Quantification of Changes for the Milne Ice Shelf, Nunavut, Canada, 1950 – 2009

Colleen Adel Mortimer

Thesis submitted to the
Faculty of Graduate and Postdoctoral Studies
In partial fulfillment of the requirements
For the MSc degree in physical geography

Department of Geography
Faculty of Arts
University of Ottawa

Supervisor
Dr. Luke Copland, University of Ottawa

Committee members
Dr. Laurence Gray, Canadian Centre for Remote Sensing
Dr. Andre Viau, University of Ottawa

Abstract

This study presents a comprehensive overview of the current state of the Milne Ice Shelf and how it has changed over the last 59 years. The 205 km^2 ice shelf experienced a 28% (82 ±0.8 km^2) reduction in area between 1950 – 2009, and a 20% (2.5 ±0.9km^3 water equivalent (w.e.)) reduction in volume between 1981 – 2008/2009, suggesting a long-term state of negative mass balance. Comparison of mean annual specific mass balances (up to -0.34 m w.e. yr^{-1}) with surface mass balance measurements for the nearby Ward Hunt Ice Shelf suggest that basal melt is a key contributor to total ice shelf thinning. The development and expansion of new and existing surface cracks, as well as ice-marginal and epishelf lake development, indicate significant ice shelf weakening. Over the next few decades it is likely that the Milne Ice Shelf will continue to deteriorate.

Acknowledgments

Support for this project has been provided by a National Sciences and Engineering Research Council of Canada (NSERC) Discovery Grant, NSERC Alexander Graham Bell Canada Graduate Scholarship, the Garfield Weston Foundation, the Northern Scientific Training Program, the Polar Continental Shelf Project, Canada Foundation for Innovation, Ontario Research Fund, CRYO-EX, the University of Ottawa, the Canadian National Air Photo Library, and the Canadian Ice Service.

I would like to thank my supervisor, Dr. Luke Copland for his continued patience and support throughout the process and for the many incredible experiences along the way. Luke, thank you for exposing me to the field of glaciology and for providing me the opportunity to study 'snow'. Never have I felt more at home than on a glacier, digging a snowpit, or traversing the remote areas of Canada's North.

I would also like to thank Dr. Derek Mueller for assistance in field data collection and for his continued guidance over the course of this project. I would like to acknowledge Sierra Pope for her assistance in field data collection. Members of the Laboratory for Cryospheric Research provided advice and camaraderie throughout the project. Comments and suggestions from thesis committee members Dr. Andre Viau and Dr. Laurence Gray improved the quality of the manuscript. Faculty members were always available to answer questions and provide important advice along the way. I would especially like to thank Sylvie Theriault and Elba Douglas, without their patience and support I would not have been able to complete this project.

I would not be where I am today if it were not for my family; together we have gone through a great deal and somehow made it this far. I am incredibly lucky to have very understanding parents, Alan and Pat Mortimer and I could have never asked for a better big sister. Sandra has always been there to look out for me and help in whatever capacity necessary. Mom, dad, and Sandra; I owe much of this thesis to the three of you.

Table of contents

Abstract……...….**I**

Acknowledgments……..…**II**

List of Tables…….....**VI**

List of Figures…….……....**VII**

Chapter 1: Introduction……..…**1**
1.0 Introduction.....**1**
1.1 Arctic change……..…**1**
1.1.1 Arctic temperature change……..……**1**
1.1.2 Arctic land ice change…….....**4**
1.1.3 Arctic sea ice change…….……..**6**
1.1.4 Arctic ice shelf change……**9**
1.1.5 Future projections and ice shelf impacts…….....**13**
1.2 Goals and objectives…….....**14**
1.3 Thesis layout…….....**15**

Chapter 2: Literature review…….....…**16**
2.1 Ice shelf background…….....**16**
2.1.1 Ice shelf definition and distribution……..……**16**
2.1.2 Ice shelf mass balance……..……**16**
2.1.3 Ellesmere Island ice shelf types……..…….....**18**
2.1.4 Ellesmere Island ice shelf surface topography……..……**20**
2.2 Ellesmere Island ice shelf formation……...…….**22**
2.2.1 Ice shelf-sea ice interaction.....**23**
2.3 Historical research conducted on northern Ellesmere Island ice shelves…….....**23**
2.3.1 Early expeditions: late 1800s to early 1900s…….....**23**
2.3.2 Ice islands and ice shelves: 1930s - 1960s……..…….**24**
2.3.2.1 Ice islands…….....**24**
2.3.2.2 Ice shelves…….……..**30**
2.4 Historical research on the Milne Ice Shelf…….……..**31**
2.4.1 Radio-echo sounding: 1966…….……..**31**
2.4.2 Radio-echo sounding: 1981…….……..**37**
2.4.3 Ground observations: Jeffries, 1982 – 1985……..…**41**
2.5 Milne Ice Shelf morphology……...……..…**42**
2.5.1 Outer Unit and Milne Re-entrant area…….…..**44**

2.5.2 Central Unit……..…**52**
2.5.3 Inner Unit…….……**52**
2.6 Glacier inputs……**57**
2.6.1 Ice caps and tributaries……..**57**
2.6.2 Milne Glacier……..…**57**
2.7 21st century research on the Milne Ice Shelf……**60**

Chapter 3: Study area and methods…….…….....**61**
3.1 Study Site……..…**61**
3.1.1 Ellesmere Island……**61**
3.1.2 Milne Ice Shelf……..……**61**
3.2. Climate…….……**63**
3.2.1 CAA Climate……..…**63**
3.3 Methods……**65**
3.3.1 Area changes……..…....……**65**
3.3.1.1 Aerial photography: history and background……..…**65**
3.3.1.2 Satellite imagery: history and background……**76**
3.3.1.3 Passive remote sensing: visible satellite imagery……..…**76**
3.3.1.4 Active remote sensing: synthetic aperture radar……**78**
3.3.1.5 Satellite imagery data sets……..……**79**
3.3.2 Ice shelf thickness……..…**80**
3.3.2.1 Ground penetrating radar (GPR): history and development……...**80**
3.3.2.2 GPR theory: basic principles…….….**82**
3.3.2.3 GPR considerations for glaciology…….……**83**
3.3.2.4 Previous GPR applications in glaciology……...……**88**
3.3.3 Ice shelf thickness data sets……...……**90**
3.3.3.1 2008 GPR data set……..……**90**
3.3.3.2 2009 GPR data set……..……**92**
3.3.3.3 *GPR data processing and analysis*…….……**96**
3.3.3.4 *Radio-echo sounding: 1981*……**97**
3.3.4 Ablation stakes……...……**97**

Chapter 4: Results……..……**101**
4.0 Introduction…….…**101**
4.1 Area change……...…**101**
4.1.1 Area change 1950 – 1959……**105**
4.1.2 Area change 1959 – 1974/1959 – 1984……...…**108**
4.1.3 Area change 1984 – 1993……**112**
4.1.4 Area change 1993 – 2009……....**113**
4.1.5 Area change: assessment of uncertainty……..…**118**

4.2 Quantification of ice thickness: 1981 – 2008/2009……**119**
4.2.1 Ice thickness error analysis…….……**122**
4.3 2008/2009 ice shelf thickness and volume…….....**123**
4.4 Ice Shelf thickness and volume change: 1981 – 2008/2009…….…..**130**
4.4.1 Direct-line comparison of thickness change: 1981 – 2008/2009……**130**
4.4.1.1 Milne Ice Shelf specific mass balance: 1981 – 2008/2009……...…**132**
4.4.2 Spatial patterns of ice thickness and volume change: 1981 – 2008/2009…...**132**
4.4.2.1 Assessment and interpretation of 1981 and 2008/2009 DEMs…...**134**
4.4.3 Volume change 1981 – 2008/2009……..**139**
4.4.4 Volume change: assessment of uncertainty…….……**140**
4.5 Ice shelf mass gains and losses……...……**142**
4.5.1 Tributary glaciers 1950……**142**
4.5.2 Milne Glacier: 1950 – 2009…….....**150**

Chapter 5: Discussion and conclusions…….……**155**
5.0 Discussion……...……**155**
5.1 Overall pattern of Milne and northern Ellesmere Ice Shelf area change: 1950- 2009...**156**
5.1.1 20th century change……..**156**
5.1.2 21st century change……..**157**
5.1.3 MLSI change……...**158**
5.2 Interpretation of ice shelf thickness measurements……**159**
5.2.1 Comparison of Milne Ice Shelf thickness change with northern Ellesmere Island ice shelf (Ward Hunt Ice Shelf) thickness change……...…….**160**
5.3 Milne and northern Ellesmere Island Ice Shelf mass balance……....**161**
5.3.1 Milne Ice Shelf mass balance gradient……**162**
5.4 Comparison with Canadian Arctic Archipelago glaciers and ice caps……...**163**
5.5 Recent observations in context of long-term northern Ellesmere Island ice shelf history……..…**164**
5.6 Ice shelf-climate context……**165**
5.6.1 Large-scale synoptic influences……..**165**
5.6.2 Northwest Ellesmere Island climate……**165**
5.7 Assessment of current Milne Ice Shelf stability…….……**168**

Chapter 6: References……...……**170**

Appendix 1: Air photo georeferencing information……...…….**182**

List of Tables

Table 1.1: Major Ellesmere Ice Shelf ice calving events over the period 2000-2008. Adapted from Copland (2009)……**10**

Table 2.1: List of all major ice islands previously tracked in the Canadian High Arctic Source: VanWychen and Copland (2011)…….….**27**

Table 3.1: Climate normals, 1971 – 2000 for Alert and Eureka. Source: Environment Canada, National Climate Data Information Archive, www.climate.weatheroffice.gc.ca, September 11, 2010……**64**

Table 3.2: List of remotely sensed imagery used in this study……**66**

Table 3.3: Typical electrical properties for selected earth surface materials. Source: Hubbard and Glasser (2005), Macheret et al. (1993), Woodward and Burke (2007)……..…**89**

Table 3.4: Ground penetrating radar system settings for 2008 and 2009……....**95**

Table 4.1: Milne Ice Self area change (1950 – 2009)…….…..….**102**

Table 4.2: Milne Glacier terminus change (1950 – 2009)…….…**106**

Table 4.3: Temporal and spatial change in MLSI extent for the Milne Ice Shelf front from 1993 – 2009 computed from satellite imagery (Table 3.2). Region A consists of the area to the NE of the Re-entrant and Region B consists of the Re-entrant area (Figure 4.7)……..**115**

Table 4.4: Ground penetrating radar ice thickness cross-point error analysis (Figure.4.9)……...**125**

Table 4.5: Milne Ice Shelf thickness (m) descriptive statistics for 2008/2009 derived from GPR measurements……..……**127**

Table 4.6: Specific mass balance measurements for 1981 – 2008/2009 from the ~8.5 km long direct line comparison (Figure 4.11)……...…….**133**

Table 4.7: Milne Ice shelf area and volume for 1981 and 2008/2009……...**141**

List of Figures

Figure 1.1: Annual average change in near surface air temperature (°C) from stations on land north of 60°N relative to the average from 1900 to 2003 (Source: ACIA 2004)……..……..**2**

Figure 1.2: Decadal average global surface air temperature (°F) for 1901 – 2000. Decadal averages are displayed with respect to the 100 year mean. Positive values indicate above average temperatures whereas negative values indicate below average decadal mean temperature. Adapted from NOAA (2010: http://www.ncdc.noaa.gov/bams-state-of-the-climate).....**3**

Figure 1.3: Cumulative net mass balance for glaciers and ice caps of the Queen Elizabeth Islands (1960-2001) (Source: Demuth and Pietroniro 2007)……..……**5**

Figure 1.4: Mean spring ice thickness change for (a) 1982-1987, (b) 1988-1995, (c) 1996-2000, and (d) 2001-2007. (e) Mean 1982-1987 thickness minus mean 1993-1996 thickness. (f) Mean 1993-1996 thickness minus mean 2001-2007 thickness. Source: Maslanik et al. (2007)…….**8**

Figure 1.5: Reconstructed ice shelf extent along northern Ellesmere Island in 1906 overlaid on a MODIS TERRA August 2005 satellite image. Inset indicates location of Ellesmere Island (red circle). Reconstruction based on Vincent et al. (2001). Image adapted from Copland (2009)……..…**11**

Figure 1.6: Map of Ellesmere Island showing location of remaining ice shelves in 2008 (blue), and locations of former ice shelves and Yelverton Bay multi-year landfast sea ice. The former Ellesmere Island Ice Shelf extended from Clements Inlet to Nansen Sound (green). Image: MODIS TERRA satellite August 2005……..…….**12**

Figure 2.1: Schematic diagram of a typical floating ice shelf…….…..**17**

Figure 2.2: Dominant sources of accumulation (mass gains) and ablation (mass losses) for arctic ice shelves. Image courtesy of D. Mueller……..…**19**

Figure 2.3: Roll and trough topography as seen by air (A) and on the ground (B). Photos: (A) Luke Copland 16 May 2009, (B) Colleen Mortimer 23 May 2009…..…**21**

Figure 2.4: Map showing location of Marvin's 1906 ocean depth soundings and Hattersley-Smith's (1954) soundings between Cape Richards and Moss Point. Ocean depth soundings taken at edge of ice fringe are used to reconstruct 1906 ice shelf extent (dashed line). Image adapted from Bushnell (1969)……..…….....**25**

Figure 2.5: A) Ellesmere Island Ice Shelf extent in 1906 reconstructed by Vincent et al. (2001). B-F) Changes in the sector surveyed my Marvin (Figure 2.4) in 1906. Stipple indicates thick, landfast sea ice. Estimates were made using a combination of maps, air photos, and other images. The 1998/99 extent was estimated from RADARSAT-1 imagery Vincent et al. (2001)……..**26**

Figure 2.6: Ice islands from air photo imagery. A) T-3 Ice Island (1952) air photo mosaic created by the U.S. Air Force, adapted from Crary (1958). B) Aerial oblique photograph of Hobson's Choice Ice Island off the north coast of Ellesmere Island in April 1985, ~9 km long and 6 km wide (Jeffries and Sackinger, 1990). Source: Jeffries (1992a)……...**29**

Figure 2.7: A) Radio Echo Sounding system set-up used by Evans and Robin (1966). B) Four-wire 35 MHz RES system custom fitted to a Single Otter aircraft. C) Schematic illustration of nadir and off-nadir sounding used to correct for ice thickness. Source: Hattersley-Smith et al. (1969)……..**32**

Figure 2.8: A) Map of Northern Ellesmere Island showing location of April 1966 flight lines conducted by Evans and Robin. Red box highlights flight over the Milne Glacier and Milne Ice Shelf shown in part B. B) Milne Glacier flight line map, April 19, 1966. Numbers indicate distance in kilometers, referred to in Figure 2.9. Adapted from Hattersley-Smith et al. (1969)……...**33**

Figure 2.9: A) Depth profile of rear of Milne Ice Shelf and Milne Glacier derived from RES survey conducted April 19, 1966. B) Film print of RES data from April 19, 1966 survey conducted by Evans and Robin. Note: Depth scale (y-axis) in meters may be applied to echo delay times within the ice (vertical propagation is assumed) and that the horizontal scale is non-linear between the km marks and the features marked, which correspond to those on the map (Figure 2.8) and profile. Adapted from Hattersley-Smith et al. (1969)……..……...**35**

Figure 2.10: 1959 air photo mosaic of confluence of Milne Glacier's tributaries. Solid white curved lines indicate approximate location of the grounding line (adapted from Hattersley-Smith et al. 1969)…….**36**

Figure 2.11: Location map showing northern Ellesmere Island and 1981 flight lines covering Mt. Oxford Ice Cap, Disraeli Glacier and Milne Glacier. Numeric annotations on the flight lines indicate travel distances in kilometers. Source: Narod et al. (1988)……..**38**

Figure 2.12: Depth profile for the Milne Glacier determined from the 100 km longitudinal flight down the Milne Glacier in April 1981 (Fig. 2.11). The upper and lower lines are ice surface and bottom respectively; dashed lines denote areas where the identified reflections may actually be diffractions. Figure adapted from Narod et al. (1988)……..**39**

Figure 2.13: Radargram for a 100 km long flight line conducted in April 1981 (Fig. 2.11). RES returns are displayed in unit time (two-way travel time). Image adapted from Narod et al. (1988)…….....**40**

Figure 2.14: (A) Location map of ice cores and snow pits collected from the Petersen and Milne Ice Shelves, northern Ellesmere Island between 1982 and 1984 (Part B, red box). Adapted from Jeffries (1985). (B) Map of north coast of Ellesmere Island showing location of snow pits, ice cores, and mass balance networks between 1982 and 1985. Insert map shows the location of the study area in relation to the Queen Elizabeth Islands. Adapted from Jeffries (1985) and Jeffries and Krouse (1987)……..…**43**

Figure 2.15: Map of the surface features and units of Milne Ice Shelf derived from July 1959 air photos (adapted from Jeffries 1986b). Numbers 1 to 4 and 6 are glaciers marked on Figure 2.18……..**45**

Figure 2.16: (A) Ice shelf ice thickness contour map derived by Prager (1983) from RES survey data from April 1981. (B) Basal PRC interpretation for Milne Ice Shelf derived by Prager (1983) from 1981 radio-echo sounding survey. Brackish ice may be present in regions where basal PRC is less than -30 dB. Source: Prager et al. (1983)…….....**46**

Figure 2.17: Milne Fiord Ice types identified by Mueller et al. (2006). Stipple indicates ice rises and glaciers, a simple hatch indicates exposed basement ice, solid grey indicates iced firn and cross hatch indicates floating glacier portions of ice shelves. Multiyear landfast sea ice (MLSI) is outlined to the seaward side of several ice shelves. Bold, straight lines are the over-flight transects. Sample sites on the ice are denoted by open circles. Adapted from Mueller et al. (2006)……..**47**

Figure 2.18: Milne Ice Shelf index map used in this study, naming conventions adapted from Jeffries (1986b). Yellow star indicates location of debris field depicted in Figure 2.21……..**48**

Figure 2.19: Outer edge of Milne Ice Shelf (May 30, 2009). Smooth Ice shelf ice (right hand side is comprised of both land ice and some MLSI. Rough sea ice is pushed up against the ice shelf. Height of freeboard was estimated to be at least 3 m. Photo: Colleen Mortimer……....**49**

Figure 2.20: Airborne X-band SAR image of the Milne Ice Shelf (center) February 1988. The ribbed texture identifies the undulating ice shelf surface. A large multiyear landfast sea ice floe, the Milne reentrant (arrow), separated from the ice shelf by a roughly S-shaped refrozen lead, has broken off the front of the west side of the Milne Ice Shelf. Image courtesy of the Canarctic Shipping Company Limited. Image adapted from Jeffries (1992a)……...**51**

Figure 2.21: Debris field and large conical mound (~15 m high) in central unit (Yellow star, Figure 2.18). May 30 2009. Photo: Colleen Mortimer, May 30, 2009...**53**

Figure 2.22: View of the Milne Glacier and Milne Epishelf Lake taken from the rear of the Central Unit. Photo: Colleen Mortimer, May 23, 2009……..…...….**55**

Figure 2.23: Milne Epishelf Lake profiles for 1983 – 2009. Point measurements from 1983 indicated by purple diamonds. Data sources: 1983 obtained from Jeffries (1985); 2004, 2006, 2007 obtained from Veillette et al. (2008); 2009 profile collected during 2009 field campaign (current study)…….....**56**

Figure 2.24: Glaciers issuing from the western side of Milne Fiord. A) Glacier 4 (hanging glacier) B) Glacier 3 with crevassed section. Photo: Colleen Mortimer May 23 and 30 2009……**58**

Figure 3.1: Map of Ellesmere Island showing major geographical features. Base image: MODIS TERRA, Aug. 13 2005……..…**62**

Figure 3.2: Air photo flight lines over the Milne Ice Shelf and surrounding areas for 1950. Flight lines overlaid on sub-scene of NTS map sheet 340F 49AN$^{1/2}$. Source: National Air Photo Library, Ottawa……...…**68**

Figure 3.3: Images used for the 1950 air photo mosaic with corresponding flight line and image numbers from Figure 3.2. Detailed information for all photos used in this study is found in Appendix 1, Table A1……..**69**

Figure 3.4: Air photo flight lines over the Milne Ice Shelf and surrounding areas for 1959. Flight lines overlaid on sub-scene of NTS map sheet 'B' 340F & 560E. Source: National Air Photo Library, Ottawa……..**70**

Figure 3.5: Air photos used for 1959 air photo mosaic with corresponding flight lines and image numbers from Figure 3.4. Detailed information for all photos used is found in Appendix 1, Table A2……..…**71**

Figure 3.6: Air photo flight lines over the Milne Ice Shelf and surrounding areas for 1974. Flight lines overlaid on sub-scene of NTS map sheet "B" 340F & 560E. Source: National Air Photo Library, Ottawa……..**72**

Figure 3.7: Air photos used for 1974 air photo mosaic with corresponding flight lines and image numbers from Figure 3.6. Detailed information for all photos used is found in Appendix 1, Table A3…….…….**73**

Figure 3.8: Air photo flight lines over the Milne Ice Shelf and surrounding areas for 1984. Flight lines overlaid on sub-scene of NTS map sheet "E" 340F & 560E. Source: National air photo Library, Ottawa…….…..**74**

Figure 3.9: Air photos used for 1984 air photo mosaic with corresponding flight lines and image numbers Figure 3.8. Detailed information for all photos used is found in Appendix 1, Table A4……**75**

Figure 3.10: Visible (ASTER) and SAR (RADARSAT-1) satellite image pair of outer Milne Ice Shelf and Milne Re-entrant area. (A) Early summer ASTER Scene; (B) Late summer ASTER scene; (C) Winter RADARSAT-1 scene; (D) summer RADARSAT-1 scene……....**77**

Figure 3.11: Field measurements on the Milne Ice Shelf May 23 – June 3, 2009. (A) Ground penetrating radar profiling; (B) Ablation stake measurements and snow pits; (C) Shallow ice coring. Photos: Colleen Mortimer and Luke Copland 2009…….…….**81**

Figure 3.12: Schematic diagram of what happens to energy emitted a GPR transmitter when it meets an internal reflector horizon (IRH). Some energy is absorbed at the interface between the two materials, some is reflected back to the receiver and a portion is transmitted through the IRH to penetrate greater depths in the material……..…….**84**

Figure 3.13: Common Midpoint Survey. Source: PulseEKKO PRO User Guide (2006)...**85**

Figure 3.14: GPR Radargram produced in EKKO View Deluxe for a ~ 3 km long transect along the Milne Ice Shelf (June 3 2009). Dark purple line represents the bed (ice-water reflector horizon). DVL gain, GPS coordinates, and velocity of 0.170 m ns^{-1} applied. The apparent undulating bed topography is a product of surface rolls……...……..**87**

Figure 3.15: Diffraction patterns for certain features. The heavy lines represent expected diffraction patterns from (A) bottom crevasse, (B) surface crevasse, (C) unsoundable block of ice (likely caused by brine infiltration), and (D) step decrease in ice thickness. The shaded portion is impenetrable ice, rock, or water. Image reproduced from Prager (1983, p. 36)……..….**91**

Figure 3.16: Field measurement sites for 2008 and 2009 on the Milne Ice Shelf overlaid on a 21 July 2009 ASTER image. Yellow star indicates location of common midpoint survey (section 4.2). C3/M1 indicates location of June 2009 epishelf lake water profile (Figure 2.24)……...…….**93**

Figure 3.17: Ground penetrating radar field set-up. (A) 50MHz GPR system custom fitted onto a komatiq; (B) Custom fitting 250 MHz GPR into plastic sled; (C) GPR sled pulled behind a skidoo. Photos: Luke Copland (A&B), Colleen Mortimer (C)……...…**94**

Figure 3.18: Flight line map for 1981 radio echo-sounding survey of the Milne Ice Shelf Prager (1983)……..……**98**

Figure 3.19: Radar section for the Milne Ice Shelf from 1981 RES survey. A and B refer to start and end points of radargram section (Figure 3.16). Two large bottom crevasses are indicated by the downward-opening hyperbolae (red boxes) which consist of gaps with no clear bottom reflection Prager (1983) suggests that this may imply that the ice between the crevasses is brackish. Source: Prager (1983)……..**99**

Figure 4.1: Milne Ice Shelf extent for 1950 to 2009. 1950, 1959, and 1984 polygons are overlaid on air photo mosaics. Polygons for 1993 (ERS-1: 19 May 1993), 2001 (ASTER: 23 May and 19 September 2001) and 2009 (ASTER: 21 July 2009) are overlaid on satellite imagery……...….**103**

Figure 4.2: Temporal change in ice shelf extent (1950 – 2009) overlain on 1959 air photo mosaic. Numbers 1-6 indicate location of glaciers referred to in Figs. 4.15 – 4.19……...**104**

Figure 4.3: Lake development for the Milne Ice Shelf 1950 – 2009; A (1950 air photo) and B (1959 air photo) show development of Milne Epishelf lake between 1984 and 1993. C (1993 ERS-1 scene) and D (2009 ASTER scene) show change of inner unit from rolls and troughs to epishelf lake ice. Lake area (ice-marginal and Milne Epishelf Lake) is given for 1959, 1984, and 2009.....**107**

Figure 4.4: Change in northwest corner of Milne Ice Shelf front between 1959 and 1974 air photo mosaics. A calving event, leading to a loss of 26 km^2 of ice shelf area, occurred sometime during this period. Dark black lines highlighted with red dotted line indicate cracks that likely acted as lines of weakness. Note position and shape of 1974 front is very similar to the large cracks……....**109**

Figure 4.5: Temporal change in Milne Ice shelf front and fractures between 1950 and 2009 overlaid on a 1974 air photo mosaic. Development of Milne Re-entrant in 1974 from 1974 air photo also shown. 1993 and 2001 omitted due to insignificant change over this period (same position as 2009)…….**110**

Figure 4.6: MLSI extent delineated on satellite scenes for May 19, 1993 (ERS-1), September 19, 2001 (ASTER), June 19, 2005 (ASTER), July 21, 2009 (ASTER), May 15, 2009 (RADARSAT-2)……..**114**

Figure 4.7: Sub-regions used to quantify spatial changes in MLSI from 1993 – 2009 overlaid on a July 21, 2009 ASTER scene. Inset graph shows MLSI area for 1993, 2001, 2005, and 2009. 2009A indicates measurements made from the July 21, 2009 ASTER scene and 2009R is from the May 15, 2009 RADARSAT-2 scene…….....**117**

Figure 4.8: Radargram section for ground penetrating radar transect from the Outer Unit, June 3, 2009. The red star indicates location of crack. Location of GPR transect is shown on a July 21, 2009 ASTER scene, identified by black line, starting at point A and ending at point A'…….….**121**

Figure 4.9: Cross point sites for 2008 and 2009 ground penetrating radar thickness error analysis measurements overlaid on a July 21, 2009 ASTER scene…….**124**

Figure 4.10: A) Milne Ice Shelf thickness from spring 2008 and 2009 GPR measurements. Black triangle indicates location of thickest ice recorded. Points A and B correspond to beginning and end of re-profiled transect displayed in figure 4.9. B) RADARSAT-2 March 15, 2009 scene, showing location of new crack……..**128**

Figure 4.11: A) Ice thickness along an 8.5 km transect from point A to B (Figure 4.8). 1981 ice shelf thickness extracted from Prager (1983) radargram. Estimated horizontal positional error is ~300 m between the two survey lines. B) Radargram from 2008 and 2009 250 MHz GPR data showing location of crack. Dark purple line indicates ice shelf bed. Dark blue circle shows location of downward-dipping hyperbolae indicating crack sidewalls…....**128**

Figure 4.12: Milne ice shelf thickness from GPR data collected in spring 2008 and 2009 overlaid on a July 21, 2009 ASTER image. B) Milne Ice Shelf thickness contour map derived from GPR data (Figure 4.12A) overlaid on a July 21, 2009 ASTER image. C) Milne Ice Shelf thickness interpolated surface (DEM) derived from contour map (Figure 4.12B) overlaid on a July 21, 2009 ASTER image……...**129**

Figure 4.13: Change in surface height for Milne Ice Shelf measured from five ablation stakes over the period April 4, 2008 to June 3, 2009 overlaid on a July 21, 2009 ASTER scene……...……**135**

Figure 4.14: Milne Ice Shelf annual snowpack for 2007-2008, measured in snow water equivalent (SWE) April 4, 2008 overlaid on a July 21, 2009 ASTER scene…….**136**

Figure 4.15: Digital elevation model of ice thickness (m) for 1981. Thickness was interpolated from 1981 contour map produced by Prager (1983) from radio echo sounding data…….……..**137**

Figure 4.16: Milne Ice Shelf thickness change 1981 to 2008/2009……...…**138**

Figure 4.17: Temporal change of Glacier 1 terminus 1950 – 2009……...**144**

Figure 4.18: Temporal change of Glacier 2 terminus 1950 – 2009……...…**145**

Figure 4.19: Temporal change of Glacier 3 terminus 1950 – 2009. Insufficient coverage for 1984 to determine terminus extent……..…….**146**

Figure 4.20: Temporal change of Glacier 4 terminus 1950 – 2009. 1993 not outlined due to poor image quality……...….**147**

Figure 4.21: Temporal change of Glacier 6 terminus 1950 – 2009……...……**148**

Figure 4.22: Temporal change of the five tributary glaciers studied for 1950 – 2009. Glacier terminuses delineated from air photo mosaics and satellite imagery (Figures 4.16 – 4.19). Naming conventions adapted from Jeffries (1986b)……...…...**149**

Figure 4.23: 1950 -2009 terminus extent for Milne Glacier main tributary, southwest tributary, and remnant glacier ice…….**151**

Figure 4.24: Measurements of temporal change of the Milne Glacier 1950 – 2009. A) Main tributary measurement axes (solid black lines) connect selected points (solid black circles); B) Southwest tributary measurement axes (dashed black lines) connect selected 'points' (solid black circles)……..**152**

Figure 4.25: Temporal change of Milne Glacier A) Main tributary and B) Southwest tributary for 1950 – 2009…….....**153**

Figure 4.26: Rate of Milne Glacier terminus advance (m yr^{-1}) for the main tributary (blue line) and the southwest tributary (red line) for 1950 – 2009……**153**

Chapter 1: Introduction

1.0 Introduction

Canada has lost > 90% of its ice shelf area over the last century (Vincent et al. 2001). Recent northern Ellesmere ice shelf breakups (2000 – present), such as the complete loss of the Ayles and Markham Ice Shelves, have highlighted the importance of assessing the present state of northern Ellesmere's remaining ice shelves. Although these features are being lost at an alarming rate, little is known about their morphology, history or dynamics. This study presents the most comprehensive assessment to date of the ice thickness and volume of any northern Ellesmere ice shelf. A combination of historical data and recent observations are used to assess changes in Milne Ice Shelf area and thickness over the past half century. These changes are presented in the context of ice shelf breakups, sea ice losses, and high arctic glacier mass balance. The following section provides an overview of recent arctic change under which the current study is being undertaken.

1.1 Arctic change

1.1.1 Arctic temperature and climate change

Over the last 50 years air temperatures in the arctic (above 60°N) have increased at twice the global average of 0.13°C decade^{-1} (ACIA 2004; Lemke et al. 2007) Although periods of increasing (1920 – 1960; 1980 to present) and decreasing (1900 – 1920s; 1960 - 1980) surface air temperatures were observed over the last century (1900 – 2003), a distinct warming trend has been observed beginning in the 1960s (Figure 1.1). The last three decades (1980 to present) are now the warmest on record (Figure 1.2) (ACIA 2004; Lemke 2007; NOAA2010:*http://www.ncdc.noaa.gov/sotc/?report=global&year=2010&month=6.*). Arctic temperature change is most pronounced in the winter months and least pronounced in the summer season (ACIA 2004; Lemke et al. 2007; Lesins et al. 2010). The IPCC (2007) predicts that arctic air temperatures will increase by an additional 3°C to 11°C over the next

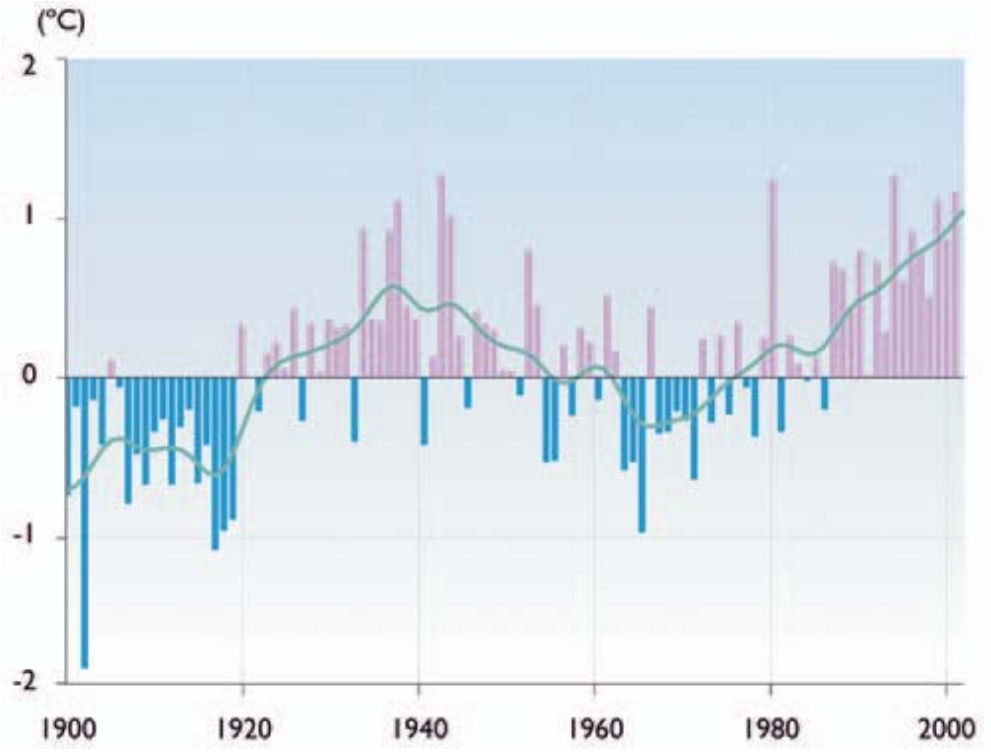

Figure 1.1: Annual average change in near surface air temperature (°C) from stations on land north of 60˚N relative to the average from 1900 to 2003 (Source: ACIA 2004).

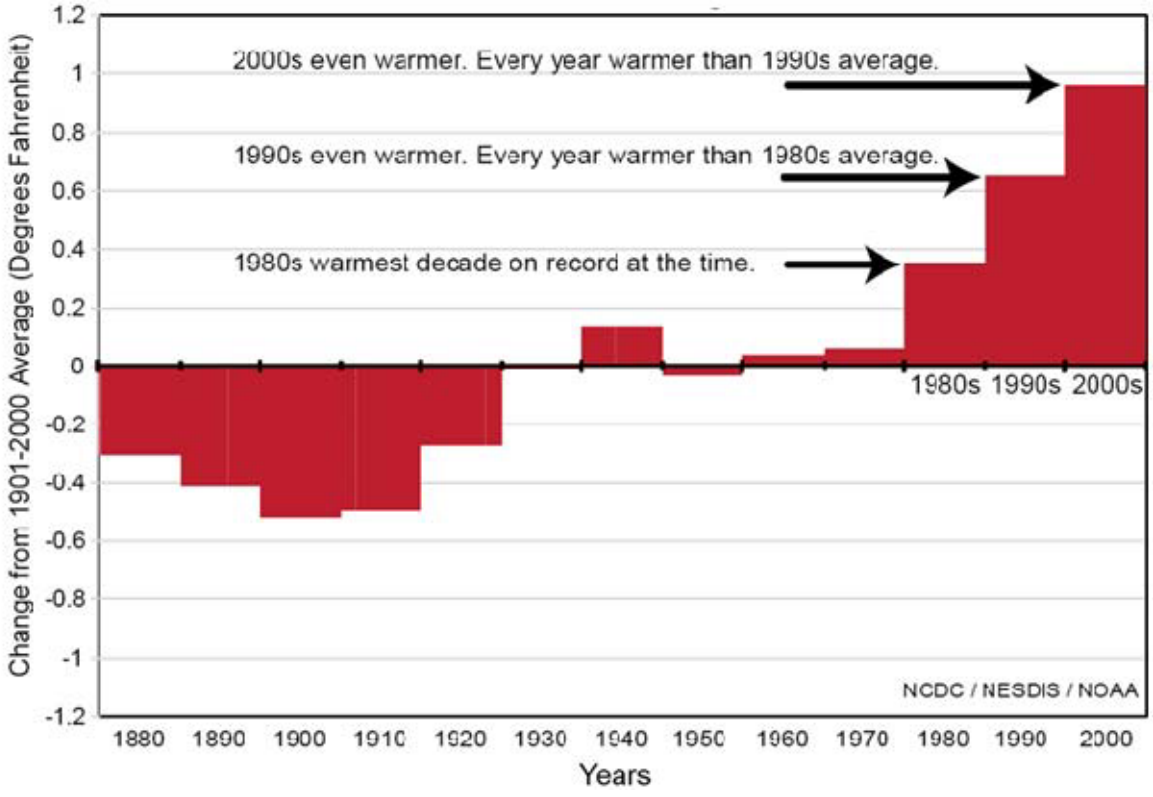

Figure 1.2: Decadal average global surface air temperature (°F) for 1901 – 2000. Decadal averages are displayed with respect to the 100 year mean. Positive values indicate above average temperatures whereas negative values indicate below average decadal mean temperature. Adapted from NOAA (2010: http://www.ncdc.noaa.gov/bams-state-of-the-climate).

century. In addition to changes in temperature, an increase in precipitable water (particularly in the spring, summer and fall), an increase in summer wind speeds and a decrease in winter cyclonic activity were observed at Eureka, located in the Canadian Arctic Archipelago (CAA), between 1954 and 2007 (Lesins et al. 2010). Observed increases in surface air temperatures are also reflected in changes in snow and land ice cover. Northern Hemisphere annual snowcover has decreased at a rate of 1.3% per decade over the last 40 years (European Environmental Agency 2008) and the duration of annual lake ice cover, dominated by an earlier melt onset and later freeze-up, has also decreased (Duguay 2006). Observed and predicted warming trends are likely to significantly impact the cryosphere, leading to further large-scale changes in sea ice and land ice, including ice shelves.

1.1.2 Arctic land ice change

Observed anthropogenic warming could significantly affect the mass balance of glaciers and ice caps, which are important contributors to global sea level rise (Abdalati 2006; Boon et al. 2010; Lemke et al. 2007). Glaciers and ice caps in the CAA comprise the largest concentration of land ice (~151,057 km^2) outside of Greenland and Antarctica (Koerner 2002). Measurements of several glaciers and ice caps in the Queen Elizabeth Islands (QEI) indicate that mass balances have become increasingly negative since the 1950s (Figure 1.3) (Braun et al. 2001; Demuth and Pietroniro 2007; Koerner 2002). This trend, which has accelerated since the 1990s, coincides with the aforementioned increases in temperature (Koerner 2005). Repeat laser altimetry surveys (1995 and 2000) of several ice caps in the CAA showed an estimated regional mass loss of 23 $km^3\ yr^{-1}$ (Abdalati et al. 2004; Abdalati 2006).

Studies of individual glaciers and ice caps confirm these broader trends. For example, the Murray Ice Cap, Hazen Plateau, Ellesmere Island, experienced an overall reduction in area of ~28% between 1959 and 2000 and a 1999 - 2000 net mass balance of -0.12 to -0.87 m water equivalent (w.e.). The mass balance for nearby Simmons Ice Cap

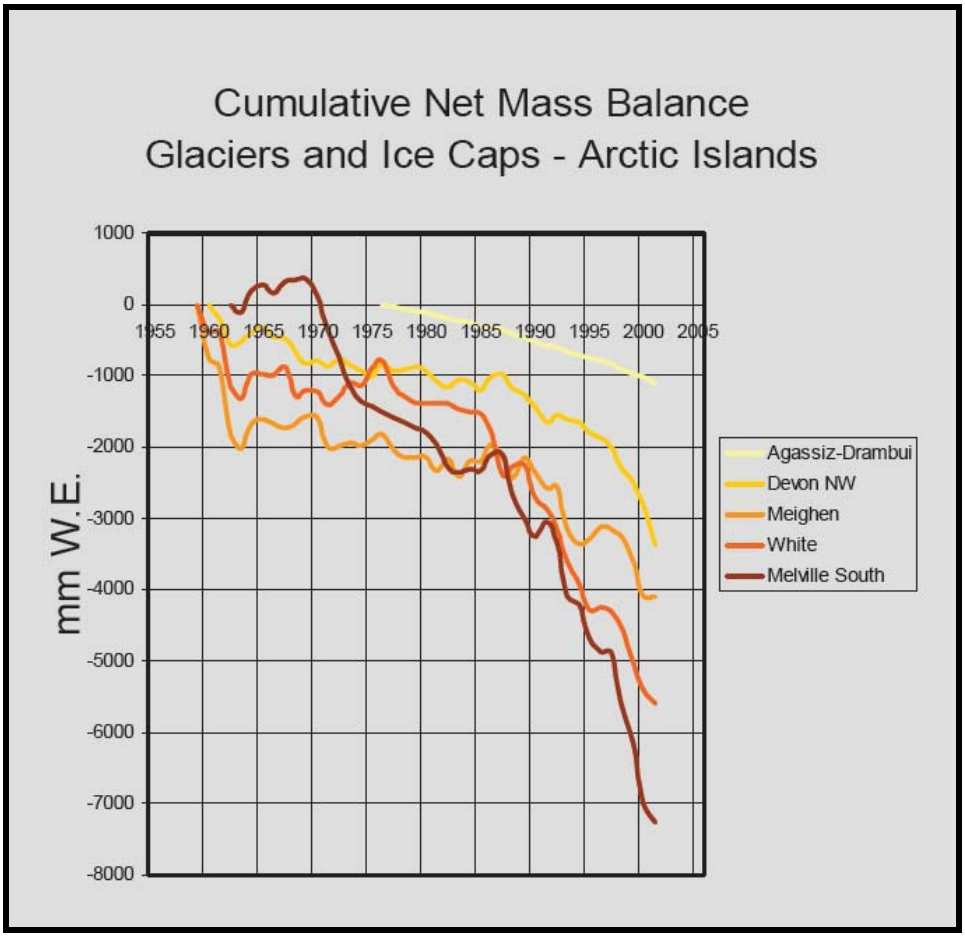

Figure 1.3: Cumulative net mass balance for glaciers and ice caps of the Queen Elizabeth Islands (1960-2001) (Source: Demuth and Pietroniro 2007).

ranged from -0.21 to -0.77 m w.e. over the same 1-year time period (Braun et al. 2001). Accelerated thinning of the Barnes Ice Cap, observed by Sneed et al. (2007), also coincides with observed atmospheric warming in the Canadian Arctic. For the period 1970 – 1984 the south dome of Barnes Ice Cap thinned at a rate of 0.12 m yr^{-1}, increasing to ~0.76 +/- 0.35 m yr^{-1} for the period 1984-2006. Between 1959/1960 and 1999/2000 the surface area of the Devon Ice Cap decreased 2.4%, with thinning and associated volume losses estimated at -67 +/- 12 km^3 (Boon et al. 2010; Burgess and Sharp 2004). Finally, model results (1959 – 2006) of Laika Glacier, Coburg Island, Nunavut showed a predicted area decrease of 23%, volume loss of 24%, and an increase in mass balance gradient (Huss et al. 2008). Under future climate warming scenarios, complete wastage of the Laika Glacier is predicted by the end of the 21st century.

1.1.3 Arctic sea ice change

Sea ice is a key cryospheric component in regulating the global climate system. Not only does its high albedo reflect a significant amount of incoming direct solar radiation, the presence of sea ice provides a physical barrier which separates the relatively warm ocean from the cold atmosphere in winter. According to the ACIA (2004), average arctic sea ice extent decreased between 15 and 20% over the last three decades. These marked area reductions (reduction of 7.8% per decade for 1953-2006), and an earlier melt onset attributed to warmer air and ocean temperatures, have created a weaker barrier for heat exchange between the atmosphere and ocean (Perovich et al. 2008; Serreze et al. 2007; Stroeve et al. 2007). From 1958 to 1990, reductions in sea ice were greatest in the eastern and central parts of the Arctic Ocean, with smaller reductions in the Beaufort and Chukchi Seas (Rothrock et al. 1999; Serreze et al. 2007). Beginning in the late 1990s, parts of the western Arctic Ocean including the Beaufort and Chukchi Seas witnessed the sharpest declines (Maslanik et al. 2007; Rothrock et al. 1999). Rapid reductions in the western Arctic have extended well into the 21st century.

Coincident with a decrease in extent has been a decrease in the age and thickness of the Arctic's sea ice cover (Figure 1.4) (Maslanik et al. 2007; Nghiem et al. 2007). Between March 2005 and 2007, the extent of multiyear sea ice (MYI), defined as sea ice that has survived at least one melt season, decreased 23% (Nghiem et al. 2007). Few areas of very old sea ice (8+ years old) remain. Instead the bulk (58%) of the MYI is comprised of 2 – 3 year old ice; a 35% increase since the 1980s. Regions containing at least 50% of 5 year old MYI at the end of the winter season (March) decreased by 56% between 1985 and 2007. Although the trend towards a younger, thinner Arctic sea ice cover has accelerated in recent years, thinning has been observed from the 1950s onwards. Analysis of end of melt season sea ice draft thickness between 1958 and 1999 showed an average decrease of ~1.3 m, with the largest change being observed in the eastern Arctic where draft decreased from 3.3 m (1958 – 1976) to 1.5 m (1999). Changes in circulation patterns and an increase in sea ice export through Fram Strait has further accelerated the loss of MYI, which has largely been replaced with younger and thinner first year ice (FYI) (Maslanik et al. 2007; Nghiem et al. 2007).

Sea ice melt onset in 2009 was up to two weeks earlier in some regions compared to the 1979-2000 mean (NSIDC 2009), and September 2007 minimum extent (4.28×10^6 km^2) surpassed the previous record minimum (September 2005) by 23% and the long-term mean (1979-2000) by 39% (Maslanik et al. 2007). Observed low sea ice coverage has been attributed in part to high temperatures and strong winds (Comiso et al. 2008). Minimum sea ice extent for 2010 was the third lowest on record (4.60 million km^2 on September 19, 2010), below that of 2009 (NSIDC Arctic Sea Ice News and Analysis, http://nsidc.org/arcticseaicenews).

The presence of sea ice provides an important buttressing effect that helps to stabilize ice shelves and tidewater glaciers (Reeh et al. 2001; Rignot et al. 2004; Scambos et al. 2004; Williamson et al. 2008). The removal of sea ice exposes ice shelves to increased dynamic effects of ocean winds, tides and currents (Copland et al. 2007; Jeffries 2002; Serreze et al. 2007). The dramatic reductions in sea ice extent and volume therefore have

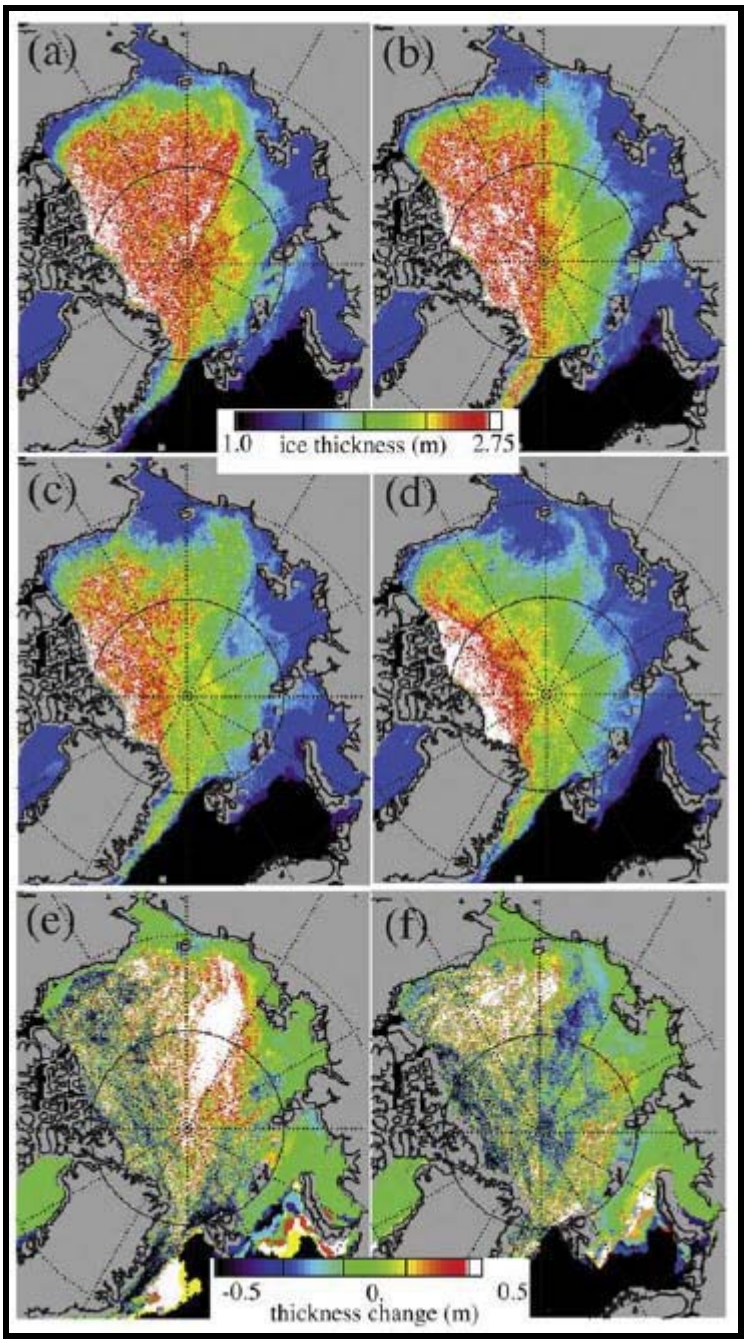

Figure 1.4: Mean spring ice thickness change for (a) 1982-1987, (b) 1988-1995, (c) 1996-2000, and (d) 2001-2007. (e) Mean 1982-1987 thickness minus mean 1993-1996 thickness. (f) Mean 1993-1996 thickness minus mean 2001-2007 thickness. Source: Maslanik et al. (2007).

potentially important consequences for the future survival of arctic ice shelves (Alt et al. 2006; Maslanik et al. 2007; Vincent et al. 2001).

1.1.4 Arctic ice shelf change

Ice shelves are thick (>20 m) floating masses of ice attached to land (Jeffries 2002). Large ice shelves are common around Antarctica where they cover approximately 55% of the coastline (Glasser et al. 2009) and are up to 1000 m thick. Much smaller ice shelves exist in the Canadian Arctic north of 82°N, along the northwest coast of Ellesmere Island (Jeffries 1992a). These ice shelves are the remnants of a large (~9000 km^2) ice shelf fringe that formed between 3000 and 4500 years ago along northern Ellesmere and Axel Heiberg Islands (Figure 1.5) (Bradley et al. 1990; England et al. 2008; Evans and England 1992; Vincent et al. 2001).

Since the late 19th century Canada has lost over 90% of its ice shelf area. Much of this loss occurred in the early to mid-20th century. By the mid-1900s, the once continuous Ellesmere Ice Shelf had been reduced to several small individual ice shelves (Bradley 1990; England et al. 2008; Evans and England 1992; Vincent et al. 2001). Significant ice shelf area was lost in the early to mid-20th century (1920s to 1960s) via large-scale calving events including the loss of ~600 km^2 from the Ward Hunt Ice Shelf between 1961 and April 1962 (Hattersley-Smith 1963). The 1980s saw another period of ice shelf loss which included calving of the ~40 km^2 Hobson's Choice Ice Island from the Ward Hunt Ice Shelf sometime between 1982 and 1983 as well as a 33.3 km^2 piece of the Milne Ice Shelf between 1959 and 1974 (Jeffries 1986b).

Disintegration of the ice shelves continued throughout the first decade of the 20th century, decreasing the total number of ice shelves from six to four (Table 1.1; Figure 1.6). Fracturing of the Ward Hunt Ice Shelf (2000 – 2002) was followed by the loss of the entire Ayles Ice Shelf (87.1 km^2) in August 2005 (Copland et al. 2007). In 2008 the remaining ice

Table 1.1: Major Ellesmere Ice Shelf ice calving events over the period 2000-2008. Adapted from Copland (2009).

Year(s)	**End of summer ice shelf area (km^2)**	**Calving event(s)**	**Area lost (km^2)**
2000-2002	1043 km^2	Fracturing of Ward Hunt Ice Shelf	6 km^2
2005	943 km^2	Entire Ayles Ice Shelf 20% of Petersen Ice Shelf	87 km^2 13 km^2
2006-2007	935 km^2	Part of Petersen Ice Shelf	8 km^2
2008	720 km^2	Part of Ward Hunt Ice Shelf Entire Markham Ice Shelf 60% of Serson Ice Shelf	42 km^2 50 km^2 122 km^2

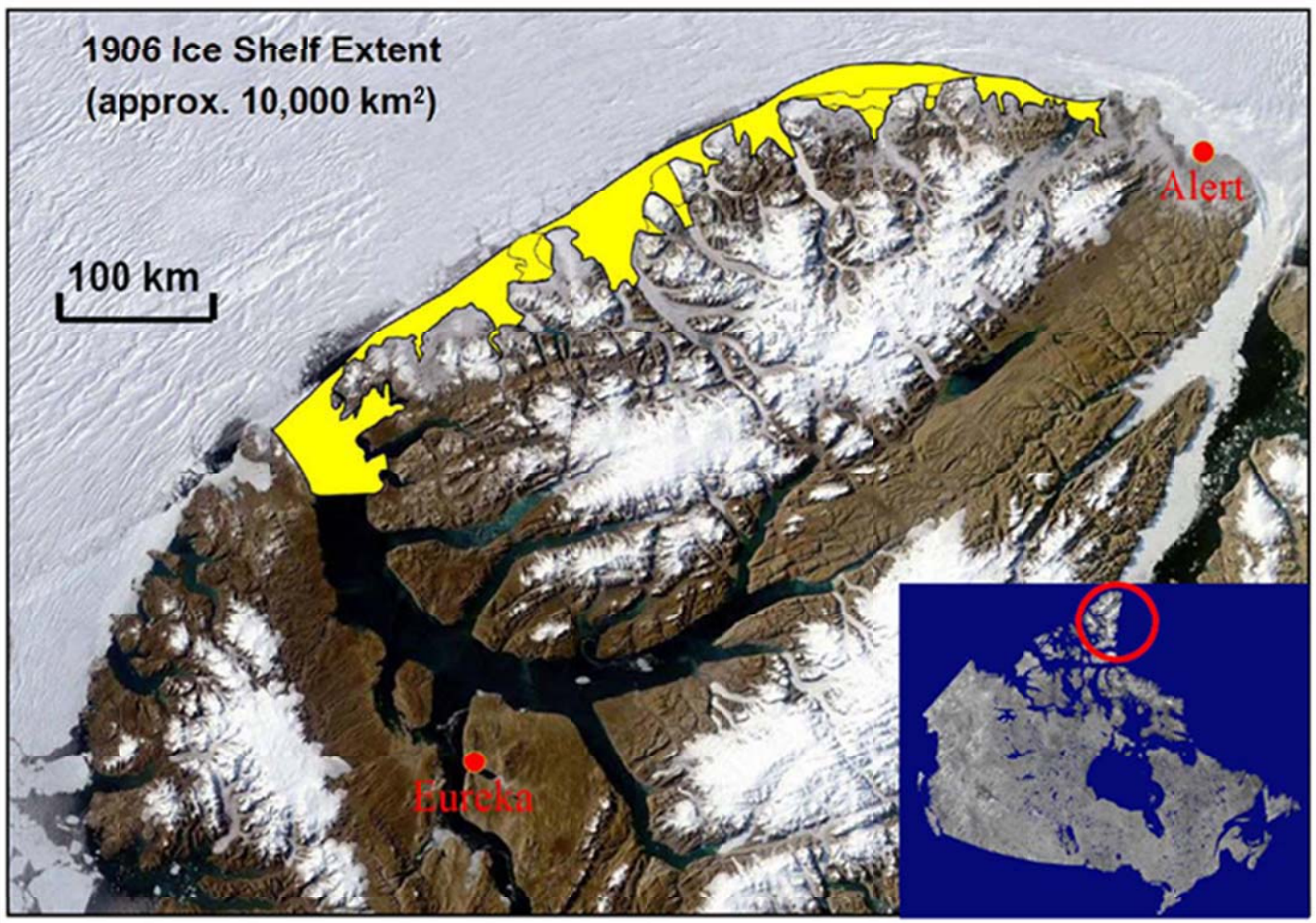

Figure 1.5: Reconstructed ice shelf extent along northern Ellesmere Island in 1906 overlaid on a MODIS TERRA August 2005n satellite image. Inset indicates location of Ellesmere Island (red circle). Reconstruction based on Vincent et al. (2001). Image adapted from Copland (2009).

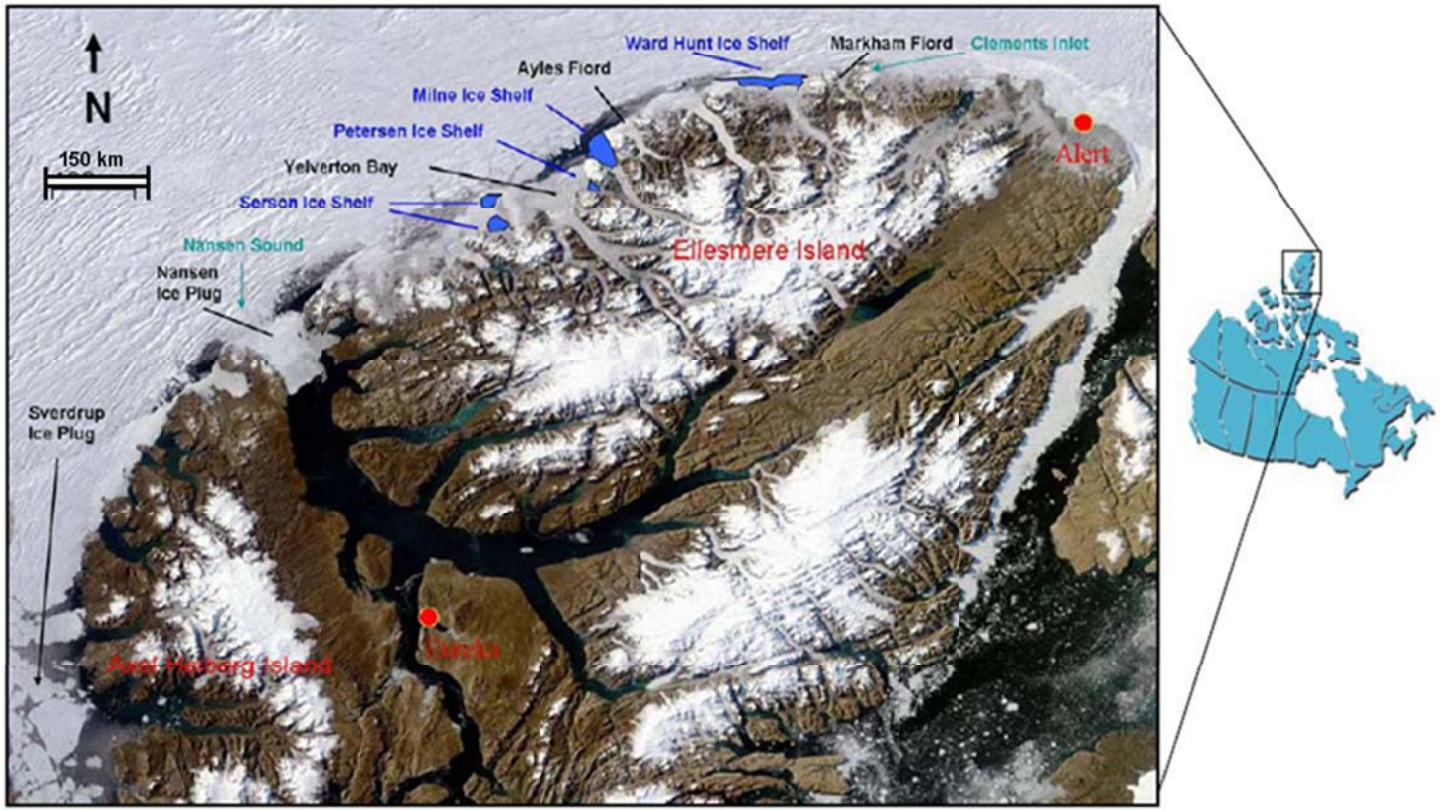

Figure 1.6: Map of Ellesmere Island showing location of remaining ice shelves in 2008 (blue), and locations of former ice shelves and Yelverton Bay multi-year landfast sea ice. The former Ellesmere Island Ice Shelf extended from Clements Inlet to Nansen Sound (green). Image: MODIS TERRA satellite August 2005.

shelf area decreased by a further 23% (Mueller 2008). Losses included 60% of the Serson Ice Shelf (122 km^2), the entire Markham Ice Shelf (50 km^2), and part of the Ward Hunt Ice Shelf (42 km^2) (Table 1.1). Significant periods of ice shelf disintegration (1930s - 1960s and 2000 – present) appear to coincide with periods of relatively warm air temperatures in the 1930s and 1950s (1.0°C to 1.5°C above 1900-2000 mean) and 1980s to present (2.0°C above 1900 - 2000 mean), as well as periods of light sea ice (Copland et al. 2007; Mueller 2008; Vincent et al. 2001).

Since the 1950s, Ellesmere Island's ice shelves have experienced a net mass loss (Copland et al. 2007; Vincent et al. 2001). Ablation stake measurements for the Ward Hunt Ice Shelf reveal a recent acceleration in negative surface mass balance, with the 2002-2003 surface mass balance (-0.54 m w.e.) far exceeding the 45 year rate of -0.069 m w.e. yr^{-1} (Braun et al. 2004a; Braun 2011). Ice shelf area decrease and accelerated negative surface mass balance provide unequivocal evidence that arctic ice shelves have undergone significant change since the beginning of the 21st century.

1.1.5 Future projections and ice shelf impacts

Ice shelves can break up in response to both short-term (days to years) and long-term (years to decades) external changes. Studies of ice shelves in the Arctic and Antarctic (Copland et al. 2007; Glasser et al. 2009; Jeffries 2011; Scambos et al. 2004; Vincent et al. 2001) indicate that short-term forcing can arise from high air temperatures, strong offshore winds, low sea ice conditions, and an increase in open water. Long-term forcing includes negative mass balance, increase in crevassing and an increase in surface ponding leading to a decrease in structural strength and ice thickness (Braun et al. 2004a; Copland et al. 2007). These long-term forcings, which have been attributed to an increase in mean annual air temperatures over the last half century, pre-weaken the ice shelf making it more susceptible to abrupt, short-term changes (Braun et al. 2004a; Scambos et al. 2004). Ice shelves can therefore serve as important sentinels for climate-related impacts in the Canadian High

Arctic (Braun et al. 2004b; Copland et al. 2007; Mueller et al. 2003). Arctic ice shelf disintegration appears to occur as a threshold response related to an augmentation of air and ocean temperatures (Glasser et al. 2009). For instance, Copland et al. (2007) attributed the break-up of the Ayles Ice Shelf (August 2005) to a temperature threshold of >200 positive degree days (PDD) per year.

The break-up of an ice shelf does not have a direct contribution to sea level rise since the ice is already floating. However, the loss of these features can have other important consequences. For instance, the breakup of Larsen B Ice Shelf triggered an acceleration of four surrounding glaciers which can in turn contribute to sea level rise (Scambos et al. 2004). Ice shelves are also ecologically important. In the Canadian Arctic, ice shelf disintegration frequently triggers the drainage of epishelf lakes and the associated loss of unique cryo-habitats (Mueller et al. 2003; Mueller et al. 2006; Vincent et al. 2001). These fresh and brackish water lakes support rare microbial communities that are extremely sensitive to external change.

The loss of >90% of Canada's ice shelves over the last century has provided unequivocal evidence that the arctic is changing. However, limited long-term studies concerning Ellesmere Island's Ice Shelves have been carried out. Previous research has been conducted to determine changes in overall ice shelf extent (e.g., Mueller et al. 2009; Vincent et al. 2001), but little is known about the impact of warming on changes in ice shelf thickness. This study addresses this knowledge gap.

1.2 Goals and objectives

The goal of this project is to quantify recent volume and area changes of the Milne Ice Shelf, Ellesmere Island, Nunavut. Changes in surficial area (1959-2009) and ice thickness (1981 – 2009) are determined via a combination of fieldwork and analysis of remotely sensed imagery. This project provides some of the most detailed measurements to

date of the changes of an ice shelf in the Canadian Arctic over the past 25+ years. As such, it will provide important insight as to how Nunavut's coastline is changing. Changes in Arctic sea ice have been studied extensively in the past, but little work has been carried out to examine land ice changes related to features such as ice shelves.

1.3 Thesis layout

This thesis follows a traditional format. This introduction is followed by a brief overview of ice shelf formation, distribution and mass balance, and a comprehensive review of previous work conducted on northern Ellesmere's ice shelves with a specific focus on the Milne Ice Shelf. Chapter 3 presents the methods used to complete this study. Results are presented in Chapter 4, as is an assessment of error and an evaluation of the methods used. Chapter 5 provides both a discussion and conclusion.

Chapter 2: Literature review

2.1 Ice shelf background

2.1.1 Ice shelf definition and distribution

An ice shelf is defined as a floating mass of ice attached to land with a minimum thickness of 20 m and a minimum freeboard of 2 m (Jeffries 2002; Lemmen et al. 1988; Mueller et al. 2006). These buoyant features are in hydrostatic equilibrium with the ocean, so only a small fraction (~10%) of their total thickness is typically visible above sea level (Figure 2.1). Globally, the largest concentration of ice shelves is found in the Antarctic where ~55% of the coastline is fringed with them (Dowdeswell and Jeffries 2011; Glasser et al. 2009). Ice shelves are also found in the Eurasian High Arctic, Greenland, and the Canadian High Arctic (Dowdeswell 2011). Arctic ice shelves are considerably smaller than Antarctic ice shelves (by up to 3 orders of magnitude), and are largely confined to fiords. In contrast, Antarctic ice shelves are generally unconfined, extending outward in large embayments (Dowdeswell and Jeffries 2011). Further, unlike their Antarctic counterparts, which are largely glacially fed, arctic ice shelf growth typically relies on surface accumulation and basal freeze-on (Dowdeswell and Jeffries 2011; Jeffries 2002; Jeffries 2011; Mueller et al. 2006; Vaughan 1998; Vincent 2001). The largest concentration of Arctic Ice Shelves is found along the northeastern coast of Ellesmere Island. The remaining sections of this chapter are concerned primarily with northern Ellesmere's ice shelves, with specific emphasis on the Milne Ice Shelf.

2.1.2 Ice shelf mass balance

Glacier and ice shelf mass balance is defined as the sum of all accumulation (mass gains) and ablation (mass losses) over a specified period of time (Anonymous 1969). When mass gains equal mass losses the ice shelf's (or glacier) mass balance is said to be zero. A positive mass balance is associated with ice shelf mass gain whereas a negative mass balance indicates mass loss. Ice shelf accumulation occurs via glacier inflow, surface

$h_d = h_i \times 0.90$

h_f = ice shelf freeboard

h_d = ice shelf draft

h_i = ice shelf thickness

0.90 = ice density

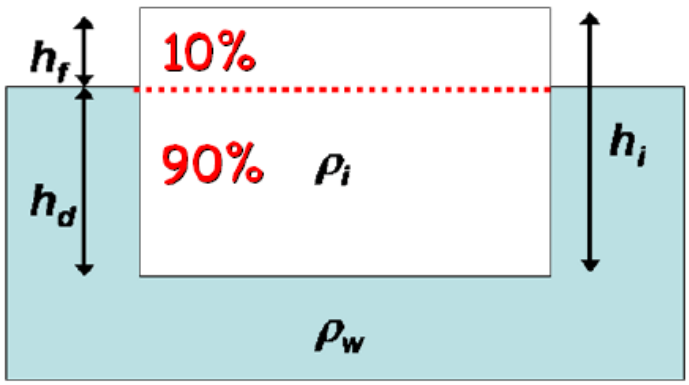

Figure 2.1: Schematic diagram of a typical floating ice shelf.

snowfall, and basal freeze-on of sea water. Ablation occurs via surface and basal melt, and iceberg calving (Jeffries 2011; Figure 2.2). Glacial input is currently of limited importance for most ice arctic ice shelves except for parts of the Milne (Jeffries 1986a; Jeffries 1986b; Jeffries 2011). However, as evidenced by many remnant glacier tongues present on former ice islands, glaciers were previously important in the formation of the Ayles, Serson, Petersen, and Milne Ice Shelves (Copland et al. 2007; Jeffries 1986a; Jeffries 1986b; Jeffries 1992a; Jeffries 2002; Mueller 2003). Calving, resulting in the production of large ice islands has been the most visible sign of mass loss and change in areal extent for arctic ice shelves. Surface and basal melt may also contribute to ice shelf thinning; however, no quantitative studies regarding ice shelf thinning have been carried out on Ellesmere Island.

For a typical Antarctic ice shelf, the accumulation zone is located towards the rear of the ice shelf where land-based glaciers flow out onto the floating ice shelf. The ablation zone, dominated by iceberg calving, is located at the ice shelf front (Benn and Evans 2010). This contrasts with observations of northern Ellesmere's ice shelves where mass gains are greatest at the front of the ice shelf and ablation dominates with distance from the coast. This pattern, termed a '*reversed'* mass balance gradient, is evidenced by the development of many large epishelf lakes at the rear of the Ward Hunt, Ayles, Milne, and Peterson Ice Shelves.

2.1.3 Ellesmere Island ice shelf types

Globally, ice shelves are classified according to processes of formation and ice type (Vaughan 1998). The three principal ice shelf types on northern Ellesmere Island are: *sea-ice ice shelves* composed primarily of marine ice (e.g. Ward Hunt Ice Shelf), *glacier ice shelves* made up primarily of meteoric ice (e.g. Milne Ice Shelf), and *composite ice shelves* made up of a mixture of both meteoric and marine ice (e.g. Serson Ice shelf) (Jeffries 2002; Mueller et al. 2003; Mueller et al. 2006; Jeffries 2011) (Figure 1.6). *Marine ice* (also referred to as basement ice by Marshall 1960 and Lyons et al. 1971) originates from the

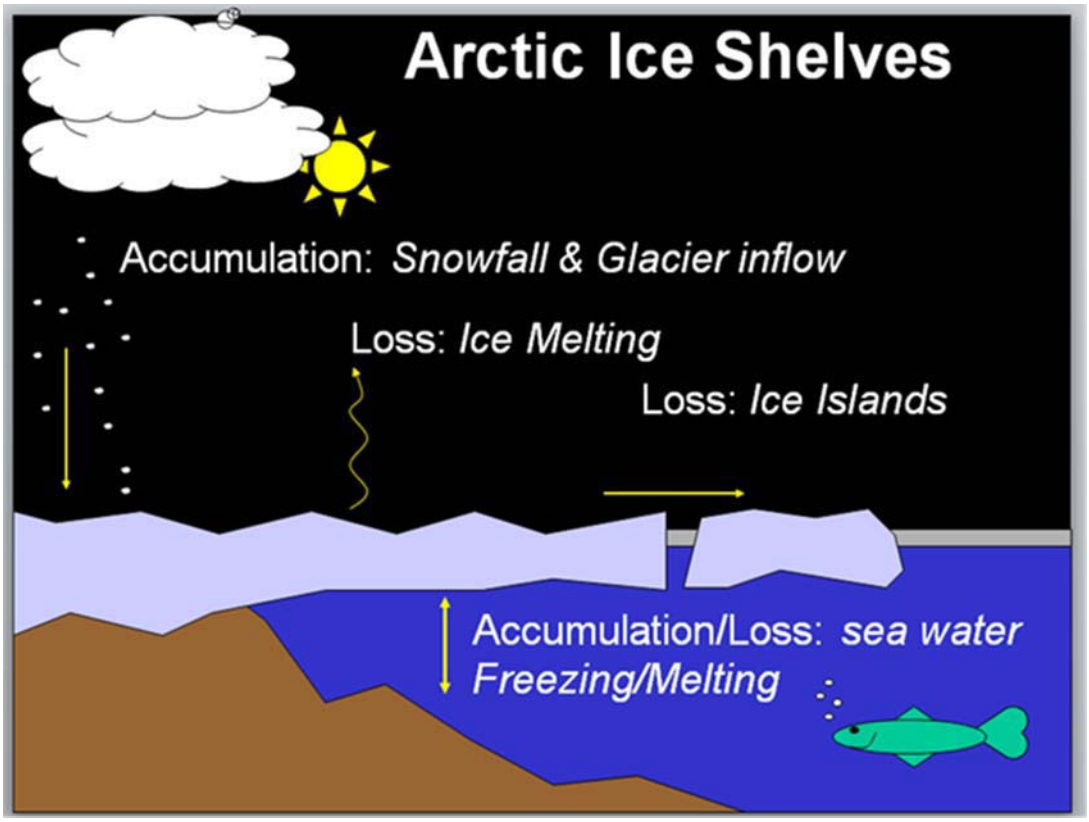

Figure 2.2: Dominant sources of accumulation (mass gains) and ablation (mass losses) for arctic ice shelves. Image courtesy of D. Mueller.

freezing of sea water and brackish water. It has a higher salinity content and a lower compressive strength than meteoric ice (Jeffries 2002; Mueller et al. 2006; Vincent et al. 2001). *Meteoric ice* includes iced-firn, superimposed ice, surface precipitation, and lake ice (both young ponded ice found in troughs and older lake ice found in epishelf lakes). It is formed on land or in situ, and in some cases via basal accretion (Jeffries 2002; Jeffries 2011; Mueller et al. 2006; Vincent et al. 2001). Meteoric ice also includes inputs from glaciers. *Iced-firn* is formed by the meltwater percolation and refreezing of snow and ice and is an important component of Ellesmere Island's composite and meteoric ice shelves.

2.1.4 Ellesmere Island ice shelf surface topography

The surface topography of Ellesmere's ice shelves is characterized by a series of distinctive rolls and troughs which parallel the coast and prevailing wind direction (Figure 2.3) (Hattersley-Smith 1957; Jeffries 1986b). Hattersley-Smith (1957), who provided the first comprehensive study of these features, proposed that they were produced by wind action. He argued for a process similar to that observed on sand dunes, where offshore winds create the initial rolls and troughs which are then perpetuated by meltwater ponds. This theory was used to explain the larger rolls and troughs observed in older ice shelf ice compared to younger multiyear landfast sea ice (MLSI).

Conversely, Crary (1960) suggested that wind action serves to align the randomly distributed rolls and troughs which are produced by surface melt. Rolls are then elongated via a combination of solar heating and convective currents. Holdsworth (1987) later hypothesized that the rolls originated from pack ice pressure where the undulations develop as a result of buckling in the ice and were maintained by the secondary processes related to surface meltwater ponds. Finally, Jeffries (1992a) suggests that the undulating topography is likely due to a series of processes including wind action, solar radiation, convective circulation and gravity flow of meltwater in the summer. In conclusion, although the undulating topography has been debated for decades, its origin and subsequent development remains inconclusive (Crary 1958; Crary 1960; Hattersley-Smith 1957; Holdsworth 1987;

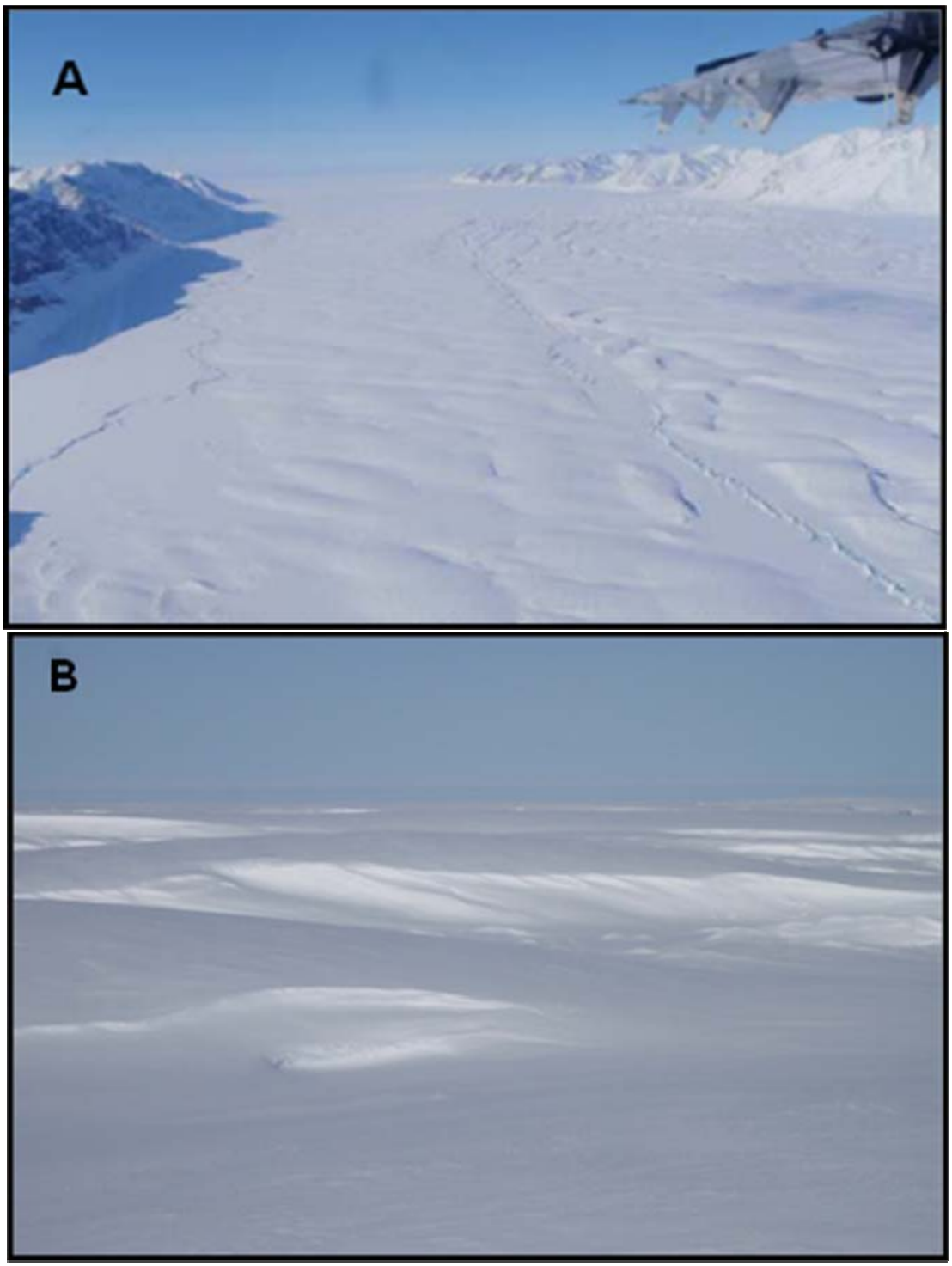

Figure 2.3: Roll and trough topography as seen by air (A) and on the ground (B). Photos: (A) Luke Copland 16 May 2009, (B) Colleen Mortimer 23 May 2009.

Jeffries 1986b; Jeffries 2011). Further, the relationship between surface wavelength (L) and ice thickness (H) has also been investigated (see: Hattersley-Smith 1957; Holdsworth 1987; Jeffries 1992a; Jeffries 2002 and Jeffries 2011), although few consistent patterns have been found.

The annual snowpack on the ice shelves of northern Ellesmere Island is characterized by considerable stratification, including a large depth hoar layer that forms in the winter/spring. An intermediate snow layer, consisting mainly of loose granular snow overlain with fine grained snow, lies beneath a hard wind-slab surface layer with sastrugi (Jeffries 1985; Jeffries and Krouse 1987). The mean annual snow density collected in the region of the ice shelves between Clements Markham Inlet and Nansen Sound from 1982 to 1985 ranged from 0.3 to 0.4 kg m^{-3} (Jeffries and Krouse 1987).

2.2 Ellesmere Island ice shelf formation

The long-term history of Ellesmere Island's sea ice and ice shelves has previously been reconstructed via a combination of proxy methods including investigations of organic material, geomorphological evidence and ice cores (Dyke et al. 1997; Bradley 1990; Lemmen and England 1992; England et al. 2008; England et al. 2011). England et al. (2008) used radiocarbon dating of 69 driftwood samples collected inland of the Ward Hunt Ice Shelf to determine that it began to form ~5500 yrs. B.P., but that permanent ice cover wasn't established in Markham Inlet until ~3500 yrs. B.P. Driftwood, which has been found on raised beaches on land behind the ice shelves, is believed to have been transported in sea ice to northern Ellesmere from continental Russia by the Transpolar Drift (Bradley 1990; Dyke et al. 1997; Lemmen and England 1992). Ice shelves and MLSI fill fiords and embayments blocking the land from driftwood deposition. The presence and absence of driftwood therefore serves as a proxy for the presence of ice shelves along the coast of Ellesmere Island. Crary (1960) also estimated a mid-Holocene formation of the Northern Ellesmere Ice Shelf (~4400 yrs. B.P.), inferred from the location of tidal cracks as well as the location and

age of a sediment layer on ice island T3 (Bradley 1990; Crary 1960). Milne Fiord was likely covered by landfast sea ice ~4200 – 4100 B.P. which was later replaced by glacier tongues (Jeffries 1986b). These estimates for ice shelf formation are supported by ice core analysis from the Meighen Ice cap where regrowth began ~3000-4500 yrs. B.P. (Koerner and Patterson 1974).

2.2.1 Ice shelf-sea ice interactions

The presence and absence of sea ice was an important factor in the formation and continued growth and thickening of northern Ellesmere's ice shelves. The continued existence of these ice shelves is contingent on the presence of a thick, stable sea ice pack and the development of old multiyear landfast sea ice (MLSI). When sea ice is pushed up against the MLSI fringe, it physically holds the ice shelves in place and acts as a barrier to protect them from oceanic influences and prevents direct collisions with the mobile pack ice (Alt et al. 2006; Copland et al. 2007; Kwok and Cunningham 2010). The removal of old MLSI has been observed during periods of low sea ice conditions, warmer air and ocean temperature and high offshore winds (Alt et al. 2006; Jeffries 2002; Pope et al. 2011). In turn, the removal of the MLSI has been associated with ice shelf break-up (Reeh et al. 2001). For example, removal of MLSI from the front of the Ayles Ice Shelf in August 2005 exposed the ice shelf to unusually high winds which lead to the 13 August 2005 breakup event (Copland et al. 2007).

2.3 Historical research conducted on northern Ellesmere Island ice shelves

2.3.1 Early expeditions: late 1800s to early 1900s

The 1875 – 1876 British Arctic Expedition led by Lt. Pelham Aldrich (Royal Navy) was the first to identify the existence of an ice fringe along the coast of northern Ellesmere Island (Hattersley-Smith 1969; Koenig et al. 1952; Jeffries 1986; Jeffries 1992). Reports

from sledging parties led by explorers such as Robert Peary (1906, US Navy) and Aldrich identified a continuous 400 - 500 km long ice fringe stretching from Point Moss to Nansen Sound (Jeffries 1987; Jeffries 2002; Vincent et al. 2001). This 8,900 km^2 – 10,000 km^2 ice fringe was later renamed the Ellesmere Island Ice Shelf (Figure 1.5) (Crary 1958; England et al. 2008; Jeffries 1992a; Vincent 2001). Ocean depth soundings taken at the edge of the ice shelf by Ross Marvin during Peary's 1906 expedition have aided in reconstructing the 1906 ice shelf extent between Cape Discovery and Cape Nares (Bushnell 1956; Vincent et al. 2001) (Figures 2.4 and 2.5). Naval reports from Robert S. James, Second Officer on the voyage of the *D.G.S. Arctic* confirmed Aldrich and Peary's land observations of the existence of an Ellesmere Island Ice Shelf fringe (Jeffries 1987). It should be noted that these expeditions coincided with the end of the Little Ice Age (LIA), which may also coincide with the maximum recent extent of the Ellesmere Ice Shelf (England et al. 2008; England 2011).

2.3.2 Ice islands and ice shelves: 1930s - 1960s

2.3.2.1 Ice Islands

By the mid-1900s, the continuous Ellesmere Ice Shelf had been reduced to six small individual ice shelves (Bradley 1990; Copland et al. 2007; Copland 2009; England et al. 2008; Evans and England 1992; Vincent et al. 2001). Much of what is currently known regarding changes to the Ellesmere Island Ice Shelf comes from sightings of ice islands, the first of which were reported by the Russian military in the 1930s. These large tabular icebergs which calve from ice shelves are distinguishable from sea ice floes by their ridged surface, large size and large freeboard above the surrounding ocean (Jeffries 1992a; Koenig et al. 1952). The American military first reported sightings of ice islands in the Beaufort Sea sector of the Arctic Ocean between 1946 and 1950 which included T1 in 1946, and T2 and T3 in 1950 (Cary 1958; Cary 1960; Jeffries 1987; Jeffries 1992a; Jeffries 1992b; Koenig et al. 1952). These findings were made public in November 1950 at the First Alaskan Science

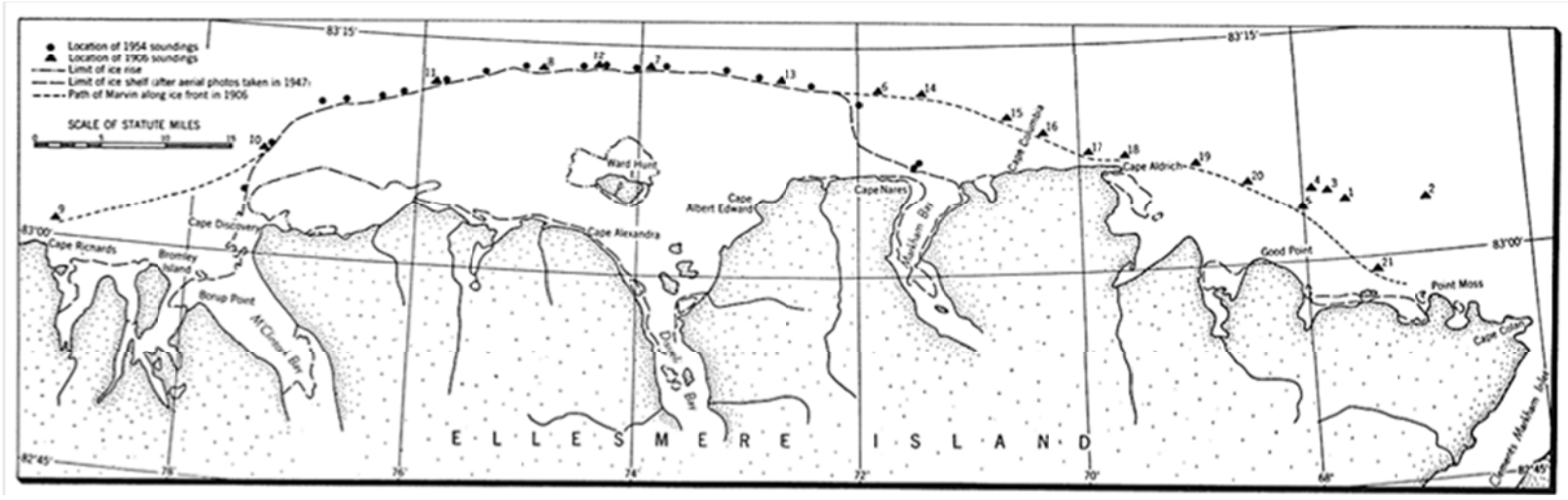

Figure 2.4: Map showing location of Marvin's 1906 ocean depth soundings and Hattersley-Smith's (1954) soundings between Cape Richards and Moss Point, Ocean depth soundings taken at edge of ice fringe are used to reconstruct 1906 ice shelf extent (dashed line). Image adapted from Bushnell (1969).

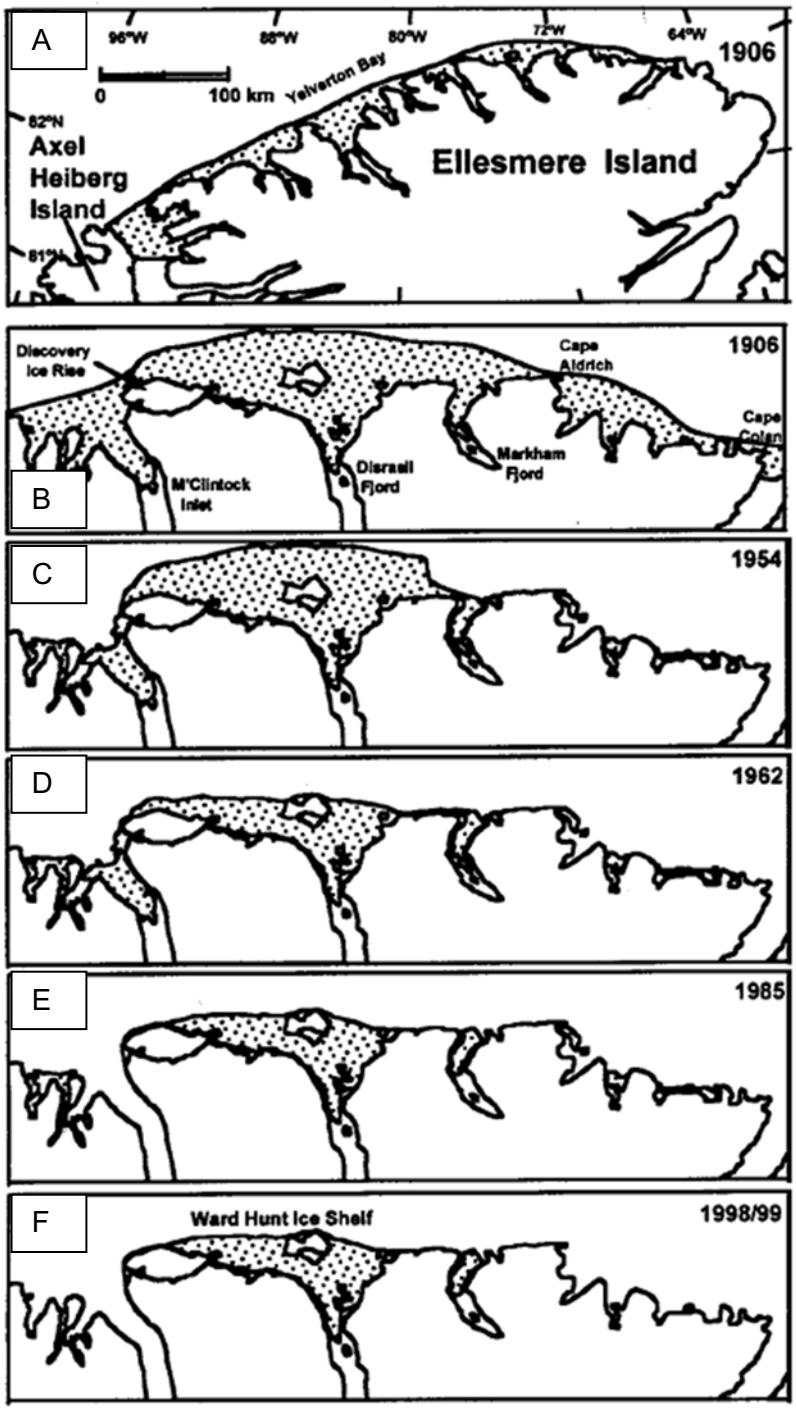

Figure 2.5: A) Ellesmere Island Ice Shelf extent in 1906 reconstructed by Vincent et al. (2001). B-F) Changes in the sector surveyed my Marvin (Figure 2.4) in 1906. Stipple indicates thick, landfast sea ice. Estimates were made using a combination of maps, air photos, and other images. The 1998/99 extent was estimated from RADARSAT-1 imagery Vincent et al. (2001).

Table 2.1: List of all major ice islands previously tracked in the Canadian High Arctic Source: VanWychen and Copland (2011).

Name	Origin	Year of calving	Year of breakup	Location of breakup	Tracking Method(s)	Duration (years)	Size	Refs
T-1	Ellesmere Island	1946+	1971	N coast Ellef Ringnes Island	Aerial photos, ice atlases	Approx. 25	~27x33 km	1,5
T-2	Ellesmere Island	1950+	1951	Atlantic Ocean	Aerial photos, ice atlases	Unknown	~31x33 km	1,9, 10
T-3 /Fletcher's	Ellesmere Island	1935	1984	Southern tip of Greenland	Aerial photos, research station, ice atlases	Approx. 40	~8x16.5 km	1,2, 11
ARLIS-II	Serson (Alfred Ernest) Ice Shelf	1955	1964	Exited into Greenland Sea	Aerial photos, research station, inferences from other ice islands	9	2.4x5.6 km	2,3
WH-1	Ward Hunt Ice Shelf	1961-1962	1968	NW coast Banks Island	Ice atlases, aerial reconnaissance	At least 3	73.5 km^2	1,2,5
WH-2	Ward Hunt Ice Shelf	1961-1962	1968*	N. Meighen Island	Ice atlases, aerial reconnaissance	At least 4	68 km^2	1,2,5
WH-3 /NP-19	Ward Hunt Ice Shelf	1961-1962	1966*	W coast Prince Patrick Island	Ice atlases, aerial reconnaissance	At least 3	8x14 km	1,25
WH-4	Ward Hunt Ice Shelf	1961-1962	1966*	W coast Prince Patrick Island	Ice Atlases, aerial reconnaissance	At least 3	93 km^2	1,2,5
WH-5	Ward Hunt Ice Shelf	1961-1962	1966	Grand Banks, Newfound-land	Aerial reconnaissance, tracking buoys, ice atlases	Approx. 4	~20x9 km	1,2,6
Hobson's Choice /Ice Island 3831	Ward Hunt Ice Shelf	1983	1992	Queens Channel	Satellite observations, tracking buoys, research station	Approx. 9	~10x5 km	2,4,10
Ayles Ice Island	Ayles Ice Shelf	August 2005	-	-	Tracking buoys, satellite observations, ice atlases	-	~15x6 km (66.4 km^2)	8

+ Year of first observation, but calving date is unknown * Year of last observation, but breakup date is unknown

References: 1 = Lindsay (1975, 1977, 1981); Lindsay et al. (1968) 2 = Jeffries (1992a); 3 = Jeffries (1992b); 4 = Jeffries and Shaw (1993); 5 = Crary (1958); 6 = Nutt (1966); 7 = Hattersley-Smith (1963); 8 = Copland et al. (2007); 9 = Koenig et al. (1952); 10 = Yan (1986); 11= Wadhams (2000)

Conference, spawning extensive research programs over the next 35 years from both the Canadian and American military (Table 2.1) (Jeffries 1992a; Koenig et al. 1952).

Ice islands were of military and scientific importance due to their ability to be used as semi-permanent floating bases (Jeffries and Sackinger 1990; Sackinger et al. 1991). Researchers such as Koenig et al. (1952) used aerial reconnaissance missions to link the rolling topography of the ice islands to their source – the ice shelves of northern Ellesmere Island (Jeffries 1992a). Early investigations incorporated low-level flying, landings, and ground measurements (Crary 1958; Crary 1960; Hattersley-Smith et al. 1969; Jeffries 1992a). The first reported landing on T3 (Figure 2.6), which would serve as a research base for the U.S.A.F. from 1952 – 1970, occurred in March 1952 as part of the U.S.A.F.'s Project ICICLE (Cary 1958; Hattersley-Smith et al. 1955; Vincent et al. 2001). The first Canadian expedition to T3 was led by Hattersley-Smith in 1953 (Hattersley-Smith et al. 1955). Analysis of trimetregon air photographs taken in 1949 and 1950 combined with observations from icebreakers identified several more ice islands during the 1950s (Crary 1958; Crary 1960; Hattersley-Smith et al. 1969; Jeffries 1992a). Jeffries (1992b) used surface geology, ridging, and air photographs to trace the origins of ice island ARLIS-II to the Serson Ice Shelf (1955 calving of 2.4 x 5.6 km). Although the majority of ice shelf area loss occurred during the first half of the 20th century, ice shelf disintegration continued throughout the 1960s including the calving of ~600 km^2 from the Ward Hunt Ice Shelf between 1961 and 1962. This constituted the largest known collection of ice islands (WH1 – WH5) in recent history (Jeffries 1992a). Developments in satellite technology aided in the identification of ice islands during the 1980s, including Hobson's Choice (~40 km^2) which calved from the Ward Hunt Ice Shelf sometime between 1982 and 1983 (Figure 2.6) (Jeffries 1992a).

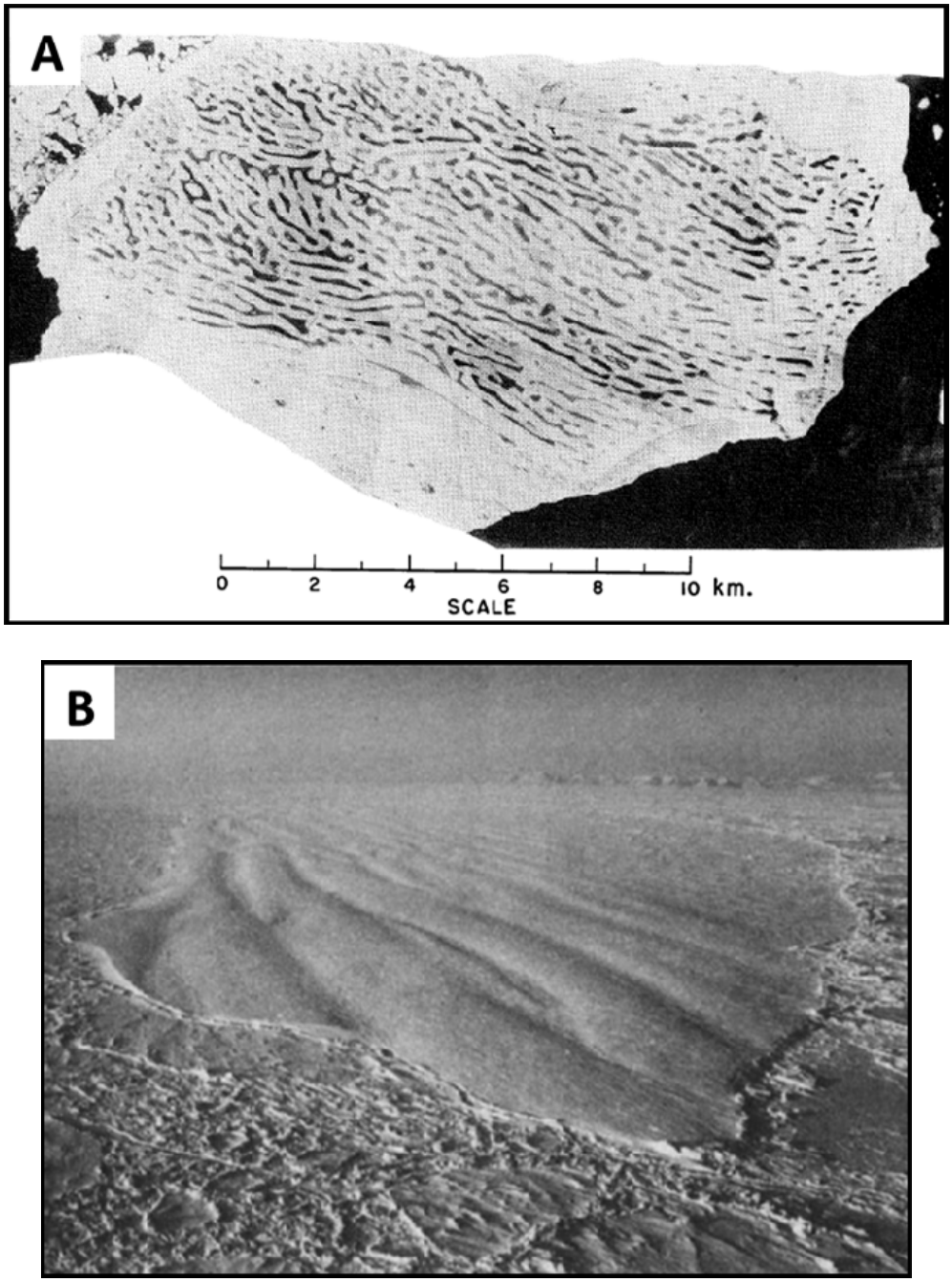

Figure 2.6: Ice islands from air photo imagery. A) T-3 Ice Island (1952) air photo mosaic created by the U.S. Air Force, adapted from Crary (1958). B) Aerial oblique photograph of Hobson's Choice Ice Island off the north coast of Ellesmere Island in April 1985, ~9 km long and 6 km wide (Jeffries and Sackinger, 1990). Source: Jeffries (1992a).

2.3.2.2 Ice shelves

The early research conducted on arctic ice islands paved the way for scientific expeditions to Ellesmere's ice shelves, the first of which was conducted by Hattersley-Smith on the Ward Hunt in 1954 (Crary 1958; Hattersley-Smith et al. 1955; Jeffries 1992a). Research was mainly descriptive in nature, outlining the physical characteristics and morphology of the ice shelves. Investigations also included shallow cores, deep drilling, analysis of internal and shallow ice temperatures and tidal levels (Cary 1958; Hattersley-Smith et al. 1955). In addition to land-based measurements, the first airborne radio-echo sounding (RES) surveys to determine the thickness of Ellesmere Island's ice caps, glaciers, and ice shelves were conducted in April 1966 by the U.K. Scott Polar Research Institute (Evans and Robin 1966; Hattersley-Smith 1969; Hattersley-Smith et al. 1969). Efforts to develop topographic maps of Canada resulted in complete air photo coverage of the ice shelves for 1959. Together, these early scientific expeditions laid the foundations for future research projects on Ellesmere's ice shelves, the majority of which were conducted on the Ward Hunt Ice Shelf (see: Koenig et al. 1952; Hattersley-Smith et al. 1955; Hattersley-Smith and Serson 1970; Serson 1979; Jeffries et al. 1986b). Research on the Ward Hunt Ice Shelf included investigations and modeling of the importance of ice rises for ice shelf stability (Sanderson 1979), significant mass balance programs and the aforementioned ice thickness measurements (Braun 2011; Jeffries 1986b; Serson 1979).

Increased oil exploration and development in the Beaufort Sea and off the North Slope of Alaska during the 1970s and 1980s renewed interest in the northern Ellesmere ice shelves. Ice islands pose a particular threat to offshore oil structures and development because of the greater thickness and high material strength of land ice compared to that of sea ice (Jeffries 1986a; Jeffries 1986b; Jeffries 1992a; Prager 1983; VanWychen and Copland 2011). Joint funding from the Defense Research Establishment, the Arctic Institute of North America (AINA), and various oil companies including Shell and Petro Canada led to the establishment of concerted field research programs during the 1980s on the Ellesmere Island ice shelves. The aim of these projects was to better understand and map ice island

drift patterns, and to assess the current state (size, stability, dynamics) of the remaining ice shelves. In addition to ice shelf and ice island stability and dynamics, research also included the first isotopic data analysis for the northern coast of Ellesmere Island (1982 -1985; Jeffries and Krouse 1987). This important data set supplements that of Koerner (1979), who analyzed stable isotopes and mass balance for the high arctic (Jeffries and Krouse 1987). The 1980s also saw the first large-scale scientific programs directed at the Milne Ice Shelf, as outlined in the next section.

2.4 Historical research on the Milne Ice Shelf

Compared to other Ellesmere Island ice shelves such as the Ward Hunt Ice Shelf, limited work on the Milne Ice Shelf has been carried out (Narod et al. 1988). Airborne radio-echo sounding profiles were conducted in 1966, but ground observations did not begin until 1982 (Evans and Robin 1966; Hattersley-Smith 1969; Hattersley-Smith et al. 1969; Jeffries 1987; Narod et al. 1988). The limited research conducted on the Milne Ice Shelf, beginning with the 1966 radio-echo sounding surveys, is described below.

2.4.1 Radio-echo sounding: 1966

Radio-echo sounding (RES) surveys of Ellesmere Island were conducted between April 13 and 20, 1966 (Evans and Robin 1966; Hattersley-Smith 1969; Hattersley-Smith et al. 1969). The 35 MHz RES system was custom fitted by H. Serson to a Single Otter aircraft and flown at an altitude of ~300 m above the ice surface (Hattersley-Smith 1969) (Figures 2.7 and 2.8). Navigation was limited to line of sight with the aid of 1959 air photo mosaics (Evans and Robin 1966; Hattersley-Smith 1969), and new airborne reconnaissance photos were taken to aid in interpreting the RES returns. Data was interpreted for ice thickness, bed conditions, and ice temperature distribution (Evans and Robin 1966).

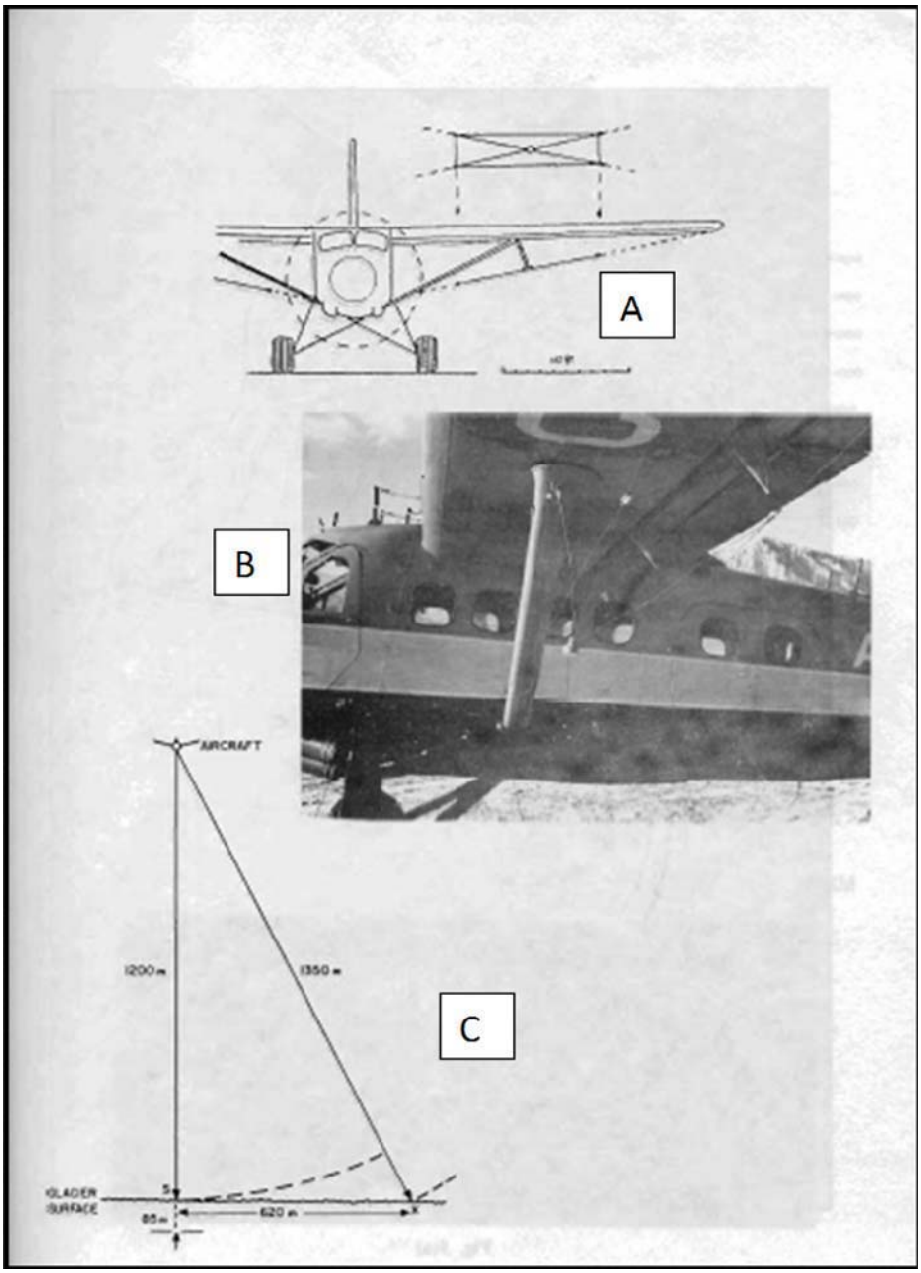

Figure 2.7: A) Radio Echo Sounding system set-up used by Evans and Robin (1966). B) Four-wire 35 MHz RES system custom fitted to a Single Otter aircraft. C) Schematic illustration of nadir and off-nadir sounding used to correct for ice thickness. Source: Hattersley-Smith et al. (1969).

Figure 2.8: A) Map of Northern Ellesmere Island showing location of April 1966 flight lines conducted by Evans and Robin. Red box highlights flight over the Milne Glacier and Milne Ice Shelf shown in part B. B) Milne Glacier flight line map, April 19, 1966. Numbers indicate distance in kilometers, referred to in Figure 2.9. Adapted from Hattersley-Smith et al. (1969).

Radio-echo sounding flights over the Milne Glacier and Milne Ice Shelf were undertaken on April 19th 1966 (Figure 2.8) (Hattersley-Smith et al. 1969). Technical difficulties over the Milne Ice Shelf (camera was not working) resulted in RES returns only being collected over the Milne Glacier. Hattersley-Smith and others (1969) analyzed the RES with the aid of reconnaissance air photos to produce the first depth profile of the Milne Glacier (Figure 2.9). Their results showed a very rough ice surface over the last 3 km of the flight line (where the glacier terminus meets the ice shelf), which they attributed to pressure from the glacier. It was also determined that the Milne Glacier which originates from the Oxford Ice Cap was comprised of three ice streams (southwest, central, northeast). The southeast and northwest ice streams joined the larger central ice stream 10 km and 19 km upglacier from the glacier terminus (Figure 2.10). Ice thickness in the terminus region ranged from ~60 m (Southwest tributary) to ~13 m (Main tributary) (Evans and Robin 1966; Hattersley-Smith 1969 et al.; Hattersley-Smith 1969). Further upglacier, ice thickness increased from ~280 m at a distance of 15 km from the terminus to ~740 m at the grounding line located ~45 km from the terminus (Figures 2.8, 2.9 and 2.10). The glacier is believed to be grounded below sea level and the ELA was estimated at ~1000 m a.s.l. (Hattersley-Smith et al. 1969). Comparisons between 1950/1959 air photographs and reconnaissance photos taken during the 1966 flights showed little change in the glacier terminus position (Hattersley-Smith 1969; Hattersley-Smith et al. 1969; Jeffries 1984; Jeffries 1987).

Differences in bottom echo strength determined from the RES data were used to identify areas of grounded (weak, scattered reflection) and floating ice (smooth, strong reflection) (Evans and Robin 1966; Hattersley-Smith 1969) (Figure 2.11). A significant change in bottom echo strength was observed ~11.5 km upglacier from the terminus (Figure 2.9), corresponding to a change from a floating glacier tongue to grounded glacier ice (Evans and Robin 1966; Hattersley-Smith et al. 1969). Sharp changes in reflection in combination with ice thickness were used to identify marginal lakes between the northeastern tongue and Milne Fiord, as well as an ice-dammed lake (ice thickness ~20 m) between the southwestern and central ice streams (Figure 2.10) (Hattersley-Smith et al. 1969).

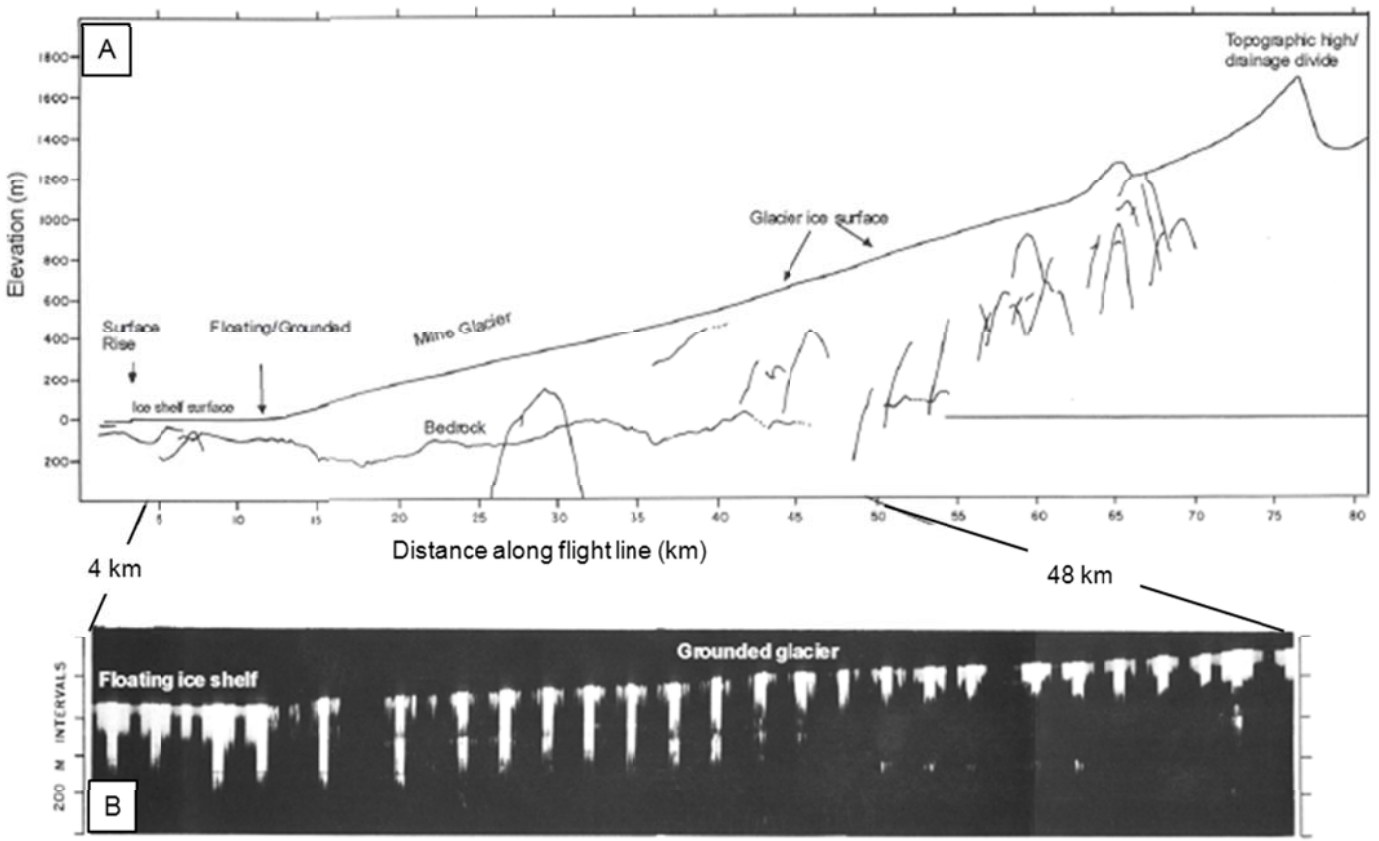

Figure 2.9: A) Depth profile of rear of Milne Ice Shelf and Milne Glacier derived from RES survey conducted April 19, 1966. B) Film print of RES data from April 19, 1966 survey conducted by Evans and Robin, Note: Depth scale (y-axis) in meters may be applied to echo delay times within the ice (vertical propagation assumed) and that the horizontal scale is non-linear between the km marks and the features marked, which correspond to those on the map (Figure 2.8) and profile. Adapted from Hattersley-Smith et al. 1969.

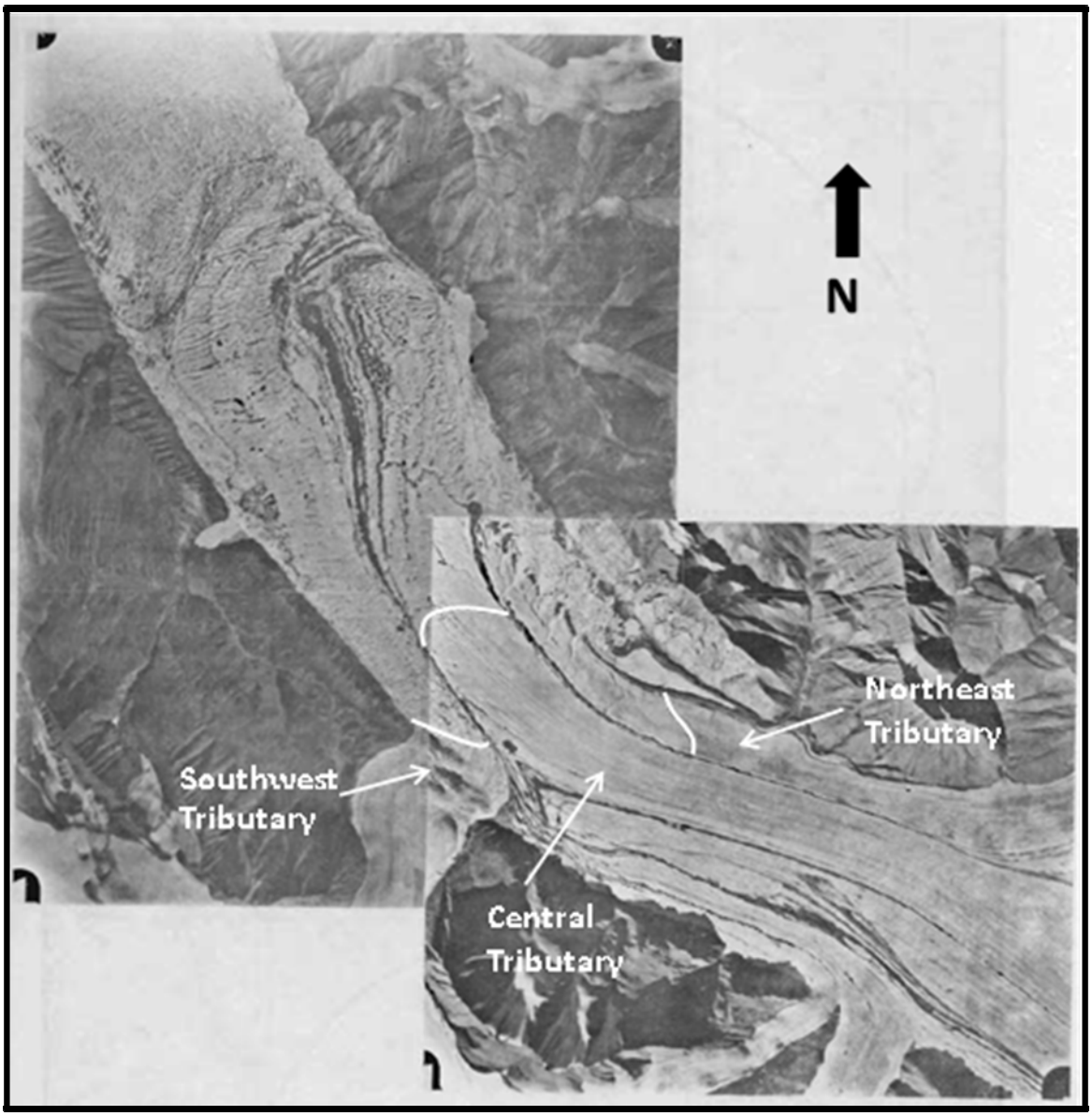

Figure 2.10: 1959 air photo mosaic of confluence of Milne Glacier's tributaries. Solid white curved lines indicate approximate location of the grounding line (adapted from Hattersley-Smith et al. 1969).

2.4.2 Radio-echo sounding: 1981

A second RES survey was conducted in June 1981 by Narod, Clarke, and Prager of the University of British Columbia (Narod and Clarke 1983; Narod et al., 1988; Prager, 1983). This study, whose principal objective was to obtain detailed surveys of both the Ward Hunt and the Milne Ice Shelves, provided valuable information concerning the physical characteristics (particularly ice thickness), of the Milne Ice Shelf. When combined with ground-based observations from Jeffries (1982 – 1985; section 2.4.3), these studies provide a comprehensive overview of state of the Milne Ice Shelf in the early to mid-1980s.

In an attempt to characterize the Milne Fiord ice system, which consists of the Milne Glacier and Milne Ice Shelf, a 100 km long flight was undertaken from the Milne Glaciers' accumulation zone (Oxford Ice Cap) to the ice shelf-sea ice boundary in June 1981 (Figures 2.11, 2.12 and 2.13). Maximum thickness for the Milne Glacier was ~750 m and ~100 m for the Milne Ice Shelf, which is in agreement with ice thicknesses obtained by Evans and Robin (1966) (Narod et al. 1988; Prager 1983) (section 2.4.1). The authors also investigated the characteristic roll and trough topography but found little to no signs of bottom expression in the RES returns (Narod et al. 1988; Prager 1983).

For RES data, the returned power of a signal at the receiver is equal to the transmitted power minus all losses (Prager 1983). As the signal passes through a material the radar wave loses power (Bingham and Siegert 2009; Copland and Sharp 2001; Prager 1983; Woodward and Burke 2007). The ratio of the returned (reflected) power to the incident power (in dB) is referred to as the power reflection coefficient (PRC). For glacier ice, dielectric attenuation and scattering by ice inclusions and roughness are the principle sources of power loss; these variations in PRC can provide insight into changes in ice type for a given region (Bingham and Siegert 2009; Narod and Clarke 1983; Narod et al. 1988; Prager 1983; Woodward and Burke 2007). Narod et al. (1988) used changes in PRC to characterize ice type and to distinguish between areas of floating and grounded ice (Prager 1983), with differences in basal PRC (BPRC) between ice shelves (~0 dB), floating glaciers

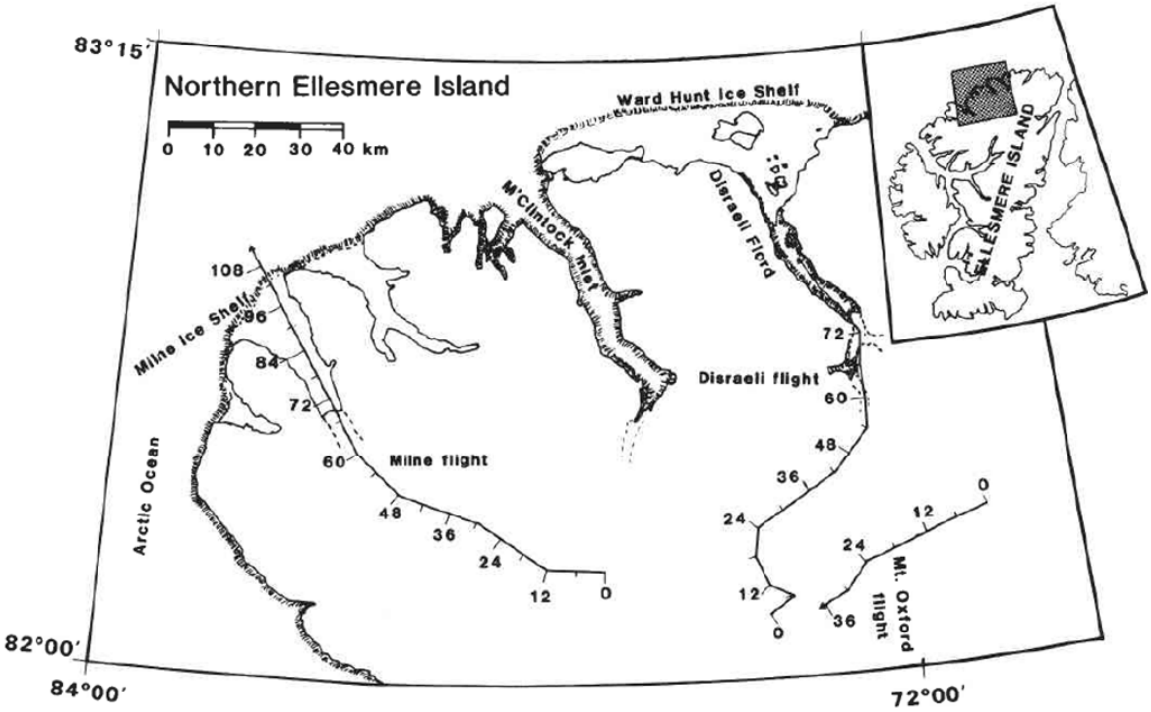

Figure 2.11: Location map showing northern Ellesmere Island and 1981 flight lines covering Mt. Oxford Ice Cap, Disraeli Glacier and Milne Glacier. Numeric annotations on the flight lines indicate travel distances in kilometers. Source: Narod et al. (1988).

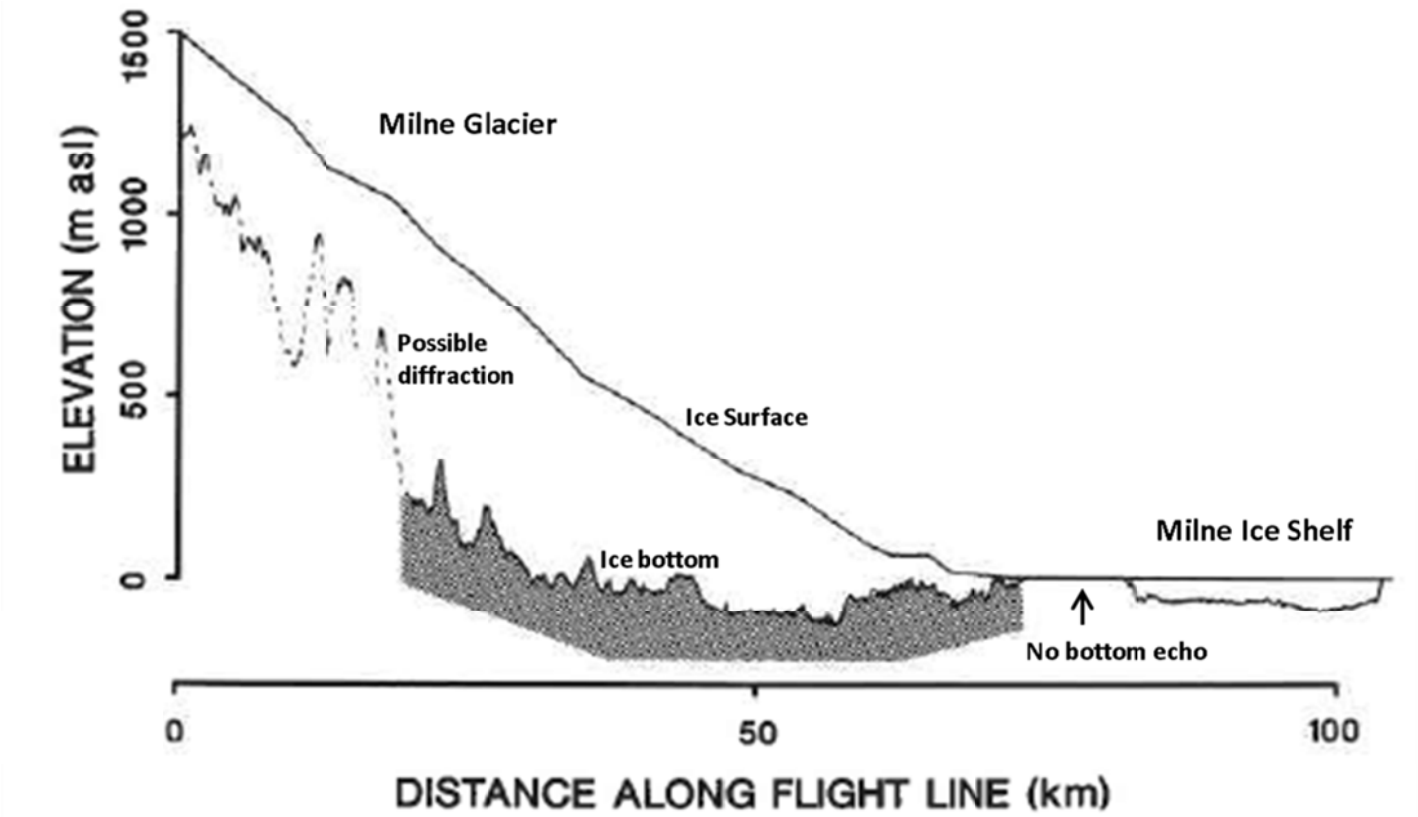

Figure 2.12: Depth profile of the Milne Glacier determined from the 100 km longitudinal flight down the Milne Glacier in April 1981 (Fig. 2.11). The upper and lower lines are ice surface and bottom respectively; dashed lines denote areas where the identified reflections may actually be diffractions. Figure adapted from Narod et al. (1988).

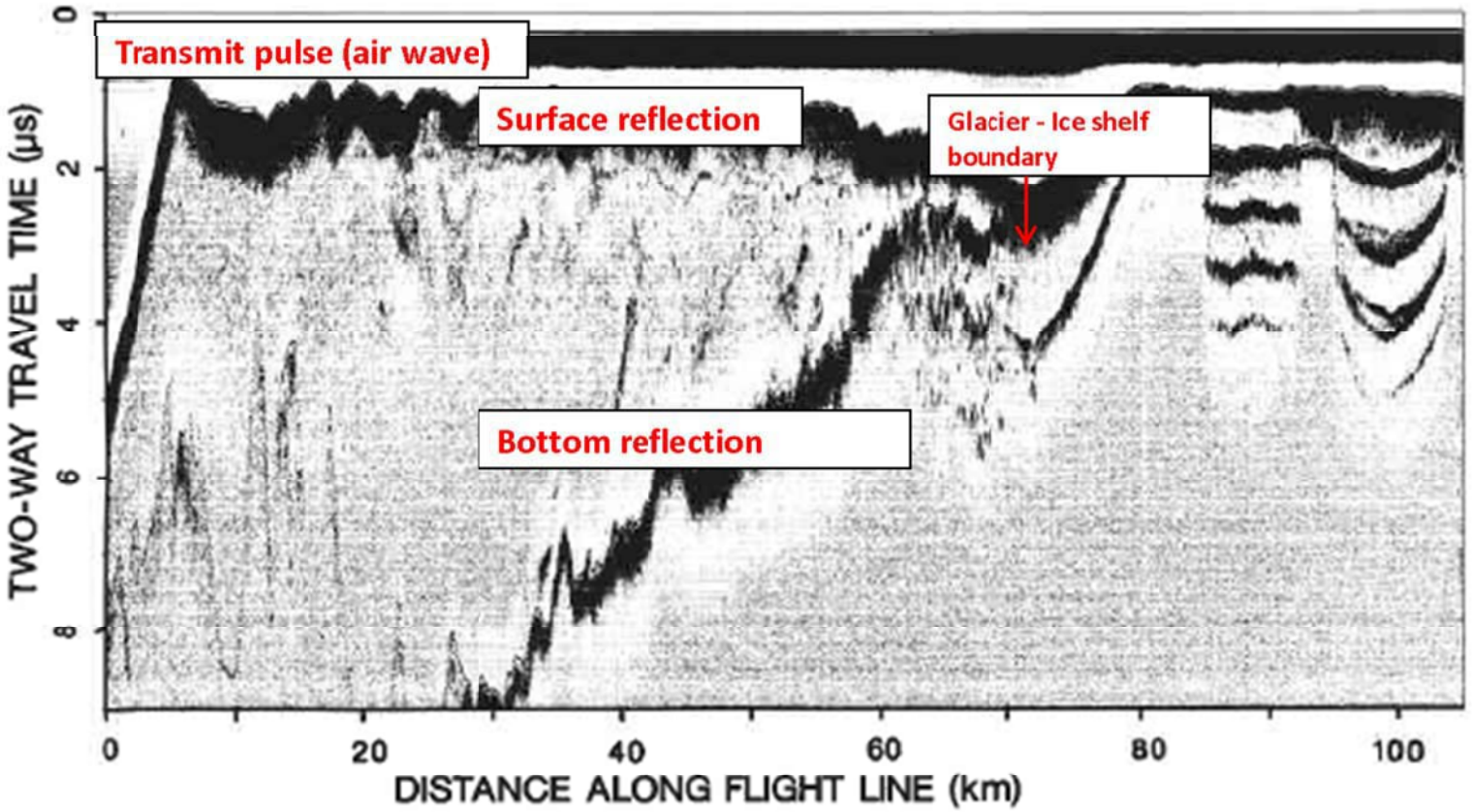

Figure 2.13: Radargram for a 100 km long flight line conducted in April 1981 (Fig. 2.11). RES returns are displayed in unit time (two-way travel time). Image adapted from Narod et al. (1988).

(-5 dB to -15 dB), and grounded ice (-30 dB) (Narod et al. 1988; Prager 1983). A sharp increase in BPRC from -30dB to -5 dB at the 68 km mark of the flight line (Figures 2.12 and 2.13) suggests that the tongue of the Milne Glacier is floating, corroborating the findings of Evans and Robin (1966). In addition to the 100 km reconnaissance flight along the Milne Glacier, detailed flights were conducted over the Milne Ice Shelf in June 1981 (section 3.3.3.4). This survey was the most comprehensive study of the thickness of the Milne Ice Shelf to date and provides an important data source for this study.

2.4.3 Ground observations: Jeffries, 1982 – 1985

In addition to RES surveys, ground observations (1982-1985) and a reconnaissance flight (1984) were undertaken by M.O. Jeffries in the early 1980s. Fieldwork included ice coring, snow sampling, observations of coastal ice conditions, rock sampling, and water profiles of lakes (Jeffries 1986b). The first ice cores (1.00 m – 2.05 m depth) were taken from the Milne Ice Shelf between 23 April and 5 June 1983, with the aim of sampling as many different ice types as possible (Jeffries 1985) (Figure 2.14a). Additional cores were taken in 1984 and 1985; snow pits were dug each summer between 1982 and 1985 (Figure 2.14) and analyzed for salinity and $\delta^{18}O$ to determine variations precipitation, temperature, and salinity.

Although no continuous mass balance studies have been conducted on the Milne Ice Shelf, Jeffries (1986b) used the height of moraines and conical mounds above the ice surface to estimate ablation and make inferences regarding mass balance. Differential ablation means that moraines protect the underlying ice, retarding ablation, while the surrounding ice melts more quickly. Jeffries (1986b) inferred a mean annual surface lowering of 10 cm yr^{-1} over a 100 year period from the height of conical mounds in the Central Unit where the maximum height of a conical debris mound (~10 m) corresponds to 10 m surface lowering. The presence of lichens and other vegetation on the moraines is given as further evidence

that the rocks have been exposed at the surface for a considerable period of time (England et al. 2008; Jeffries 1986b). More importantly, Jeffries (1986b) states that:

> "Although there has been a considerable net loss of ice at the ice shelf surface, it cannot be assumed that there has been an actual reduction in ice thickness; bottom-freezing could compensate for the surface loss, as at the Ward Hunt Ice Shelf (Serson, 1979)."

This statement provides motivation for this research project which aims to determine if any change in thickness has occurred since 1981.

2.5 Milne Ice Shelf Units

Differences in surface topography (rolls and troughs), ice thickness, and ice type have been used to previously classify the Milne Ice Shelf into distinct units. Jeffries (1986b) used changes in surface roll and trough wavelength and orientation to divide the ~290 km^2 ice shelf (as measured by Jeffries in 1986 from 1959 aerial photographs) into Outer (175 km^2), Central (75 km^2), and Inner (60 km^2 in 1959; 40km^2 in 1984) Units (Figure 2.15). Narod et al. (1988) characterized the ice shelf according to ice thickness and basal PRC (Figure 2.16), noting conformity with Jeffries' morphological units. More recently, Mueller et al. (2006) classified the Milne Ice Shelf according to ice type inferred from backscatter in RADARSAT-1 imagery, reconnaissance flights (spring/summer 2001), and near-surface ice samples (spring/summer 2001). They found that 76.7 km^2 consists of glacier ice, 129.2 km^2 iced-firn, >100 km^2 MLSI (Figure 2.17).

This ice type classification system corresponds reasonably well with divisions based on morphology, ice thickness, and bPRC suggesting a relationship between bulk ice properties and ice type (Mueller et al. 2004; Narod et al. 1988). The three morphological units identified by Jeffries (1986b) have since been adopted by several researchers studying the Milne Ice Shelf (Mueller et al. 2006; Narod et al. 1988; Veillette et al. 2008) and are

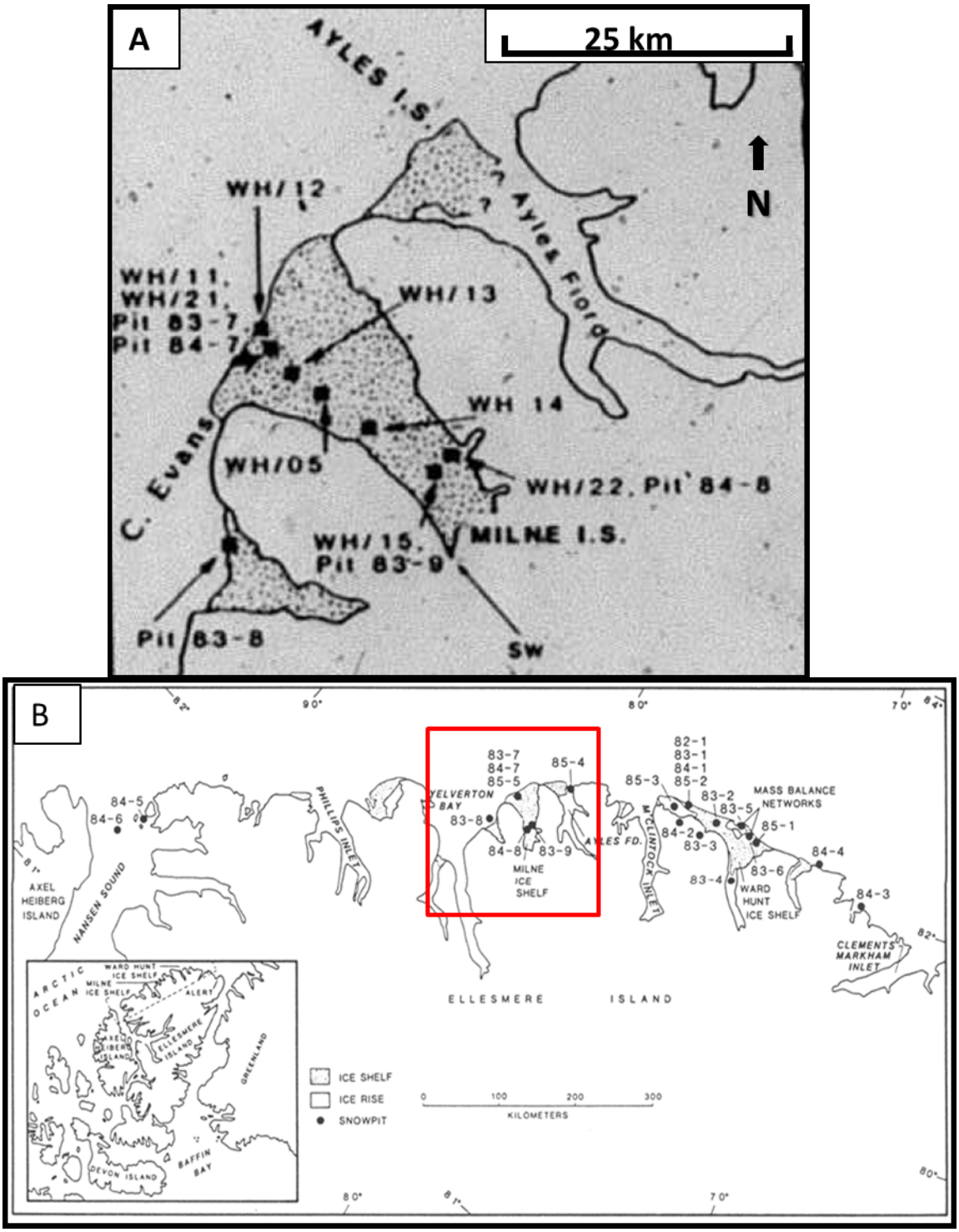

Figure 2.14: (A) Location map of ice cores and snow pits collected from the Petersen and Milne Ice Shelves, northern Ellesmere Island between 1982 and 1984 (Part B, red box). Adapted from Jeffries (1985). (B) Map of north coast of Ellesmere Island showing location of snow pits, ice cores, and mass balance networks between 1982 and 1985. Insert map shows the location of the study area in relation to the Queen Elizabeth Islands. Adapted from Jeffries (1985) and Jeffries and Krouse (1987).

used in this study (Figure 2.18). Because of the wide use of this nomenclature in the literature, each unit is described below.

2.5.1 Outer Unit and Milne Re-entrant area

The Outer Unit extends outward from its border with the Central Unit near Glaciers 1 and 6 where the Milne Fiord starts to widen (Figures 2.15 and 2.18). The front of the outer unit forms the boundary with the Arctic Ocean where a small amount of MLSI is attached to the ice shelf (Figure 2.19). Surface topography is characterized by regularly aligned SW-NE rolls and troughs with steep north-facing slopes that parallel the coast and prevailing wind direction. Mean wavelength is ~350 m and the maximum height difference (amplitude) between rolls and troughs is ~7.5 m (Jeffries 1986b; Jeffries 2002; Jeffries 2011). Meltwater ponds, which appear dark blue in summer ASTER scenes (Figure 2.18), fill the troughs. Analysis of a 1.00 m long ice core (WH/13, Figure 2.14), collected in spring 1983 from a trough in the outer unit, indicated that the meltwater forms during the ablation season and re-freezes in the winter (Jeffries 1985). The snow surface is relatively hard due to strong winds, compaction and weathering and very little debris is found on the surface of this unit (Jeffries 1986b; Jeffries 2002). The near-surface is mostly comprised of iced-firn, particularly near Cape Egerton where the basal PRC determined from 1981 RES sounding (section 2.4.2) is extremely high (> -10 dB) (Mueller et al. 2004; Narod et al. 1988; Prager 1983). The middle section of the Outer Unit has low basal reflectivity (< - 30 dB) which could be the result of brackish, basement ice freezing to the bottom of the ice shelf (Mueller et al. 2004; Narod et al. 1988; Prager 1983).

Important features of the Outer Unit include a re-healed fracture and a re-captured ice island or glacier tongue. Two large re-healed fractures, visible in remotely sensed imagery and RES surveys (Figure 2.18), could be important in the future stability of the ice shelf as indicated by the calving of 33 km^2 of ice in the 1960s where two additional fractures, seen in 1959 air photos, likely acted as lines of weakness. The second feature of

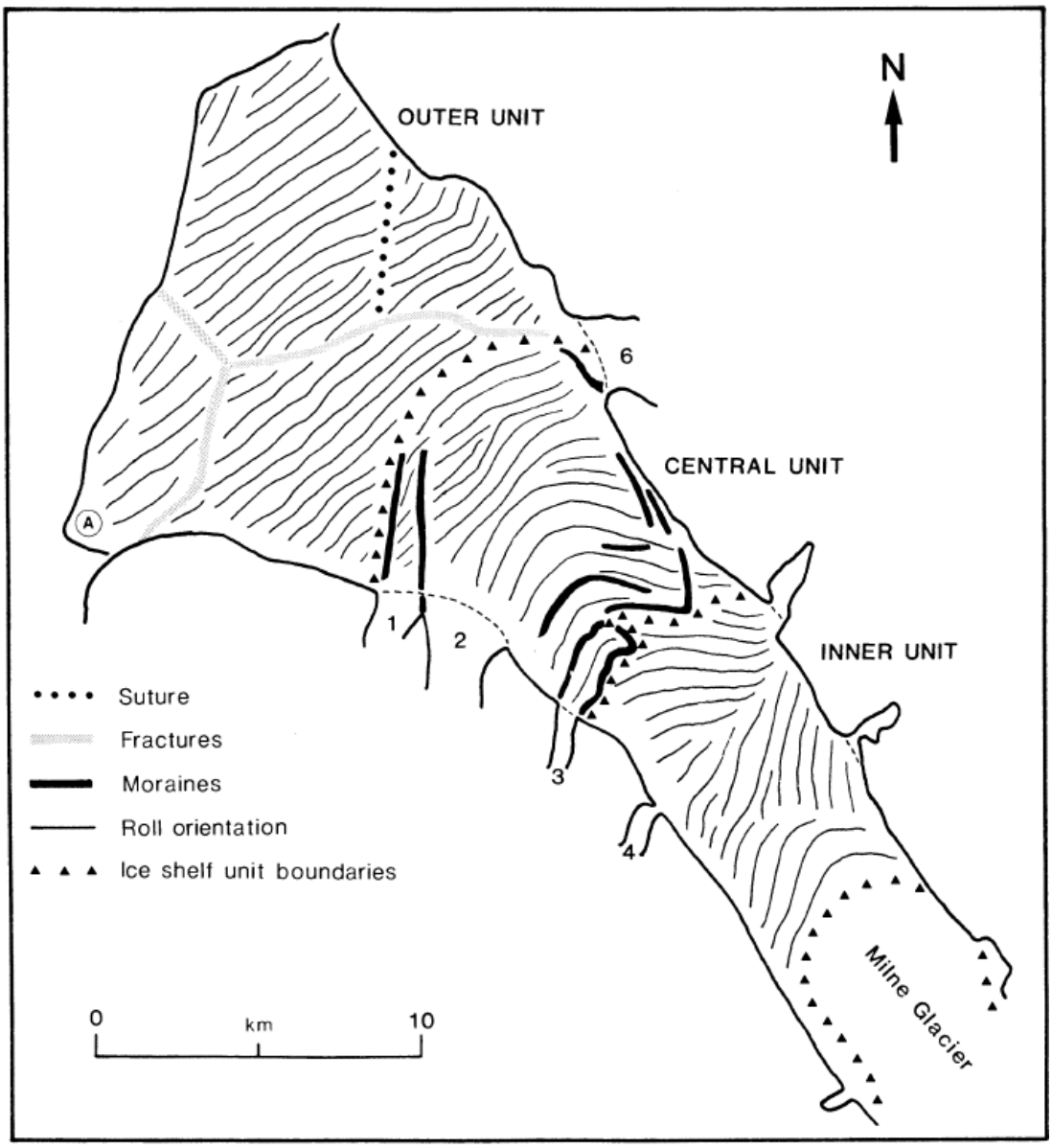

Figure 2.15: Map of the surface features and units of Milne Ice Shelf derived from July 1959 air photos (adapted from Jeffries 1986b). Numbers 1 to 4 and 6 are glaciers marked on Figure 2.18.

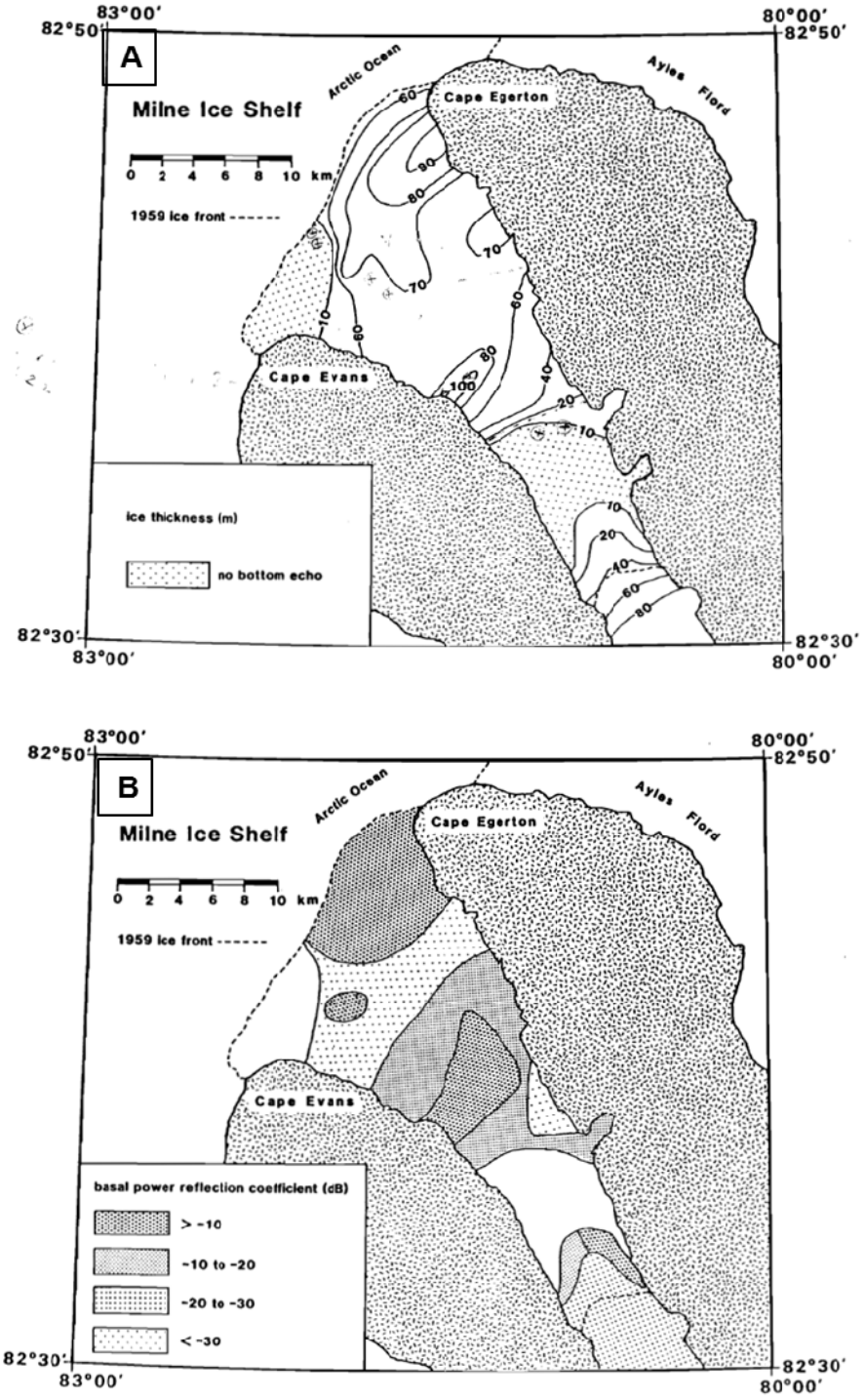

Figure 2.16: (A) Ice shelf ice thickness contour map derived by Prager (1983) from RES survey data from April 1981. (B) Basal PRC interpretation for Milne Ice Shelf derived by Prager (1983) from 1981 radio-echo sounding survey. Brackish ice may be present in regions where basal PRC is less than -30 dB. Source: Prager et al. (1983).

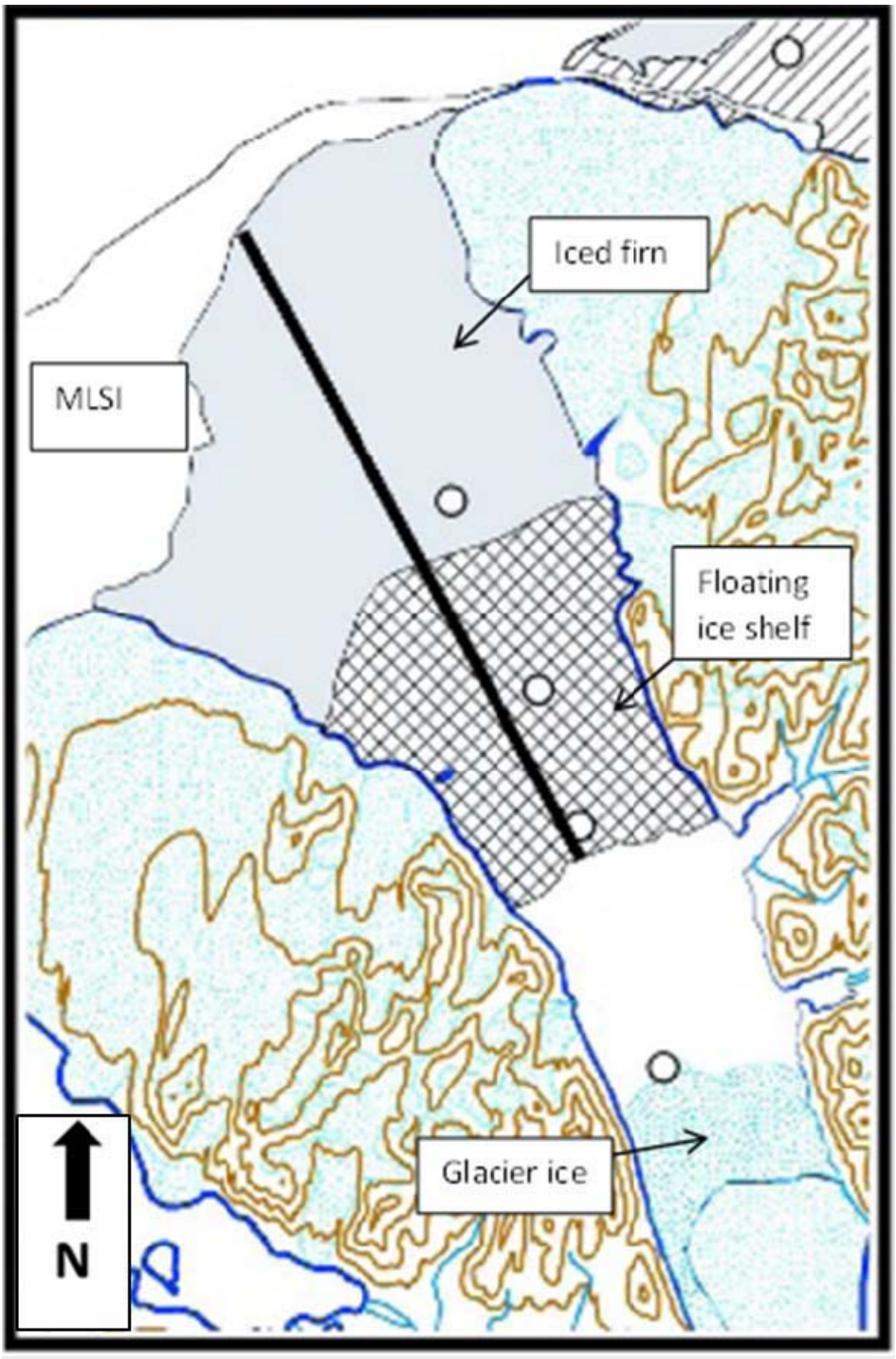

Figure 2.17: Milne Fiord Ice types identified by Mueller et al. (2006). Stipple indicates ice rises and glaciers, a simple hatch indicates exposed basement ice, solid grey indicates iced firn and cross hatch indicates floating glacier portions of ice shelves. Multiyear landfast sea ice (MLSI) is outlined to the seaward side of several ice shelves. Bold, straight lines are the over-flight transects. Sample sites on the ice are denoted by open circles. Adapted from Mueller et al. (2006).

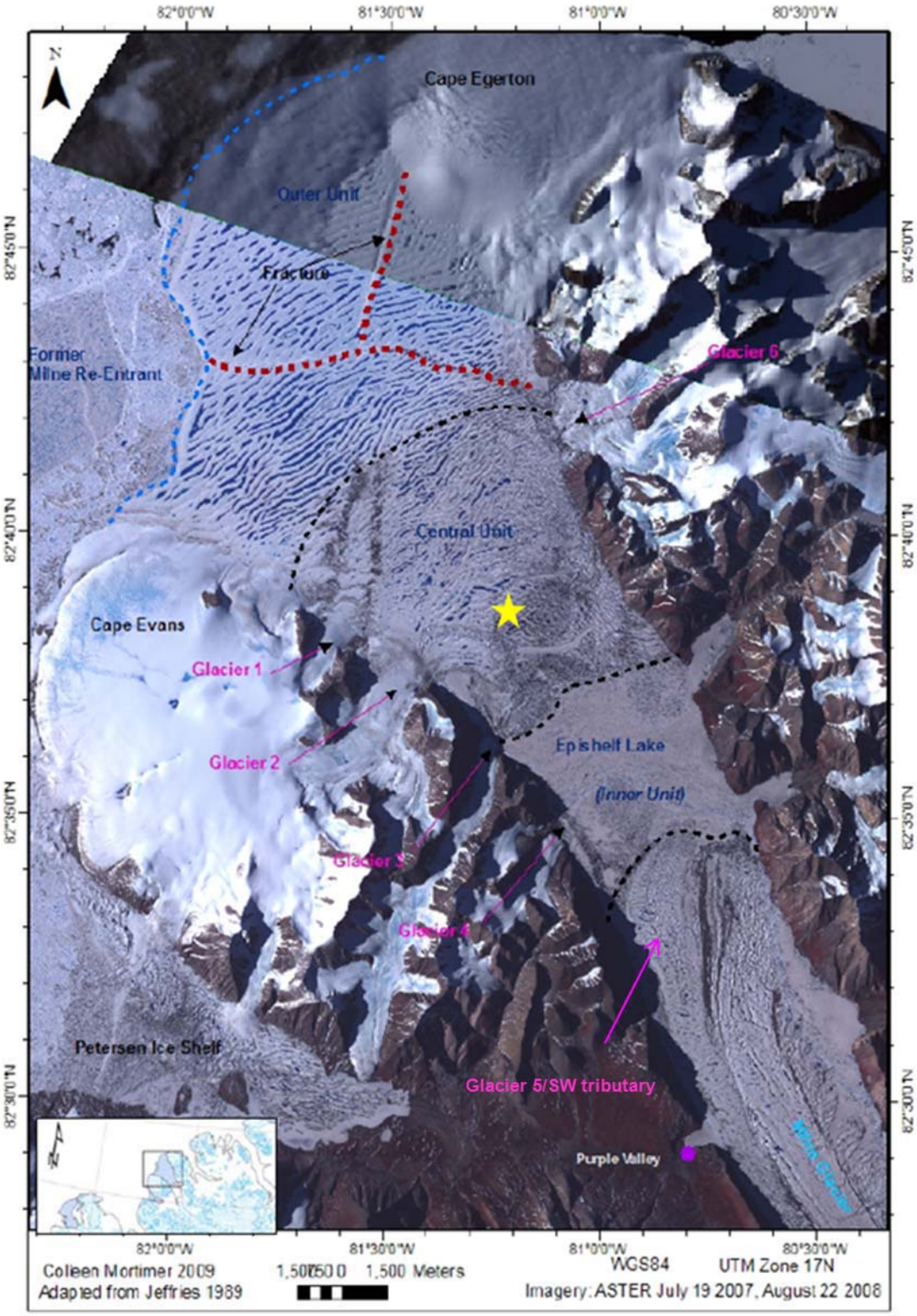

Figure 2.18: Milne Ice Shelf index map used in this study, naming conventions adapted from Jeffries (1986b). Yellow star indicates location of debris field depicted in Figure 2.21.

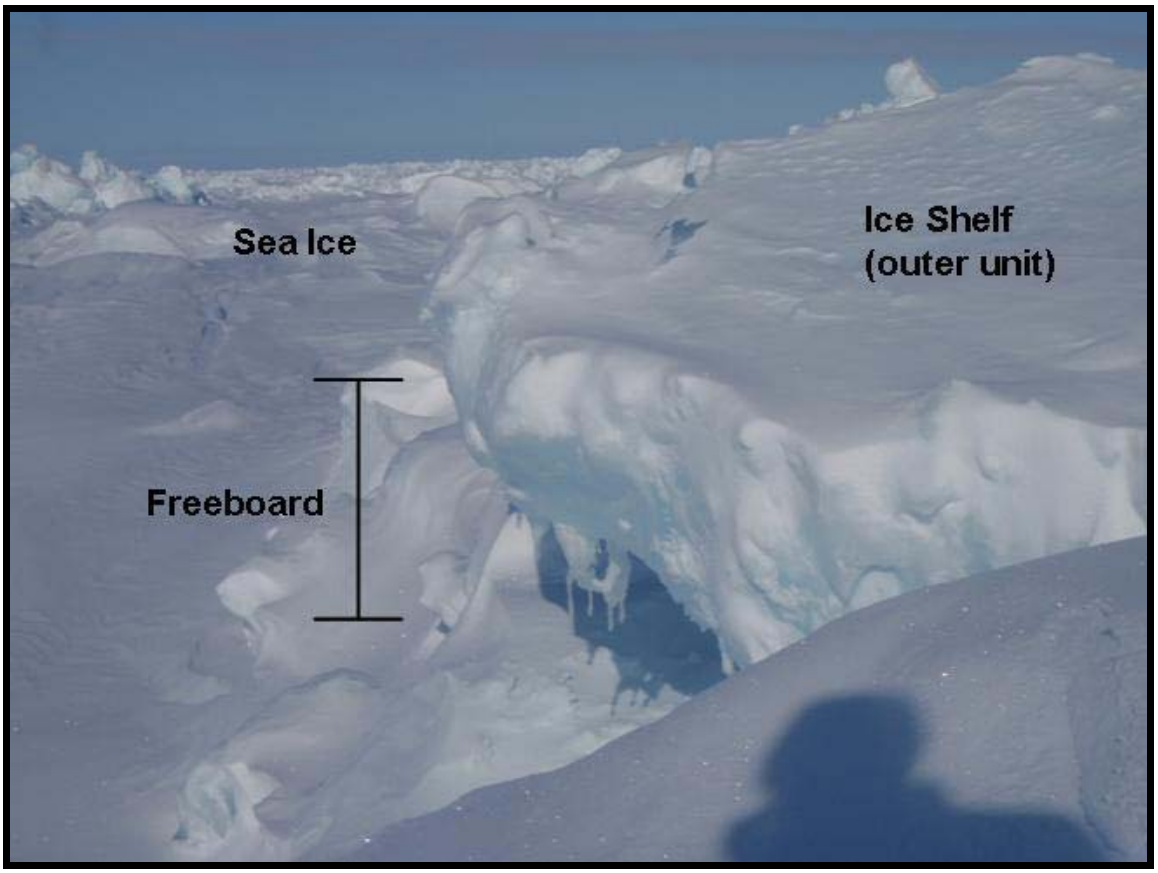

Figure 2.19: Outer edge of Milne Ice Shelf (May 30, 2009). Smooth Ice shelf ice (right hand side is comprised of both land ice and some MLSI. Rough sea ice is pushed up against the ice shelf. Height of freeboard was estimated to be at least 3 m. Photo: Colleen Mortimer.

note is an area of high reflectivity ice (> -10 dB) surrounded by low reflectivity ice in the central-western section of the Outer Unit (Figure 2.16b). Narod et al. (1988) suggest that this could be a re-captured ice island; however, Jeffries (1986b) suggests that it could be a former ice tongue which previously flowed from Cape Evans (Jeffries 1986b). This feature could provide important insight into the Milne Ice Shelf's history and formation.

The Milne Re-entrant area is located in the northwestern section of the Outer Unit near Cape Evans, and consists of old sea ice which fills an area following a calving event. The ice there is brackish and the small surface rolls and troughs (amplitude ~1 m) have a short wavelength (60-100 m). Annual snow depth obtained via snow pit analysis was 0.90 m in 1983 (pit 83-7), 0.50 m in 1984 (pit 84-7), and 0.48 m in 1985 (pit 85-5) (Figure 2.14). In the case of the Milne, MLSI filled the Re-entrant area following the calving of 33 km^2 of ice sometime between 1959 and 1974 (Figure 2.20). Jeffries and Krouse (1987) used the MLSI formation following this event to study the growth and formation of multiyear sea ice. MLSI ice thickness and stable isotope analysis from two ice cores collected in 1985 (9.80 m for a ridge and 7.24 m for a trough) indicated that the Re-entrant ice was ~20 years old, suggesting that ice shelf calving event occurred around 1965 (Jeffries 1986b; Jeffries 1992a; Jeffries and Krouse 1987). Analysis of crystal structure and stable isotopes provided insight regarding the formation of sea-ice ice shelves (section 2.2) from a basement of thick sea ice. Annual layering was observed in both the salinity and $\delta^{18}O$ profiles of ice cores taken from the Milne Re-entrant. Jeffries (1988) attributes the presence of annual layering in the salinity profile to a lack of homogenization caused by rapid brine movement, which could be a result of low temperatures or specific structural properties. The observed linear correlation between salinity and $\delta^{18}O$, together with analysis of ice texture, suggests that the MLSI growth is associated with fresh-water/sea-water stratification below the ice surface.

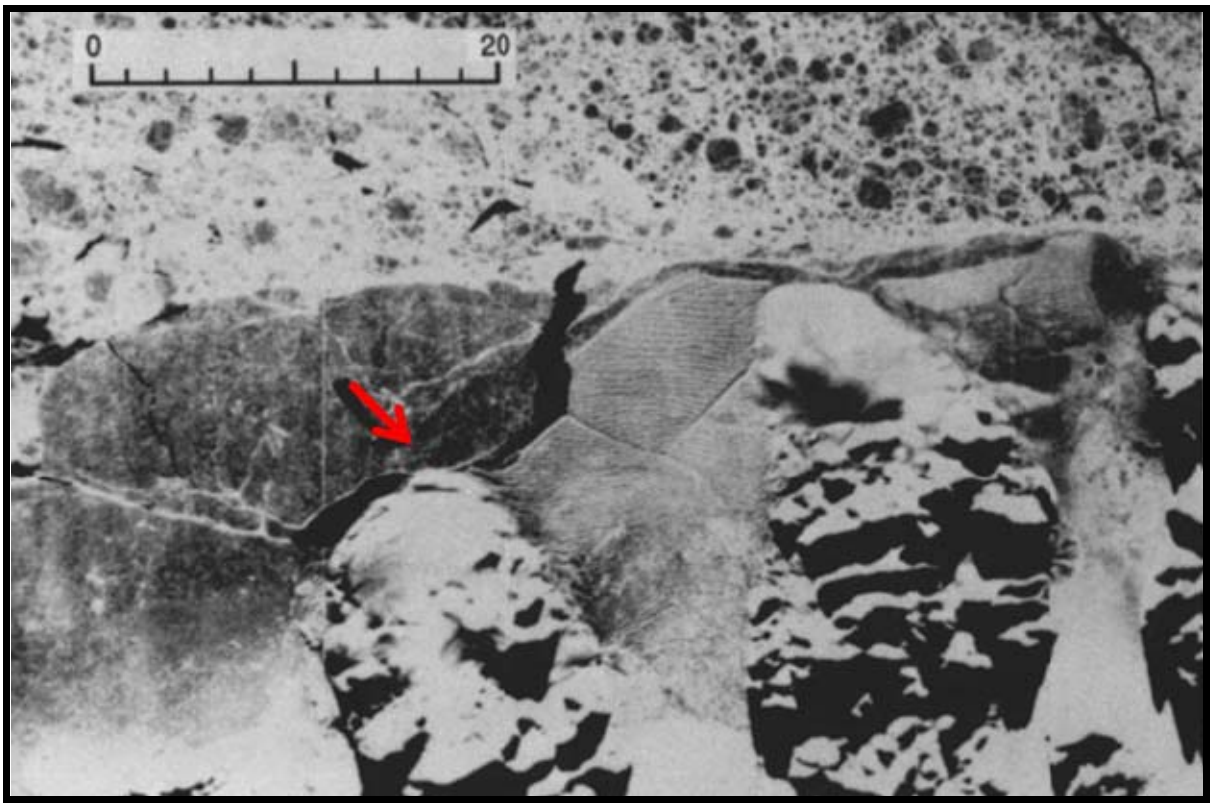

Figure 2.20: Airborne X-band SAR image of the Milne Ice Shelf (center) February 1988. The ribbed texture identifies the undulating ice shelf surface. A large multiyear landfast sea ice floe, the Milne reentrant (arrow), separated from the ice shelf by a roughly S-shaped refrozen lead, has broken off the front of the west side of the Milne Ice Shelf. Image courtesy of the Canarctic Shipping Company Limited. Image adapted from Jeffries (1992a).

2.5.2 Central Unit

The Central Unit is located behind the Outer Unit in an area where the Milne Fiord narrows (Figures 2.15 and 2.18). Current and former tributary glaciers flank the sidewalls; surface topography is characterized by contorted and bifurcating rolls and troughs which become increasingly disorganized with distance from the coast (Figure 2.15). Rolls and troughs in the central unit are steeper (~5 m amplitude) and have a shorter wavelength (~150 m to ~180 m) compared to those in the Outer Unit. Although mean ice thickness is only ~50 m, the thickest ice on the Milne Ice shelf (>90 m) is found in the Central Unit near Glacier 2 (Jeffries 1986b; Narod et al. 1988; Prager 1983). Analysis of a 2.00 m ice core (WH/14, Figure 2.14) collected in spring 1983 from a ridge in the central unit indicated that the ice was of glacial origin (Jeffries 1985). SAR image analysis and near surface sampling in summer 2001 confirmed that much of the Central Unit is comprised of glacier ice (Mueller et al. 2006). Surface debris including large conical mounds (~10 m to 20 m high), stranded ice blocks, contorted moraines, and glacial erratics (Figure 2.21), some of which are found at a considerable distance (~7 km) from the nearest glacier (Jeffries 1986b), provide further evidence of the movement of current and former glacier tongues into Milne Fiord. This extensive debris cover is used by Jeffries (2002) to explain the dark appearance of the central unit in both winter and summer SAR scenes. Finally, the high basal PRC measured in the central unit (>20 dB) is also indicative of glacier ice (Figure 2.16b) (Narod et al. 1988; Prager 1983). These measurements indicate that the composition of the Central Unit is largely influenced by tributary glaciers.

2.5.3 Inner Unit

Behind the Central Unit sits the Milne Epishelf Lake, beyond which is the Milne Glacier (Figures 2.18 and 2.22). The Epishelf Lake was originally referred to as the Inner Unit by Jeffries (1986b) (Figure 2.15) (Jeffries 2002; Mueller et al. 2003). Epishelf lakes are unique cryospheric features formed by the trapping of freshwater from summer melt of snow

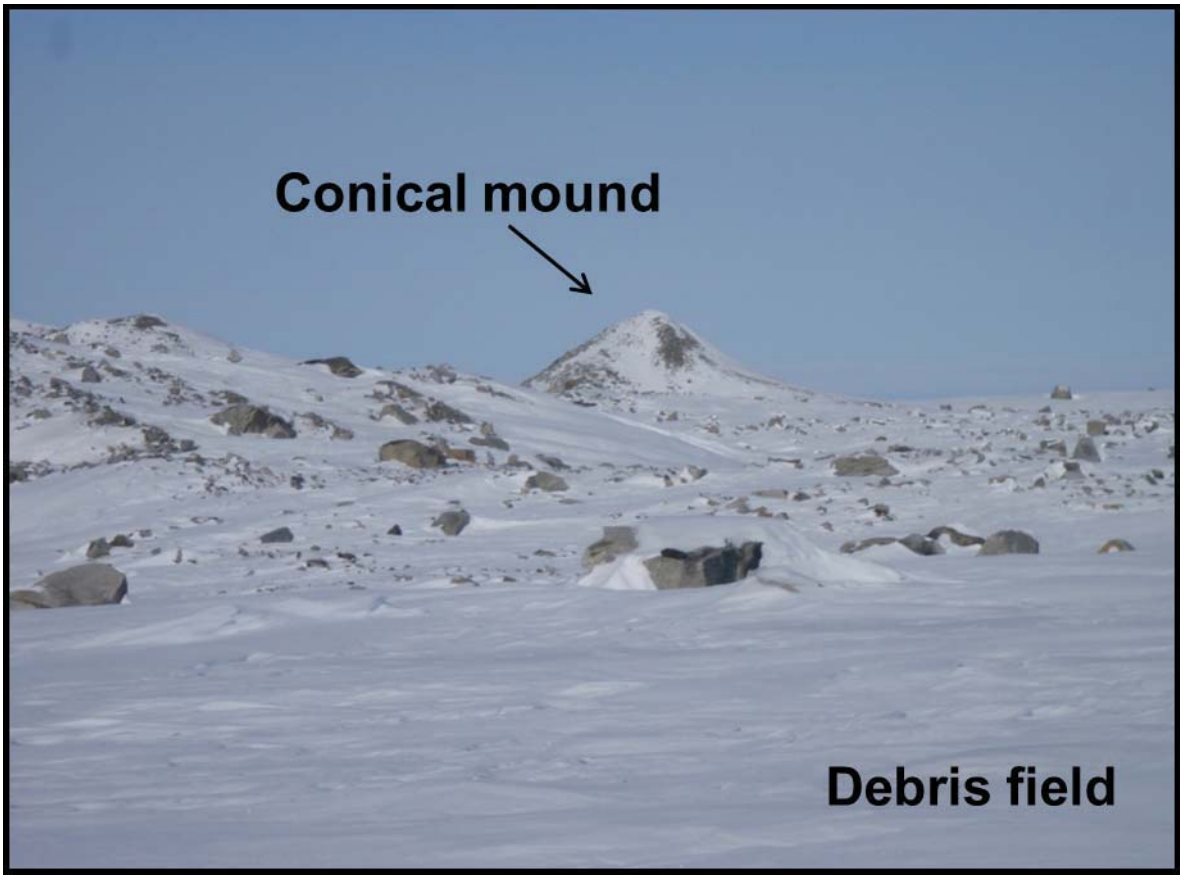

Figure 2.21: Debris field and large conical mound (~15 m high) in central unit (Yellow star, Figure 2.18). May 30 2009. Photo: Colleen Mortimer, May 30, 2009.

and glacier ice behind an ice shelf. The freshwater layer is typically covered by perennial lake ice and isolated from the underlying salt water due to the differences in water density, creating a uniquely stratified water column (Mueller et al. 2003; Mueller et al. 2004; Mueller et al. 2006; Veillette et al. 2008). Epishelf lake development in areas where ice shelves used to exist, together with the formation of ice-marginal lakes, indicates negative mass balance (Copland et al. 2007; Mueller et al. 2003; Mueller et al. 2006; Mueller 2008; Smith et al. 2007; Veillette et al. 2008; Vincent et al. 2001). Epishelf lakes also provide a means of monitoring ice shelf thickness change because hydrostatic inversion allows the depth of the freshwater layer to be used as a proxy for the minimum ice shelf draft thickness (Braun et al. 2004a; Braun 2011; Mueller 2008; Smith et al. 2007; Veillette et al. 2008). The drainage of an epishelf lake is frequently linked with ice shelf collapse (Copland et al. 2007; Mueller 2008). This drainage is visible in SAR scenes by a sudden shift from the characteristic bright white signature from the underlying freshwater layer to a grey tone indicating the presence of saltwater underneath the thin ice cover.

The Milne Epishelf Lake is characterized by a relatively smooth surface with shallow rolls and troughs (amplitude ~1 m) with short wavelength (60-100 m). Annual snow depth was 0.52 m in 1983 (pit 83-9) and 0.54 m in 1984 (pit 84-8) (Figure 2.14) (Jeffries and Krouse 1987). Ice coring in 1984 indicated that the ice is relatively thin (3.19 m), and consisted of *'fiord ice'* (Jeffries 1986b). RES surveys in 1981 showed no bottom echo in this region because the ice was thinner than the minimum 10 m depth that could be measured with the instrument (Figure 2.16a) (Narod et al. 1988; Prager et al. 1983). Density stratification was observed in water profiles collected between 1983 and 2009 (Jeffries and Krouse 1987; Jeffries 2002; Mueller et al. 2003; Veillette et al. 2008) (Figure 2.23).

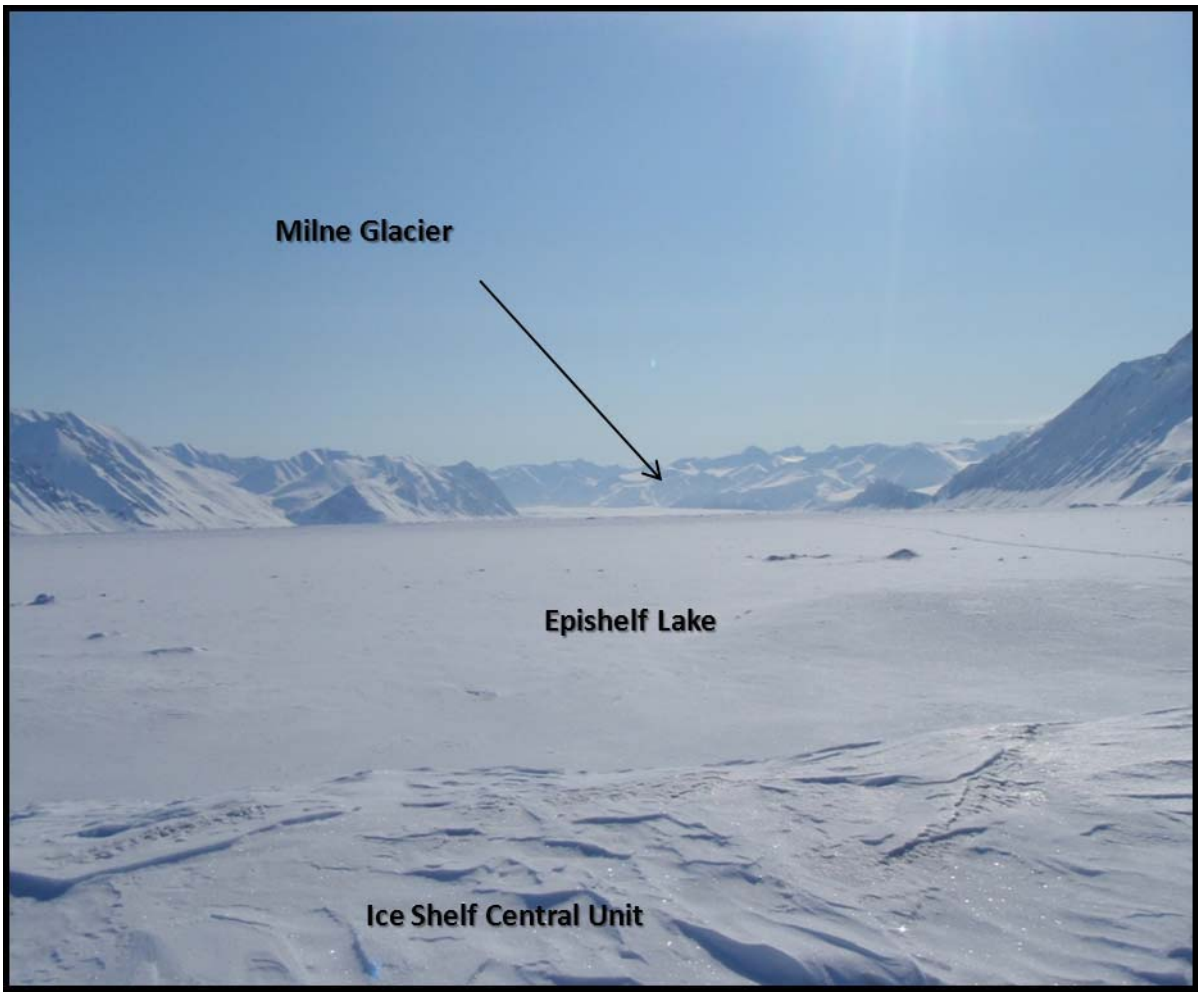

Figure 2.22: View of the Milne Glacier and Milne Epishelf Lake taken from the rear of the Central Unit. Photo: Colleen Mortimer, May 23, 2009.

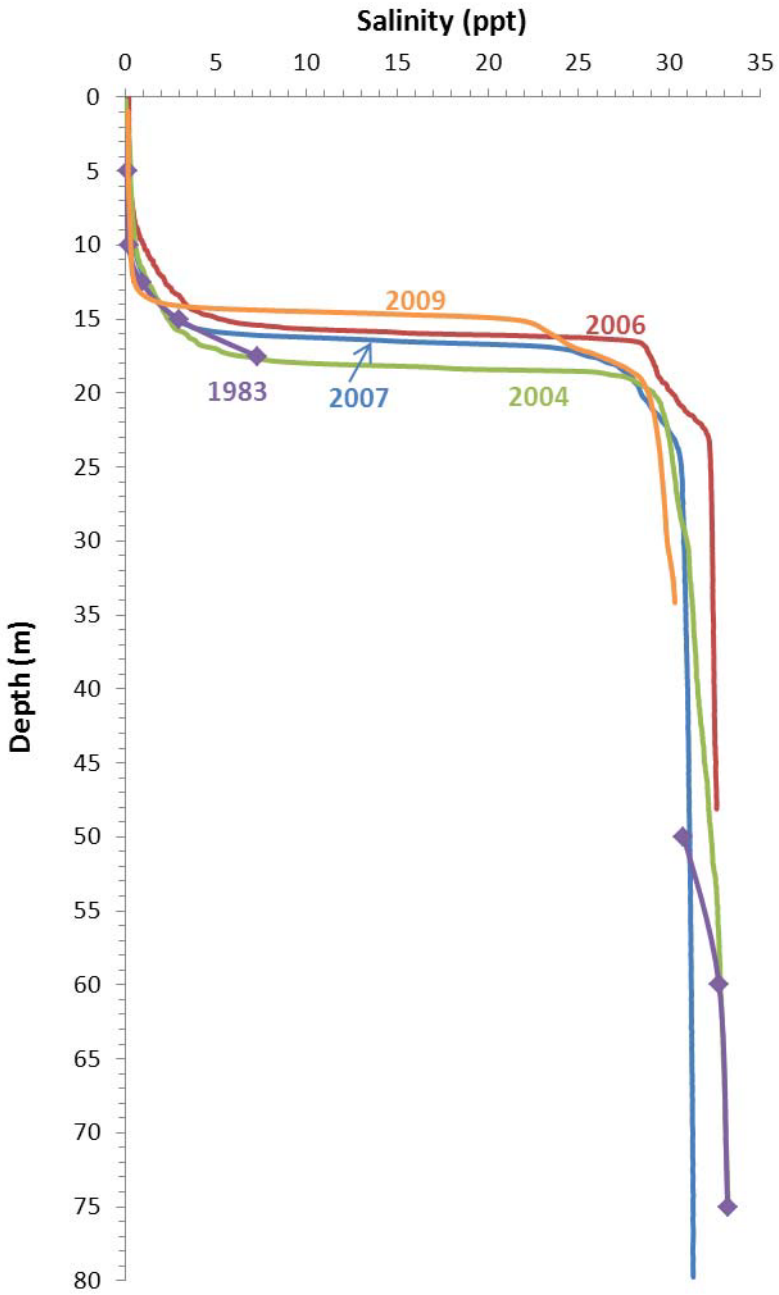

Figure 2.23: Milne Epishelf Lake profiles for 1983 – 2009. Point measurements from 1983 indicated by purple diamonds. Data sources: 1983 obtained from Jeffries (1985); 2004, 2006, 2007 obtained from Veillette et al. (2008); 2009 profile collected during 2009 field campaign (current study).

2.6 Glacier inputs

In addition to mass gains and losses from precipitation, basal accretion, calving and melt, the existence of the Milne Ice Shelf is heavily influenced by its surrounding features, specifically its glacial inputs. Changes in glacial inputs result in a decrease in mass input to the ice shelf, so monitoring the smaller tributary glaciers within Milne Fiord, as well as the larger Milne Glacier, is important when assessing the current stability of the Milne Ice Shelf.

2.6.1 Ice caps and tributaries

Glaciers issuing from small ice caps on the east (elevation ~1067 m a.s.l.) and west (elevation ~ 1219 m a.s.l.) sides of Milne Fiord terminate either on the Milne Ice Shelf or remain as hanging glaciers along the valley walls (Figures 2.18 and 2.24). Jeffries (1986b) named six of these tributaries (Glaciers 1 through 6) (Figures 2.15 and 2.18). In this study, Glacier 5 is considered to be part of the Milne Glacier (SW tributary). Flow from the two large, low-lying ice caps on Cape Evans (west) and Cape Egerton (east) may also provide important land ice to the Milne Ice Shelf (Figure 2.18). As previously discussed (section 2.2.1) current and former glacier tongues likely played an important role in the formation, current stability, and mass balance of the Milne Ice Shelf. However, knowledge concerning temporal and spatial changes in tributary glaciers and their mass input to the ice shelf is limited.

2.6.2 Milne Glacier

Behind the Milne Epishelf Lake sits the 55 km long, 4 to 5 km wide, 750 m thick Milne Glacier (Hattersley-Smith 1969; Jeffries 2002; Narod et al. 1988; Prager 1983) (Figures 2.18 and 2.22). As discussed above (sections 2.3.1 and 2.3.2), early reports from the 1960s and 1980s concluded that the glacier was contiguous with the Milne Ice Shelf and

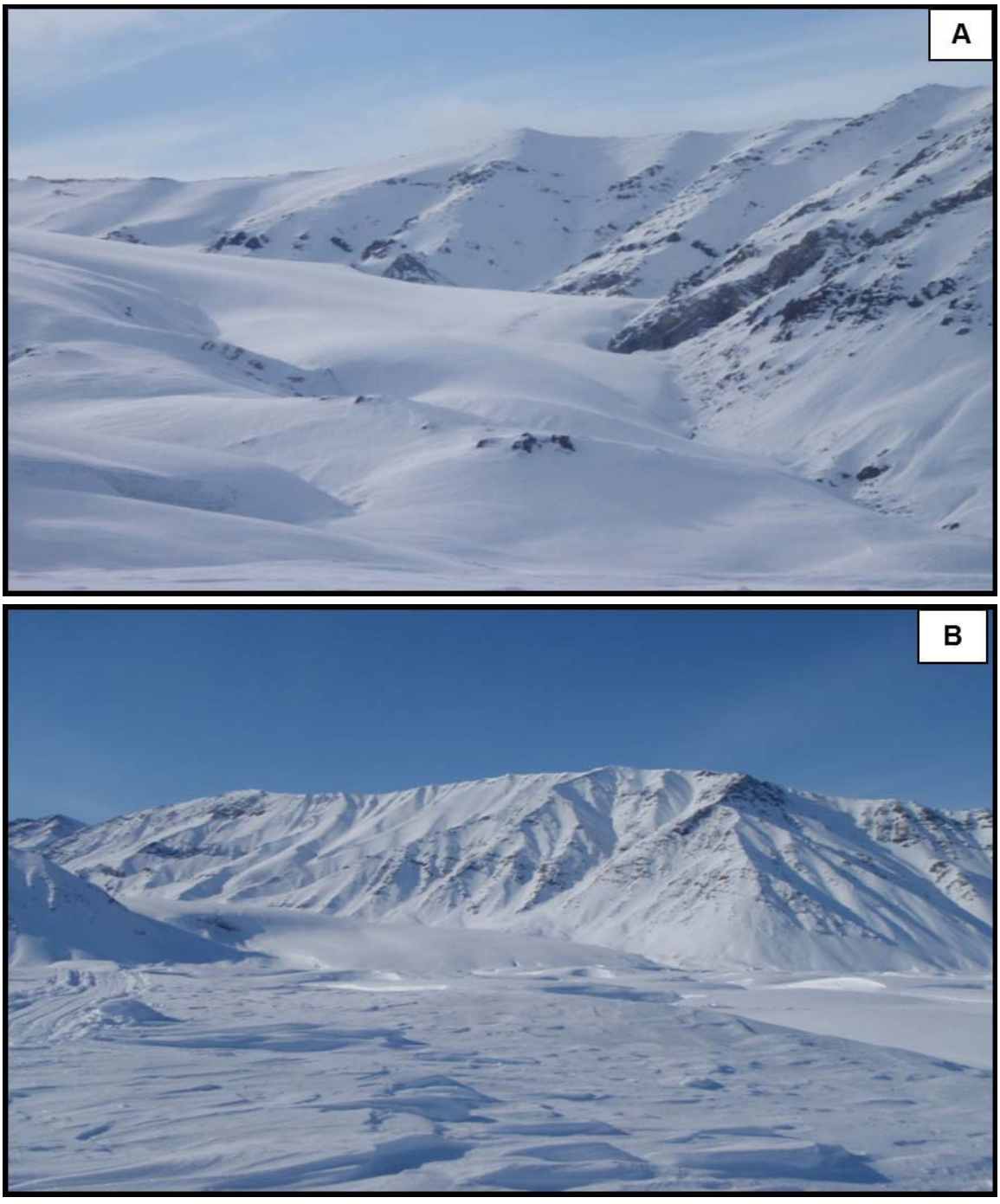

Figure 2.24: Glaciers issuing from the western side of Milne Fiord. A) Glacier 4 (hanging glacier) B) Glacier 3 with crevassed section. Photo: Colleen Mortimer May 23 and 30 2009.

that the tongue was floating (Evans and Robin 1966; Hattersley-Smith et al 1969; Jeffries 1984; Jeffries 1986b; Prager 1983). Jeffries (1984) identified the Milne Glacier to be a surge type glacier based on data collected during an April 1984 reconnaissance flight, ground observations in 1983, and aerial photography.

Surge-type glaciers are characterized by cyclical flow, alternating between a long quiescent phase (tens to hundreds of years) of relatively slow velocity and a short active surge-phase (months to years), of rapid advance (Benn and Evans 2010, p.169; Copland et al. 2003; Grant et al. 2009). During the quiescent phase, mass builds up in the reservoir area. At the same time thinning occurs in the lower part of the glacier, increasing the overall glacier gradient. During a surge, mass is transferred downglacier from the reservoir area, resulting in a rapid advance of the glacier terminus. Mass buildup in the reservoir area then begins a new surge cycle (Benn and Evans 2010 p.169; Copland et al. 2003; Grant et al. 2009).

Surge-type glaciers are not uncommon along Ellesmere Island as Hattersley-Smith (1969) noted a possible 5 to 6 km surge of the nearby Otto Glacier and 37 of the 51 high arctic surge-type glaciers identified by Copland et al. (2003) were located on Ellesmere Island. Jeffries (1984) cited the location of a pressure ridge beyond the location of the 1959 terminus, the presence of contorted moraines, irregular surface drainage and significant buckling of the inner unit as evidence of glacier surging. Comparisons of air photos (1950 and 1959) and satellite imagery (airborne X-band SAR and RADARSAT) indicates that the Milne Glacier advanced 10 m a^{-1} between 1950 and 1959, did not advance between 1959 and 1966, but advanced an additional ~2.5 km between 1966 and 1988 and another 2 km between 1988 and 2000 (Jeffries 2002). In this study the Milne Glacier is not considered part of the ice shelf proper, so advances of the Milne Glacier can result in a replacement of ice shelf ice with glacier ice and therefore a decrease in ice shelf area.

2.7 21st century research on the Milne Ice Shelf

Since the work of Narod and Jeffries during the 1980s, limited research on the physical properties of the Milne Ice Shelf has been carried out. However, measurements have been taken on the Milne Ice Shelf to explore the microbiological diversity of Ellesmere Island's cryohabitats (Mueller et al. 2003; Mueller et al. 2009; Veillette et al. 2008; Vincent et al. 2001). Backscatter from RADARSAT-1 imagery was used by Mueller et al. (2006) to classify numerous biological indicators and total cryo-habitat area (4.1 km^2). Images and near-surface ice samples taken during a helicopter transect over the Milne Ice Shelf in 2001 were used in part to verify these classifications. In a study to determine the structure of ice-dammed lake ecosystems along the northern coast of Ellesmere Island, Veillette et al. (2008) conducted water profiles (temperature and salinity) of the Milne Epishelf Lake between 2004 and 2007. These research projects were mainly restricted to the Milne Epishelf Lake, with little work being carried out on the ice shelf itself.

Chapter 3: Study area and methods

3.1 Study Site

3.1.1 Ellesmere Island

Ellesmere Island (79°49'59"N 78°0'0"W) is the largest (196,235 km^2) and most northerly island in the CAA (Figure 3.1). It is heavily glaciated with a total land ice area of approximately 84,000 km^2 (Williamson et al. 2008). The island is bordered by the Arctic Ocean to the north-northwest, Nares Strait to the east, and Nansen and Greely Fiords to the southwest (Figure 3.1). Its topography is dominated by several elongate mountain ranges trending from SW to NW (e.g. British Empire Range, United States Range; Figure 3.1).

The Agassiz (19,500 km^2), Prince of Wales (20,704 km^2) and Manson (6233 km^2) Ice Caps occupy east and southeast Ellesmere Island, while the Northern Ellesmere Ice Cap (24,372 km^2) occupies the northwest (Figure 3.1). Numerous valley and lobate glaciers originate from these ice caps where they drain from high elevations (~2286 m a.s.l.) to sea level (Williamson et al. 2008). A central desert, stretching from Eureka to Alert, is largely unglaciated (Koerner 2002) (Figure 3.1). The northwest coast of Ellesmere Island is home to North America`s only remaining ice shelves (Figure 1.6). In winter, sea ice fringes the coast and fills bays and inlets. In the past a large amount of multi-year landfast sea ice (MLSI) remained attached to the northern coast year-round; however, much of this MLSI has recently been lost and replaced by first year ice that melts in the summer (Maslanik et al. 2007; Nghiem et al. 2007). Increasingly, large open water leads occur near the Arctic Ocean coast in summer.

3.1.2 Milne Ice Shelf

The Milne Ice shelf (~205 km^2) is located at the head of Milne Fiord (82°44'0"N 81°45'0"W), between Cape Evans and Cape Egerton on the northwest Coast of Ellesmere

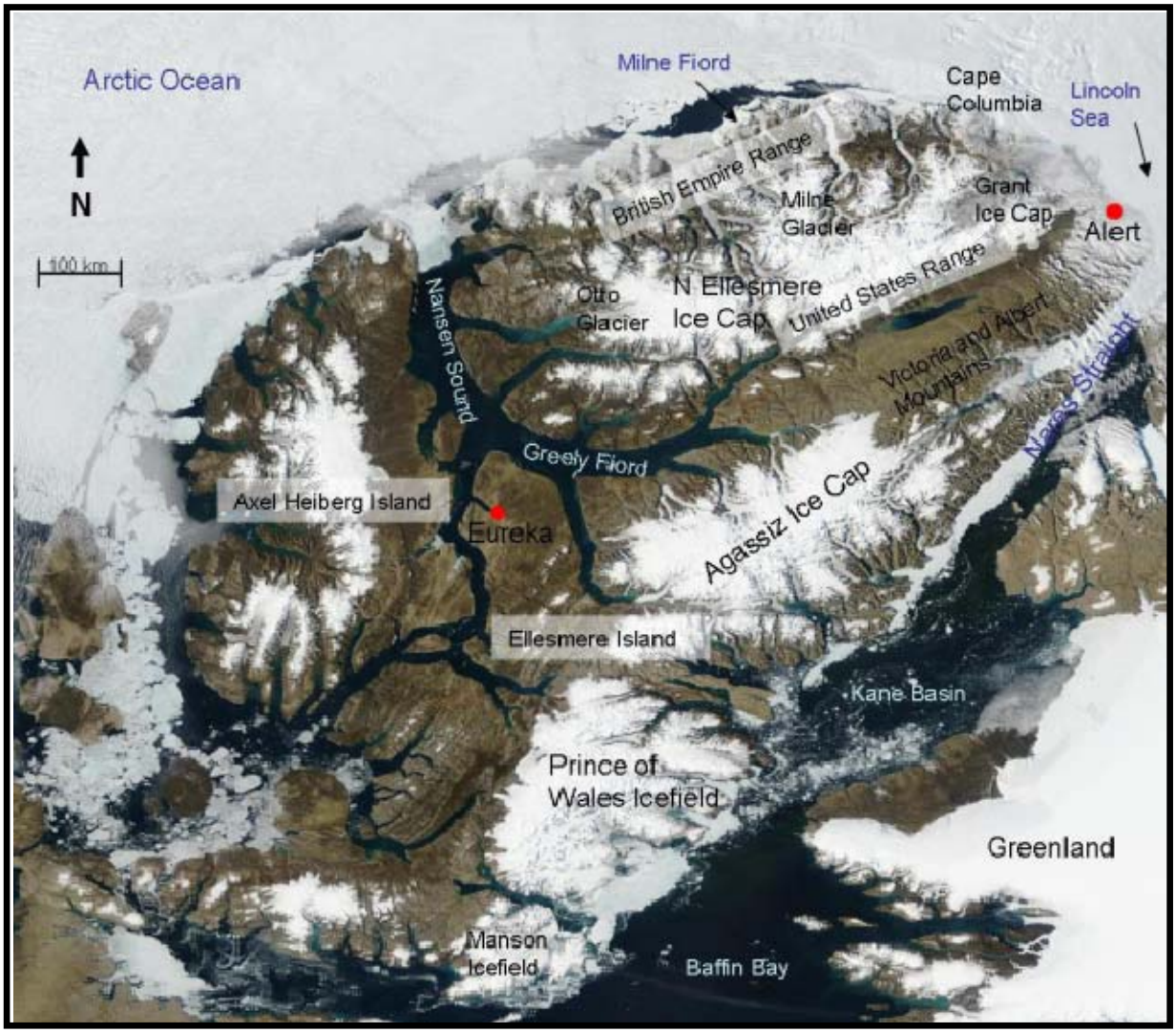

Figure 3.1: Map of Ellesmere Island showing major geographical features. Base image: MODIS TERRA, Aug. 13 2005.

Island. It is the thickest of the remaining arctic ice shelves with a thickness of ~100 m (Jeffries 2011; Figures 1.6 and 3.1). Behind the Milne Ice Shelf sits a large epishelf lake beyond which flows the 55 km long, 4-5 km wide Milne Glacier (Figures 2.12 and 2.13). The sides of the steep-walled Milne Fiord are flanked with long valley glaciers (Figures 2.18 and 2.24), some of which likely still provide mass input to the ice shelf.

3.2. Climate

3.2.1 CAA Climate

The northern CAA experiences cold temperatures and low levels of precipitation. Weather stations at Alert (82°32'12"N, 62°16'8"W) and Eureka (79°58'8"N, 85°55'8"W), located equidistant (~320 km) from the Milne Ice Shelf, reported average annual temperatures of -18°C and -20°C respectively (Table 3.1; 1971-2000 Climate Normals). Total annual average precipitation was 75 mm at Eureka and 153 mm at Alert over this same period (www.climate.weatheroffice.ec.gc.ca). Eureka experiences a continental climate, located on the lee side of the surrounding mountains, while Alert's climate is heavily influenced by the Lincoln Sea (Lesins et al. 2010; Figure 3.1). Average surface air temperature at Purple Valley, Nunavut (rear of the Milne Ice Shelf) between June 1, 2009 and May 31, 2010 was -17°C, with maximum and minimum temperatures of 14°C and -49°C, respectively (http://tinyurl.com/milnewx). NCEP/NCAR reanalysis indicates that surface air temperatures (SATs) along the northwest coast of Ellesmere Island increased by 0.5°C per decade over the period 1948-2007 (Copland et al., 2007; Mueller et al. 2009).

Sites along the northwest coast of Ellesmere Island are characterized by considerable differences in climate over short distances owing to the varying topography in this mountainous region, and distance from the coast (Abdalati et al. 2004; Copland et al. 2007; Vincent et al. 2001). Katabatic winds, funnelling of winds along the coastline, and proximity to open water sources strengthen this microclimatic variability. During the spring and summer, open water along the coast sees the development of low stratus clouds which move

Table 3.1: Climate normals, 1971 – 2000 for Alert and Eureka. Source: Environment Canada, National Climate Data Information Archive, www.climate.weatheroffice.gc.ca, September 11, 2010.

	Daily average temperature (°C)	Average daily maximum temperature (°C)	Average daily minimum temperature (°C)	Total annual precipitation (mm)	Total annual snowfall (cm)	Total annual rainfall (mm)
Alert	-18.0	-14.7	-21.3	153.8	173.3	16.1
Eureka	-19.7	-16.4	-22.9	75.5	58.5	26.2

inland and settle in the fiords (Figure 3.2). This heavy fog can increase long-wave radiation, thereby enhancing summer melt (Hock 2003). The lowest glacier equilibrium altitudes (ELAs) in the Northern Hemisphere are found along the northern coast of Ellesmere Island, attributed to what Braun et al. (2004a) termed the 'Arctic Ocean Effect', where reduced summer melt and enhanced snow accumulation manifest itself by low-elevation, coastal ice caps and ice shelves (Andrew and Barry 1978; Braun et al. 2004b; Braun 2011; Koerner 1979; Miller et al. 1975). This is reflected in the fact that snow accumulation decreases with distance inland from the coast of northern Ellesmere Island giving rise to a *reversed mass balance gradient* (section 2.1.2).

3.3 Methods

A combination of field measurements (undertaken in April 2008 and May/June 2009) and remotely sensed imagery were used to quantify changes in areal extent (1950-2009), thickness (1981-2009), and volume (1981-2009) of the Milne Ice Shelf. This section outlines the methods used to quantify these changes, and describes relevant background and theory where necessary. Table 3.2 lists imagery used in this study.

3.3.1 Area changes

3.3.1.1 Aerial Photographs: history and background

Aerial photography is one of the oldest forms of airborne remotely sensed imagery (Campbell 2002), although coverage of the high Arctic only extends as far back as the 1940s and 1950s (Jeffries 2002). Air photos were used in several early studies of the Ellesmere Ice Shelves to determine total areal extent as well as changes in surface features (e.g. Jeffries 1984; Jeffries 1986a; Jeffries 1986b). These studies often manually mosaicked images together, using visual or manual measurement techniques.

Table 3.2: List of remotely sensed imagery used in this study.

Sensor	Resolution	Date	Image ID
Air photo	2.1m	15/07/1950	T405C: 235 – 237 , T407C: 6 – 12, 204 - 209
Air photo	2.8 m	29/07/1959 17/08/1959	A16709: 7 – 9 A16785: 65 – 70, 81 – 83, 211 - 215
Air photo	1.17 m	11/07/1974	A29343: 70 - 80
Air photo	1 m	24/07/1984 24/08/1984	A26534: 3 -61 A26534: 63 - 93
ASTER Level 1B	15 m	23/05/2001	AST_L1B_00305232001222836
ASTER Level 1B	15 m	19/09/2001	AST_L1B_00309192001223125
ASTER Level 1B	15 m	19/06/2005	AST_L1B_00306192005204020
ASTER Level 1B	15 m	19/06/2005	AST_L1B_00306192005221820
ASTER Level 1B	15 m	19/07/2007	ASTER_L1B_ 00307192007230820
ASTER Level 1B	15 m	22/08/2008	AST_L1B_00308222008000337
ASTER Level 1B	15 m	21/07/2009	AST_L1B_00307212009223745_203
ERS-1 Standard beam	30 m	19/05/1993	19930519_e1_09623_213R1
RADARSAT-1 Standard Beam	28 m	26/01/2005	2005_20050126_r1_48181_214
RADARSAT-1 Standard Beam	28 m	05/06/2005	2005_20050605_r1_50039_213
RADARSAT-1 Standard Beam	28 m	16/07/2005	2005_20050716_r1_50625_213
RADARSAT-1 Standard Beam	28 m	29/08/2006	2006_R1_060829_124822_01f
RADARSAT-2 Wide Beam	40 m	15/03/2009	20090315_202620_r2_w1___vx_a_utm17n_.tif
RADARSAT-2 Wide Beam	40 m	15/03/2009	20090315_202620_r2_w1___vx_a_utm17n_tog.tif
RADARSAT-2 Wide Beam	40 m	03/03/2010	20100303_135045_r2_w2___hx_a_utm17n_.tif

Recent studies have taken advantage of software advances to better analyse changes in glaciers and ice shelves over time. For instance, Copland et al. (2007) used similar air photos to reconstruct the extent of the Ayles Ice Shelf in 1959 with imaging software and rubber sheeting techniques (Mueller, pers. comm., 2009). Similarly, DeBeer and Sharp (2009) mosaicked 1951 air photos of the Monashee Mountains, British Columbia, using a thin plate spline method in PCI Geomatica. The air photo mosaics were georeferenced to a LANDSAT DEM for analysis (DeBeer and Sharp 2009). These modern digital mosaics provide more accurate measurements of area and surface change (Jeffries 2002).

Monochrome trimetregon and vertical aerial photographs of the Milne Ice Shelf are available for 1950, 1959, 1974, and 1984 and housed at the National Air Photo Library (NAPL), Ottawa. Complete coverage is only available for 1959 (Figures 3.4 and 3.5), while near complete coverage is available for 1950 and 1984 (Figures 3.2, 3.3, 3.8 and 3.9). Coverage for 1974 is limited to the ice shelf front (Figures 3.6 and 3.7). Trimetregon air photos, which consist of three air photos taken simultaneously (right-looking oblique, centre down-looking, and left-looking oblique), were collected by the Royal Canadian Air Force (RCAF) in July 1950. For this study only the centre (down-looking) photos were georeferenced. From 1959 onward the more common vertical stereoscopic air photos were used.

Air photo prints measuring 10" X 10" were scanned in full colour at 600 dpi in uncompressed .tif format. The digital colour images were converted to greyscale, the outer borders cropped and loaded into ArcMAP 9.3. Ground control points (GCPs) selected from a July 21, 2009 ASTER scene were used to georeference all of the air photos to a common reference image. Stationary features such as mountain peaks and fiord valley walls were chosen for the GCPs, and where possible a minimum of 20 evenly distributed GCPs and a root mean squared error (RMSE) <15 m was used for each photo. In some cases achieving these criteria was not possible due to poor photo quality (e.g., cloud, fog) or a lack of suitable GCPs (e.g., photo only contained ice shelf). Georeferenced images were rectified using a 1st order polynomial and mosaicked in ENVI 4.4 (Table 3.2 and Appendix 1).

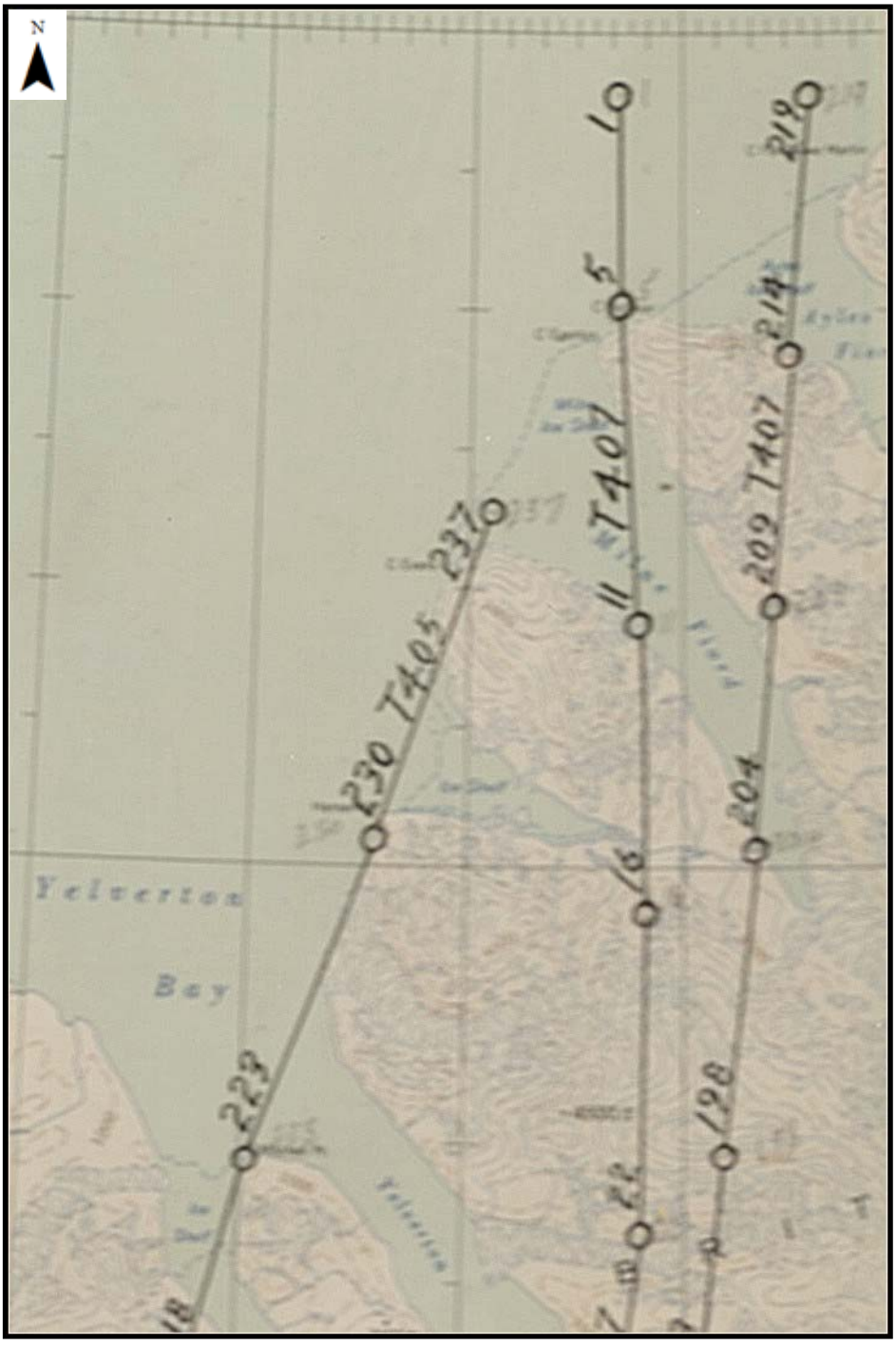

Figure 3.2: Air photo flight lines over the Milne Ice Shelf and surrounding areas for 1950. Flight lines overlaid on sub-scene of NTS map sheet 340F 49AN[1/2]. Source: National Air Photo Library, Ottawa.

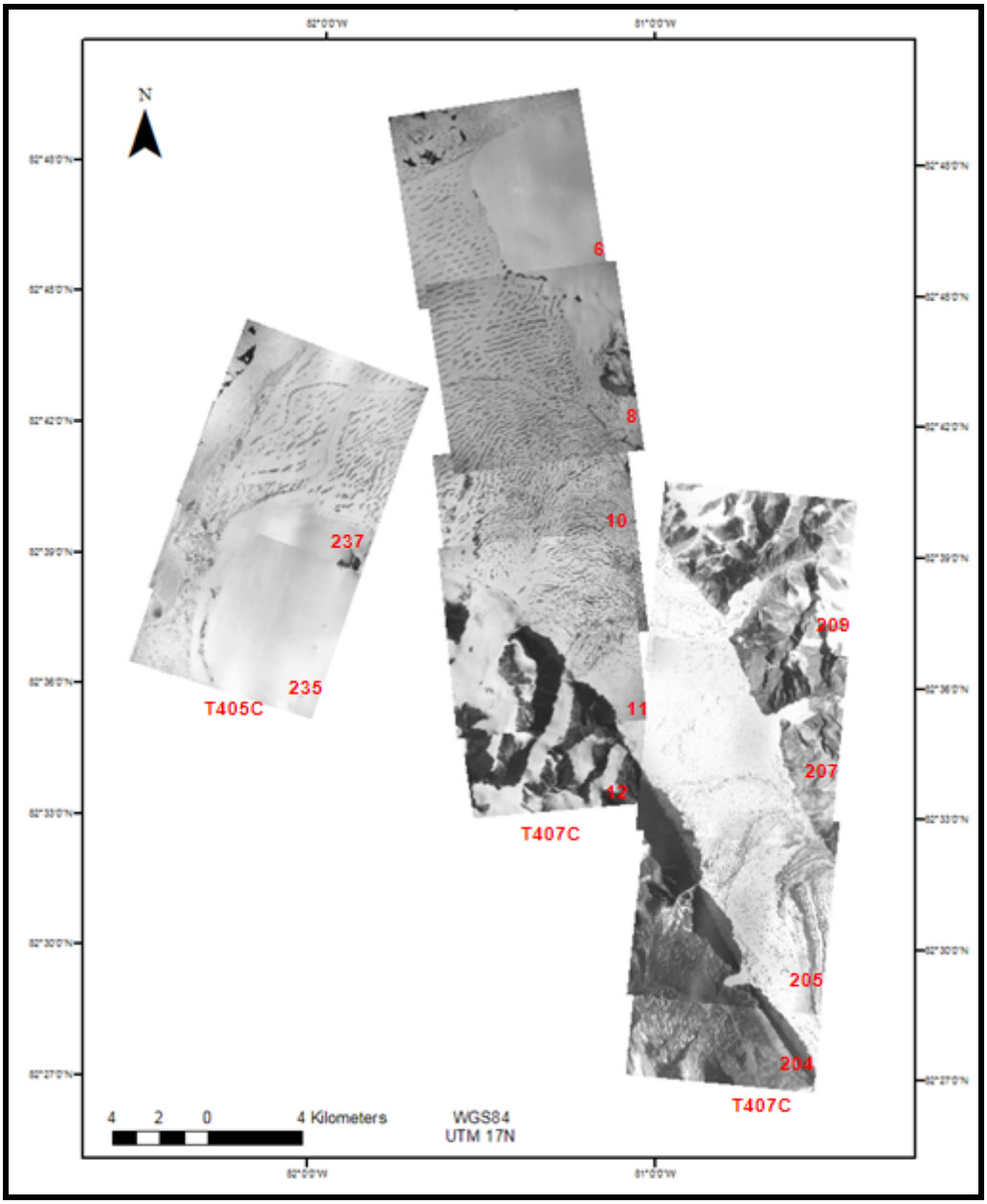

Figure 3.3: Images used for the 1950 air photo mosaic with corresponding flight line and image numbers from Figure 3.2. Detailed information for all photos used in this study is found in Appendix 1, Table A1.

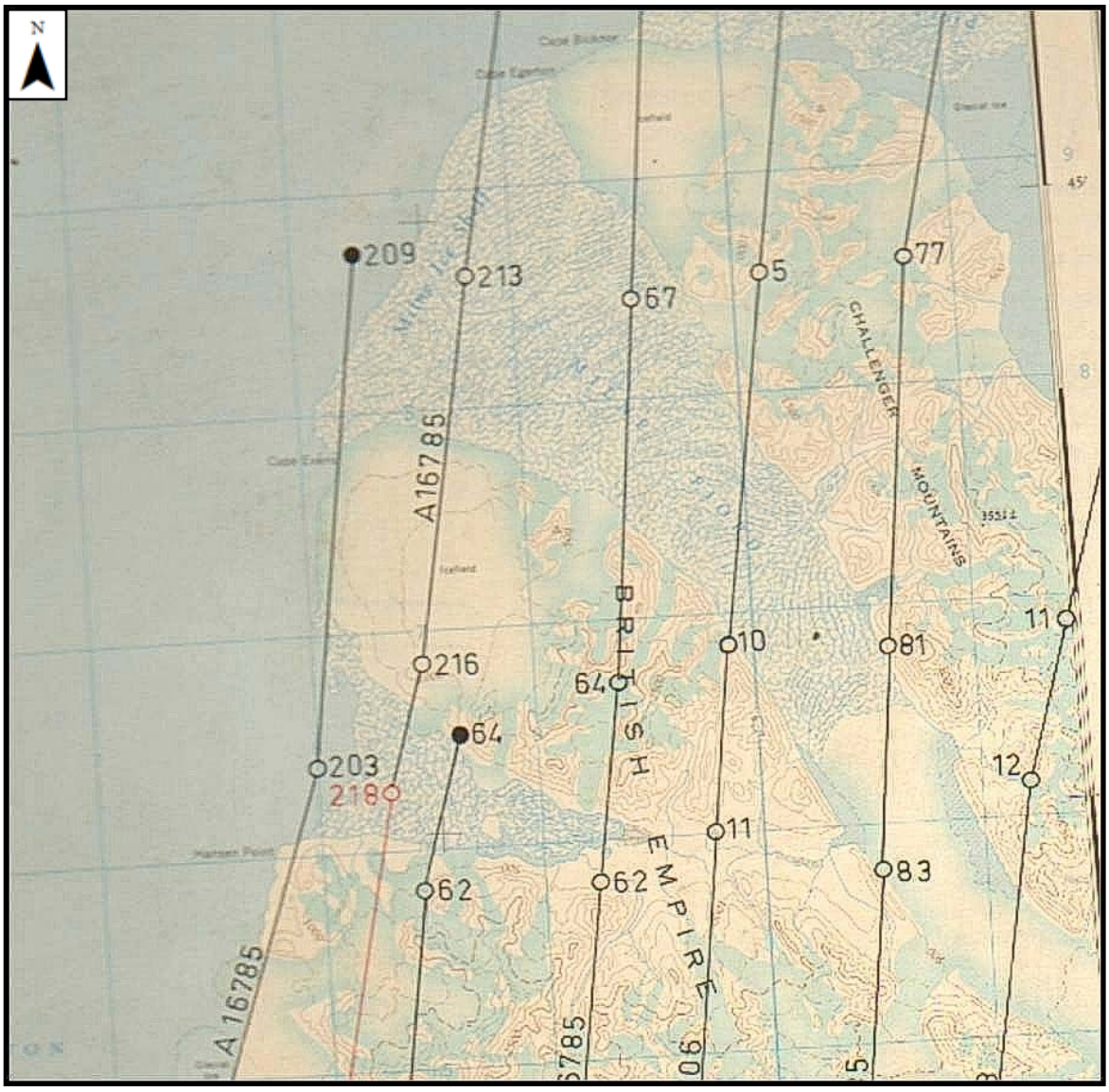

Figure 3.4: Air photo flight lines over the Milne Ice Shelf and surrounding areas for 1959. Flight lines overlaid on sub-scene of NTS map sheet 'B' 340F & 560E. Source: National Air Photo Library, Ottawa.

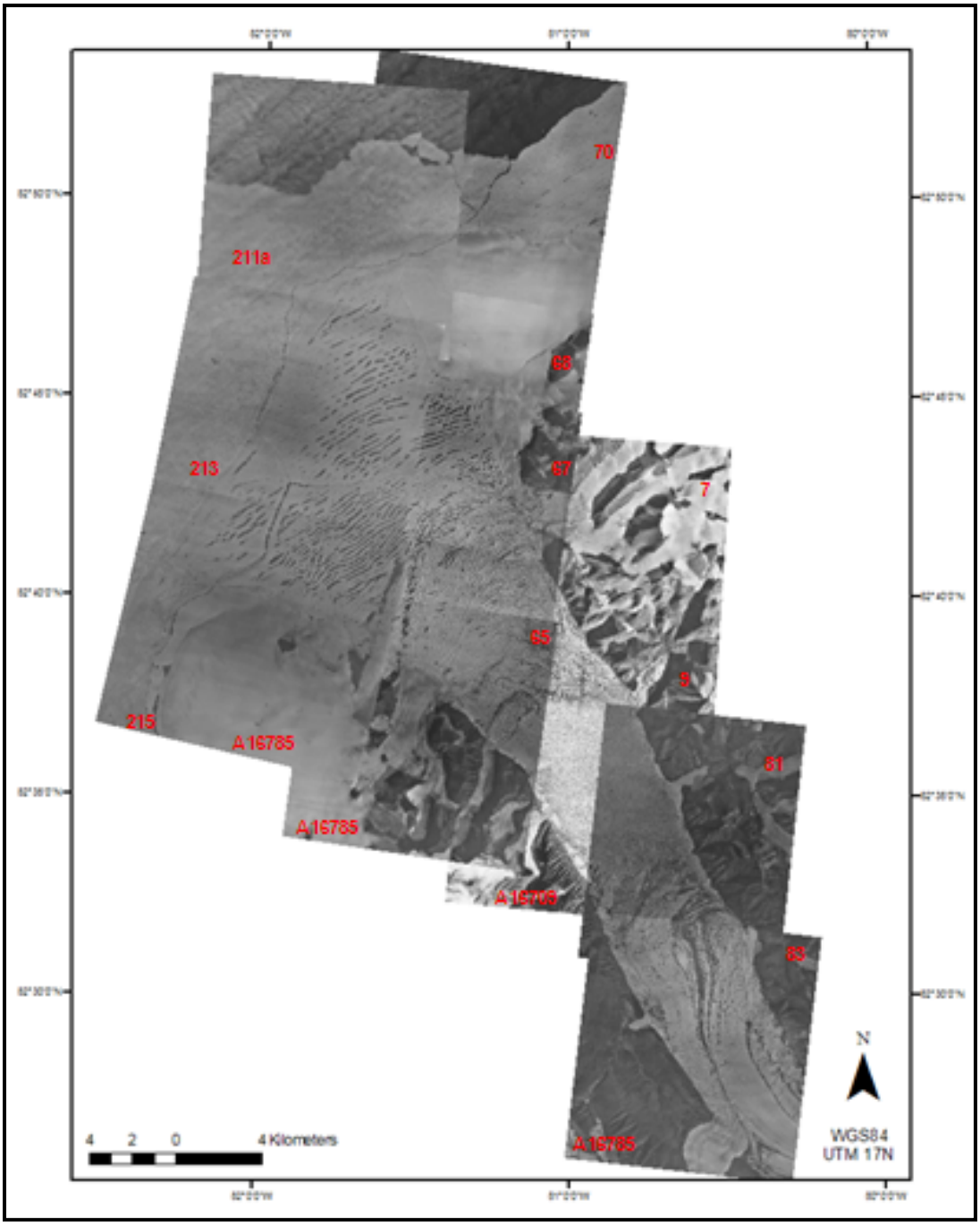

Figure 3.5: Air photos used for 1959 air photo mosaic with corresponding flight lines and image numbers from Figure 3.4. Detailed information for all photos used is found in Appendix 1, Table A2.

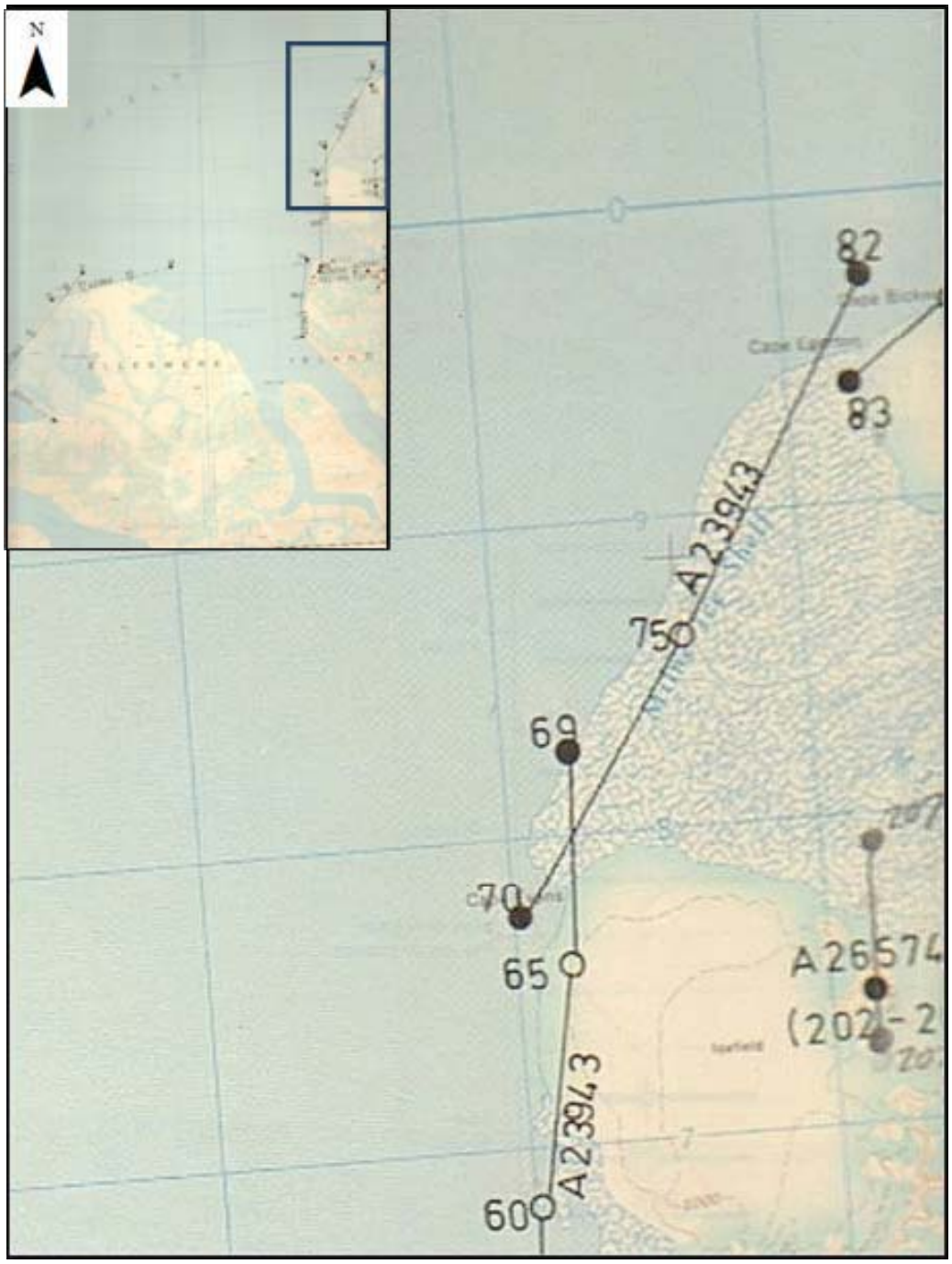

Figure 3.6: Air photo flight lines over the Milne Ice Shelf and surrounding areas for 1974. Flight lines overlaid on sub-scene of NTS map sheet "B" 340F & 560E. Source: National Air Photo Library, Ottawa.

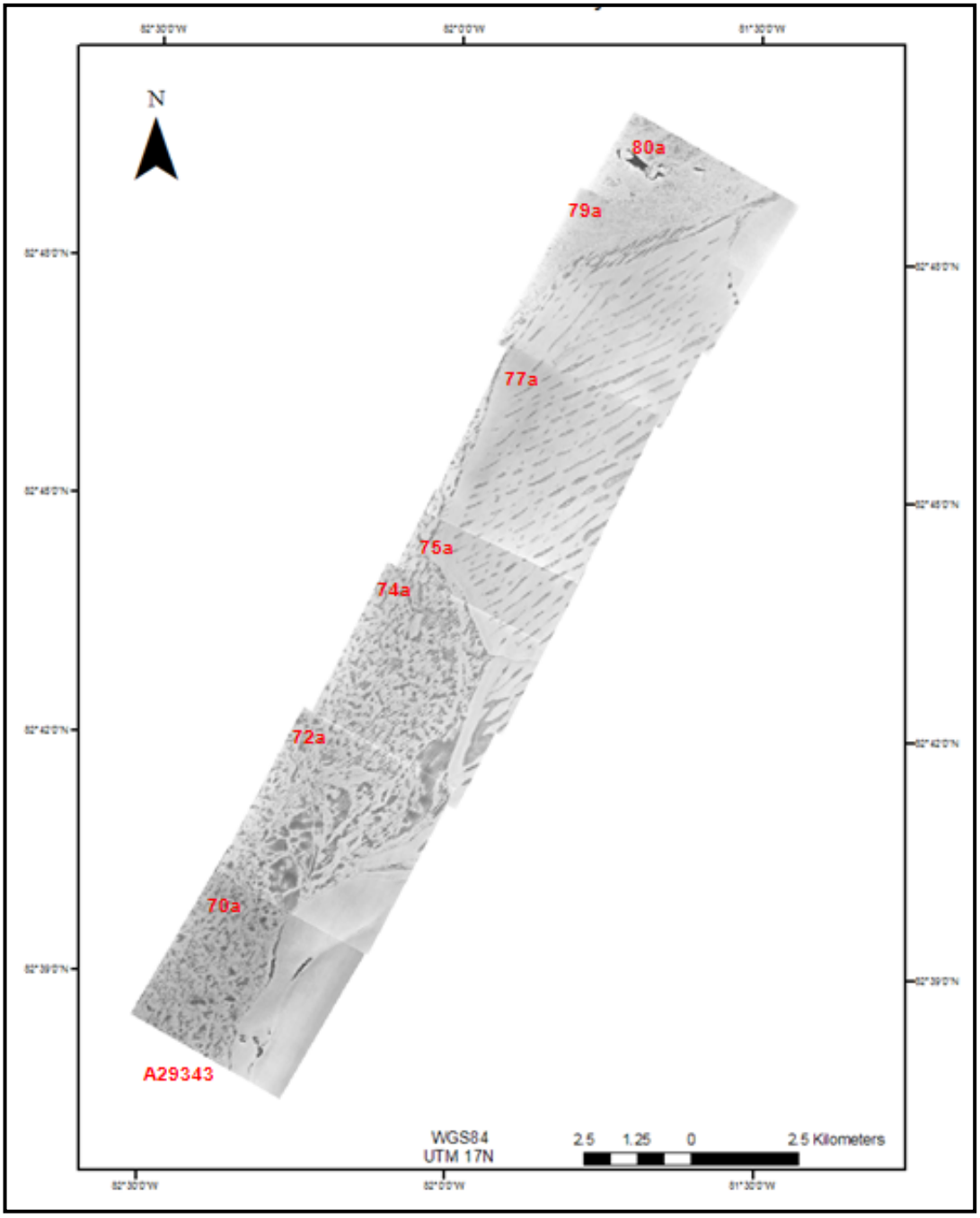

Figure 3.7: Air photos used for 1974 air photo mosaic with corresponding flight lines and image numbers from Figure 3.6. Detailed information for all photos used is found in Appendix 1, Table A3.

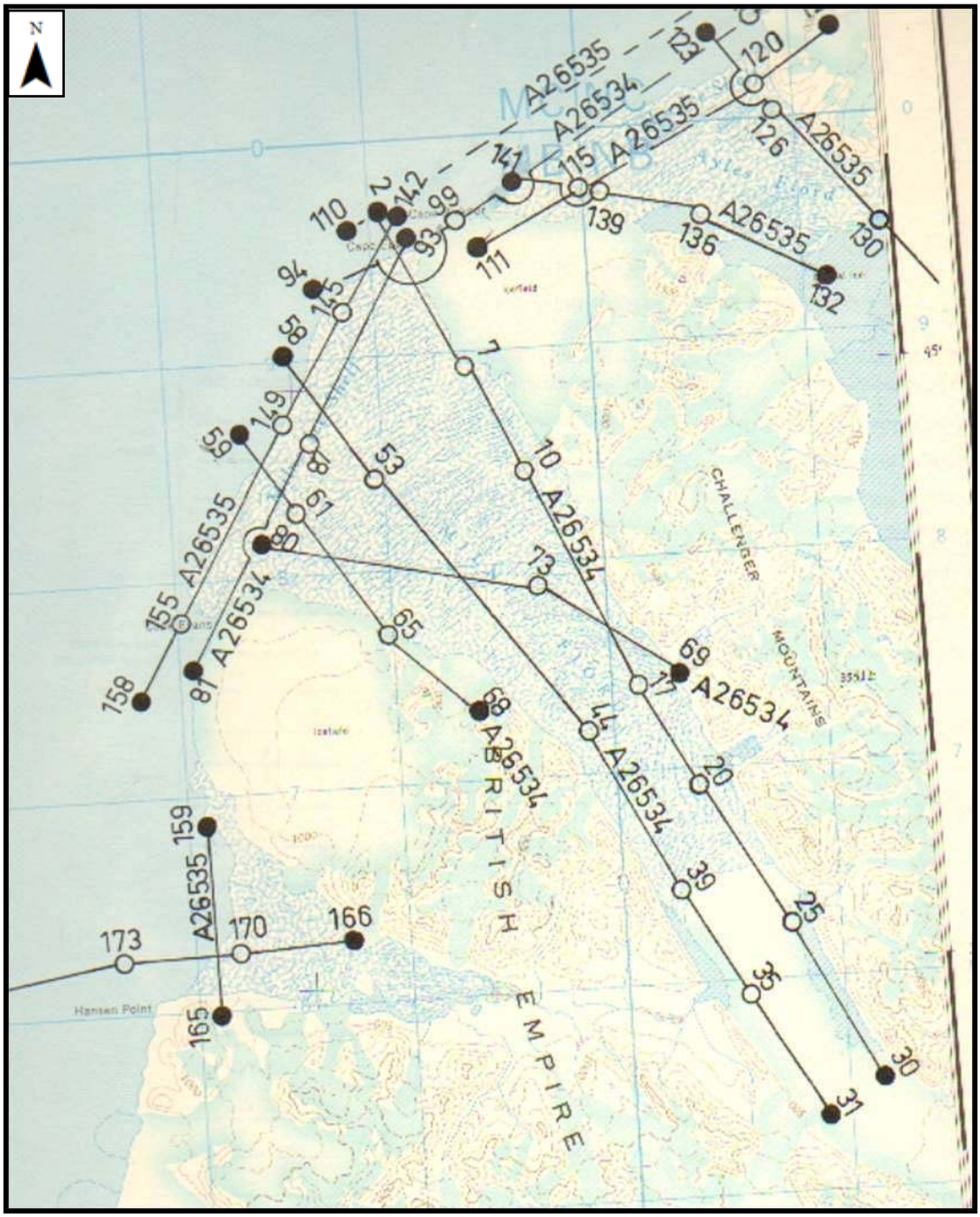

Figure 3.8: Air photo flight lines over the Milne Ice Shelf and surrounding areas for 1984. Flight lines overlaid on sub-scene of NTS map sheet "E" 340F & 560E. Source: National air photo Library, Ottawa.

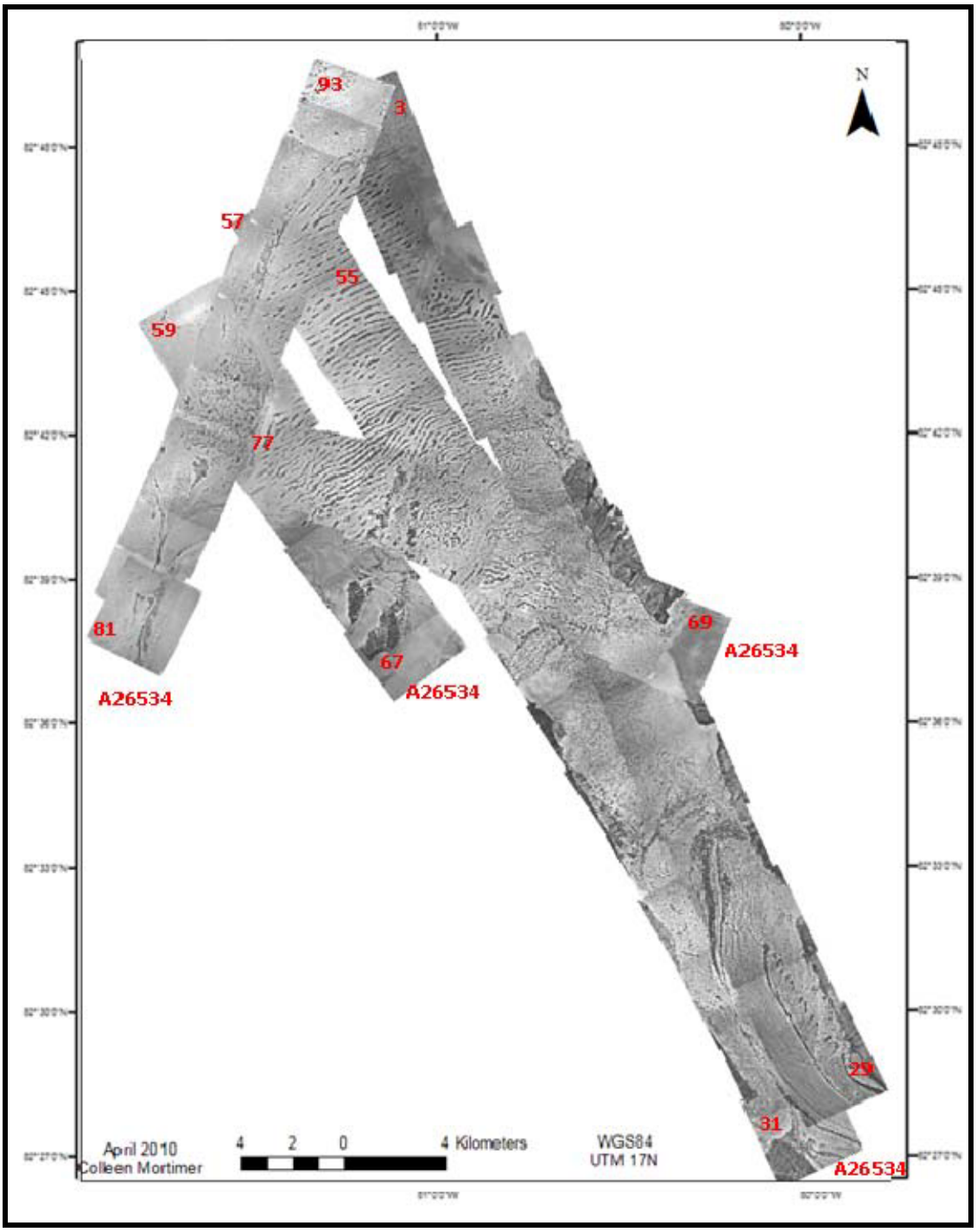

Figure 3.9: Air photos used for 1984 air photo mosaic with corresponding flight lines and image numbers Figure 3.8. Detailed information for all photos used is found in Appendix 1, Table A4.

3.3.1.2 Satellite imagery: history and background

Satellite imagery provides much greater spatial and temporal coverage compared to aerial photography, although imagery covering the northwest coast of Ellesmere Island has only been available since the 1990s. The lack of early coverage was due to the relatively southerly orbital paths of early satellites (e.g., Landsats 1-5 were unable to image further north than ~80°N). Consequently, regular imaging of the northwest coast, including the Milne Ice Shelf, did not begin until the mid to late 1990s. The two primary types of remotely sensed imagery available for the ice shelves, passive and active, are described below.

3.3.1.3 Passive remote sensing: visible satellite imagery

Passive satellite sensors detect energy that is naturally available (reflected or emitted) at the earth's surface. Advantages of passive imagery include ease of interpretation and less feature distortion compared to SAR scenes. Disadvantages include the inability to penetrate cloud and the need for sunlight. Thus, in the Arctic these sensors only provide useful imagery during the summer months (Bamber and Payne 2004; Campbell 2002; Jeffries 2002).

Products obtained from NASA's Advanced Spaceborne Thermal Emission and Reflection Radiometer (ASTER), aboard the TERRA satellite (launched in December 1999), provide images up to 15 m resolution using 14 bands (visible through thermal) in northern regions during the summer (http://asterweb.jpl.nasa.gov/). Among passive sensors, ASTER imagery offers some of the best available coverage of the Milne Ice Shelf due to its relatively northerly orbit and ability to image off-nadir. ASTER imagery therefore forms the bulk of the passive satellite data used in this project, with the image pair in Figures 3.10a and 3.10b illustrating some features of interest on the Milne Ice Shelf that are

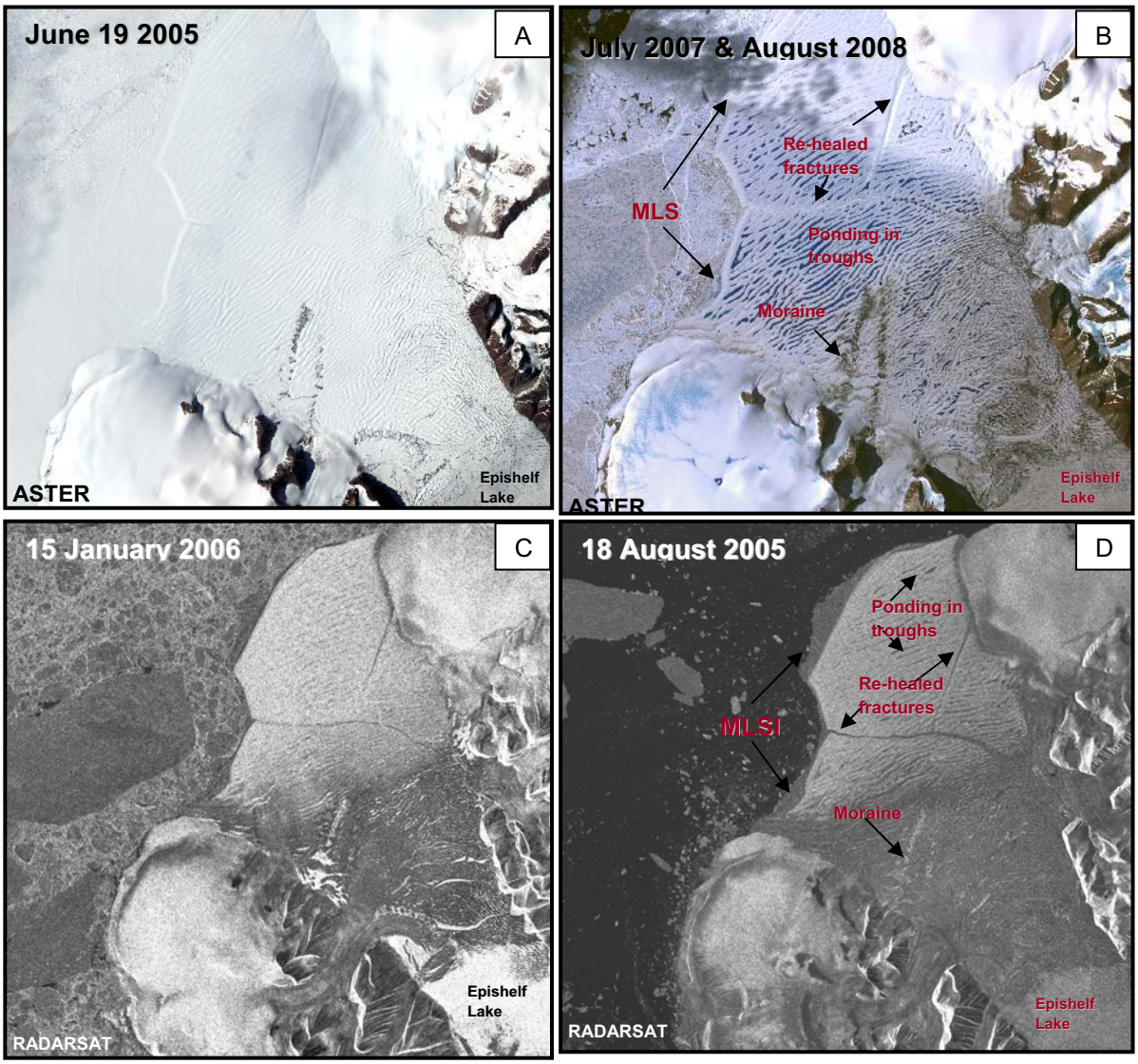

Figure 3.10: Visible (ASTER) and SAR (RADARSAT-1) satellite image pair of outer Milne Ice Shelf and Milne Re-entrant area. (A) Early summer ASTER Scene; (B) Late summer ASTER scene; (C) Winter RADARSAT-1 scene; (D) summer RADARSAT-1 scene.

distinguishable in visible imagery. Of note is the rapid development of melt ponds in the surface troughs from an early summer snow-covered surface. Glacier moraines, debris, and large cracks are also much more noticeable later in the summer than in the spring.

LANDSAT-7 (launched 15 April 1999; 30 m resolution for multispectral bands) provided the first regular imaging of the southern part of the Milne Ice Shelf, although many recent scenes have large stripes across them due to failure of the Scan Line Corrector in May 2003 (Campbell 2002, Jeffries et al. 1992). Due to this failure and the availability of higher resolution images that cover the northern margin of the ice shelf, LANDSAT data was not used for this study.

MODIS imagery, available since 1999, provide scenes at up to 250 m resolution, with the high repetition of the MODIS (TERRA and AQUA) satellites over the poles enabling the tracking of changes over very short time periods (less than hourly at high latitudes). For this study, MODIS imagery was used as a first order qualitative data source to identify rapid changes at the ice shelf front, and to refine the timeline of specific, short-term events. MODIS imagery was not used for quantitative analysis due to its relatively low resolution.

3.3.1.4 Active remote sensing: synthetic aperture radar

Synthetic aperture radar (SAR) sensors emit their own electromagnetic energy to image the earth's surface and near-surface, and as such have been used in many studies of the Canadian High Arctic because of their ability to obtain imagery year-round. Jeffries and Sackinger (1990) also used SAR imagery to detect and monitor ice islands. In fresh ice, the longer wavelength (compared to optical images) can penetrate through the surface and aid in interpreting sub-surface features including re-healed crevasses (Bamber and Payne 2004, p.413). Disadvantages include significant foreshortening, layover and shadow, particularly in steep-walled valley fiords (Campbell 2002, p.204-224). Further, summer melt leads to

wet ice which attenuates the radar wave, leading to dark images that prevent distinction between ice shelf ice types. In one of the first uses of active SAR imagery, Jeffries (1992a) used an airborne X-band SAR scene to identify calving of the Milne Re-entrant area in winter 1988 (Figure 2.20).

RADARSAT-1, launched on November 4, 1995, provides good coverage of the Milne Ice Shelf during both winter and summer for 1997 to 2009. This C-Band (0.058 m wavelength), 5.3 GHz sensor has daily coverage of the Arctic (Jeffries 2002). For this project, RADARSAT-1 imagery, available via an agreement with the Canadian Ice Service (CIS), was the primary data source for SAR scenes. RADARSAT-2 (launched 14 December 2007) was used for 2008 and 2009. Finally, ERS-1 imagery, available through an agreement with the Alaska Satellite Facility, was used to extend the duration of satellite imagery for the Milne Ice Shelf as far back as 1993. Table 3.2 lists all satellite imagery used in this study.

Differences in greyscale, related to variations in salinity, surface roughness, and moisture content, are used to distinguish features in SAR scenes. For example, the RADARSAT-1 pair in Figure 3.10c & 3.10d illustrates some key features of Milne Ice Shelf and Fiord. Brackish ice appears darker than fresh ice, helping to identify different ice types. The epishelf lake appears extremely bright in the winter owing to the freshwater layer below a thin layer of land ice, but dark in late summer because of surface melt (Jeffries 2002; Mueller et al. 2009). The re-healed fractures appear dark in both scenes. This could be due to brackish ice which has formed in these cracks (Jeffries 2002). The central unit appears dark in both winter and summer, most likely due to brine inclusions, surface debris and high surface roughness.

3.3.1.5 Satellite imagery data sets

Satellite imagery was used to delineate ice shelf area and track surface features for the Milne Ice Shelf for the recent past (1993 – 2009). To quantify changes in overall areal extent, scenes were collected for 1993, 2001, and 2009. A higher temporal resolution (~4yrs:

1993, 2001, 2005 and 2009) was used to analyze changes in MLSI and landfast sea ice, which exhibit more year to year variability. SAR scenes were used in combination with shallow ice cores and GPR data to infer information about ice type. Image georectification was conducted in ArcMAP 9.3 using ground control points derived from a July 21, 2009 ASTER scene. Scenes were shifted to correct for position but pixels were not resampled. A full list of images used in this study is found in Table 3.2.

3.3.2 Ice shelf thickness

Present-day ice thickness for the Milne Ice Shelf was determined from ground penetrating radar (GPR) measurements from 2008 and 2009 (Figure 3.11). A detailed contour map was produced from the GPR measurements, from which a thickness DEM was produced. To determine changes over time, the present-day ice thickness measurements were compared to the radio-echo sounding measurements made in 1981 (Prager 1983). To place these long-term changes in context, ablation stake measurements were taken over a 1-year period (2008 to 2009) to provide information regarding short term variations in accumulation and ablation. Error analysis of the 2008 and 2009 GPR data is described in section 4.2.1.

3.3.2.1 Ground penetrating radar (GPR): history and development

Ground penetrating radar is a geophysical radar technique that can be used to investigate subsurface features (Annan 2002; Barrett et al. 2007; Bingham and Siegert 2007; Woodward and Burke 2004). The roots of modern GPR can be traced back to the 1950s when the USAF noted aircraft altimeter returns over Greenland that resulted from radar frequencies penetrating through the ice surface (Annan 2002; Bamber and Payne 2004; Bingham and Siegert 2007; Crabtree and Doake 1986). In 1966, radio-echo sounding

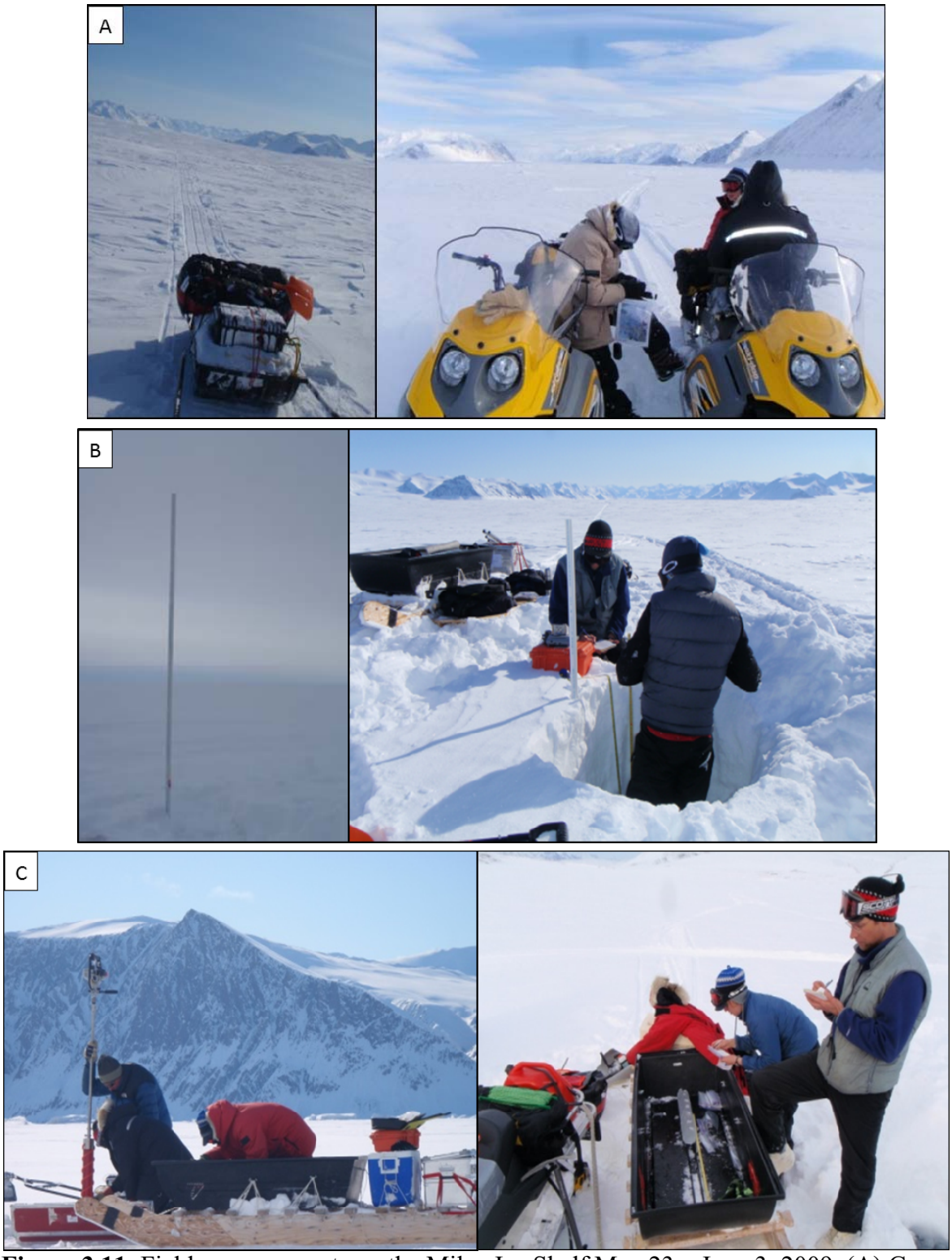

Figure 3.11: Field measurements on the Milne Ice Shelf May 23 – June 3, 2009. (A) Ground penetrating radar profiling; (B) Ablation stake measurements and snow pits; (C) Shallow ice coring. Photos: Colleen Mortimer and Luke Copland 2009.

surveys carried out over northern Ellesmere Island returned promising results of glacier and ice shelf thickness, including ice thickness for parts of the Milne Glacier (Evans and Robin 1966; Hattersley-Smith 1969; Hattersley-Smith et al. 1969). Technological improvements during the 1980s spawned a new era of RES and the subsequent development of smaller, more portable units that form the basis of modern GPR systems (Annan 2002; Narod and Clarke 1983).

3.3.2.2 GPR theory: basic principles

GPR works by exploiting the principle that the propagation speed (velocity) of electromagnetic waves is dependent upon the dielectric properties of earth's materials (Annan 2002; Bingham and Siegert 2007; Evans and Robin 1966; Hattersley-Smith et al 1969; Hubbard and Glasser 2005; Woodward and Burke 2004). The propagation velocity, v, of a radio wave through a material is proportional to the material's dielectric constant ε (Table 3.3):

$$v = \frac{c}{\sqrt{\varepsilon`_r}} \quad (1)$$

Where c is the speed of light in a vacuum (3.0×10^8 m s^{-1}), and $\varepsilon`_r$ is the material's dielectric permittivity. The relationship between velocity, frequency and wavelength in any medium is given by equation (2), with higher frequencies corresponding to shorter wavelengths and vice versa:

$$f = \mathrm{v}/\lambda \quad (2)$$

Outside a vacuum the wavelength is altered according to a material's dielectric constant, where a lower dielectric constant leads to a faster velocity and longer wavelength. GPR systems emit electromagnetic pulses of a pre-defined frequency into a material from a transmitter. Pulses are returned to the receiver from dielectric discontinuities known as internal reflector horizons (IRHs). The nature of the reflector horizon can be interpreted from the amplitude and polarity of the reflection coefficient, R:

$$R = \frac{\sqrt{\varepsilon_1} - \sqrt{\varepsilon_2}}{\sqrt{\varepsilon_1} + \sqrt{\varepsilon_2}} \quad (3)$$

Equation (3) indicates that strong reflecting horizons result from large contrasts in dielectric properties (Hubbard and Glasser 2005; Irvine-Fynn 2006; Macheret et al. 1993; Prager 1983). When the transmitted (incident) wave reaches an internal reflector horizon (IRH), some of the pulse's energy is transmitted through the IRH to subsequent layers, a portion is absorbed by the material, and finally a portion is reflected back to the receiver (Figure 3.12). For each electromagnetic pulse, the amount of energy returned and the total transit time, also known as the two-way-travel-time (TWTT), are recorded by the receiver. Unit time is converted to unit depth by applying the material's specific velocity (Annan 2002; Bingham and Siegert 2007; Hubbard and Glasser 2005; Macheret et al. 1993; Woodward and Burke 2004):

$$\text{Depth} = (v)\ (t/2) \quad (4)$$

The propagation velocity for a material can be determined at the study site via a common midpoint survey (CMP). This technique involves repeatedly moving both the transmitter and receiver a set distance from a central point (midpoint) (Figure 3.13). A pulse is fired at each survey point. As the distance from the midpoint reflector increases so does the path length and thus the TWTT. With a known distance and transit time the material's velocity can then be computed (Barrett et al. 2007; Macheret et al. 1993).

3.3.2.3 GPR considerations for glaciology

Most GPR systems use two shielded dipole antennae separated by a fixed distance to transmit and receive electromagnetic pulses at a predefined frequency. Pulses are fired from the receiver at a set rate (sample interval) as the GPR is towed across the surface. The

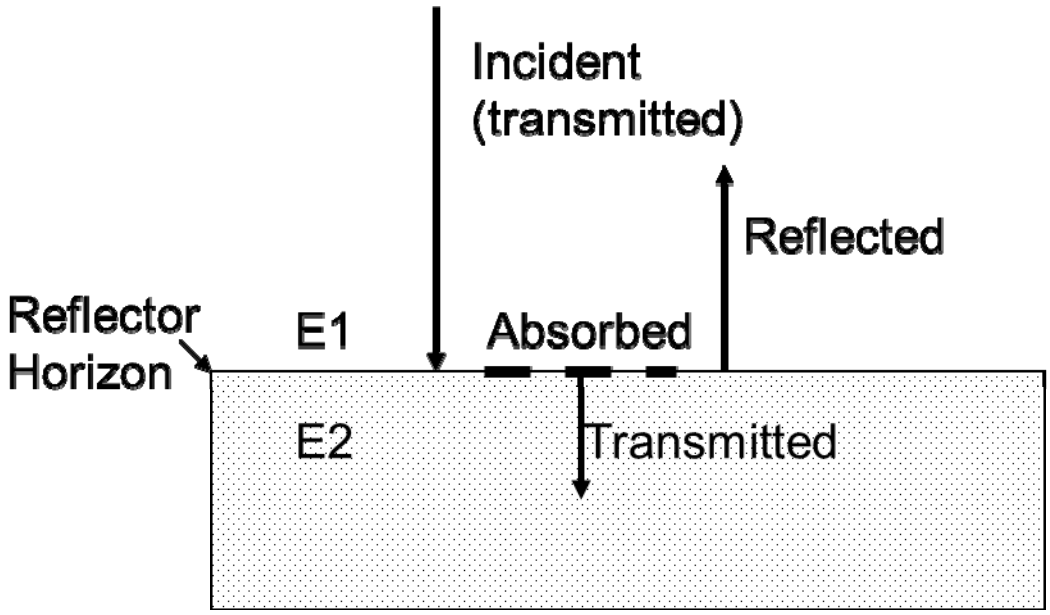

Figure 3.12: Schematic diagram of what happens to energy emitted a GPR transmitter when it meets an internal reflector horizon (IRH). Some energy is absorbed at the interface between the two materials, some is reflected back to the receiver and a portion is transmitted through the IRH to penetrate greater depths in the material.

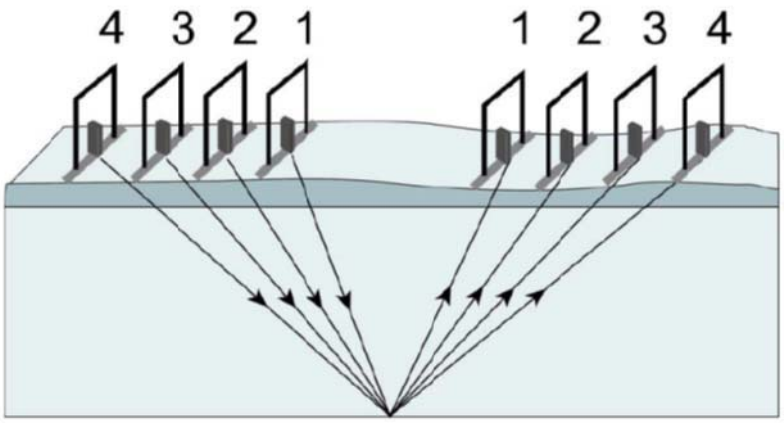

Figure 3.13: Common Midpoint Survey. Source: PulseEKKO PRO User Guide (2006).

receiver records the returned signals to build an image of the subsurface (radargram) (Figure 3.14). The conical nature of the pulse results in geometric spreading, which leads to a signal which is more dispersed with increasing distance from the source (Hubbard and Glasser 2005; Plewes and Hubbard 2001). The rate of loss of electromagnetic energy with distance, *d*, from the source due to signal spreading is given by equation 5:

$$\text{Geometrical spreading} = 1/d^2 \quad (5)$$

In addition to geometrical spreading, attenuation and scattering affect the strength of the returned signal. Attenuation (energy loss as the radar wave passes through a material) is caused by both scattering and absorption. Scattering depends on the size of particles and irregularities within the material, while absorption depends on dielectric properties (Hubbard and Glasser 2005; Woodward and Burke 2007). In glaciology, attenuation, scattering and absorption are primarily related to water content, salt/brine inclusions, debris content and crystal orientation (Bingham and Siegert 2007; Palli et al. 2002; Plewes and Hubbard 2001; Woodward and Burke 2007). Water molecules absorb electromagnetic energy, so wet (temperate) glacial ice absorbs more energy and attenuates the radar pulse much more than in cold dry ice. Changes in crystal orientation relative to the transmitter also increase scattering; differences in c-axis orientation can lead to anisotropic responses (Kovacs and Morey 1978; Nyland 2004; Pringle et al. 2009). This is of particular concern in sea ice or ice with salt/brine inclusions.

The physical size of a GPR antenna is inversely proportional to wavelength, with low frequency systems having very large antennas which can impose logistical constraints (e.g., a typical 5 MHz antenna has a length of ~20 m). Secondly, there exists a trade-off between penetration depth and resolution. For similar materials, a higher frequency GPR system yields higher resolution but shorter penetration depth due to increased attenuation and scattering at shorter wavelengths. These trade-offs must be taken into account when selecting the appropriate frequency, as it is desirable to be able to penetrate the maximum required depth with the highest possible resolution. The minimum resolvable feature is equal

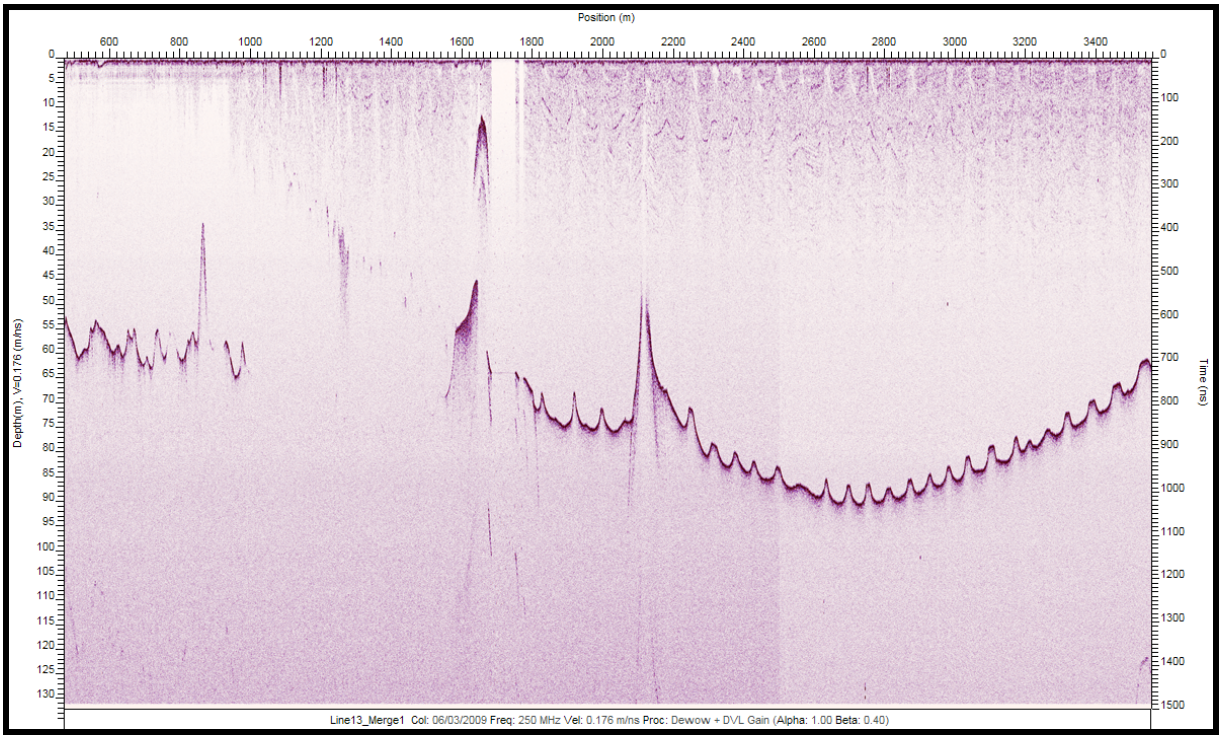

Figure 3.14: GPR Radargram produced in EKKO View Deluxe for a ~ 3 km long transect along the Milne Ice Shelf (June 3 2009). Dark purple line represents the bed (ice-water reflector horizon). DVL gain, GPS coordinates, and velocity of 0.170 m ns^{-1} applied. The apparent undulating bed topography is a product of surface rolls.

to one quarter of the instrument's wavelength, so a frequency should be chosen that is approximately one half-wavelength greater than the size of the particle of interest (Hubbard and Glasser 2005, p.156-157). For this study, a PulseEKKO Pro GPR system with a center frequency of 250 MHz was used that best met these limitations. Data from a 50 MHz GPR system collected in 2008 was also included.

3.3.2.4 Previous GPR applications in glaciology

GPR has been widely used to study ice properties and determine the thickness of many of the world's glaciers and ice caps (Bingham and Siegert 2007; Bingham and Siegert 2009; Hubbard and Glasser 2005; Irvine-Fynn et al 2006; Woodward and Burke 2007). It is also frequently used in combination with snow pits and ice cores to study annual snow layers, snowmelt processes, and snow accumulation variability (Dunse et al. 2008; Palli et al. 2002). Early radio echo sounding surveys of the Ellesmere Island ice shelves by Evans and Robin (1966) and Prager (1983) proved the technique to be successful for non-saline ice (Hattersley-Smith et al. 1969; Narod et al. 1988). Recent studies of northern Ellesmere Island's ice shelves have successfully used GPR to obtain ice thicknesses for both marine and meteoric ice areas, as well as for MLSI regions (Copland 2009; Mueller 2008).

In addition to determining ice shelf thickness, GPR has been used to infer structural characteristics of glacier ice and phase changes identified in GPR returns have been used to infer internal reflector horizon type (Hubbard and Glasser 2005; Irvine-Fynn 2006; Woodward and Burke 2007). For typical ice shelf imaging the ice-water interface returns a wavelet with the same polarity as the transmitted waveform [when $\varepsilon_1 < \varepsilon_2$], whereas a reversed polarity wavelet is returned [when $\varepsilon_1 > \varepsilon_2$] at the ice-air interface (Equation 3). The strong relative differences in dielectric constant between ice and water make the base of floating glaciers and ice shelves typically easy to identify (Table 3.3) (Hubbard and Glasser 2005; Prager 1983).

Table 3.3: Typical electrical properties for selected earth surface materials.
Source: Hubbard and Glasser (2005), Macheret et al. (1993), Woodward and Burke (2007).

Material	**Dielectric constant (E)**	**Velocity (m ns^{-1})**
Air	1	0.3
Snow	1.2 – 2.0 (dry); 1.5 – 3.3 (wet)	0.194 – 0.252
Cold ice	3 – 4	0.167 – 0.170
Warm (temperate) ice	1.9 – 2.1	0.14 – 0.16
Fresh water	80	0.033
Sea water	80	0.01

Differences in emitted signal power compared to returned signal power have previously been exploited to determine bed type and internal ice properties. Prager (1983) determined the basal power reflection coefficient (BPRC) and propagation loss rate from radio echo sounding data to infer ice type for the Milne Ice Shelf. Copland and Sharp (2001) used changes in bed reflection power (BRP_r) from radio echo sounding data to determine thermal and hydrological properties of John Evans Glacier, Nunavut. Significant englacial features including crevasses (bottom and surface) and impenetrable material (brine inclusions) have been successfully imaged and identified with the aid of GPR (Irvine-Fynn et al., 2006; Prager 1983; Woodward and Burke 2007). Identification of such features can provide additional information concerning an ice shelf's condition, particularly when repeated GPR surveys from a number of different years are available (e.g. stability and development of new cracks). Types of reflections that some of these objects may return are illustrated in figure 3.15.

3.3.3 Ice shelf thickness data sets

3.3.3.1 2008 GPR data set

In April 2008, GPR data was collected by Derek Mueller and Luke Copland during the Canadian Ranger's 2008 Op Nunalivut Patrol. Pulse EKKO Pro 250 MHz and 50 MHz GPR systems were used (Table 3.4). The 250 MHz system was custom fitted into a plastic sled and pulled behind a skidoo (~19 km hr^{-1}) by Kevin Attagutalukutuk and Douglas Nakoolak of the Rangers Patrol. The 50 MHz GPR system was custom fitted on a komatiq sled ~20 cm above the snow surface and towed at a speed of ~20 km hr^{-1} (Figures 3.11, 3.16 and 3.17). For both surveys, a built-in non-differential GPS (accuracy +/-5 m) was used to record position. System specifications are found in table 3.4.

Preliminary processing of the 2008 GPR data showed that the 250 MHz system was able to penetrate depths of up to ~100 m on the Milne Ice Shelf, corresponding to the

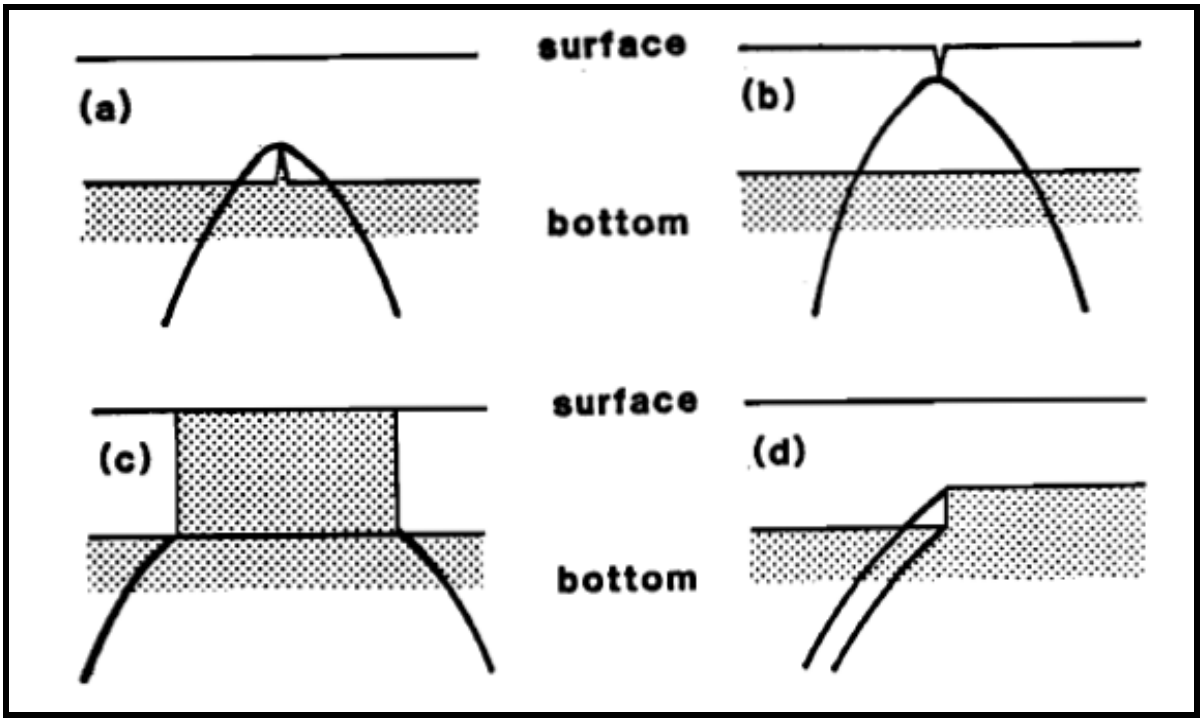

Figure 3.15: Diffraction patterns for certain features. The heavy lines represent expected diffraction patterns from (A) bottom crevasse, (B) surface crevasse, (C) unsoundable block of ice (likely caused by brine infiltration), and (D) step decrease in ice thickness. The shaded portion is impenetrable ice, rock, or water. Image reproduced from Prager (1983, p. 36).

thickest known ice found by Prager (1983). Thus, the 250 MHz system, which is smaller and therefore much easier to tow, was used for 2009.

3.3.3.2 2009 data set

The 2009 data set was collected by Colleen Mortimer and Luke Copland to derive general ice depths and re-profile Prager's (1983) survey lines (Figures 3.11, 3.16 and 3.17). To this end, the 1981 flight line map was georeferenced to a July 21st 2009 ASTER satellite image in ArcMAP 9.3. Specific routes to be driven were loaded onto handheld GPS devices using Fugawi Global Navigator software. Surveys were undertaken between 23 May 2009 and 3 June 2009. GPR system specifications are given in table 3.4.

A preliminary investigation was carried out 23 May 2009 to confirm that the 250 MHz system could penetrate the thickest known areas of ice, identified from the 1981 and 2008 surveys. The 250 MHz GPR system was mounted in a plastic sled (similar to set-up used in 2008) and pulled behind a skidoo at a speed of ~20 km hr^{-1} (Table 3.4; Figures 3.11, 3.16 and 3.17). A built-in GPS receiver (accuracy +/- 5m) inserted the position of each trace as it was recorded, providing specific location information to facilitate processing and interpretation of depth measurements. For navigation, a handheld GPS unit (accuracy +/-5 m) was mounted on the skidoo. Local topography, weather conditions (fog and snow), and safety (crevasses and open water) made following some flight lines difficult, particularly in the Central Unit of the ice shelf. A common midpoint survey (CMP) performed on May 28, 2009 on the Milne Epishelf Lake confirmed that a radio-wave velocity of 0.170 m ns^{-1} was appropriate for this study.

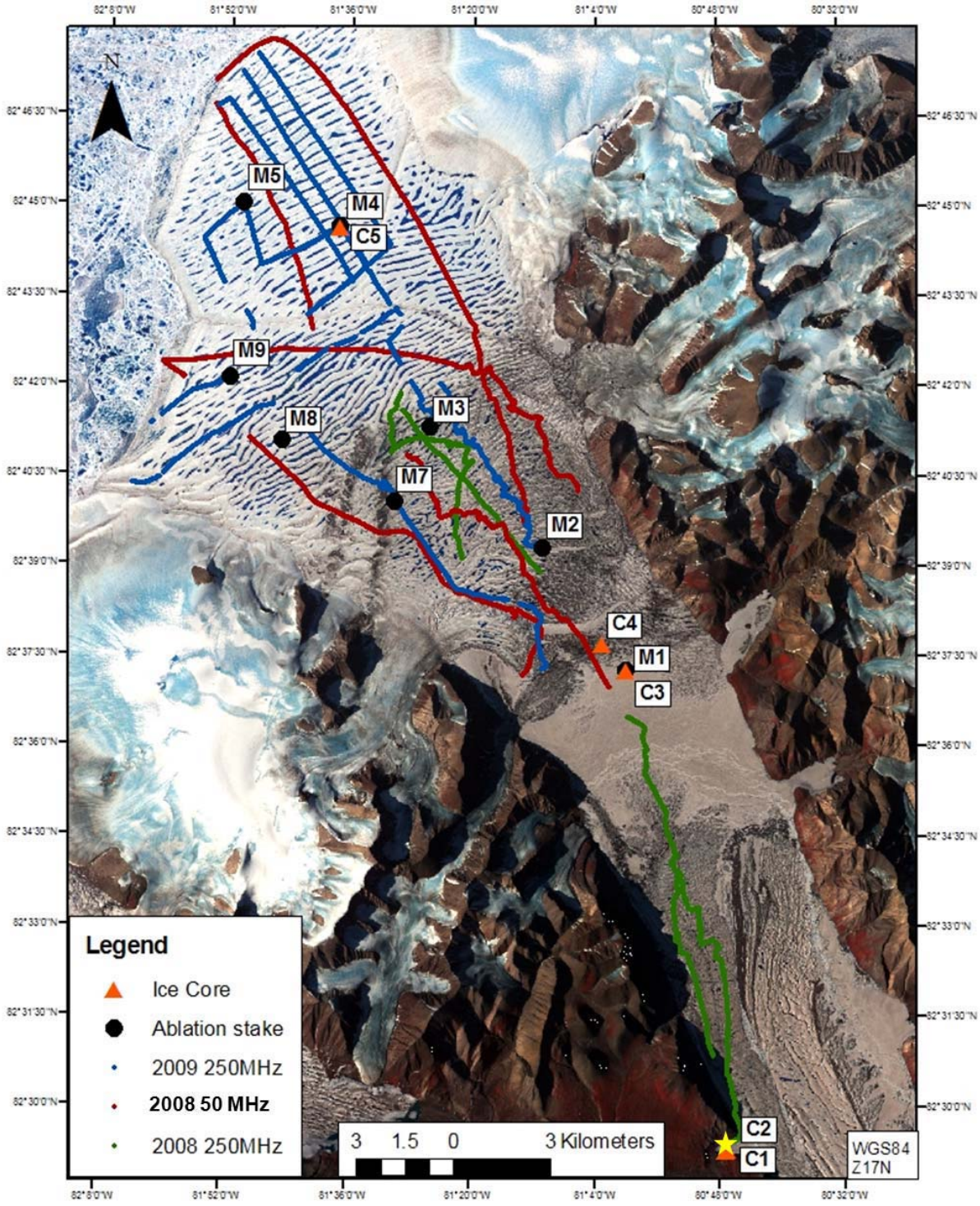

Figure 3.16: Field measurement sites for 2008 and 2009 on the Milne Ice Shelf overlaid on a 21 July 2009 ASTER image. Yellow star indicates location of common midpoint survey (section 4.2). C3/M1 indicates location of June 2009 epishelf lake water profile (Figure 2.23).

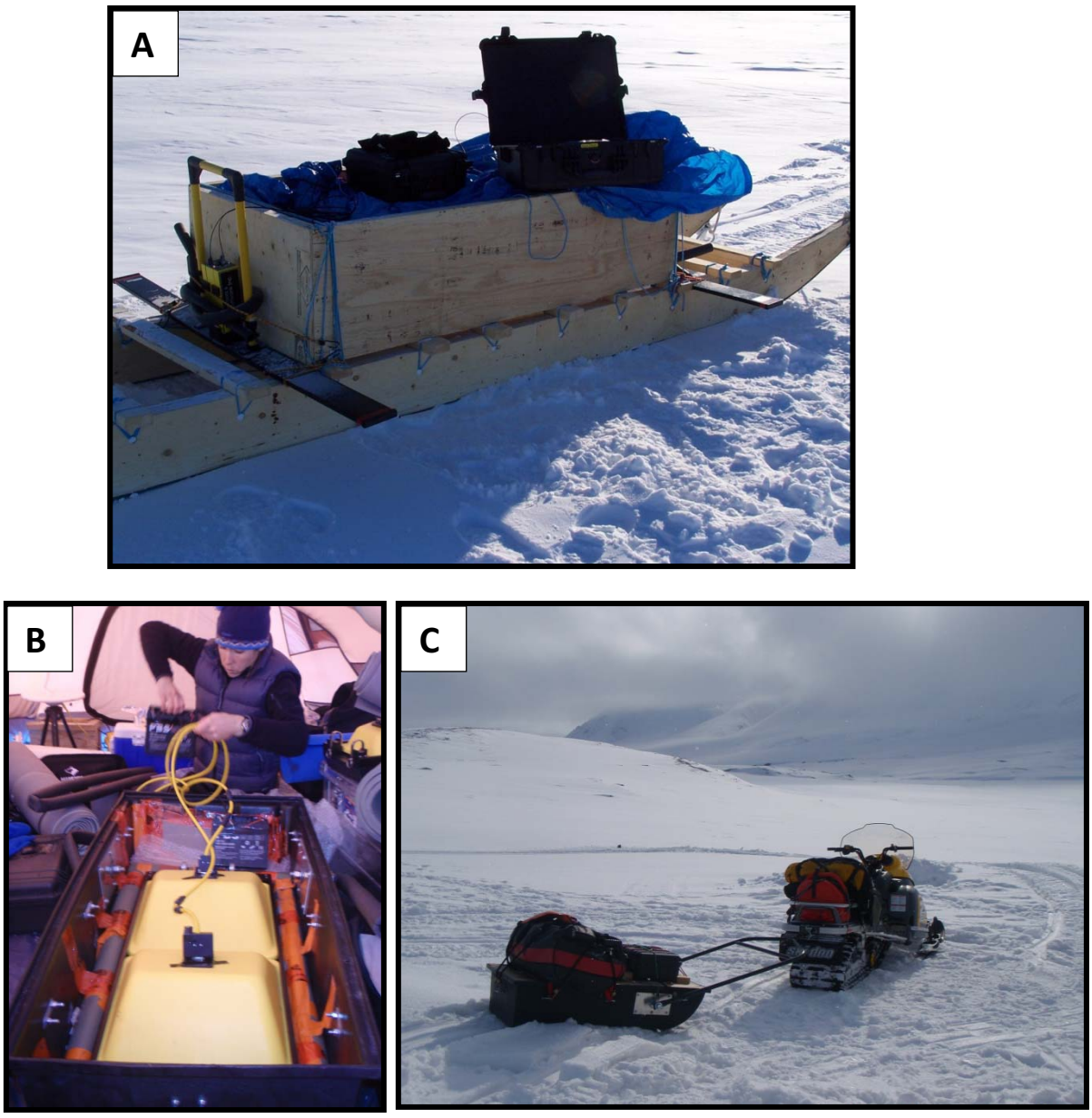

Figure 3.17: Ground penetrating radar field set-up. (A) 50MHz GPR system custom fitted onto a komatiq; (B) Custom fitting 250 MHz GPR into plastic sled; (C) GPR sled pulled behind a skidoo. Photos: Luke Copland (A&B), Colleen Mortimer (C).

Table 3.4: Ground penetrating radar system settings for 2008 and 2009.

	2009	**2008**	**2008**
Principal Investigator	Luke Copland and Colleen Mortimer, University of Ottawa	Derek Mueller, Carleton University	Luke Copland, University of Ottawa
Date	23 & 30 May 2009 3 June 2009	15 April 2009	April 4 2008 April 5 2008
GPR frequency	250 MHz	250 MHz	50 MHz
Time window	2000 ns	2070 ns	2000 ns
Sample interval	0.4 ns	0.6 ns	2.0 ns
Stacking	8 fold	8 fold	8 fold
GPS	Every trace	Every trace	Every 10^{th} trace
Survey type	Reflection	Reflection	reflection
Trace delay	0.5 s (23 & 30 May) 0.2 s (3 June)	0.2 s	NA
Antenna separation	0.40 m	0.40 m	2.0 m
Average speed	20 km hr^{-1}	19 km hr^{-1}	20 km hr^{-1}

3.3.3.3 GPR data processing and analysis

GPR data post-processing, including data editing and the application of spatial and temporal filters, was performed in EKKOView Deluxe to visually enhance the reflection at the ice shelf base. Initially, a DEWOW filter was applied to all traces, which removes low frequency signals resulting from near-field echoing, reflector roughness, and ice inclusions while preserving high frequency signals (Maurer 2006; Prager 1983). Trace differencing (a high pass spatial filter) was applied to enhance rapidly changing features such as the ice-water interface while suppressing flat-lying, constant features, and other artefacts. A two stage DVL gain filter was then applied to account for the reduction in returned power with depth. This filter first applies a linear gain function (Beta) to enhance signals at the desired depth followed by an '*s*-shaped' function (Alpha) which corrects for specific system response. This gain was used to visually enhance the bottom reflection at the expense of sensitivity to internal resolution. The post-processed radargrams (Figure 3.14) were then used to determine ice depths and used to identify cracks and other internal features.

Ice thickness was determined using Sensors and Software's IcePicker R4 software using a combination of automated and manual picking. The ice shelf base was identified in unit time (ns) and converted to depth by equation (6), which takes into account antenna separation and ice velocity.

$$T(m) = (((t + s / 0.3)\, V_I / 2)^2 - s^2 / 4)^{1/2} \quad (6)$$

Where t is the two-way travel time (ns), V_1 is the velocity for cold ice (0.170 m ns^{-1}), and s is the antenna separation. Final ice thickness measurements were displayed in ArcMAP 9.3 and error analysis was performed.

3.3.3.4 Radio-echo sounding: 1981

Present-day (2008/2009) thickness of the Milne Ice Shelf is compared with ice thickness measurements collected in June 1981 by Narod and Clarke (1983) and Prager (1983). The 1981 dataset was collected as part of a large-scale study which surveyed ~2000 km of flight lines over glaciers and ice shelves of northern Ellesmere Island (section 2.4.2), including the Milne Ice Shelf (Jeffries 1986b; Narod et al. 1988; Narod and Clarke 1983; Prager 1983). An 840 MHz radar system designed at UBC was mounted on a Twin Otter Aircraft. Parallel lines with a spacing of 1 km were flown at an airspeed of ~215 km hr^{-1} and ground clearance of ~120 m (Figure 3.18). Pulses were transmitted from the 90° corner-reflecting antenna at a rate of 10 KHz (10 ns separation). Returned signals were recorded on analogue magnetic tapes and later processed for ice shelf thickness and basal power reflection coefficient (BPRC) (Prager 1983). Omega navigation (uncorrected absolute accuracy of ~3 km, corrected accuracy of ~1 km) was used for positional information. It is noted that data for the Milne Ice Shelf yielded particularly good results for ice thickness and BPRC. Data available from this study for comparative analyses included a 15 km radargram section (Figure 3.19), a thickness contour map (Figure 2.16a), and BPRC map (Figure 2.16b).

3.3.4 Ablation stakes

Ablation stakes are used to measure the change in surface height over a specified period of time as a result of accumulation or loss of snow and ice (Hubbard and Glasser 2005). This method has traditionally been used in mass balance studies on small alpine glaciers where dense networks of stakes are easy to maintain. The longest continually monitored mass balance network, located at Storglaciaren Sweden, began in 1945 (Zemp et al. 2010). Along northern Ellesmere Island ablation stakes have been used to study the mass balance of the Ward Hunt Ice Shelf since 1959 (Braun et al. 2004; Braun 2011), and on nearby Axel Heiberg Island they have been used to determine the mass balance on Baby Glacier over a similar period (Adams et al. 1998) .

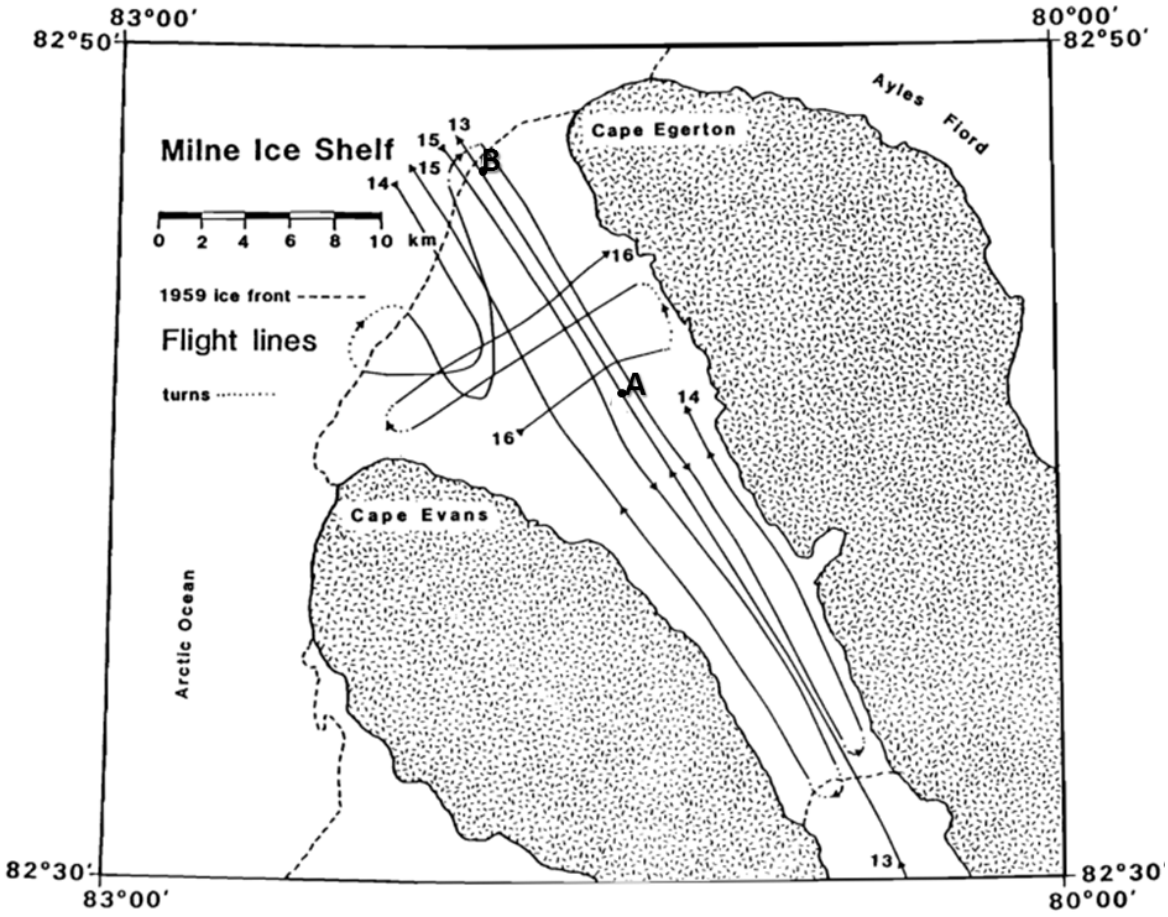

Figure 3.18: Flight line map for 1981 radio echo-sounding survey of the Milne Ice Shelf Prager (1983).

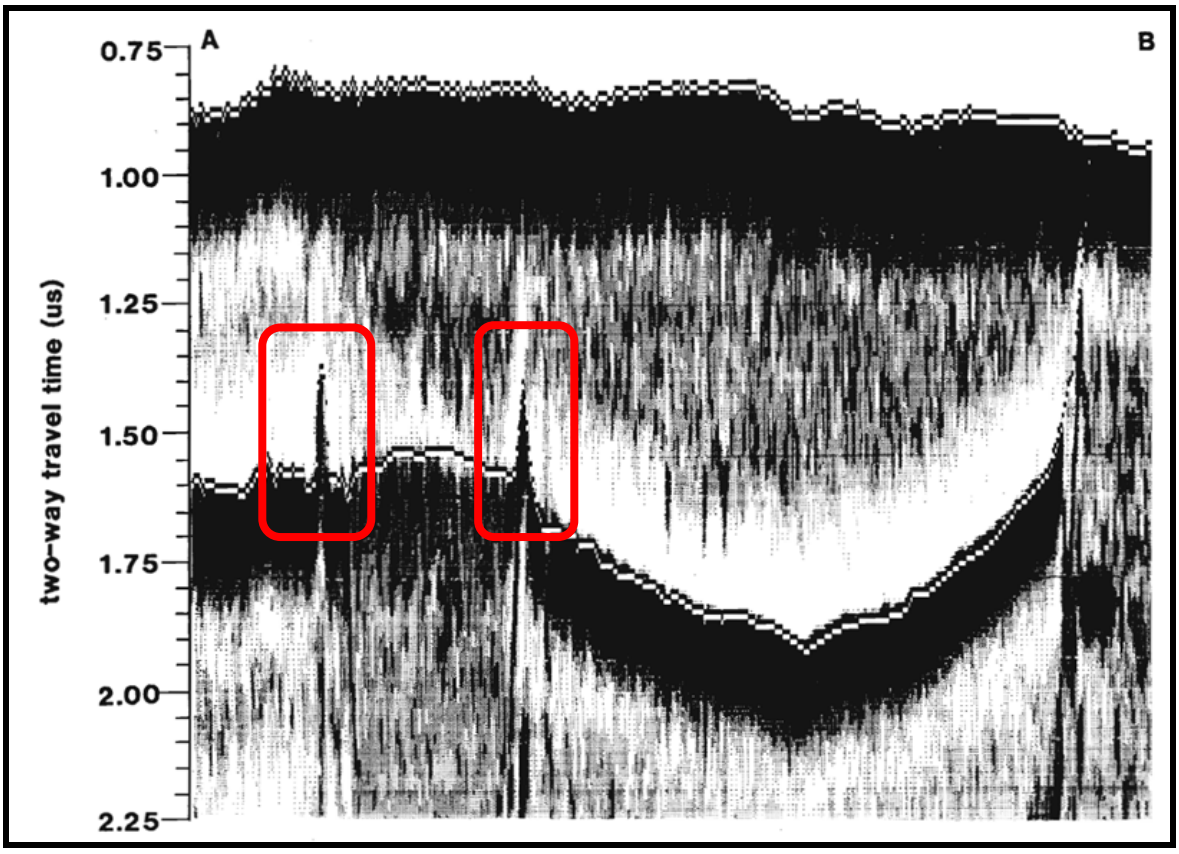

Figure 3.19: Radar section for the Milne Ice Shelf from 1981 RES survey. A and B refer to start and end points of radargram section (Figure 3.16). Two large bottom crevasses are indicated by the downward-opening hyperbolae (red boxes) which consist of gaps with no clear bottom reflection Prager (1983) suggests that this may imply that the ice between the crevasses is brackish. Source: Prager (1983).

Ablation stake measurements were taken over a 1-year period (2008 to 2009). Eight 3.04 m (10 ft.) long ablation stakes were installed on the Milne Ice Shelf in early April 2008 using a Kovacs hand auger (Figures 3.11 and 3.16). Five of these stakes were recovered on June 3, 2009 (Figure 3.16). The height of the pole out of the ice (measurement does not include snow) was taken and compared to the previous year's measurements. At each location, snow depth and density were measured and GPS coordinates were taken (Figure 3.11). These measurements are used to provide information regarding short term variations in accumulation and ablation when interpreting longer-term (1981 – 2009) mass balance change.

Chapter 4: Results

4.0 Introduction

This chapter summarizes the current state of the Milne Ice Shelf and how it has changed over the last 59 years. Field data and satellite imagery are used to provide a summary of the current (2008/2009) state of the Milne Ice Shelf. This is followed by an analysis of area change between 1950 and 2009. Thickness and volume change is quantified for the period 1981 – 2008/2009. Changes in surface characteristics (cracks and fractures) and sources of mass inputs (glaciers) and losses (calving and lake development) are monitored and used to interpret the observed area and volume changes and to assess the current stability of the Milne Ice Shelf.

In determining change over time, it is acknowledged that the change reported is a net change from one date to another and does not include any variability that may have occurred within each time period. In this study the term *between* refers to net change. Attempts are made, where possible, to indicate situations where important smaller scale variability may have occurred that was not captured in the image analysis. Further, it is noted that minimum ice shelf thickness values reported here are less than the 20 m thickness used to define an ice shelf. Since ice shelf ice thinner than 20 m has already been reported for the Milne Ice Shelf (Narod et al. 1988), a broader range of ice thickness values enables greater comparison.

4.1 Area change

Changes in Milne Ice Shelf area between 1950 and 2009 were determined from air photo mosaics (1950, 1959, 1974 and 1984) and satellite imagery (ERS-1, ASTER, RADARSAT-1, RADARSAT-2 for 1993, 2001 and 2009) (Table 4.1; Figure 4.1). A polygon was created to delineate the ice shelf in each image, from which the area was computed (Figure 4.2). Polygon differencing revealed a 28 ±1.0 % reduction in areal extent

Table 4.1: Milne Ice Self area change (1950 – 2009).

Time period	**Time interval (number of years)**	**Total area loss (km^2)**	**Rate of area change ($km^2\ yr^{-1}$)**
1950 – 1959	9	6	0.67
1959 – 1984	25	31	1.24
1984 – 1993	9	36	4.0
1993 – 2001	8	8	1.0
2001 – 2009	8	1	0.13
1950 – 2009	59	82	1.39

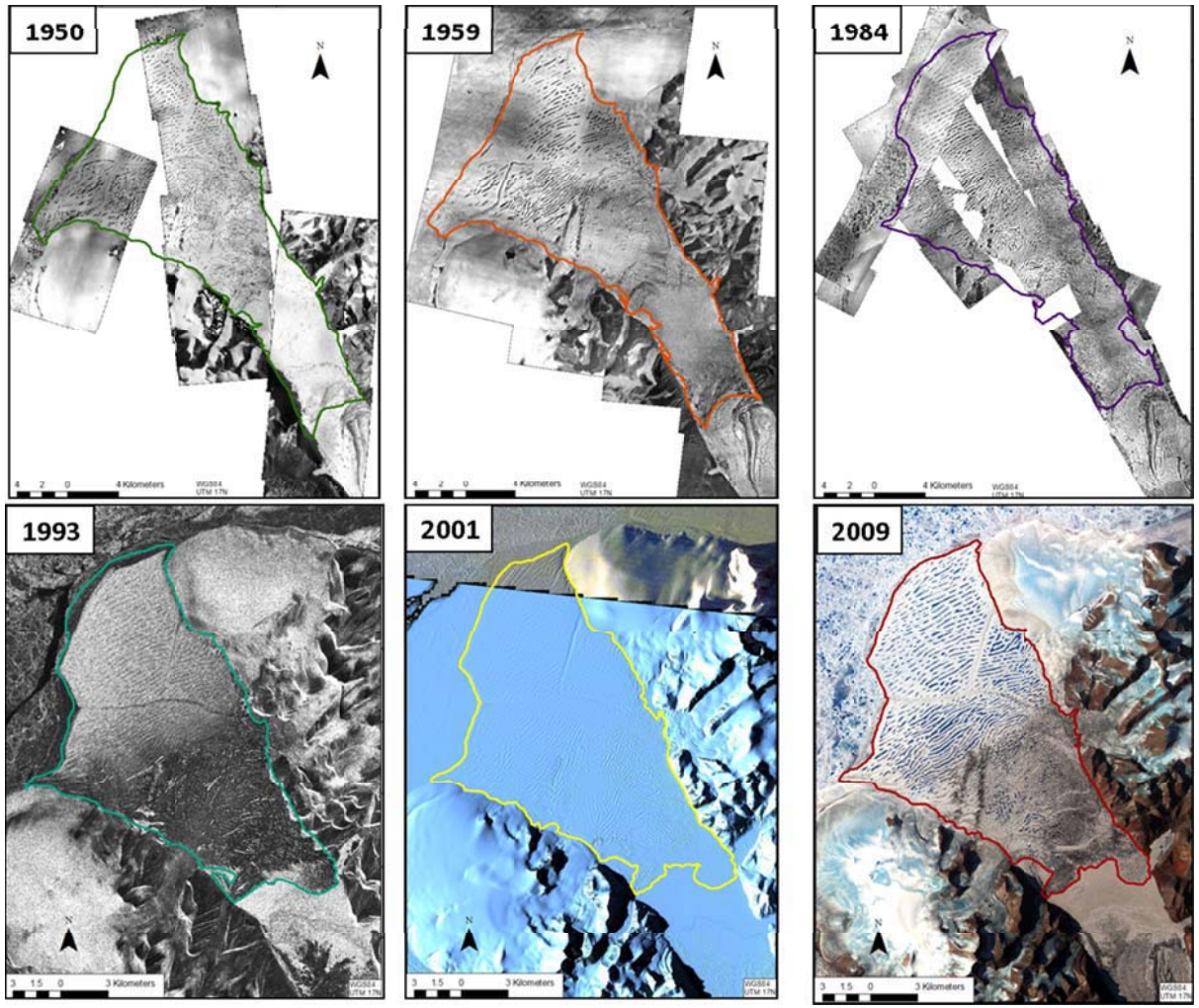

Figure 4.1: Milne Ice Shelf extent for 1950 to 2009. 1950, 1959, and 1984 polygons are overlaid on air photo mosaics. Polygons for 1993 (ERS-1: 19 May 1993), 2001 (ASTER: 23 May and 19 September 2001) and 2009 (ASTER: 21 July 2009) are overlaid on satellite imagery.

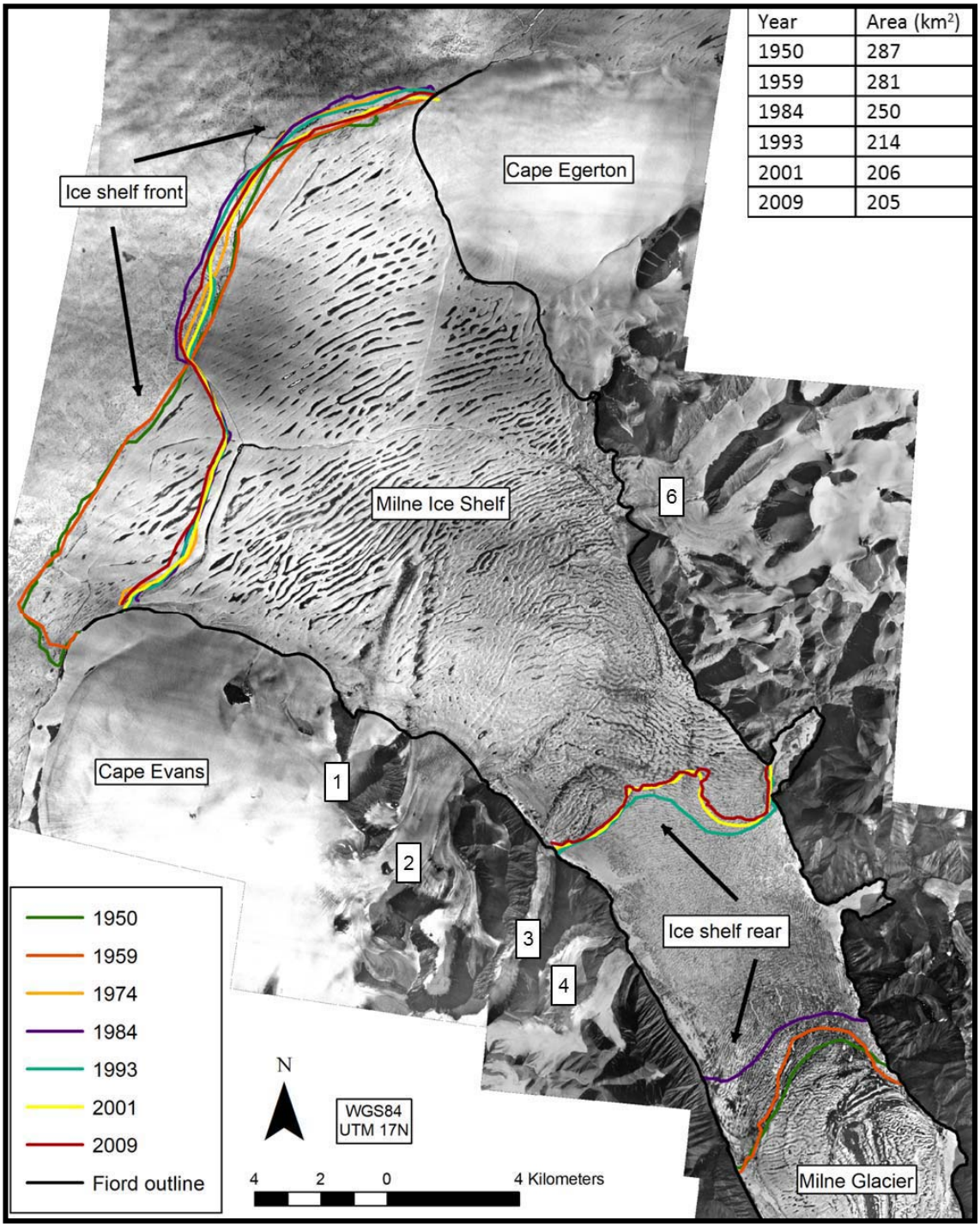

Figure 4.2: Temporal change in ice shelf extent (1950 – 2009) overlain on 1959 air photo mosaic. Numbers 1-6 indicate location of glaciers referred to in Figs. 4.15 – 4.19.

between 1950 (287 km^2) and 2009 (205 km^2). A reduction in ice shelf area was observed over each successive time period measured, with the largest losses between 1959 and 1984 (29 km^2) (Figure 4.1). Decreases in total area occurred due to: 1) calving from the ice shelf front; 2) advancement of the Milne Glacier at the rear of the ice shelf; and 3) development of ice-marginal and epishelf lakes. Overall changes observed at the rear of the ice shelf were much more pronounced than those at the front (Figure 4.2). The relative contribution of each of these processes differs over the various time periods studied, and are outlined in detail below.

4.1.1: Area change 1950 – 1959

A 6 km^2 decrease in ice shelf area occurred between 1950 (287 km^2) and 1959 (281 km^2). This is mainly attributed to the advance of the Milne Glacier, where the main tributary advanced ~660 m and the SW tributary ~600 m into the Inner Unit at the rear of the ice shelf (Table 4.2). A smaller amount of the area loss occurred due to an increase in ice dammed lake area from ~6 km^2 to ~8.5 km^2 between 1950 and 1959. Increased lake area results in a decrease in ice shelf area since these regions are not considered part of the ice shelf. These features mainly exist along the ice shelf margins adjacent to the fiord walls and, on the air photo mosaics, are distinguishable from the surrounding ice shelf ice by their smooth ice surface (absence of rolls and troughs) and reflective light grey tone and texture (Figure 4.3). The lake ice surface appears to be at a lower elevation than the surrounding ice shelf in the air photos and satellite imagery, which was confirmed by field observations (Figure 2.22). From the hydrostatic equilibrium principle discussed in section 2.5.3, this suggests that these lakes penetrate the entire ice shelf thickness, separating it from the fiord sidewalls (Braun 2011, Smith et al. 2007).

Table 4.2: Milne Glacier terminus change (1950 – 2009).

Time period	Time interval (number of years)	Main tributary total advance (m)	Southwest tributary total advance (m)	Main tributary rate of advance ($m\ yr^{-1}$)	Southwest tributary rate of advance ($m\ yr^{-1}$)
1950 - 1959	9	662.9	598.7	73.7	66.5
1959 - 1984	25	1410.0	1502.2	56.4	60.1
1984 - 1993	9	1155.9	1559.0	128.4	173.2
1993 - 2001	8	951.3	1182.9	118.9	147.9
2001 - 2009	8	975.8	740.4	122.0	92.5
1950 - 2009	59	5137.9	5583.8	99.9	108.0

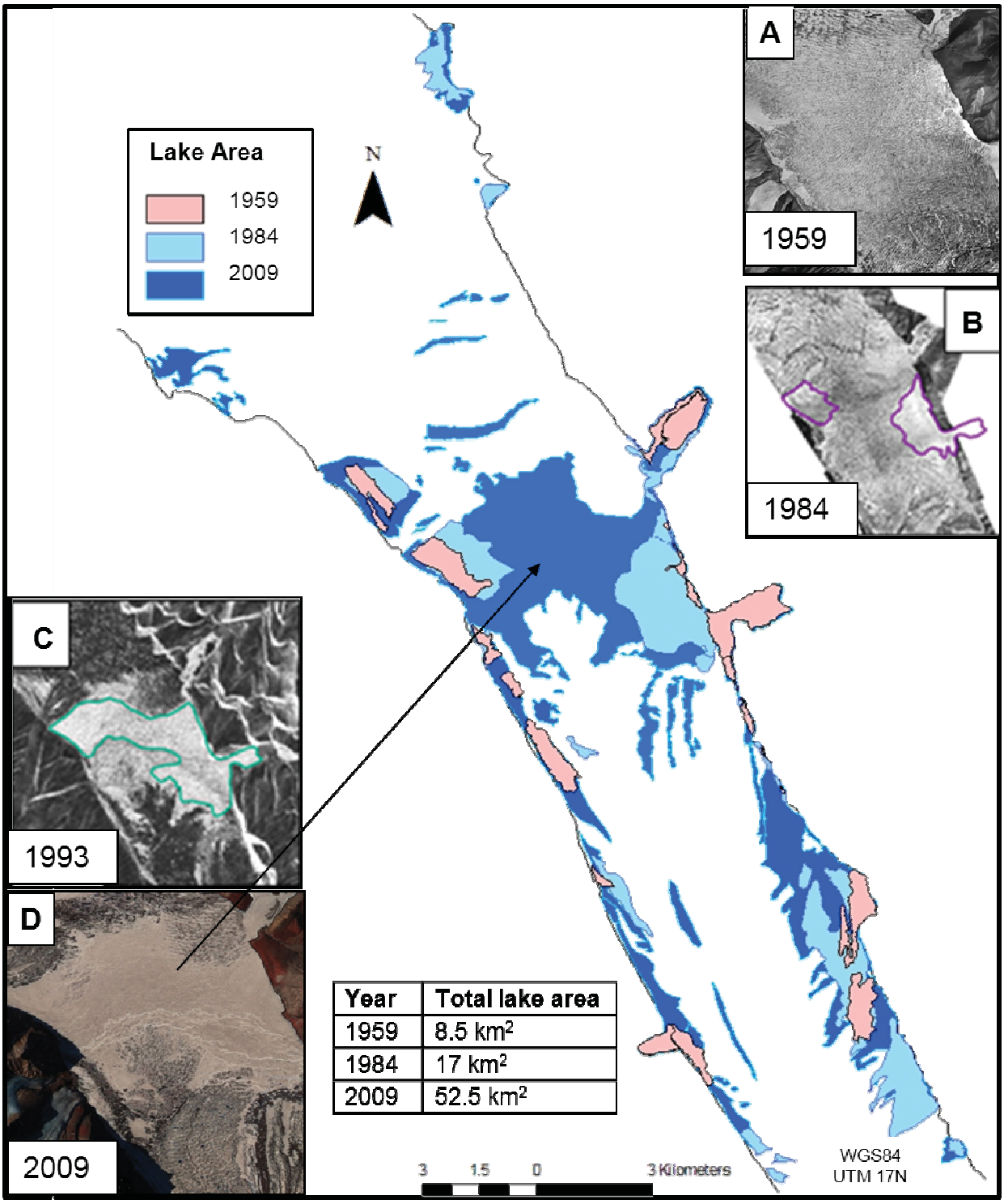

Figure 4.3: Lake development for the Milne Ice Shelf 1950 – 2009; A (1950 air photo) and B (1959 air photo) show development of Milne Epishelf lake between 1984 and 1993. C (1993 ERS-1 scene) and D (2009 ASTER scene) show change of inner unit from rolls and troughs to epishelf lake ice. Lake area (ice-marginal and Milne Epishelf Lake) is given for 1959, 1984, and 2009.

4.1.2 Area change 1959 – 1974/1959 – 1984

Between 1959 and 1984 the Milne Ice Shelf experienced an 11% (31 km^2) reduction in area (Figures 4.1 and 4.3). Over this 25 year period significant changes were observed at both the front and rear of the ice shelf. Significant expansion of ice dammed lakes, particularly in the Inner Unit, were also observed. Air photo analysis revealed the removal of 26 km^2 of ice from the northwestern corner of the Milne Ice Shelf, near Cape Evans, sometime between 1959 and 1974 (Figure 4.4). This calving event, which was the most significant change in the ice shelf front over the entire study period (1950 – 2009), was identified from air photo mosaics by a change in ice type. In 1959 the ice in the northwest corner had a well-developed ridge and trough surface, similar in appearance to the ice in the rest of the Outer Unit, suggesting that it was old, thick ice shelf ice. Two large fractures, visible in the 1959 imagery, appear to separate much of this old ice from the rest of the ice shelf and probably acted as lines of weakness for this calving event (Figures 4.4 and 4.5). The ridged ice shelf ice on the seaward side of these fractures that was present in 1959 is absent in 1974, replaced by a combination of perennial sea ice, fast ice, and MLSI. The dark colour and absence of any surface ridges indicates the presence of younger sea ice instead of old ice shelf ice. This area is referred to as the Milne Re-entrant (section 2.5.1).

In this study, thick MLSI with distinctive rolls and troughs is considered to be *incipient ice shelf* and is included in calculations of total ice shelf area. Younger MLSI that has not developed significant ridging and has a dark signature in SAR scenes (usually ice that is < 3 years old) is not considered to be part of the ice shelf. The slight ridging observed on the surface of the ice in the Re-entrant area in 1974 (Figure 4.5) suggests that the ice has been present in that location for several years and that it is likely that the ice has been stable since the main calving event.

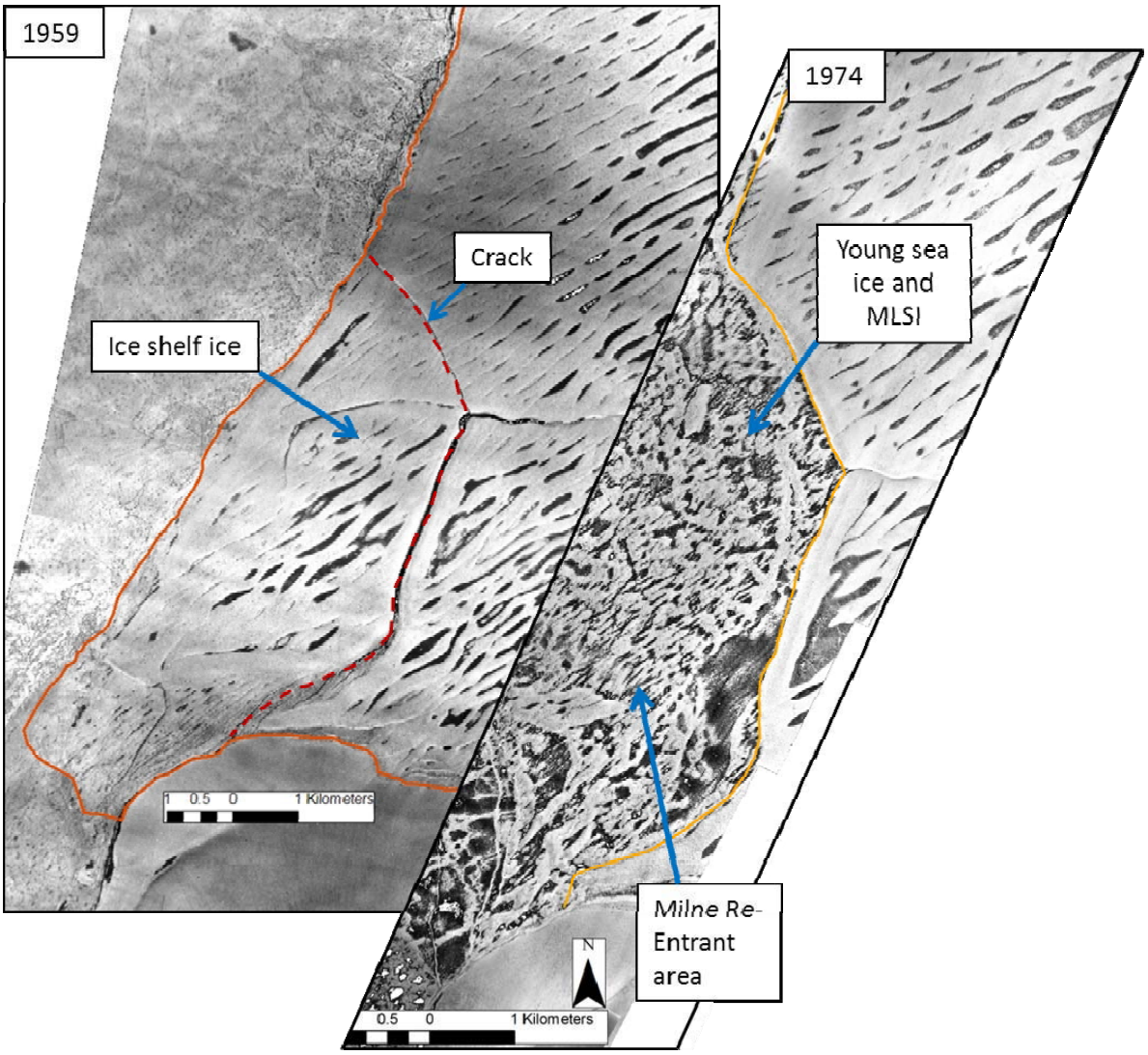

Figure 4.4: Change in northwest corner of Milne Ice Shelf front between 1959 and 1974 air photo mosaics. A calving event, leading to a loss of 26 km^2 of ice shelf area, occurred sometime during this period. Dark black lines highlighted with red dotted line indicate cracks that likely acted as lines of weakness. Note position and shape of 1974 front is very similar to the large cracks.

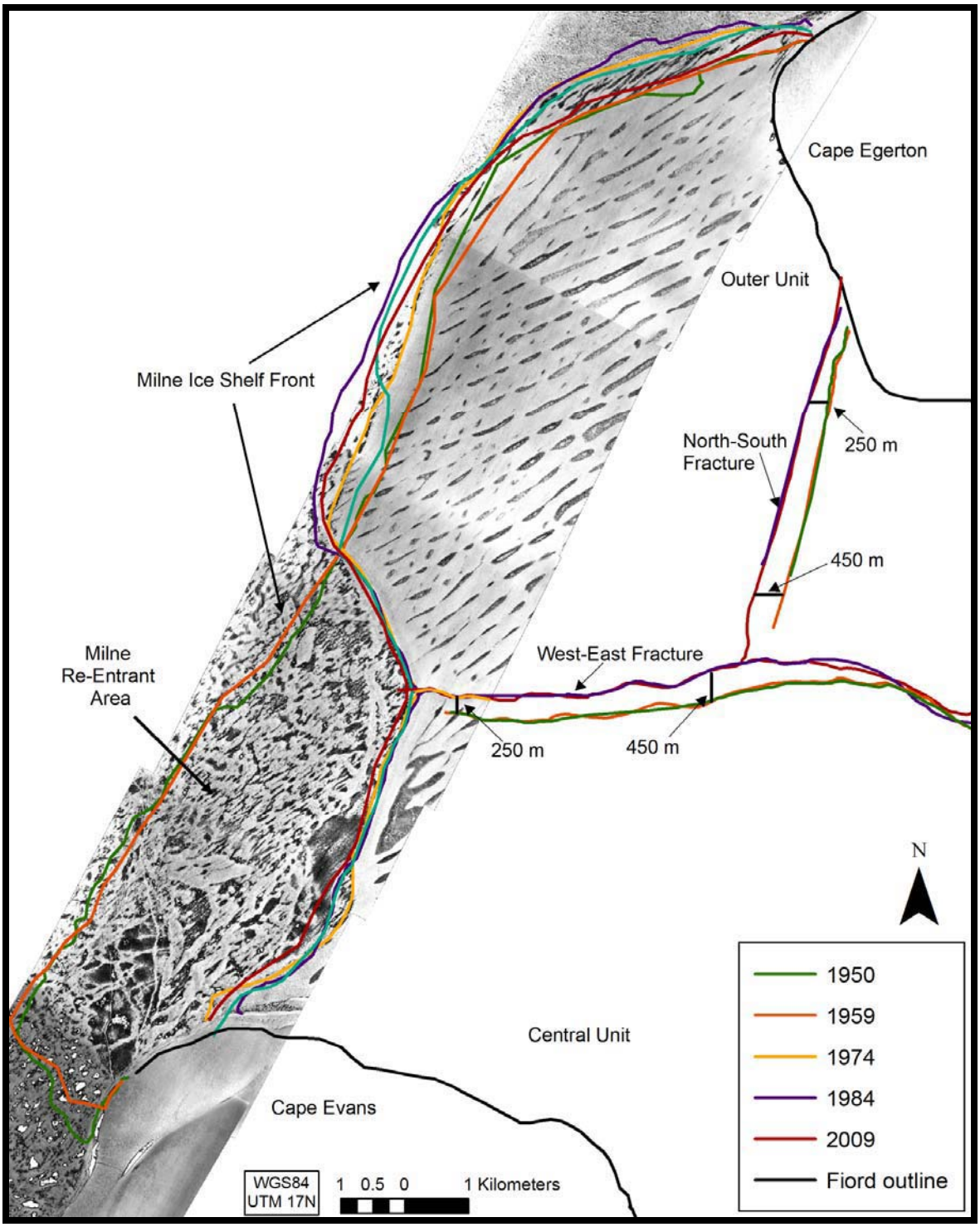

Figure 4.5: Temporal change in Milne Ice shelf front and fractures between 1950 and 2009 overlaid on a 1974 air photo mosaic. Development of Milne Re-entrant in 1974 from 1974 air photo also shown. 1993 and 2001 omitted due to insignificant change over this period (same position as 2009).

This event is likely the same calving event identified by Jeffries (1986a) who reported a loss of ~33 km^2 from the northwest corner sometime around 1965 (section 2.3.2) . Area loss measured in the current study is 21% smaller than reported by Jeffries (1985; 1986a; 1992a). Much of this discrepancy can be attributed to improvements in technology and measurement techniques not available at the time of the Jeffries (1986a) study. In particular, Jeffries (1986a) manually mosaicked the 1959 and 1974 air photos and approximated the area lost by multiplying the dimensions of the primary axes (3.75 x 8.75 km) of the calved ice island. In contrast, we digitally mosaicked and georectified the same air photos in ArcMAP 9.3 (section 3.3.1) to obtain a more precise measurement of area loss. Shallow ice cores collected by Jeffries and Krouse (1987) in spring 1985 from the Re-entrant area indicated the presence of 20-year old MLSI (sections 2.4.3 and 2.5.1). This suggests that the ice in the Re-entrant area did not undergo significant change (removal and re-building) between 1974 and 1984 following the calving event.

Coincident with the loss of 26 km^2 of ice from the northwest corner of the ice shelf was a change in the position of both the ice shelf front and the two characteristic re-healed fractures (Figure 4.5). The re-healed fractures appear as dark grey-black lines on the air photos and form a 'Y' shape on the central-outer portion of the ice shelf. Between 1959 and 1974 the position of these two fractures advanced seaward by ~250 – 450 m (Figure 4.5). In 1974 the ice shelf front to the east of the Re-entrant area is located ~450 m seaward compared to 1959 (Figure 4.5). Additional seaward advance (~500 m) of the ice shelf front was observed in this region between 1974 and 1984. Although this advance equates to an area increase of 8 km^2, reductions at the sides and the rear of the ice shelf as well as the large Re-entrant calving event itself resulted in a net reduction in ice shelf area between 1959 and 1984.

Reductions in area at the sides and rear of the ice shelf were only computed for the period 1959 to 1984 because the 1974 air photo mosaic was limited to the ice shelf front. Total lake area increased from 8.5 km^2 in 1959 to 17 km^2 in 1984 (Figure 4.3). The majority of this increase was the result of the conversion of Inner Unit ice to lake ice, identified from

air photo analysis by the conversion of ridged ice shelf ice to smooth lake ice (section 2.5.3). In 1959, surface rolls and troughs, which indicate the presence of older ice shelf, cover most of the Inner Unit. In 1984 two large areas of smooth ice with a reflective, grey tone and texture are visible along the sides of the fiords that extend into the centre of the ice shelf in the Inner Unit. These were not present in 1959. Further area reductions from the advance of the Milne Glacier by ~1.5 km between 1959 and 1984 were also observed (Table 4.2).

4.1.3 Area change 1984 - 1993

A 36 km^2 reduction in ice shelf area was observed between 1984 (250 km^2) and 1993 (214 km^2) (Figure 4.2). Aside from a small reduction in MLSI extent in the center of the ice shelf front, the position of the ice shelf front is essentially the same in both images (Figure 4.2). It is noted that Jeffries (1992a) reported calving of ice from the re-entrant area from a 1988 airborne SAR image. It was not possible to quantify area changes for this shorter time interval because the SAR imagery (February 1988 airborne X-band image) was not available. This time period also marks a change in data source from air photos to satellite imagery (section 3.3.1).

The 14.4% decrease in ice shelf area over this 9-year period is primarily the result of the establishment of the Milne Epishelf Lake. Between 1984 and 1993 two large ice dammed lakes that were visible in the 1984 air photo mosaic (Figure 4.3B) grew from locations along the fiord walls to form one large lake that is continuous across the full width of Milne Fiord (Figure 4.3C). The lake ice that had a smooth texture on the air photos appears bright white on the 19 May 1993 ERS-1 scene. In this spring SAR scene, the white reflectance of the Epishelf Lake, caused by a freshwater layer underlying it, is distinguishable from that of the Outer Unit in part due to an absence of roll and trough topography (Mueller et al. 2009; sections 2.5.3; 3.3.1). The presence of an epishelf lake during this period is corroborated by water profiles collected by Jeffries, who noted density stratification (freshwater layer above more saline water) below the ice surface at the rear of

the fiord in 1983 (Figure 2.14) (Jeffries 1985, Jeffries and Krouse 1987). In 1993, for the first time in this study, the Milne Ice Shelf was no longer connected to the Milne Glacier. This means that the Milne Glacier no longer provides direct glacier mass input to the Milne Ice Shelf, and advancement of the Milne Glacier terminus into the Milne Epishelf Lake does not affect total ice shelf area.

4.1.4 Area change 1993 – 2009

Between 1993 and 2009, ice shelf area decreased an additional 11 km^2 (Figure 4.2). The majority of this loss (10 km^2) occurred between 1993 and 2001 with negligible change (1 km^2) between 2001 and 2009. The 5% reduction in areal extent over this 16-year period (1993 – 2009) is attributed to: (a) the conversion of Inner Unit ice on the SW side of the ice shelf to Epishelf Lake ice (at the ice shelf rear), and (b) a decrease in MLSI extent (at the ice shelf front).

Cycles of MLSI calving and growth have been documented by Jeffries (2002) and Copland et al. (2007) for the Re-entrant area for periods shorter than the 16-year timespan investigated above. However, the extent to which this same process occurs across the entire front has not been investigated. The higher temporal resolution provided by satellite imagery (1993 – 2009) compared to air photo data sets (1950 – 1984) permitted quantification of spatial and temporal change in MLSI across the entire front of the Milne Ice Shelf over roughly 4-year time intervals. MLSI was delineated for 1993, 2001, 2005, and 2009 and polygon differencing was performed; 1993 was included to extend the time period for this MLSI study (Figure 4.6). MLSI extent for 2009 is taken as the average extent measured from ASTER and RADARSAT scenes (Table 4.3). Images used for this part of the study are listed in Table 3.2.

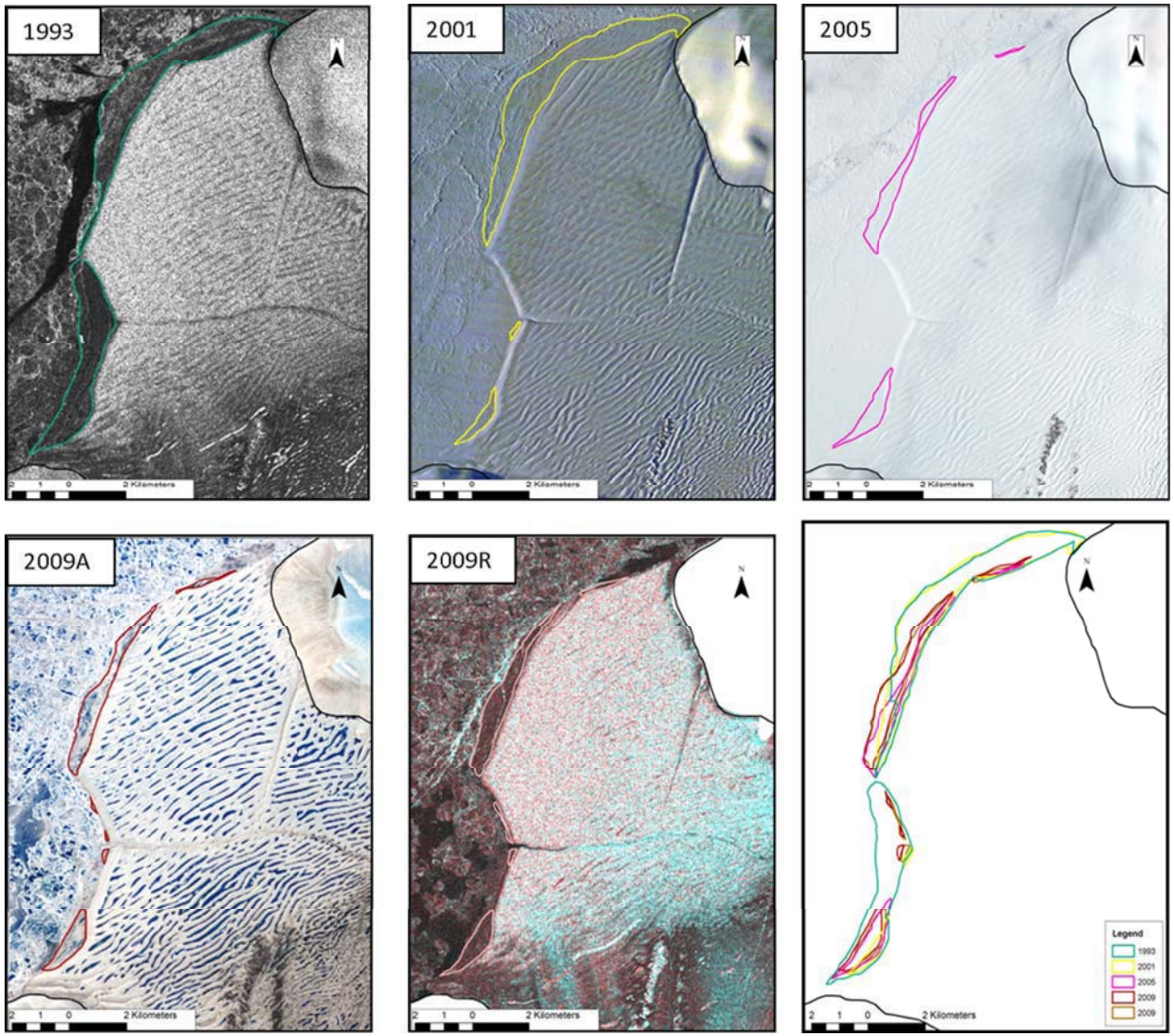

Figure 4.6: MLSI extent delineated on satellite scenes for May 19, 1993 (ERS-1), September19, 2001 (ASTER), June 19, 2005 (ASTER), July 21, 2009 (ASTER), May 15, 2009 (RADARSAT-2).

Table 4.3: Temporal and spatial change in MLSI extent for the Milne Ice Shelf front from 1993 – 2009 computed from satellite imagery (Table 3.2). Region A consists of the area to the NE of the Re-entrant and Region B consists of the Re-entrant area (Figure 4.7).

Year	**Region A km^2**	**Region B km^2**	**Total MLSI km^2**
1993	8.7	6.4	15.1
2001	8.93	0.7	9.7
2005	1.30	1.2	1.4
2009 Aster	3.0	1.3	4.2
2009 Radarsat-2	3.1	1.4	4.5
2009 average	3.06	1.32	4.37

To permit comparison between years, high resolution satellite images from the same time of year were used. Early summer scenes, acquired prior to melt-onset, provide the best data because visible scenes are not completely snow-covered and SAR scenes are not too dark from attenuation of the signal by water content from summer melt. Change detection is limited by the lowest resolution image, where only variability greater than the largest pixel size can be determined. The data set used here (lowest resolution data: RADARSAT-2 with pixel size of 40 x 40 m, Table 3.2) permits quantification of change greater than 0.0016 km^2.

Finally, since both SAR and visible scenes were used to compute MLSI area, a comparison was performed to determine the extent to which the different data sources affected total measured MLSI extent. MLSI area calculated from a July 21, 2009 ASTER scene was 0.3 km^2 less than that calculated from a May 15, 2009 RADARSAT-2 scene. These differences in area are likely due to both a resolution effect and differences in ice type imaged by the different sensors. However, the overall uncertainty is still much less than the area changes being measured (Table 4.3), so it is reasonable to infer that much of the measured change in MLSI area is the result of actual MLSI gains and/or losses and not simply the result of differences in satellite data sources.

To investigate spatial changes in MLSI extent over time the ice shelf front was divided into two regions. Region A consists of the area to the northeast of the large suture, Region B consists of the front in the Re-entrant area (Figure 4.7). Over the period 1993-2009, maximum MLSI area (15.1 km^2) was observed in 1993 and minimum extent (1.4 km^2) in 2005 (Table 4.3; Figure 4.7). In 1993 MLSI extent was 8.7 km^2 in Region A and 6.4 km^2 in Region B. Loss of ~5.5 km^2 of MLSI from Region B was observed between May 19, 1993 and May 23, 2001 but little or no change was observed in Region A (Figures 4.6 and 4.7). 2001 marked the minimum extent (0.7 km^2) of MLSI in the Re-entrant area and may be the result of a recent calving event. Between May 23, 2001 and June 19, 2005 partial re-growth of ~0.5 km^2 of MLSI was observed in Region B, although the removal of 7.63 km^2 from Region A resulted in a net reduction (~8.2 km^2) over this period. Re-growth of ~1.8 km^2 of MLSI in Region A was observed between 2005 and 2009. Over the same period,

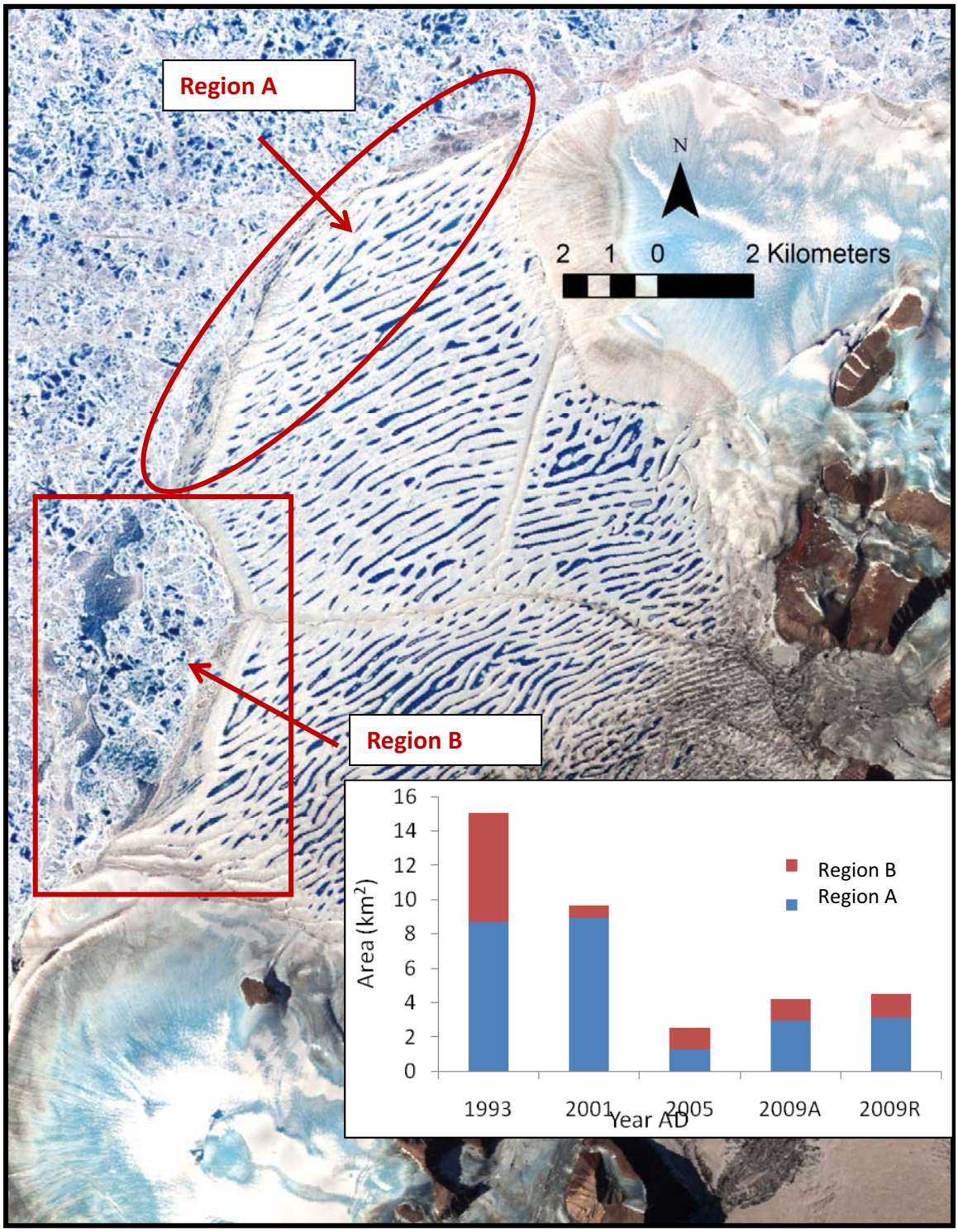

Figure 4.7: Sub-regions used to quantify spatial changes in MLSI from 1993 – 2009 overlaid on a July 21, 2009 ASTER scene. Inset graph shows MLSI area for 1993, 2001, 2005, and 2009. 2009A indicates measurements made from the July 21, 2009 ASTER scene and 2009R is from the May 15, 2009 RADARSAT-2 scene.

MLSI extent in Region B remained relatively stable (Table 4.3; Figures 4.6 and 4.7). Overall, although periods of increasing and decreasing MLSI occurred between 1993 and 2009, a net reduction of 10.7 km^2 (71%) was observed.

4.1.5 Area change: assessment of uncertainty

In computing total ice shelf area and area change from air photo mosaics and satellite imagery several sources of uncertainty arise. Air photos were georectfied to assign spatial coordinates from the base image (21 July 2009 ASTER scene) and the root mean squared error (RMSE) was recorded (Appendix 1). In the image mosaicking process, the RMSE represents only one source of error as it provides information about the transformation's accuracy, but not the registration's accuracy. The computed RMSE error is the difference (residual error) between the specified control point on the base image and the location of the tie point on the image being georeferenced after the specified function is applied (1^{st} order polynomial was used for all images, section 3.3.1.1) (ArcMAP 9.3 Desktop Help). Photos with a larger footprint (e.g. 1950 and 1959) tended to have a higher RMSE than those with a smaller footprint (e.g. 1984). RMSE ranged from 4.0 m to 55.3 m. Average RMSE was computed for each year (1950: 28.7 m, 1959: 27.1 m, 1974: 17.8, and 1984, 15.3 m) from which an overall average RMSE of ~19.0 m was derived (Appendix 1).

Although error resulting from the georectification process can be quantified, other sources of uncertainty cannot. Air photo mosaicking necessitates human interpretation, which can introduce errors especially when few ground control points are available. For most air photos where a suitable number of good ground control points were available, it was possible to overlay the air photo to match the satellite base image and produce a low RMSE. However, many photos captured only ice and snow and had no good (land-based) GCPs, so large identifiable features (surface ponds) were used to join these images with ones containing land-based GCPs.

A mosaicking uncertainty of ~200 m was estimated from the difference in position of similar features on separate images after the photos had been georectified. Satellite images were shifted to adjust for position, but not resampled, so no georectification error was computed. However, a positional error on the order of ~100 m is likely. Overall uncertainty (RMSE, mosaicking uncertainty, satellite image positional error) for area change was estimated to be < 1 km^2. For all but the most recent time period (2001-2009), area changes measured were on the order of many square kilometres, so this error is relatively insignificant.

4.2 Quantification of ice thickness

This section summarizes the current ice thickness distribution across the Milne Ice Shelf, and then evaluates the change in thickness between 1981 and 2008/2009. Total volume change between 1981 and 2008/2009 is also investigated.

Before detailed ice thickness maps can be constructed, it is important to validate the effectiveness of the measurements made by the PulseEKKO Pro GPR system in this study. This was achieved via interpretation of post-processed radargrams (section 3.3.3.3), since the large contrast in dielectric properties between glacier ice and water should result in a strong reflecting horizon at the ice shelf base (section 3.3.2.1). For most GPR traces collected over the Milne Ice Shelf and Milne Epishelf Lake in spring 2008 and 2009 the ice-water interface was indeed clearly identifiable. On each radargram two continuous lines are visible (Figure 4.8). The uppermost line, which is always darker and thicker, corresponds with the air-ice interface and is referred to as the surface reflection. Discontinuous light lines in the upper 15 m of the ice thickness likely correspond to internal reflecting horizons such as ice lenses within the iced-firn layer (Figure 4.8; Copland and Sharp 2001; Fynn et al. 2006; Woodward and Burke 2004). A second mostly continuous dark purple line was usually visible much lower down on the trace. For this line, the distinct peaks and troughs visible on the radargram (prior to correcting for surface topography) correspond with the

known roll and trough topography of the ice shelf surface. This apparent roll and trough bed topography does not necessarily indicate that the bed has an undulating surface; it most likely corresponds to the observed surface topography, although an accurate determination was not possible. Correction for elevation using the GPS data removed some but not all of the bed undulations, but this process is limited by the relatively poor elevation control on the non-differential GPS data collected by the GPR system.

Comparison of the location of known cracks identified on satellite imagery, marked in the field with an independent GPS unit, and viewed on the radargram confirmed that the GPR's internal GPS system was providing accurate positional information For example, the red star on Figure 4.8 corresponds with the location of a crack identified in the field and is visible on the July 21, 2009 ASTER image. This location corresponds with the absence of a bed reflection in the radargram, combined with rapidly increasing ice thicknesses on both sides and the presence of two downward dipping hyperbolae. This type of image in GPR returns has previously been attributed to crevasses and large cracks (Prager 1983; Woodward and Burke 2004).

Based on the common midpoint survey on Milne Epishelf Lake, a velocity of 0.170 m ns^{-1} was used to convert TWTT to ice depth (Figure 3.18). This velocity is consistent with other studies for cold glacier ice (Hubbard and Glasser 2005; Macheret et al. 1993; Woodward and Burke 2007). Comparison of the GPR derived ice thickness measurements with ice cores taken from the Milne Epishelf Lake in 2009 also provides confidence in our GPR measurements.

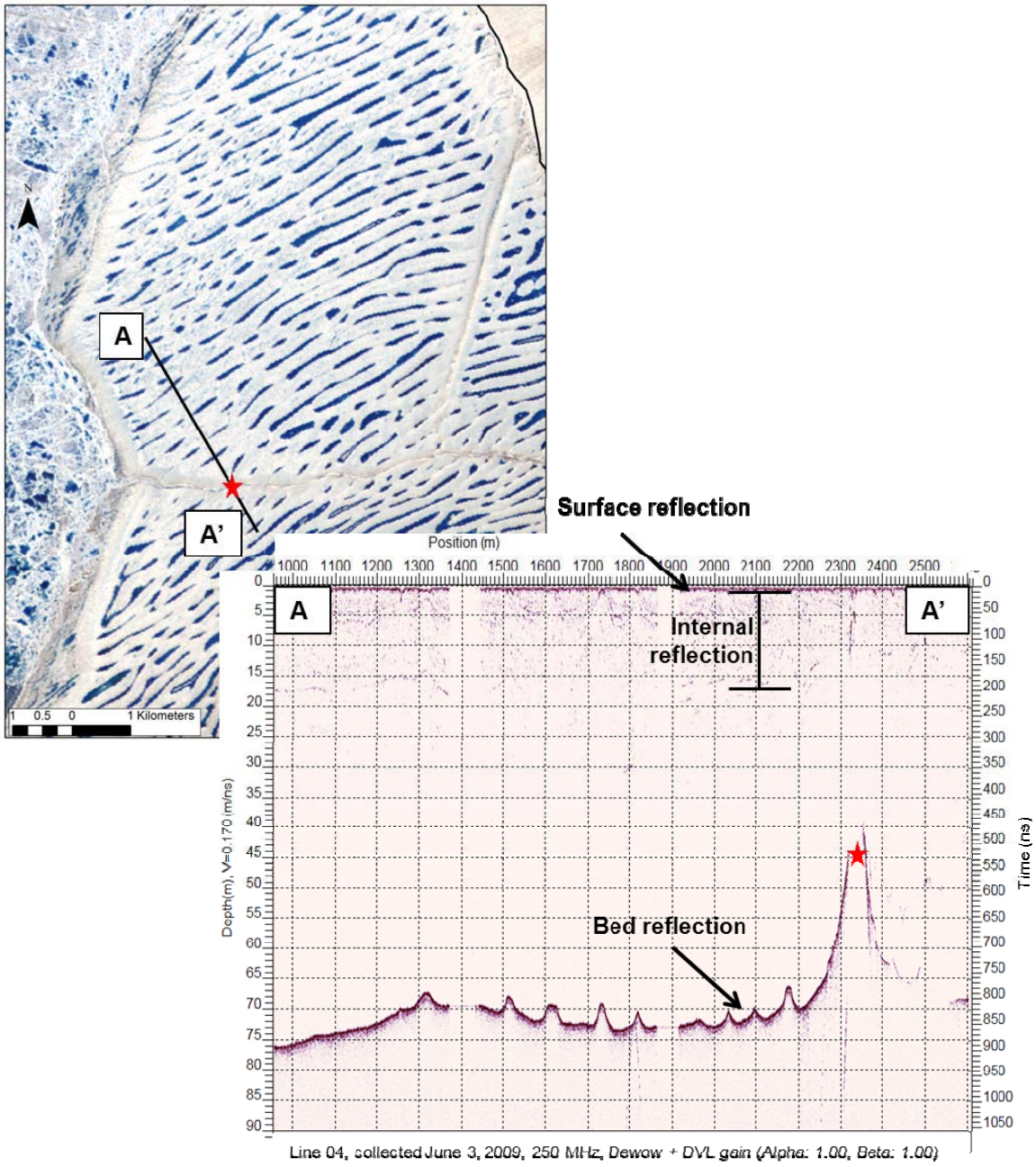

Figure 4.8: Radargram section for ground penetrating radar transect from the Outer Unit, June 3, 2009. The red star indicates location of crack. Location of GPR transect is shown on a July 21, 2009 ASTER scene, identified by black line, starting at point A and ending at point A'.

4.2.1 Ice thickness error analysis

Potential errors in the 2008/2009 ice thickness measurements arise from several potential factors:

(a) In terms of system set-up, the 50 MHz system sat ~20 cm above the snow surface, whereas the 250 MHz system sat directly on top of the snow surface. To correct for this difference, the ice-air distance was multiplied by 0.3 m ns^{-1} (speed of light) for the 50 MHz surveys and this value was then subtracted from the initial ice thickness measurement.

(b) Errors in ice depth measurements also arise from the resolution of the radio-wave in ice, and are typically quoted as $1/10^{th}$ of the transmitted wavelength (Copland and Sharp 2001). This equates to ±0.07 m for a centre frequency of 250 MHz and ±0.34 m for the 50 MHz system.

(c) In determining ice thickness it was assumed that the bed reflection occurs at the midpoint between the transmitter and the receiver. Antenna separation leads to an over-estimation of ice thickness because the ice thickness being measured is the angular distance (transmitter-bed-receiver) and not the straight line distance from the midpoint. For the 250 MHz system, this leads to an overestimation of 0.2 mm for an 80 m ice thickness and 1 mm for a 20 m ice thickness. For the 50 MHz system the overestimation is 6 mm (80 m thick) and 2.5 cm (20 m thick).

(d) Errors in depth measurement attributed to identification of the bed peak from the radargrams were quantified via a cross point analysis. For this analysis the guiding principle is that when repeat passes of a specific site are performed, the ice thickness measured at that location should be the same once GPS precision (±5 m in this study) is taken into account. After all other uncertainties and sources of error have been accounted for; most of the remaining differences in ice thickness determined at an intersection (cross-point) can be attributed to errors in manual and automated identification of the bed peak.

In this study a total of sixteen cross-points were identified (Figure 4.9). The difference in average thickness within a radius of 5 m (GPS precision) from the cross-point was computed for both transects. The difference in average thickness between the two

transects was taken to be the initial error for that cross-point. This process was repeated for all sixteen cross points. Descriptive statistics (maximum, minimum, average, spread), as well as the morphological unit (Outer, Central, Inner) and data set (year and resolution) were recorded (Table 4.4). This information was used to determine any bias or systematic error between data sets or ice shelf units and was also used to refine the thickness measurements. In this study the final cross-point error value was ±1.56 m (Table 4.4).

Total error for ice thickness measurements derived from GPR data was taken as the sum of i) the GPR resolution, ii) antenna separation iii) data processing error from the cross-point analysis. Using the average ice shelf thickness (55 m), total ice thickness uncertainty was ±1.91 m for the 50 MHz system and 1.63 m for the 250 MHz system. This equates to an uncertainty of 2.97% to 3.47% of the total ice thickness with the majority of the error attributed to GPR processing and ice-bed interface identification. For this study, an overall uncertainty of 3.5% was applied to all ice thickness measurements and provides confidence in the GPR results described below.

4.3 2008/2009 ice shelf thickness and volume

Overall, the mean thickness of the Milne Ice Shelf was ~55±1.9 m for 2008/2009, with a standard deviation of 22 m (Table 4.5). However, there were marked local variations (Figure 4.10A). The majority of the Outer Unit consists of very thick ice (70 – 80 m), with ice thickness decreasing rapidly towards the ice shelf front (20 - 30 m) and in proximity to the re-healed fractures (~20 m). Compared to the Outer Unit, ice in the Central Unit is consistently thinner (average ~50 m) and much more variable. Overall, the Central Unit also exhibits the greatest variability in ice thickness; both the maximum (94 m; Figure 4.11A black triangle) and minimum (<10 m) ice thicknesses are located there.

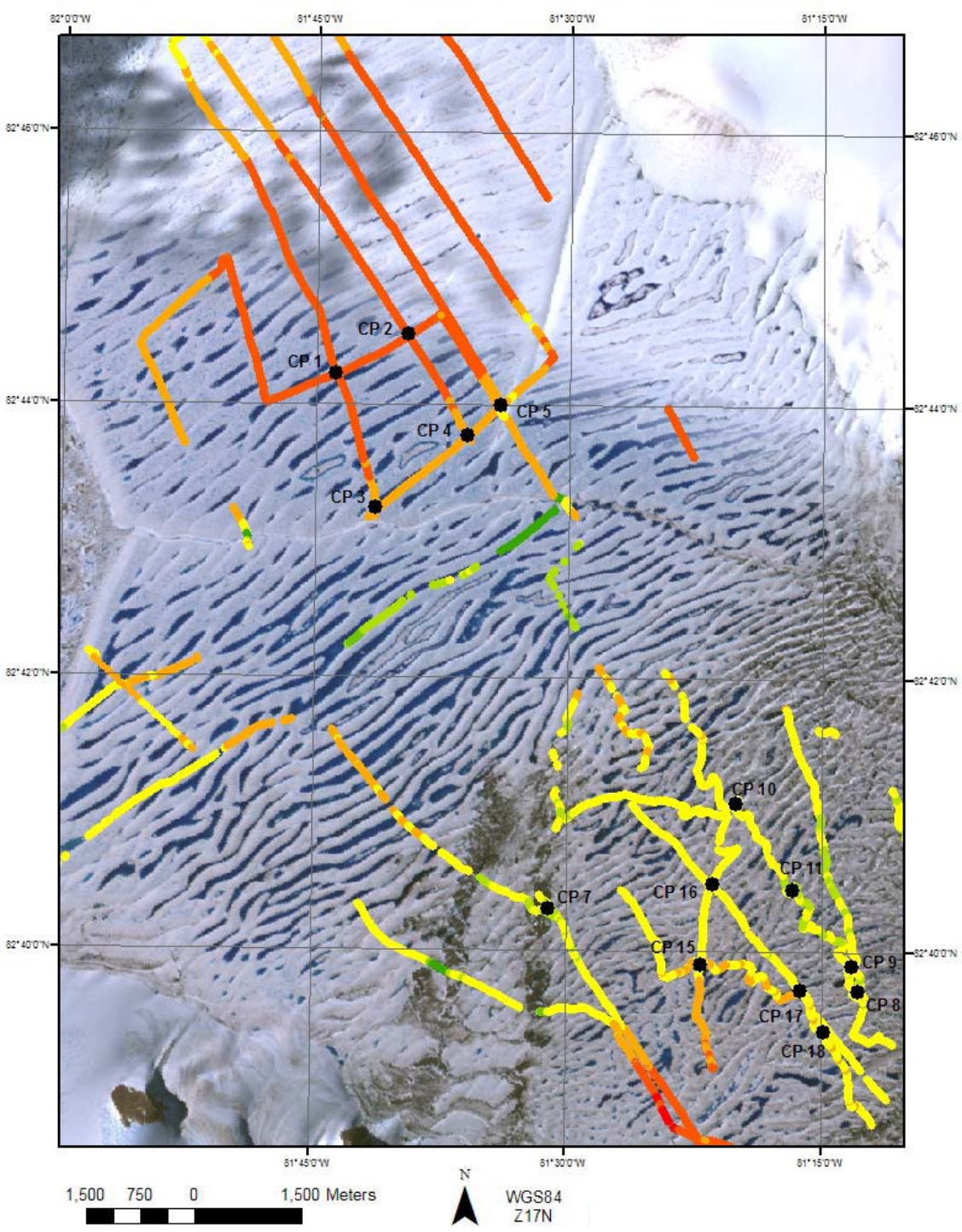

Figure 4.9: Cross point sites for 2008 and 2009 ground penetrating radar thickness error analysis measurements overlaid on a July 21, 2009 ASTER scene.

Table 4.4: Ground penetrating radar ice thickness cross-point error analysis (Figure 4.9).

Cross point	Ice Shelf Unit	Line 1 (year, frequency)	Line 2 (year, frequency)	Ice thickness (m)	Ice thickness error (m)	Ice thickness error (%)
1	Outer	2008, 50 MHz	2009, 250 MHz	83.93	3.36	4.00
2	Outer	2009, 250 MHz	2009, 250 MHz	83.49	0.02	0.03
3	Outer	2008, 50 MHz	2009, 250 MHz	67.22	2.28	3.39
4	Outer	2009, 250 MHz	2009, 250 MHz	64.88	0.26	0.40
5	Outer	2009, 250 MHz	2009, 250 MHz	56.10	0.94	2.07
7	Central	2009, 250 MHz	2009, 250 MHz	45.51	0.84	1.84
8	Central	2009, 250 MHz	2008, 50 MHz	47.22	5.47	11.60
9	Central	2009, 250 MHz	2008, 50 MHz	49.44	3.08	6.23
10	Central	2009, 250 MHz	2009, 250 MHz	49.31	0.12	0.17
11	Central	2009, 250 MHz	2009, 250 MHz	41.60	0.20	0.48
12	Central	2009, 250 MHz	2009, 250 MHz	46.43	0.26	0.21
13	Central	2009, 250 MHz	2009, 250 MHz	48.23	0.04	0.42
15	Central	2008, 250 MHz	2008, 50 MHz	55.44	2.44	4.40
16	Central	2008, 250 MHz	2008, 250 MHz	50.38	0.48	0.96
17	Central	2008, 50 MHz	2008, 250 MHz	57.08	2.26	3.90
18	Central	2008, 250 MHz	2008, 50 MHz	54.44	2.89	5.32
Average				56.29	1.56	2.84

A contour map of ice thickness was produced from the GPR point measurements. Interpretation of the ice shelf surface from 2009 satellite imagery (ASTER and RADARSAT-2) aided in the extrapolation of contour lines to areas that were not traversed with the GPR. For example, shallow contour lines were drawn around cracks and lakes which are known to have very thin ice. Higher value contour lines were drawn around areas which GPR measurements indicated were thick, such as where a glacier flows onto the ice shelf. The contour map was produced in ArcMAP 9.3 (Figure 4.12B) and an inverse distance weighting function was applied to produce a raster surface of ice thickness. The 2009 area polygon delineated from the July 21, 2009 ASTER scene was used as a mask to extract the thickness values contained within the 2009 ice shelf boundary (Figure 4.12C). This thickness DEM was used to interpret spatial variations in ice thickness and to compute total ice shelf ice volume.

In determining ice shelf volume for this study, MLSI with distinct rolls and troughs is generally included as part of the ice shelf. On the ground it is difficult to determine the exact boundary between the ice shelf ice and old MLSI as both have a gently rolling topography. Ice thicknesses from the MLSI at the front of the ice shelf were between 5 and 15 m. Thinner MLSI in the Re-entrant area did not have a ridged surface, was only 1 – 5 m thick, and had a dark signature in SAR scenes. This ice was not included as part of the ice shelf for this study. In earlier studies both MLSI and first year fast ice were usually included in estimates of ice shelf area, which would produce a slight overestimation of area and volume change between studies. Finally, quantitative analysis of ice shelf thickness was computed from the GPR data (in-situ point measurements) and not from the interpolated surface. It is recognized that the uneven spatial distribution of point measurements that arise from uneven distribution of GPR transects across the ice shelf may result in biased data. Furthermore, the maximum and minimum thickness values reported are derived from the GPR profiles and do not necessarily represent the thickest and/or thinnest ice on the entire Milne Ice Shelf.

Table 4.5: Milne Ice Shelf thickness (m) descriptive statistics for 2008/2009 derived from GPR measurements.

Milne Ice Shelf 2008/2009 thickness (m)	
Mean	54.7 m
Median	56.2 m
Mode	55.9 m
Standard deviation	22.0 m
Range	93.9 m
Minimum	0.20 m
Maximum	94.1 m

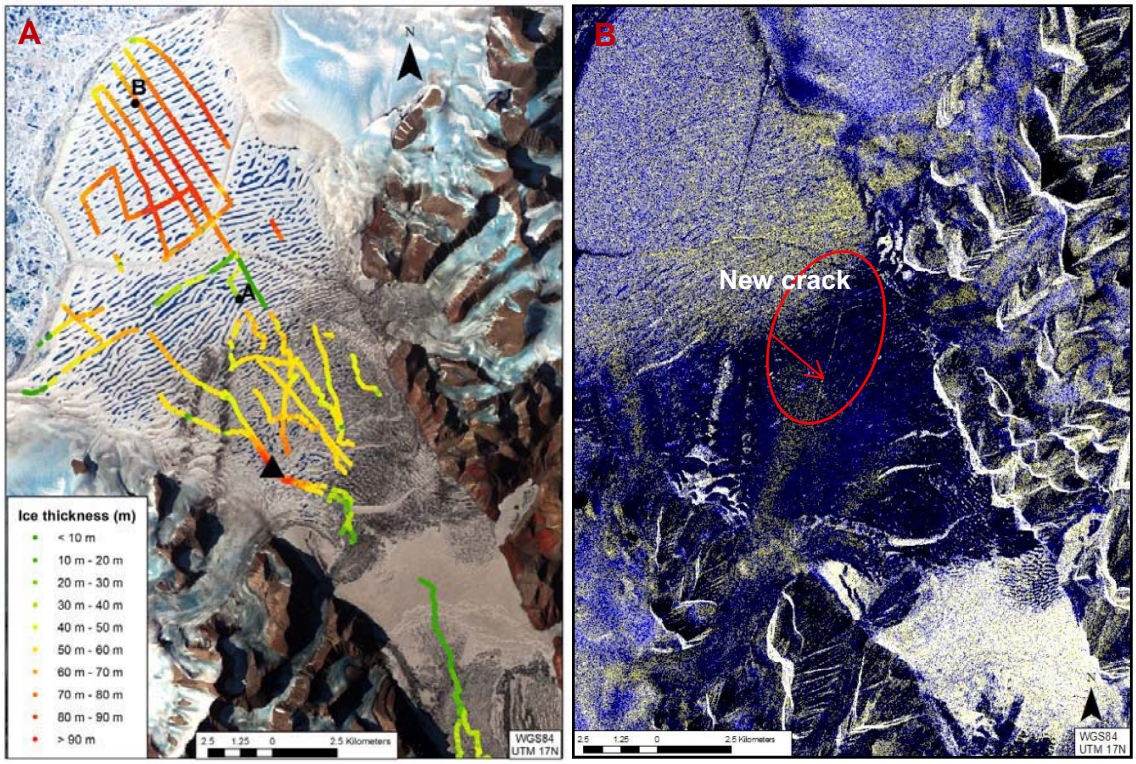

Figure 4.10: A) Milne Ice Shelf thickness from spring 2008 and 2009 GPR measurements. Black triangle indicates location of thickest ice recorded. Points A and B correspond to beginning and end of re-profiled transect displayed in figure 4.9. B) RADARSAT-2 March 15, 2009 scene, showing location of new crack.

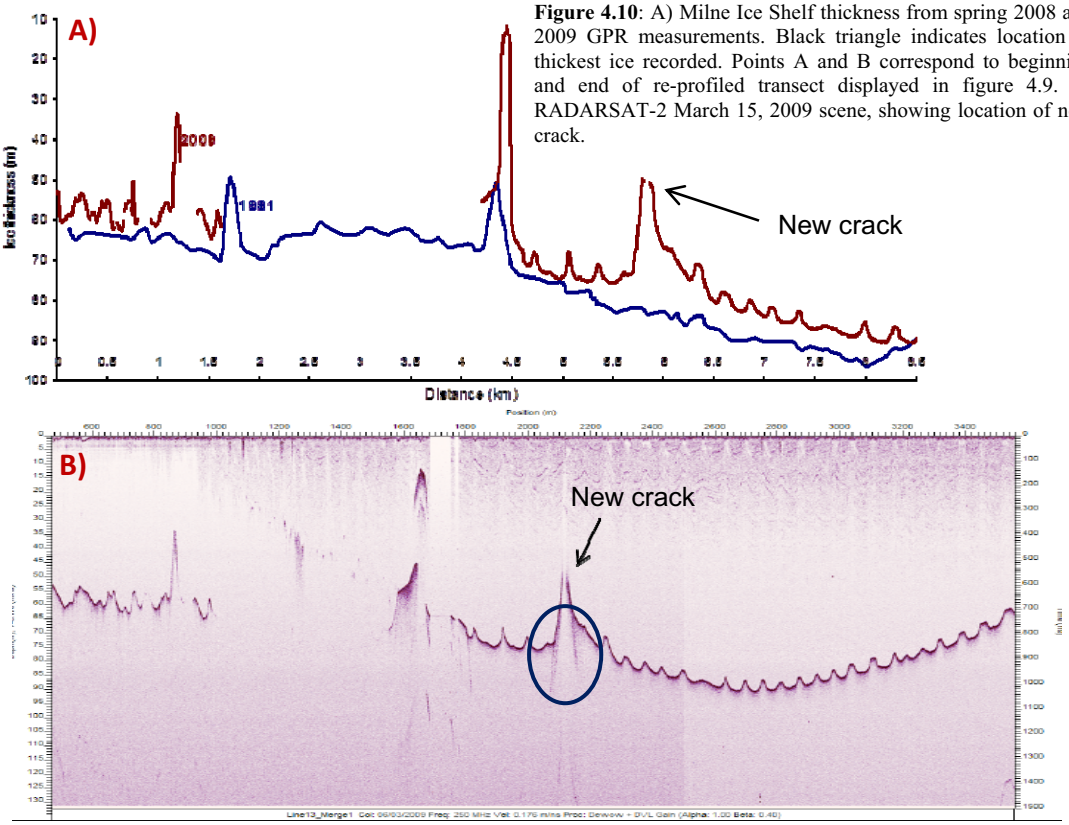

Figure 4.11: A) Ice thickness along an 8.5 km transect from point A to B (Figure 4.8). 1981 ice shelf thickness extracted from Prager (1983) radargram. Estimated horizontal positional error is ~300 m between the two survey lines. B) Radargram from 2008 and 2009 250 MHz GPR data showing location of crack. Dark purple line indicates ice shelf bed. Dark blue circle shows location of downward-dipping hyperbolae indicating crack sidewalls.

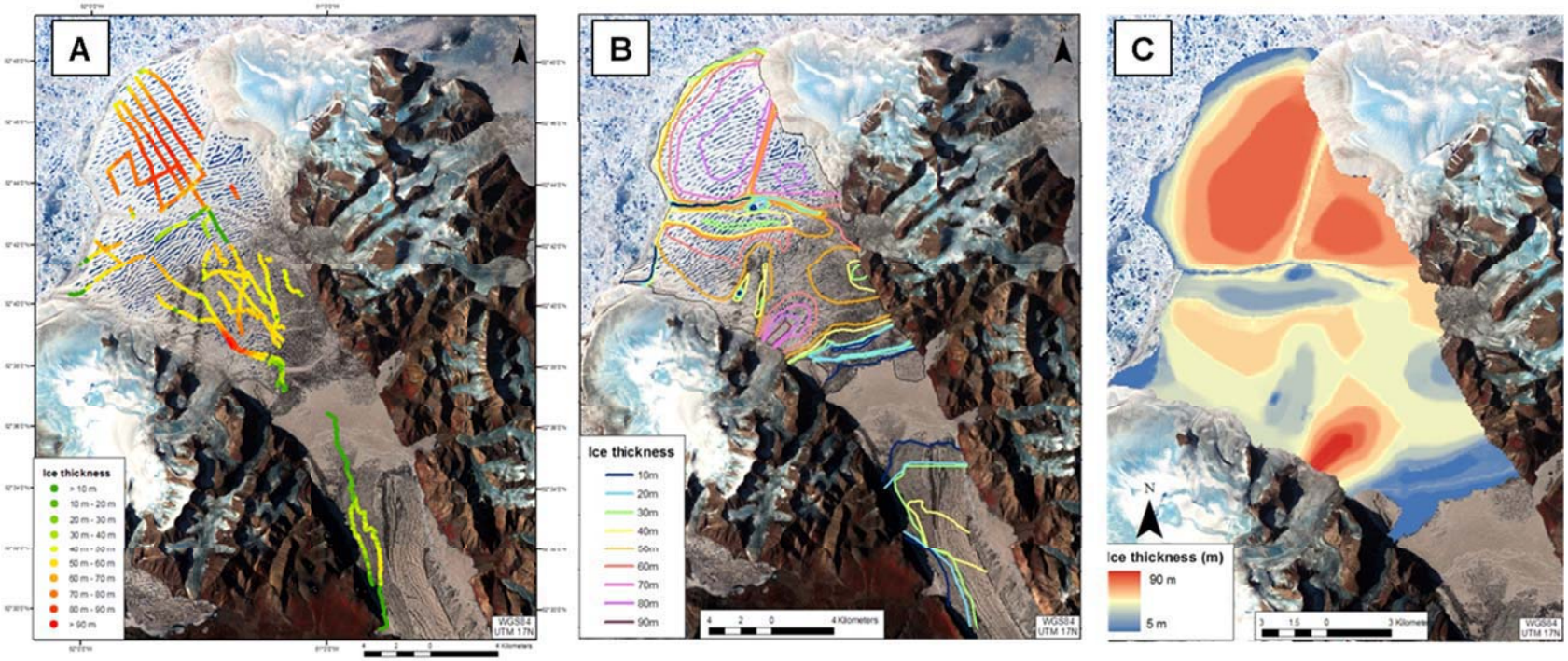

Figure 4.12: A) Milne Ice Shelf thickness from GPR data collected in spring 2008 and 2009 overlaid on a July 21, 2009 ASTER image. B) Milne Ice Shelf thickness contour map derived from GPR data (Figure 4.12A) overlaid on a July 21, 2009 ASTER image. C) Milne Ice Shelf thickness interpolated surface (DEM) derived from contour map (Figure 4.12B) overlaid on a July 21, 2009 ASTER image.

The present-day volume of the Milne Ice Shelf, computed from the thickness DEM, is 10.9 ±0.4 km^3 (9.8 km^3 w.e.) (Table 4.7). The bulk of the ice shelf's volume is contained in the Outer Unit. Thicker ice (80 - >90 m) is also observed in the Central Unit near Glacier 2 (Figure 4.12C). A large area of very thin ice (~10 - 20 m) is observed in the centre of the Milne Ice Shelf. This region is immediately to the south of the east-west running re-healed fracture, whose thickness ranges from 0 to 5 m and which separates the Outer and Central Units (Figure 4.12C). Regions of thin ice (0 – 5m) are also found at the rear of the ice shelf and in the Re-entrant area.

4.4 Ice Shelf thickness and volume change: 1981 – 2008/2009

Ice thickness measurements from 2008/2009 were compared to those collected in 1981 (Prager 1983) to determine changes in ice thickness and ice volume over the last 29 years. Mean ice thickness from the 1981 RES survey was ~70 m with a maximum depth of >100 m (Prager 1983).

4.4.1 Direct-line comparison of thickness change: 1981 – 2008/2009

A ~8.5 km long RES transect flown in 1981 was re-profiled in 2008/2009 to enable direct comparison of ice thickness changes over the 28 year period. This transect, located in the centre of the fiord, starts ~2 km inland of the two large re-healed fractures (Point A) and runs in a NW direction perpendicular to the coast to Point B, located in the middle of the Outer Unit (Figure 4.11A). Ice thickness values were extracted from the 1981 radargram (Figure 3.19, section 3.3.5.1) using image recognition software, and converted from two-way travel time to ice depth. A longitudinal transformation was applied to fit the data to marker points (e.g. cracks) that could be identified in both images. For 2008/2009 bed

reflections were only identified for the first 1.5 km and the final 4.5 km of the transect, thus only ~6 km of ice depths were directly comparable (Figure 4.11A).

The direct-line comparison revealed thinning of ~5 - 15 m between 1981 and 2008/2009 (Figure 4.12A), with an ice thickness decrease at all points surveyed. The greater variability observed in the 2008/2009 profile is likely the result of higher instrument resolution. Overall, the thickness profiles from 1981 and 2008/2009 are very similar, with thickness increasing with proximity to the coast. Over the first 1.5 km ice thickness ranged from ~65 - 70 m in 1981 compared to ~50 - 60 m in 2008/2009. Between km 4.5 and 8, ice thicknesses increased from ~70 m to >90 m in 1981 compared to ~65 - 85 m in 2008/2009. The greatest thinning (up to 15+ m) was observed between km 5 and 7 (Figure 4.11A). In 2008/2009, an absence of bed reflection near km 5.75 with rapidly decreasing ice thicknesses on either side of it, combined with presence of two downward-dipping hyperbolae, suggests the presence of a crack (Figure 4.11B). This crack is visible on a RADARSAT-2 scene from March 15, 2009 (Figure 4.10B) where a 5 km-long thin bright line running in a SW - NE direction across the Central Unit is visible. This suggests that a new crack has formed there recently, because ice at this location was ~82 m thick in 1981 and is not visible on the surface (no dark black line) from the 1984 air photo mosaic (Figure 4.1, 4.10B and 4.11A). The location of the crack on the RADARSAT-2 scene (Figure 4.10B) coincides with that from the radargram (Figure 4.11B).

At km 4.5, an absence of bed reflection with similar characteristics to the crack described above is observed for 1981 and 2008/2009 (Figure 4.11). When overlaid on the July 21, 2009 ASTER and the March 15, 2009 RADARSAT-2 scene and the 1984 air photo mosaic, this feature corresponds with a dark line running NW to SE across the Central Unit. This feature is one of two re-healed fractures described by Jeffries (1986b). Image interpretation (1984 compared to 2009) suggests that the fracture has increased in length, extending ~2 km father inland towards the eastern side of the fiord in 2009 than it did in 1984. It is not clear from the RES and GPR data if the crack has increased in width. However, it appears to penetrate a greater depth in 2008/2009 (0-10 m) compared to 1981 (~40 m) (Figure 4.11A). This direct-line comparison shows that, along this particular

transect, the ice shelf has not only undergone significant thinning over the last 29 years but that important indicators of changes in stability (i.e. cracks) have also occurred.

4.4.1.1 Milne Ice Shelf specific mass balance: 1981 – 2008/2009

To enable quantification of mass balance change, the ~8.5 km long re-profiled transect was divided into 1 km segments and the change computed for 1981-2008/9 where data allowed. This process helped smooth out resolution effects, account for some artefacts due positional error, and addressed small data gaps. Because of positional inaccuracies and data gaps between km 0.75 and 2, averages were taken over the first two kilometers and divided by two for comparison purposes (i.e. two 1 km segments). Mean annual ice thickness change was converted to water equivalent using an ice density of 0.90 g m^{-3}.

Negative mass balances were observed for all segments measured, ranging from 0.1 m w.e. yr^{-1} (km 8 to 8.5) to 0.34 m w.e. yr^{-1} (km 5 to 6), with an average mean annual mass balance of ~0.23 m w.e. yr^{-1} (Table 4.6). Mass losses were greatest between km 4 and 6 (~0.32 m w.e. yr^{-1}), with this section roughly corresponding to the northern section of the Central Unit (Figures 4.11 and 4.12). Finally, five ablation stakes measured over a 1-year period (2008-2009) all indicated surface lowering (Figure 4.13). Considerable spatial variability in the 2008 snowpack was also observed (Figure 4.14).

4.4.2 Spatial patterns of ice thickness and volume change: 1981 – 2008/2009

To determine spatial patterns of thickness change across the entire Milne Ice Shelf over time, a digital elevation model (DEM) of ice thickness was produced for 1981 (Figure 4.15). This DEM was produced from an ice thickness contour map (Figure 2.16a) developed by Prager (1983) from the 1981 RES survey data (sections 2.4.2 and 3.3.3.4). Air photo coverage for the Milne Ice Shelf is not available for 1981, so the 1984 ice shelf area

Table 4.6: Specific mass balance measurements for 1981 – 2008/2009 from the ~8.5 km long direct line comparison (Figure 4.11).

Distance along transect (km) from A to B	1981 mean ice thickness	2008/2009 mean ice thickness	Total ice thickness change (m)	Annual ice thickness change (m yr^{-1})	Annual mass change (w.e. yr^{-1})
0-2*	64.5*	57.7	6.8	0.24	0.22
0-2*	64.5*	57.7	6.8	0.24	0.22
2-3	64.8	No data	NA	NA	NA
3-4	64.1	No data	NA	NA	NA
4-5	68.1	59.2	8.9	0.32	0.29
5-6	80.4	69.9	10.5	0.38	0.34
6-7	86.9	78.7	8.2	0.29	0.26
7-8	92.6	86.7	6.0	0.21	0.19
8-8.5**	92.3	89.1	3.2	0.11	0.10

*averaged over 2 km
**averaged over 0.5 km

polygon, delineated from the 1984 air photo mosaic, was used to delineate the 1981 DEM margins (Figure 4.15).

Total ice volume computed from the 1981 DEM was 13.7 ±0.5 km^3 (Table 4.6). In 1981, the Outer Unit consisted of relatively thick ice (80 – 90 m), with relatively thin ice (10 m) in the Inner Unit (Figure 4.15). Ice thicknesses in the Central Unit were much more variable than those of the Outer and Inner Units. In particular, a large area of thick ice (70 – 90 m) was located in the Outer Unit near Cape Egerton. A second, smaller region of very thick ice (~100 m) located near Glacier 2, corresponds with the location of maximum recorded ice thickness for 1981. The thinnest ice (>10 m) was located at the front and rear of the ice shelf. The large area of very thin ice (>10 - 20m) at the rear of the ice shelf corresponds to the Inner Unit.

4.4.2.1 Assessment and interpretation of 1981 and 2008/2009 DEMs

The coarse resolution of the 1981 contour map (Figure 2.16a) resulted in an interpolated surface that fails to capture small scale features such as the re-healed fractures and likely under-represents variations in ice thickness. The greater detail in the 2008/2009 DEM is attributed to the higher density of point measurements as well as the use of satellite imagery and field observations to assist in informing the location of contour lines where GPR data was not collected or where thickness was not resolved from GPR returns (sections 3.3.3 and 4.2). Despite this, several similarities are observed between the 2008/2009 DEM (Figure 4.12C) and the 1981 DEM (Figure 4.15). In both years a large area of thick ice is located in the Outer Unit to the northeast of the large east-west running re-healed fracture and a smaller area of very thick ice is located in the Central Unit near Glacier 2. The thinnest ice (1981 and 2008/2009) is located at the front and rear of the ice shelf. Finally, a pocket of thinner than average ice along the eastern side of the fiord was present in 1981 and in 2008/2009, although the feature is more pronounced in the current (2008/2009) DEM.

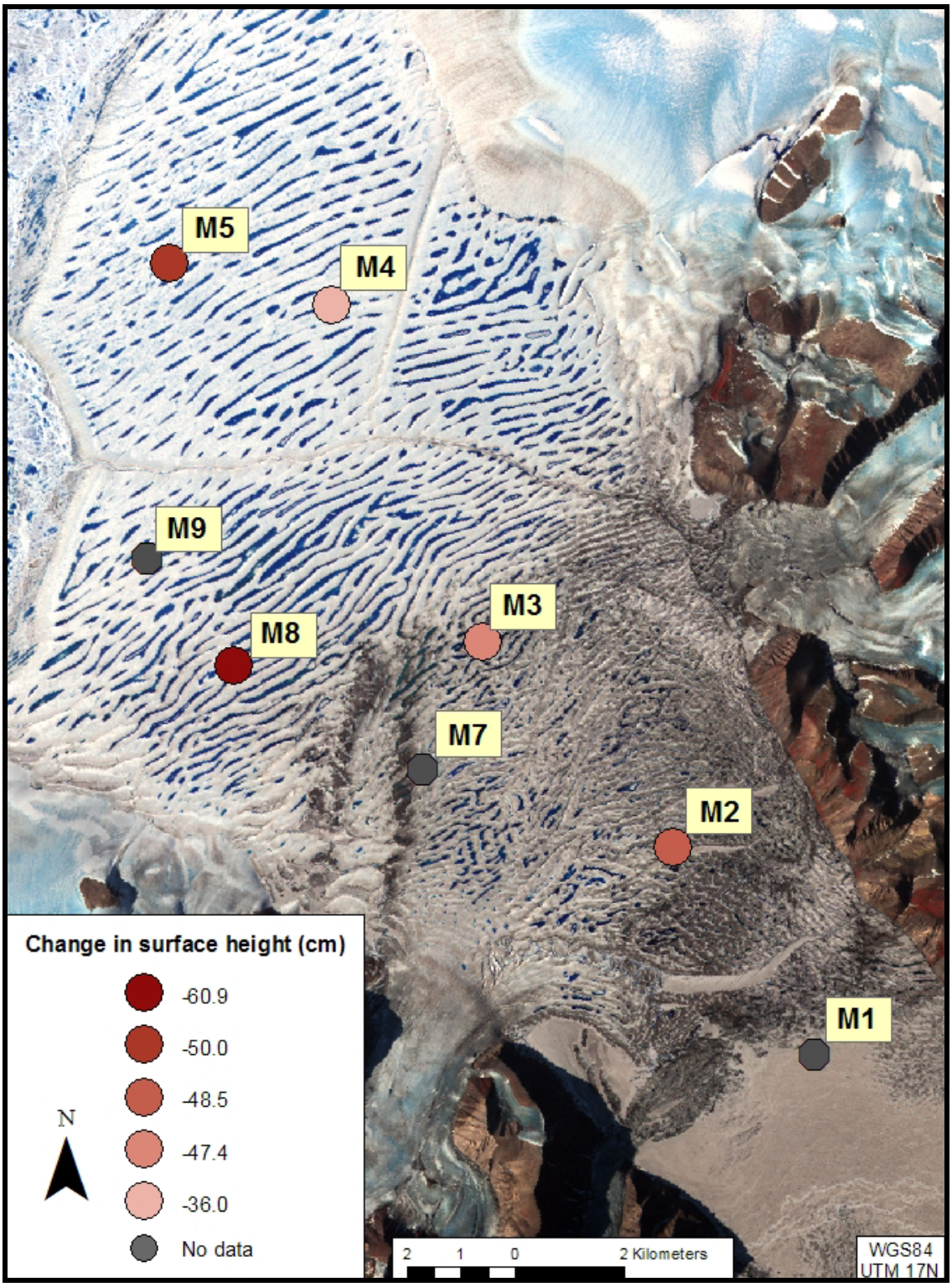

Figure 4.13: Change in surface height for Milne Ice Shelf measured from five ablation stakes over the period April 4, 2008 to June 3, 2009 overlaid on a July 21, 2009 ASTER scene.

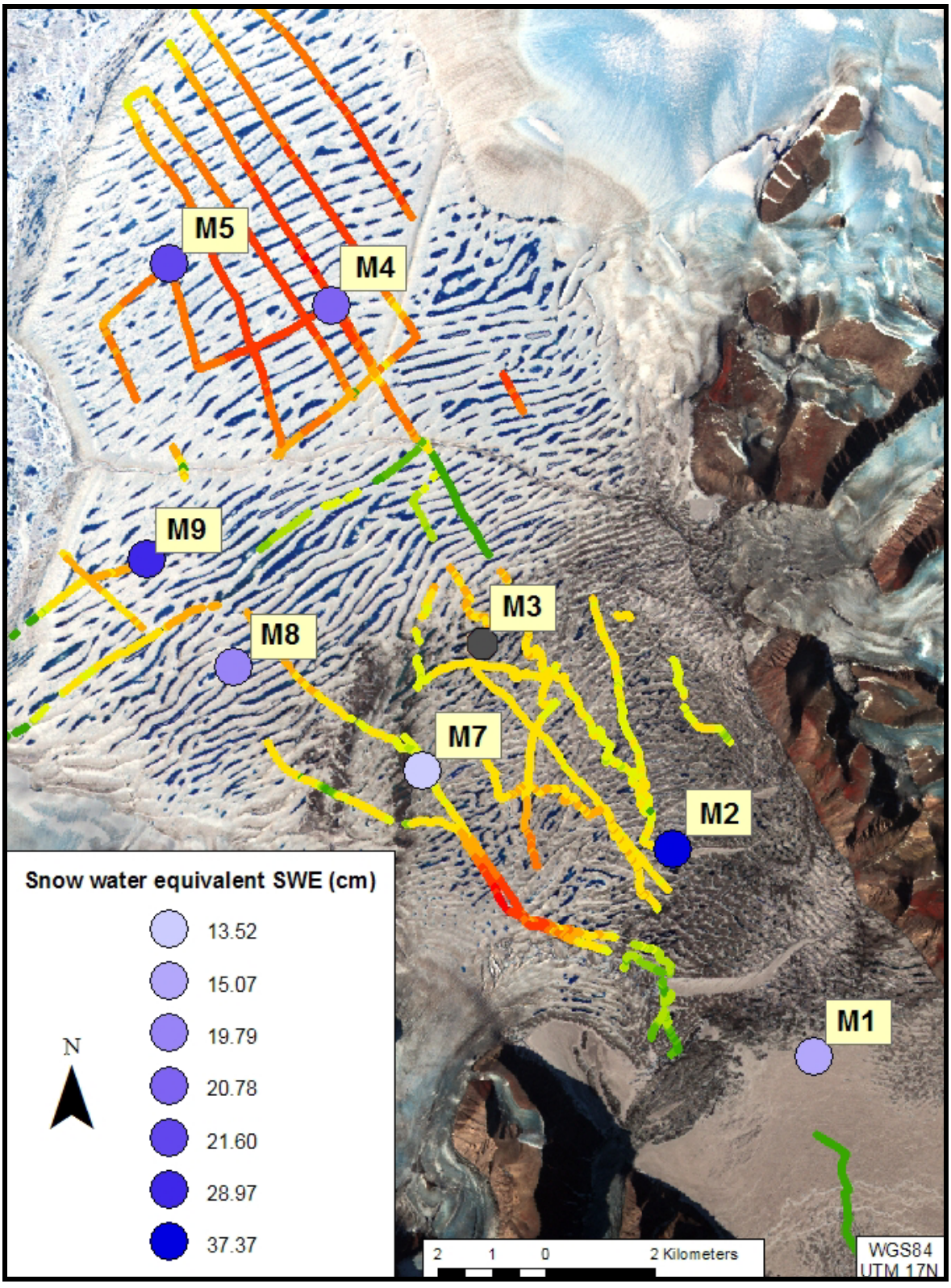

Figure 4.14: Milne Ice Shelf annual snowpack for 2007-2008, measured in snow water equivalent (SWE) April 4, 2008 overlaid on a July 21, 2009 ASTER scene.

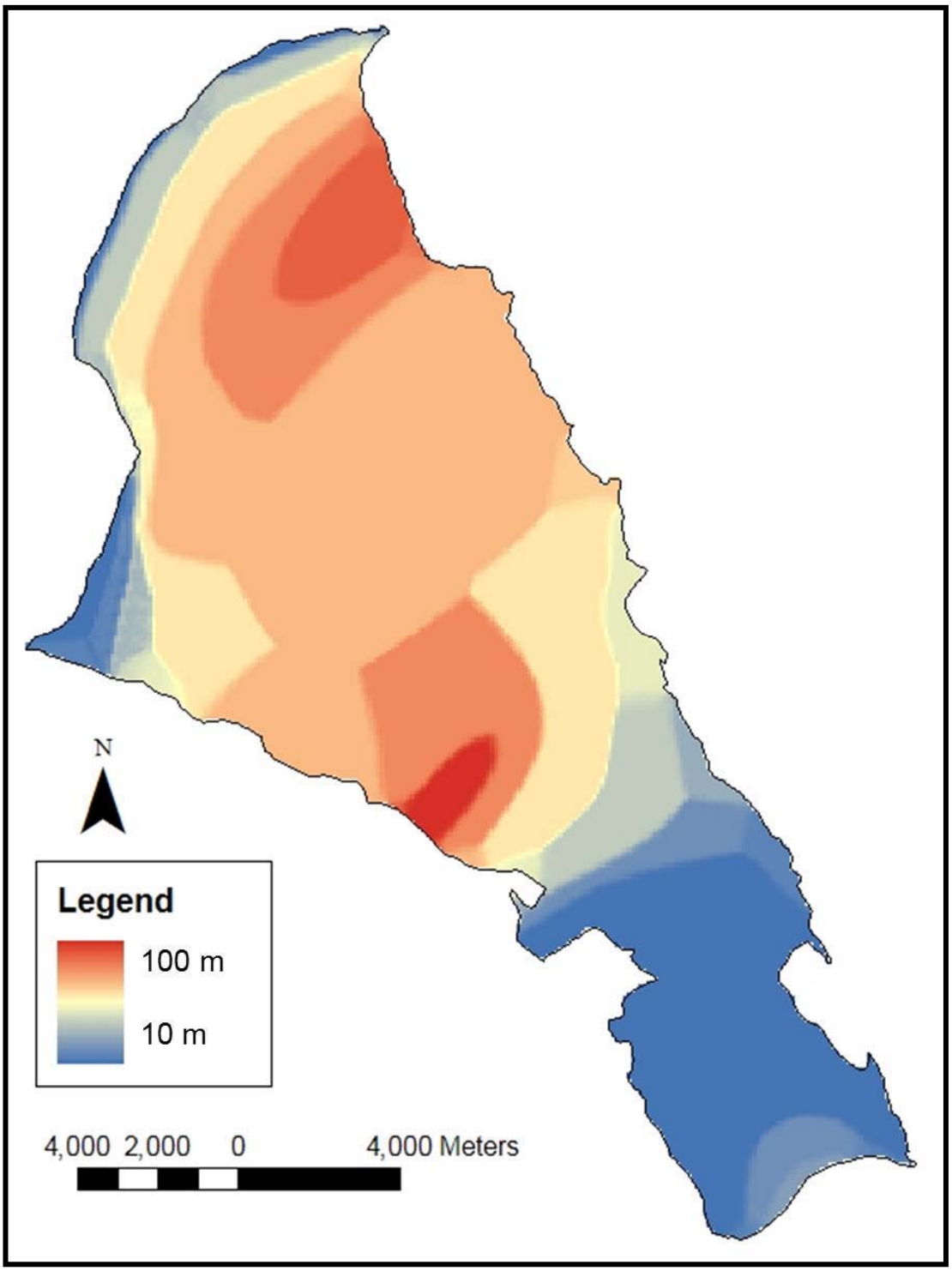

Figure 4.15: Digital elevation model of ice thickness (m) for 1981. Thickness was interpolated from 1981 contour map produced by Prager (1983) from radio echo sounding data.

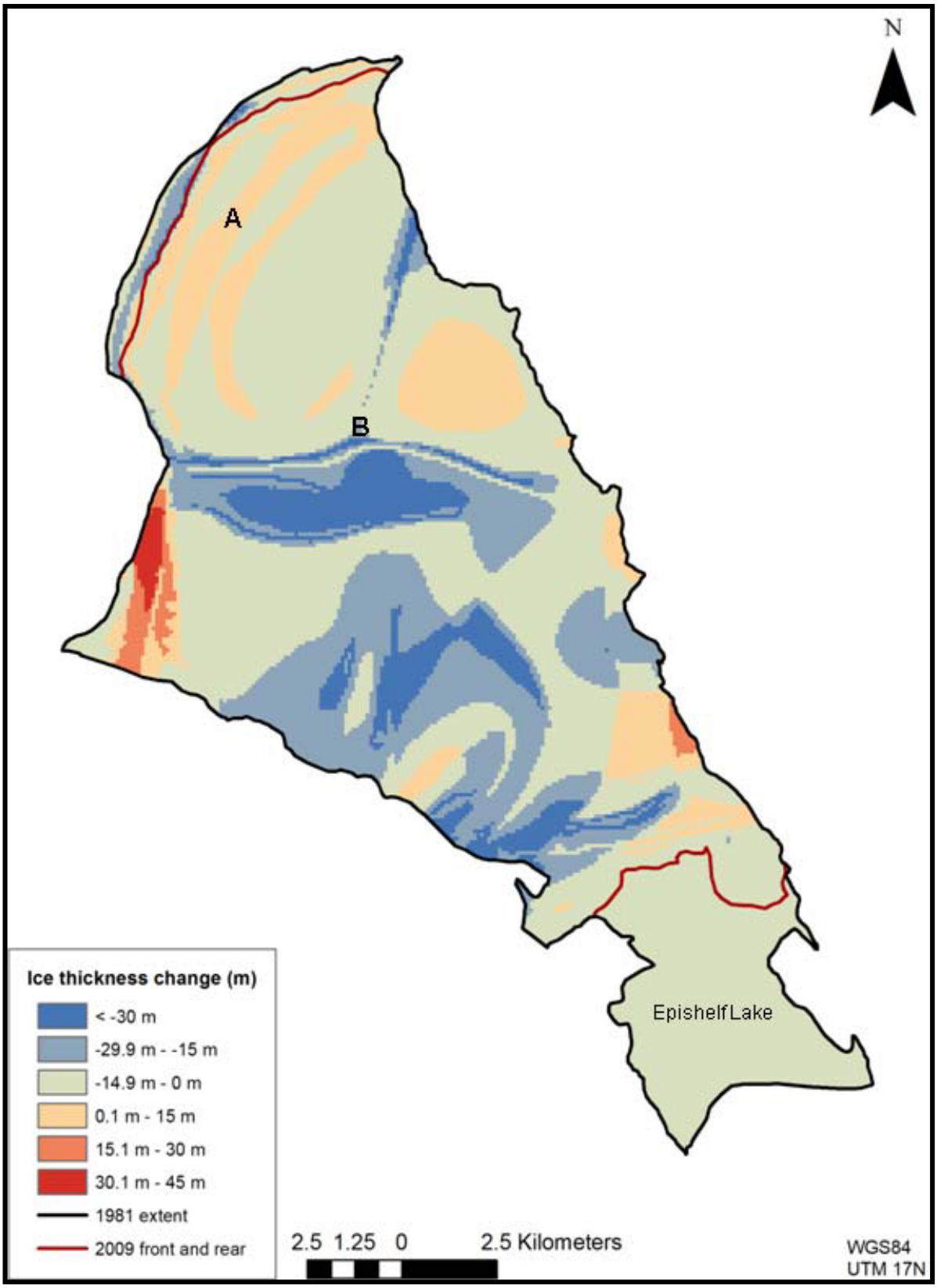

Figure 4.16: Milne Ice Shelf thickness change 1981 to 2008/2009.

Important features visible in the 2008/2009 DEM that were not observed in the 1981 DEM include two areas of thin ice in the central unit (Figure 4.12C). The former includes an area of thin ice (~30 m) immediately south of the east-west running re-healed fracture. The region of thin ice extends roughly two thirds of the way across the ice shelf in the Central Unit from west to east. A separate area of very thin ice (dark blue; ~20 m) is found in close proximity to the region just described, located to the SW of where the two re-healed fractures meet.

4.4.3 Volume change: 1981 – 2008/2009

DEM differencing was used to identify important areas of volume/thickness change between 1981 and 2008/2009. The 2008/2009 interpolated raster surface was subtracted from the 1981 interpolated surface and extracted to the 1984 area polygon. The resultant DEM (Figure 4.16) shows that most areas of the Milne Ice Shelf experienced thinning (0 – 15 m) over the last 29 years (1981 – 2008/2009). Unless otherwise specified, it is assumed that most changes are the result of physical mass gains or losses rather than interpolation artefacts and measurement errors.

The Outer Unit experienced the least amount of volume change between 1981 and 2008/2009 with changes in ice thicknesses varying from +15 m to -15 m, with higher amounts of mass loss immediately at the front of the ice shelf (-15 to -30 m). The striping effect in the Outer Unit (area 'A' in Fig 4.14) is likely an interpolation effect resulting from the contour lines in 1981 not overlapping with those from 2008/2009. However there is still good confidence that the change in this area ('A') is similar to that observed for the rest of the Outer Unit. The middle portion of the Outer Unit roughly corresponds with km 7 to 8.5 of the direct line comparison where mean annual mass balances of -0.10 to -0.19 m w.e. yr^{-1} were observed (Table 4.6).

Mass change in the Central Unit was much more variable than that observed for the Outer Unit. Apparent thickening was observed in the Re-entrant area (15 to >30 m) and on the eastern side of the fiord (0.1 – 30 m). It is unclear whether the large increase in thickness in the Re-entrant area is the result of true thickening or an interpolation effect. In the Central Unit, decreases in ice thickness of 5 to >30 m were observed. Some of these changes are termed *resolution effects* (e.g. area B, Figure 4.16) and are not necessarily indicative of real, physical change. For example, some of the decrease in ice thickness corresponding with the location of the re-healed fractures is attributed to the finer resolution of the 2008/2009 DEM which is able to resolve these features compared to the 1981 DEM. Thinning may have occurred in this region, as suggested by the direct line comparison where ice depths near the re-healed fracture were ~30 m shallower in 2008/2009 compared to 1981. This is reasonably consistent with observations of maximum mean annual mass balances of up to -0.34 m w.e. yr^{-1} (km 5 – 6) near the boundary between the Central and Outer Units (section 4.4.1.1).

Results from the DEM differencing indicate overall mass loss over the last 29 years, with the greatest mass losses occurred in the central and rear portions of the ice shelf and comparatively little mass change in the Outer Unit. A 20.4% volume loss (~2.8 ±0.98 km^3, Table 4.7), is computed by subtracting the total volume computed from the 1981 DEM (Figure 4.15) with that computed from the 2008/2009 DEM (Figure 4.12C). Of the 2.8 km^3 (2.5 km^3 w.e.) mass loss, 0.8 km^3 (0.7 km^3 w.e.) is attributed to the conversion of the Inner Unit into the Milne Epishelf Lake. If the Milne Epishelf Lake is excluded from the calculations the total volume loss between 1981 and 2008/2009 was 2.1 km^3 (15%), which equates to 1.9 km^3 w.e.

4.4.4 Volume change: assessment of uncertainty

Sources of error for total ice volume arise from area and thickness computations as well as in the interpolation method used. For this study the interpolation uncertainty was not computed so the volume error provided here is simply the summation of the error derived for areal extent with that derived for ice thickness. For 2008/2009 this equates to 4% of the

Table 4.7: Milne Ice shelf area and volume for 1981 and 2008/2009.

Year	**Area**	**Area error**	**Volume**	**Volume error**
1981	250 km^2	±1 km^2	13.7 km^3	±0.55 km^3
2008/2009	205 km^2	±1 km^2	10.9 km^3	±0.44 km^3
Total change	-45 km^2	±2 km^2	-2.8 km^3	±0.98 km^3
Percent change	-18%		-20.4%	

total ice volume. Although possible to constrain error for 2008/2009 volume reasonably well the 1981 error is much more uncertain. Corrected navigation error from Prager (1983) is 1 km and ice thickness error for an ice depth of 100 m is ± 3 m. However, considerations regarding contour map production, georectification and interpolation must also be taken into account. For the purposes of this study the 2008/2009 volume error is applied to the 1981 volume DEM. However it is acknowledged that this may underestimate the uncertainty in estimates of total volume change. Error associated with total ice volume change is thus estimated to be ~8%.

4.5 Ice shelf mass gains and losses

Observed decreases in Milne Ice Shelf areal extent, thickness, and volume are linked to changes in its mass gains and losses. Glaciers are one source of mass input to the Milne Ice Shelf, but there is limited knowledge concerning if and how the glacier mass input has changed over time. Image analysis of the Milne Glacier and five tributary glaciers was therefore conducted for 1950 – 2009 to aid in interpreting the causes of the observed ice shelf mass losses.

4.6.1 Tributary glaciers: 1950 – 2009

Air photo and satellite imagery from 1950, 1959, 1984, 1993, 2001, and 2009 was used to determine the change in terminus position of Glaciers 1, 2, 3, 4, and 6 (Figures 4.2 and 4.17 – 4.21). For all glaciers the position of their termini is located farther inland in each successive image, with the largest retreat observed between 1959 and 1984 (Figure 4.22). This suggests a decrease in mass input from the smaller tributary glaciers located on the sides of Milne Fiord since 1950.

In 1959, all five tributary glaciers terminated on the ice shelf with Glaciers 1, 2, and 6 extending at least 4.5, 2.5, and 1.5 km towards the centre of the ice shelf, respectively

(Figure 4.20). In 1984, Glaciers 1 and 4 appear to terminate near the fiord sidewall instead of extending out onto the ice shelf (Figures 4.17 and 4.20). In 1984 a small ice-dammed lake is visible in front of Glacier 4's terminus that was not visible on the 1959 air photo (Figure 4.20). The lake separates the active portion of the glacier, whose terminus is located ~3 km closer to the fiord sidewall than it was in 1959, and a remnant glacier tongue which in 1984 appears to sit on top of the ice shelf. In 1984 Glacier 1 still appears to be connected with the ice shelf even though its terminus experienced a net retreat of ~4.5 km between 1959 and 1984 (Figure 4.17 and 4.22). Glacier 6 appears to have retreated slightly (~1 km) between 1959 and 1984 (Figure 4.21).

Air photo coverage for 1984 did not include the terminus of Glaciers 2 and 3, so terminus position in 1959 was compared to that from 1993 (Figures 4.18 and 4.19). Between 1993 and 1959, negligible change (retreat of ~100 m) was observed for Glacier 2; however, the terminus of Glacier 3 retreated inland by ~3 km (Figure 4.22). In 1959 both glaciers terminated on the ice shelf, suggesting that these glaciers were still providing mass input. However, in 1993 the terminus of both glaciers had been separated by an ice dammed lake similar to that described for Glacier 1 above.

In 1993 most glacier termini were located near the fiord sidewall (Figure 4.22). Image interpretation suggests further retreat of all tributary glaciers since between 1993 – 2009 (Figure 4.22), although poor image quality inhibited clear identification of Glacier 4's terminus position for 1993 (Figure 4.20). Retreat of ~200+ m was observed for Glacier 2 between 2001 and 2009. In 2009 the glaciers located closest to the rear of the ice shelf (back of the fiord) appear to have retreated farther up-valley (Glacier 3 and 4) compared to those situated closer to the ice shelf front (Glaciers 1, 2 and 6). For example, field observations from spring 2009 indicate that Glacier 4 (Figure 2.24A), located at the back of the fiord is now a hanging glacier whereas Glacier 1, located near the head of the fiord, still terminates on the ice shelf (Figure 4.17).

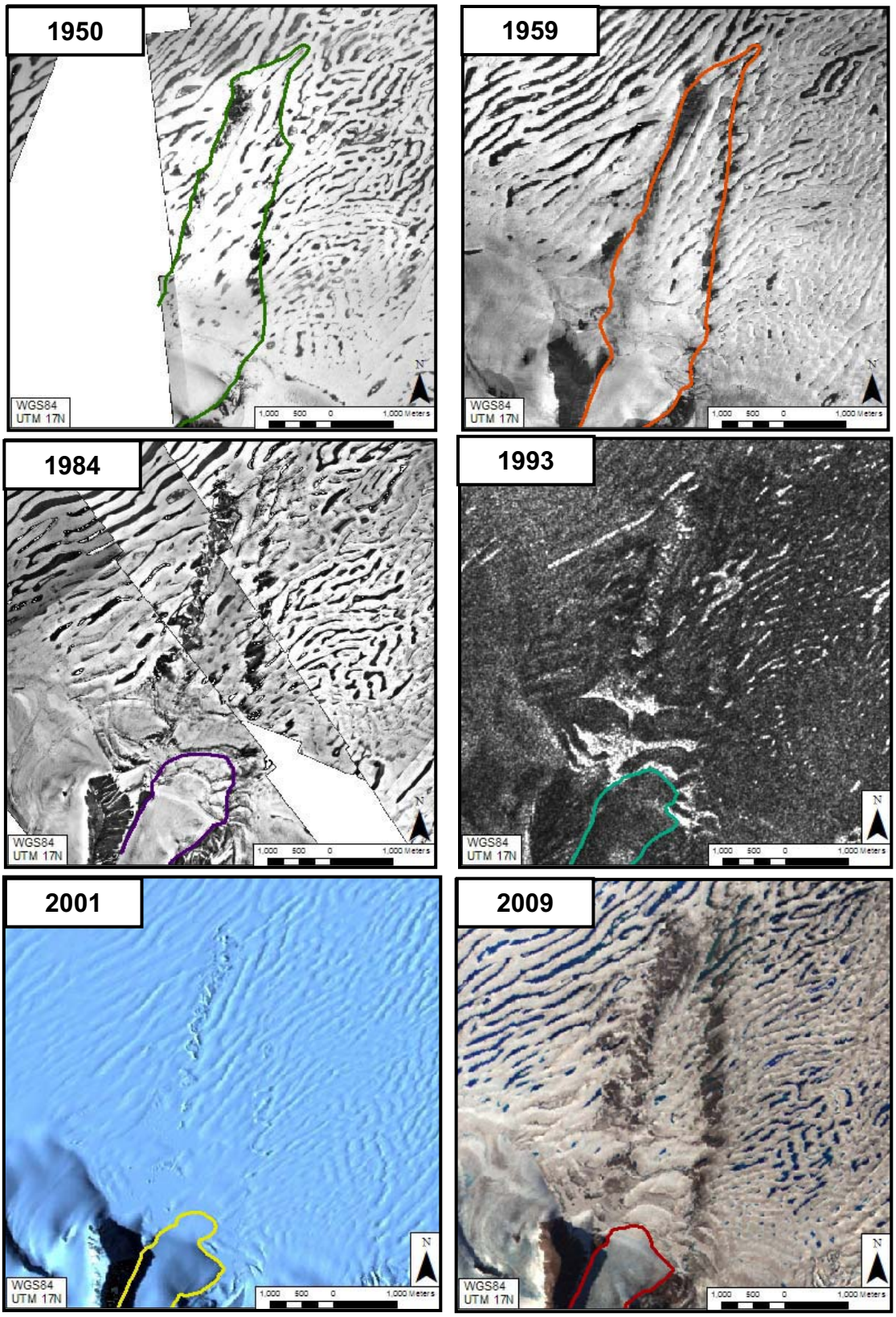

Figure 4.17: Temporal change of Glacier 1 terminus 1950 – 2009.

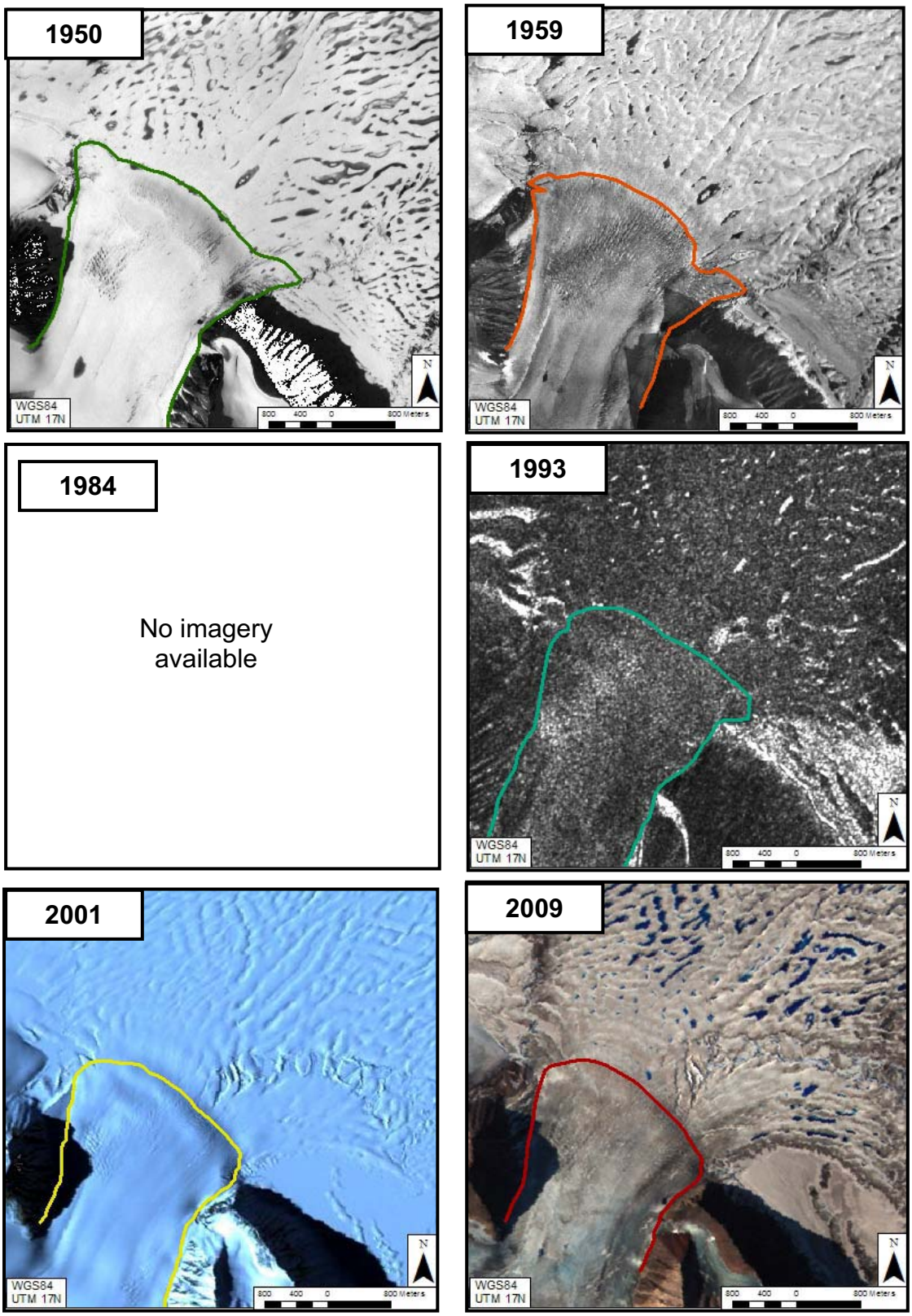

Figure 4.18: Temporal change of Glacier 2 terminus 1950 – 2009.

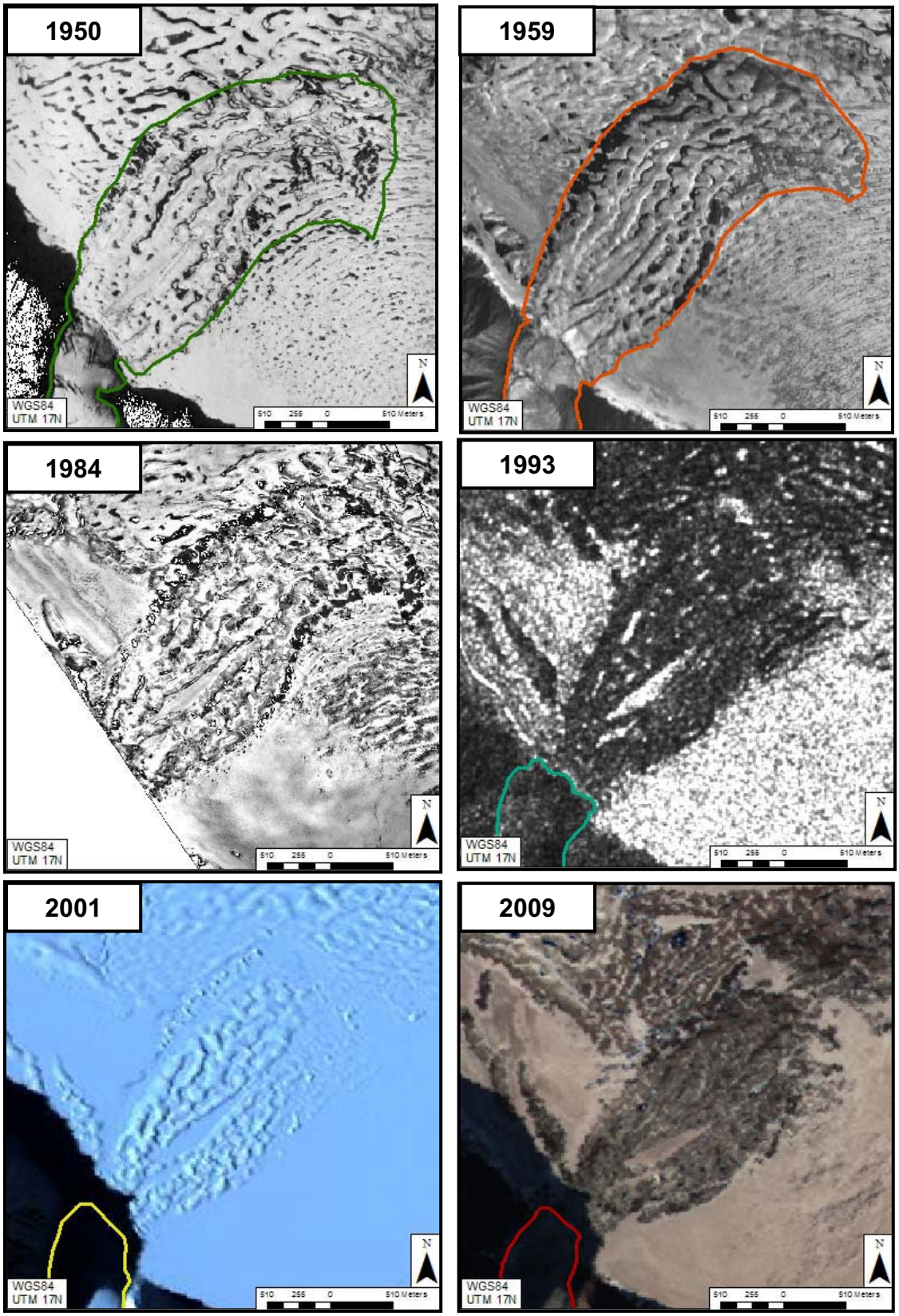

Figure 4.19: Temporal change of Glacier 3 terminus 1950 – 2009. Insufficient coverage for 1984 to determine terminus extent.

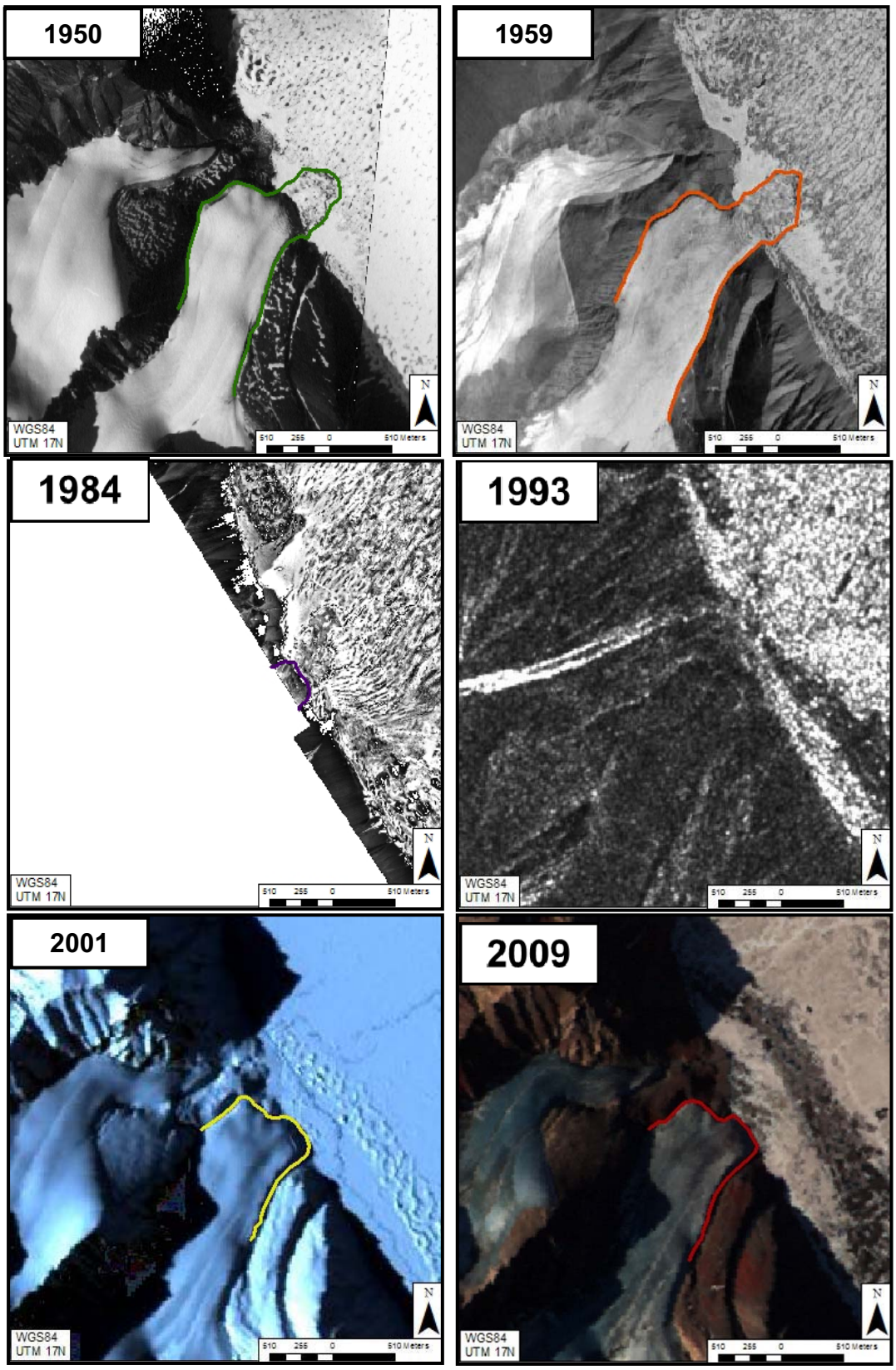

Figure 4.20: Temporal change of Glacier 4 terminus 1950 – 2009. 1993 not outlined due to poor image quality.

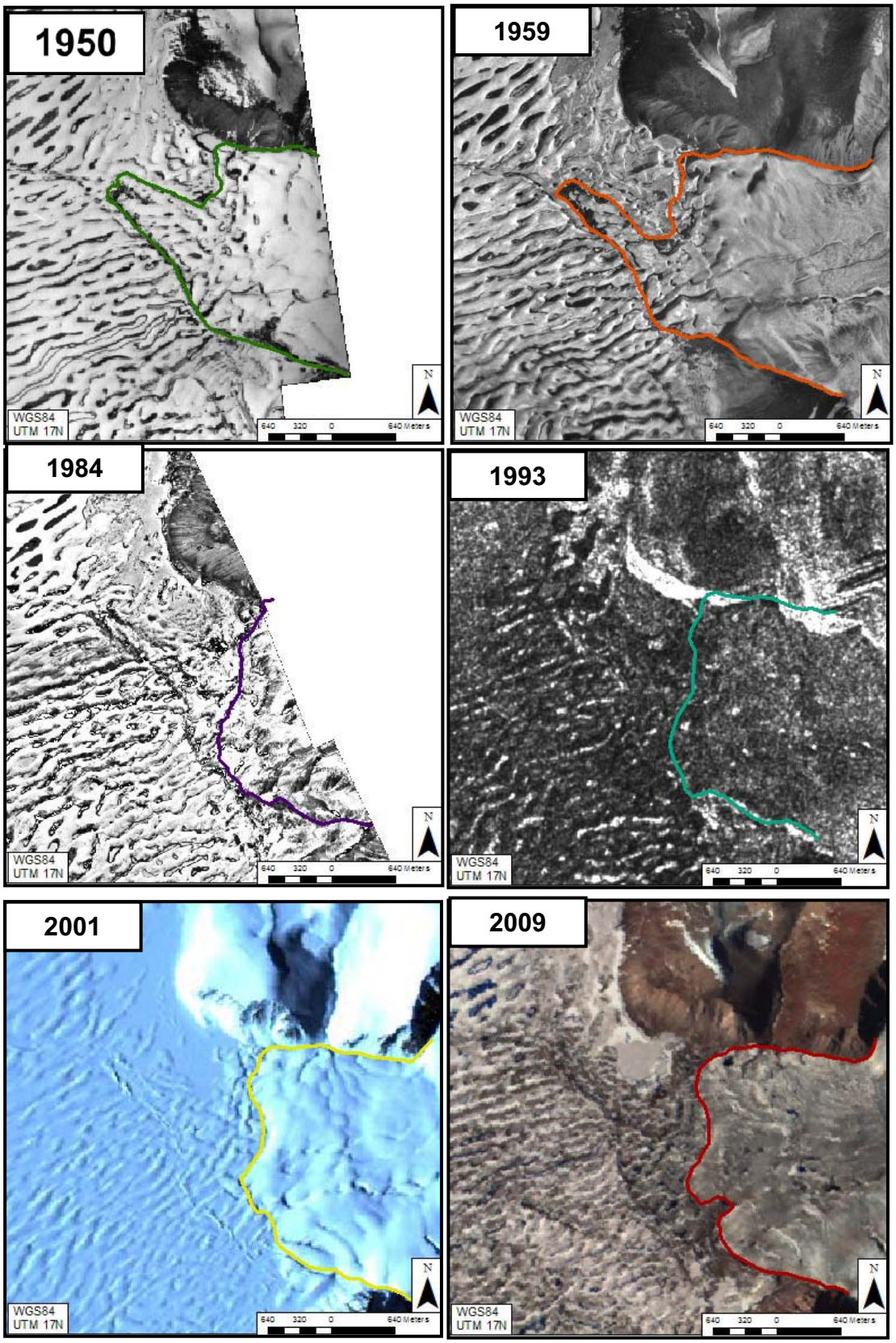

Figure 4.21: Temporal change of Glacier 6 terminus 1950 – 2009.

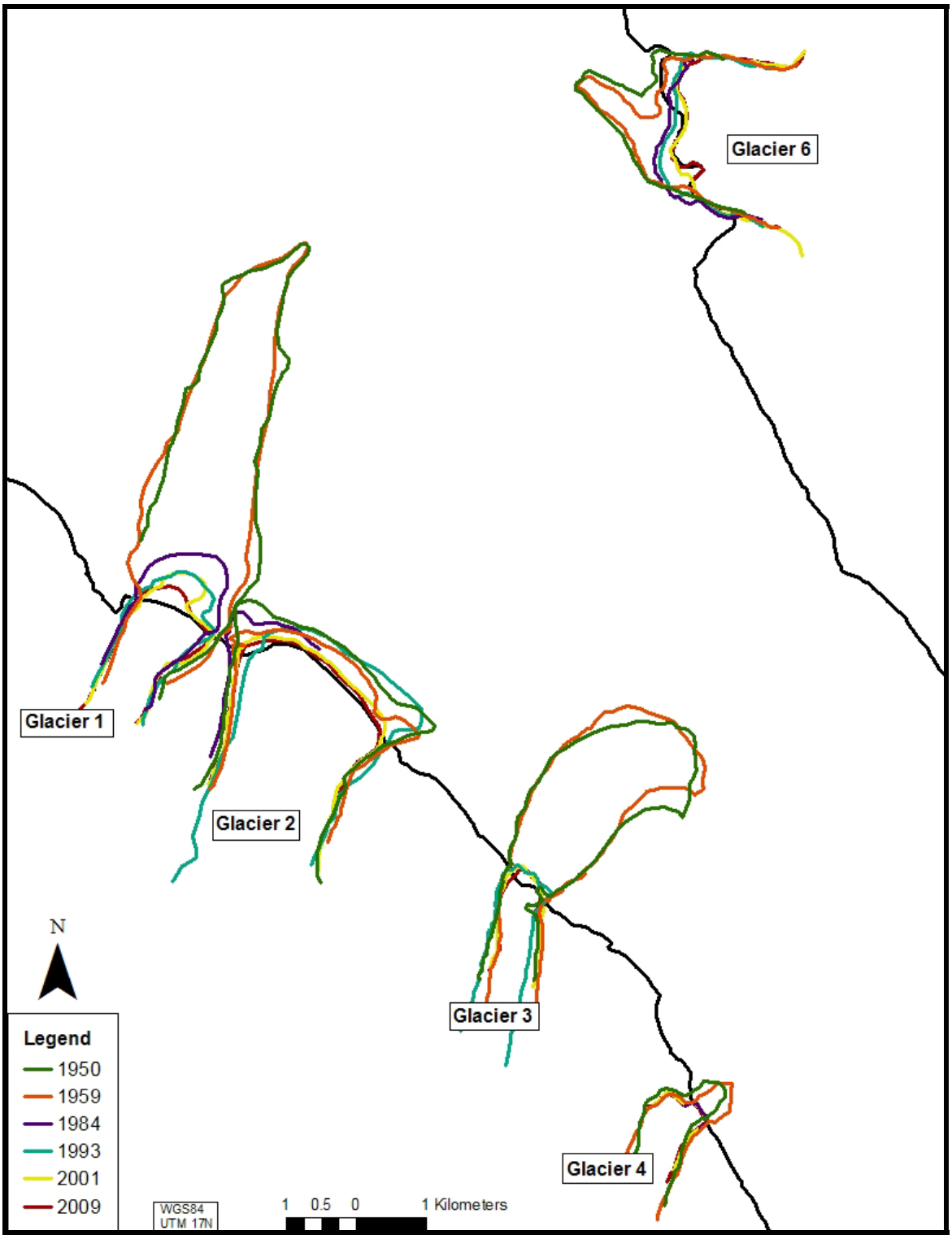

Figure 4.22: Temporal change of the five tributary glaciers studied for 1950 – 2009. Glacier terminuses delineated from air photo mosaics and satellite imagery (Figures 4.16 – 4.19). Naming conventions adapted from Jeffries (1986b).

4.6.2 Milne Glacier: 1950 – 2009

To quantify the Milne Glacier changes (Figure 4.23), identifiable features such as contorted moraines, lakes, and glacier debris were marked on each image and a measurement axis connecting the same feature over time was drawn. Five measurement axes were used to determine the rate of advance of the main terminus and four axes were used for the southwest terminus (Figure 4.24). For each time interval, the length of each axis was measured and the average computed. The total change (average of the measurement axes) and rate of change were computed for each time interval for both the main tributary and the southwest tributary (Table 4.2). Change in terminus position was determined by comparing one image with an image from a subsequent year. Measured change in terminus position was limited by the available data so it was not possible to identify rapid short-term changes.

Analysis shows successive forward movement of the Milne Glacier's terminus between each time interval, with a total advance of 5.1 km (Main tributary) to 5.6 km (Southwest tributary) between 1950 and 2009 (Table 4.2; Figures 4.23 and 4.25). The surge process appears to alternate between the dominant Main tributary, consisting of the central and northeast ice streams, and the smaller Southwest tributary (Figure 4.26). Over the 59 year period (1950 – 2009) the rate of advance of the Southwest tributary is more variable than the Main tributary (Table 4.2; Figure 4.26).

Between 1950 and 1959 the Main tributary advanced at a faster rate (73.7 m yr^{-1}) than the Southwest tributary (66.5 m yr^{-1}) (Table 4.2, Figure 4.26). Over the following 25 years (1959 – 1984) both tributaries continued to advance but at a slower rate (Main: 56.4 m yr^{-1}; Southwest: 60.1 m yr^{-1}). During this time, the slower rate of advance of the Main tributary resulted in a switch from a Main-tributary dominant to Southwest-tributary dominant ice flow (Figure 4.26). The fastest rates of advance (Main: 128.4 m yr^{-1}; Southwest: 173.2 m yr^{-1}) were observed between 1984 and 1993, coinciding with Epishelf Lake development (section 4.1.4). The development of the Epishelf Lake, sometime

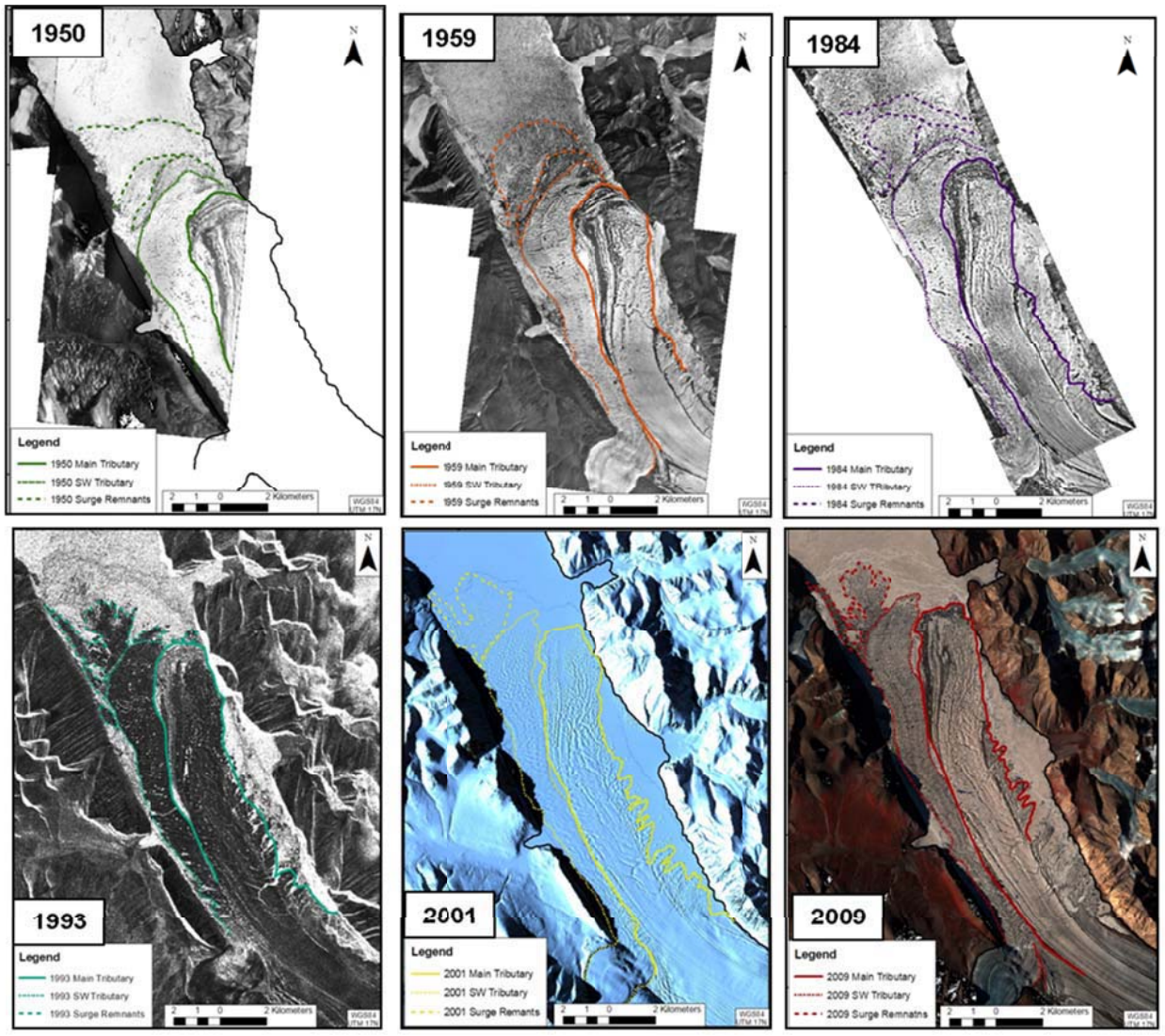

Figure 4.23: 1950 – 2009 terminus extent for Milne Glacier main tributary, southwest tributary, and remnant glacier ice.

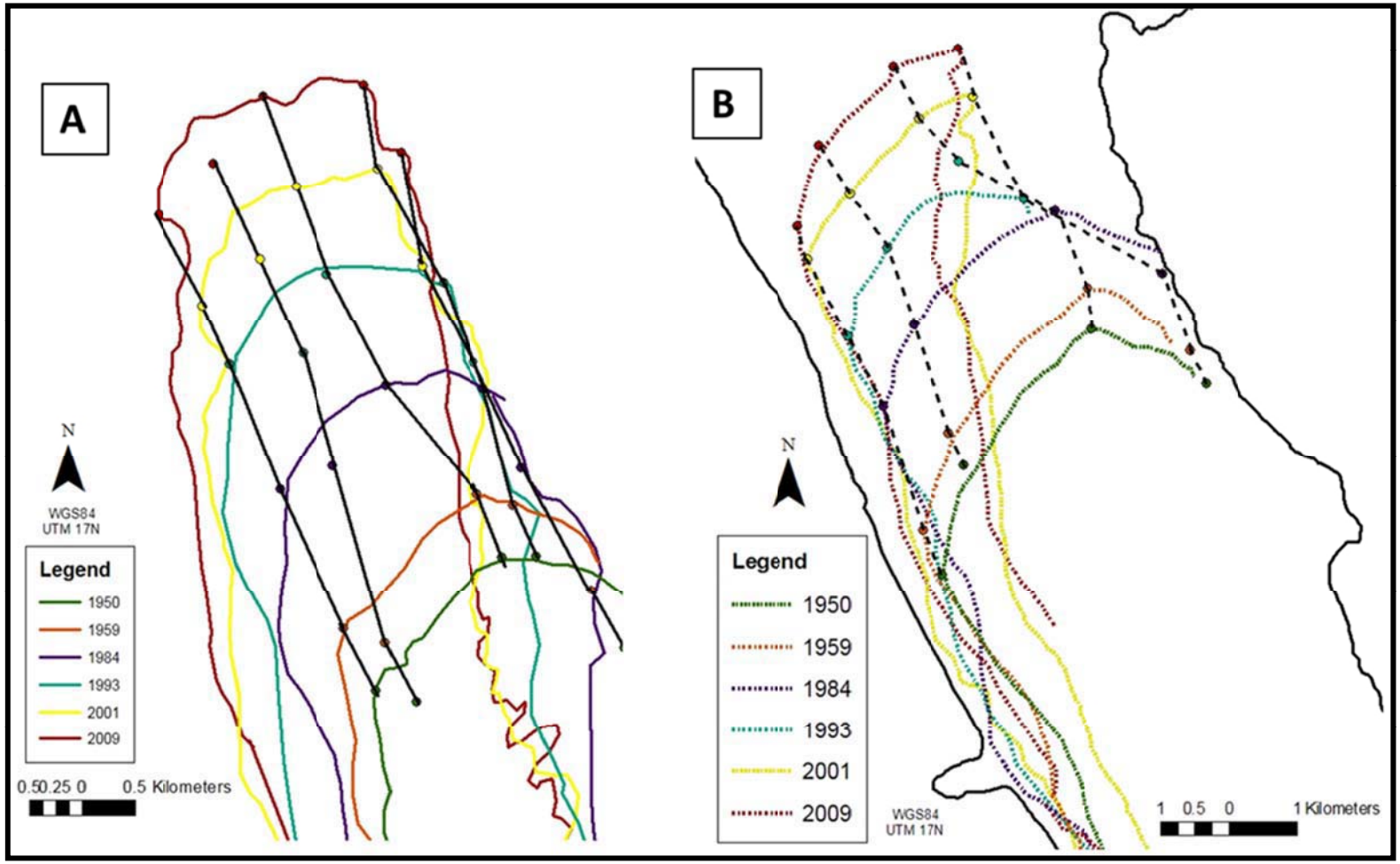

Figure 4.24: Measurements of temporal change of the Milne Glacier 1950 – 2009. A) Main tributary measurement axes (solid black lines) connect selected point (solid black circles); B) Southwest tributary measurement axes (dashed black lines) connect selected points (solid black circles).

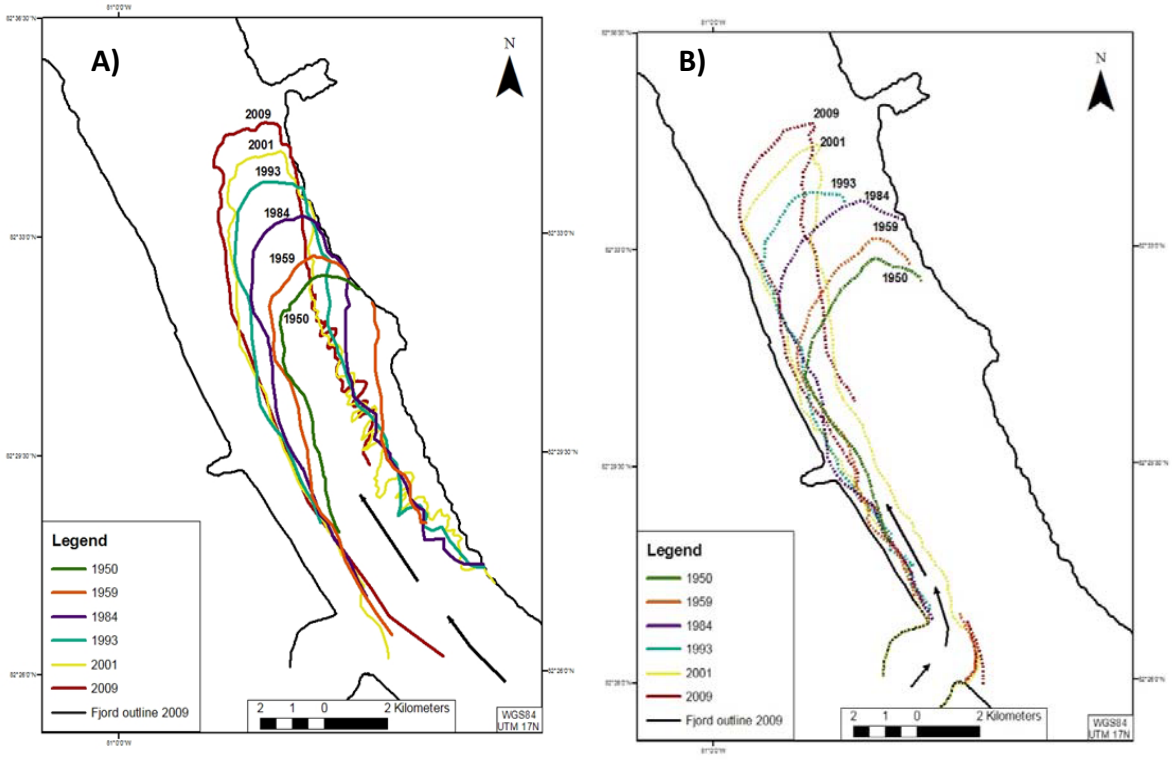

Figure 4.25: Temporal change of Milne Glacier A) Main tributary and B) Southwest tributary for 1950 – 2009.

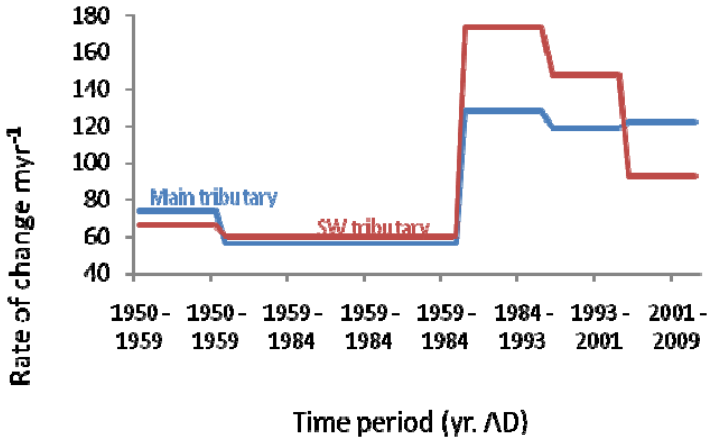

Figure 4.26: Rate of Milne Glacier terminus advance (m yr^{-1}) for the main tributary (blue line) and the southwest tributary (red line) for 1950 – 2009.

between 1984 and 1993, resulted in a loss of connection between the Milne Glacier and the Milne Ice Shelf.

Prior to ~1984 the Milne Glacier appears to have provided mass input to the Milne Ice Shelf. However, at present, melt from the Milne Glacier and surrounding catchment provides freshwater input to the Epishelf Lake but does not provide glacier mass input to the ice shelf. Between 1993 and 2001, the rate of advance of both tributaries declined slightly (Main: 118.9 m yr^{-1}; Southwest: 147.9 m yr^{-1}) compared to the previous time period (1984 – 1993) (Table 4.2; Figure 4.26). For the most recent period (2001-2009) the rate of advance increased for the main tributary (122 m yr^{-1}) but decreased for the southwest tributary (92.5 m yr^{-1}). These results illustrate the dynamic behaviour of the Milne Glacier over the last 50 years.

Chapter 5: Discussion and Conclusions

5.0 Discussion

The Milne Ice Shelf has experienced significant losses in mass since the mid-20th century. Measured reductions in ice shelf area (82 ±0.8 km^2, 26%: 1950-2009) and volume (2.8 ±0.9 km^3, 20%: 1981-2009) indicate that it has been in a state of overall negative mass balance since at least 1950. Over a similar time period, the 20% reduction in ice shelf volume between 1981 - 2008/2009 was comparable to decreases in ice shelf area of 18% (45 km^2) over the period 1984 – 2009, demonstrating that ice shelf thinning and area decrease provide similar indications of ice shelf loss.

Broken down by period, there was a decrease in mass input to the Milne Ice Shelf from the tributary glaciers during the early 1950s which continues to the present day. This was followed by significant ice shelf calving (26 km^2) sometime between 1959 and 1974. Re-building of MLSI in the Milne Re-entrant area throughout the 1970s and 1980s suggests that the ice shelf front was relatively stable during that time; however, significant reductions at the rear of the ice shelf were observed beginning in the 1980s. Negligible area change was observed over the last decade. These results have important implications for the current and future stability of the Milne Ice Shelf because thinner ice shelves are structurally weaker than thick ice shelves and are more vulnerable to mechanical stresses (Jeffries 1992a; Jeffries 1986a; Jeffries 1986b; Prager 1983; VanWychen and Copland 2011).

The changes at the Milne Ice Shelf are consistent with observed decreases in other high arctic glaciers and ice caps, ice shelves, and sea ice over the same period (Abdalati 2006; Boon et al. 2010; Braun et al. 2004b; Braun 2011; Copland et al. 2007; Maslanik et al. 2007; Mueller et al. 2009; Nghiem et al. 2007; Pope et al. 2011). This chapter interprets the observed Milne Ice Shelf changes in the context of these local (northern Ellesmere Island) and regional (Canadian High Arctic) cryospheric changes. Finally, a brief assessment of the current and future stability of the Milne Ice Shelf is presented.

5.1 Overall pattern of Milne and northern Ellesmere Island ice shelf area change: 1950 – 2009

5.1.1 20th century change

Beginning in the early- to mid-20th century, northern Ellesmere's ice shelves experienced a period of calving and mass loss. Russian and American military sightings of large ice islands in the Arctic Ocean including T1 (1946), T2 and T3 (1950) were traced back to the Ellesmere Island ice shelves (Crary 1958; Crary 1960; Koenig et al. 1952). Ice shelf calving and ice island sightings, including ~600 km^2 calved from the Ward Hunt Ice Shelf between 1961 and 1962, continued up until the mid-1960s (Jeffries 1987; Jeffries 1992a; Jeffries 1992b) (section 2.3.2.1, Table 2.1). This period of mass loss was followed by three decades of relative stability during the early 1970s to late 1990s. The exception to this pattern was the production of the ~40 km^2 Hobson's Choice ice island from the Ward Hunt Ice Shelf sometime between 1982 and 1983 during a brief warm period (Braun et al. 2004a; Jeffries 1992a; Mueller et al. 2003).

Mass losses observed for the Milne Ice Shelf (Table 4.1) are reasonably consistent with the patterns described above. Over the first ~40 years of this study area reductions were dominated by ice shelf calving (1959 – 1974) and epishelf lake development (1984 – 1993). The loss of 26 km^2 of ice shelf between 1959 and 1974, identified from air photo comparison, likely occurred around 1965 (based on evidence from ice cores; sections 2.4.3 and 2.5.1). Significant retreat of the Milne Fiord tributary glaciers (section 4.5.1), resulting in a reduction of mass input to the ice shelf, was also observed during this time (1950 – 1984). Area loss due to lake development (36 km^2, most of which is attributed to Milne Epishelf Lake development, Table 4.1) was greatest between 1984 and 1993. This period also corresponds with the loss of connection between the Milne Glacier and Milne Ice Shelf, further decreasing the glacier mass inputs to the ice shelf.

5.1.2 21st century change

Since the start of the 21st century there has been a dramatic increase in the break-up of ice shelves along northern Ellesmere Island. In particular, this has included the complete loss of the Ayles (87 km^2, 2005) and Markham (50 km^2, 2008) Ice Shelves, as well as significant fracturing and calving of the Ward Hunt (6 km^2 from 2000 - 2002, 42 km^2 in 2008), Petersen (13 km^2 in 2005, 8 km^2 from 2006-2007), and Serson (122 km^2 in 2008) Ice Shelves (Copland et al. 2007; Copland 2009; Mueller 2008; Vincent et al. 2001). It is important to note that iceberg calving can represent a temporary loss for an ice shelf, as new ice may be able to grow and replace the ice that was lost. However, the complete loss of an ice shelf, as has happened with the Ayles and Markham recently, is far more serious as it can take hundreds of years or longer for them to regrow even under favourable climate conditions (Braun 2011; England et al. 2008; Evans and England 1992; Vincent et al. 2001). Although northern Ellesmere's ice shelves have been in a state of negative mass balance for some time, these events suggest an acceleration and/or passing of a threshold over the last decade.

In contrast to all other northern Ellesmere ice shelves which experienced dramatic increases in fracturing and break-up over the last decade, the Milne Ice Shelf's area (~205 km^2) has remained unchanged since at least 2002 (Table 4.1). One explanation for the apparent stability of the Milne Ice Shelf is the favourable physiography of Milne Fiord (Braun 2011; Jeffries 1986b; Jeffries 2011). The presence of Cape Egerton, which is located on the eastern side of Milne Fiord and juts out into the Arctic Ocean, acts as a protective barrier for the Outer Unit by buffering it from the dominant sea ice drift patterns originating from the northeast (VanWychen and Copland 2011). This may be one reason why the Milne Ice Shelf did not experience any calving in the last decade whereas the entire adjacent Ayles Ice Shelf was lost in 2005. While the complex physiography of northern Ellesmere's coastline plays an important role in slowing the disintegration of the Milne Ice Shelf, it does not prevent weakening of the ice shelf interior as observed by an increase in the size and number of fractures and cracks (section 4.4), an increase in the number and size of ice

dammed lakes along the sides of Milne Fiord (sections 4.0 and 4.1), and establishment of the ~28.5 km^2 Milne Epishelf lake since the mid-1980s (section 4.1.3, Figure 4.3).

5.1.3 MLSI change

Temporal changes in multiyear landfast sea ice (MLSI) at the front of the Milne Ice Shelf display a similar trend to that observed for northern Ellesmere's ice shelves and ice plugs. Following the ~1965 ice shelf calving event, old, thick MLSI was able to establish itself in the Milne Re-entrant area and remain in place until February 1988 (Jeffries 1992a). Satellite imagery from 1993 shows the development of a ridged MLSI surface in this area, which indicates regrowth after the 1988 calving. These observations suggest that conditions favouring MLSI growth (cold temperatures and stable sea ice conditions over a period of several years) were present for much of the second half of the 20^{th} century and that calving was generally an infrequent event. This is consistent with the pattern of breakup events observed for the Nansen and Sverdrup Ice Plugs, to the west of the ice shelves, where occasional breakups in the 1970s to 1990s occurred within a context of general stability since these features were able to regrow following each loss (Pope et al. 2011).

Measurements of MLSI extent in front of the Milne Ice Shelf indicate that variability in its growth and calving has increased since the mid-1990s. Its overall area reduced by 71% (10.7 km^2) between 1993 and 2009 (section 4.1.4), with frequent calving from the same area. Similarly, ice plug losses have also become more frequent over the last decade (1998 to present). It appears that these events are now occurring within a climate where the sea ice that formed these features is no longer able to regrow to a substantial thickness between breakup events, instead being replaced by thinner and weaker first and second year ice. These changes are consistent with reports of a smaller, younger, and thinner sea ice cover over the Arctic Ocean (Comiso et al. 2008; Kwok and Cunningham 2010; Maslanik et al. 2007; Nghiem et al. 2007; Serrezze et al. 2007). Reductions in Arctic Ocean sea ice extent (7.8% $decade^{-1}$ between 1953 and 2006) and thickness (~1.3 m decrease in average sea ice

draft thickness between 1958 and 1999) have accelerated over the last decade (Maslanik et al. 2007; Stroeve et al. 2007). For example, record low September minimum sea ice cover, observed in 2007 (4.28 x 10^6 km^2) was 39% less than the 1979 – 2000 mean (~7 x 10^6 km^2). Further, in 2009, melt onset was two weeks earlier compared to the 1979-2000 mean (NSIDC Arctic Sea Ice News and Analysis, http://nsidc.org/arcticseaicenews). These observations provide further evidence that the arctic cryosphere is changing.

5.2 Interpretation of ice shelf thickness measurements

The first direct measurements of total thickness change for a northern Ellesmere Island ice shelf were determined in this study from radio-echo sounding (1981) and ground penetrating radar (2008/2009) measurements (section 4.4.1). The measured thinning of ~5 to 15 m is corroborated by changes in the depth of the halocline (freshwater-saltwater boundary) at Milne Epishelf Lake. Due to the lower density of freshwater compared to sea water, the freshwater layer floats at the top of the water column and is trapped in the Epishelf Lake at the rear of the ice shelf. The depth of the halocline thus corresponds to the minimum ice shelf thickness.

Density stratification beneath the Milne Ice Shelf was first reported by Jeffries (1985), who noted the presence of a freshwater layer of up to ~17.5 m deep in spring 1983. For this study, original data from water profiles conducted on the Milne Epishelf Lake over the period 1983 – 2009 were plotted to ensure consistent determination of halocline depth (Figure 2.24). Profiles were collected by M.O Jeffries in 1983, by Veillette et al. in 2004, 2006, and 2007, and in spring 2009 as part of the current study. Shallower, but variable, haloclines were observed over the first half of this decade (18.1 m in 2004, 15.6 m in 2006, 16.5 m in 2007, and 14.6 m in 2009; Figure 2.23), compared to those measured in 1983. Despite the use of different instruments over time, together with seasonal differences in measurement time, a reduction in the freshwater layer of ~3.5 m was observed between 1983 and 2009. This indicates a reduction in minimum ice shelf draft over time. The shallowing

of the freshwater layer confirms that the Milne Ice shelf has experienced thinning, with the strong reduction in halocline depth since ~1983 consistent with the observed increase in fractures and crevasses identified from GPR profiles and SAR imagery over this period.

5.2.1 Comparison of Milne Ice Shelf thickness change with northern Ellesmere Island ice shelf (Ward Hunt Ice Shelf) thickness change

The average Milne Ice Shelf thinning of ~15 m between 1981 and 2008/2009, derived from DEM differencing, is comparable to that documented for the nearby Ward Hunt Ice Shelf (WHIS). Information concerning longer term changes at the WHIS are available from radio-echo sounding (RES) measurements on meteoric ice sections of the ice shelf in 1966 (Hattersley-Smith et al. 1969) and 1981 (Narod et al. 1988). RES soundings for the western sector of WHIS to the north of Cape Discovery ranged from ~20-80 m (mean ice thickness ~44.5 m) in 1966 compared to 40-50 m from the eastern section in 1981. Although the sections profiled are not directly comparable, the measurements suggest ice shelf thinning during this time.

After 1981, Jeffries et al. (1988) estimated an average Ward Hunt Ice Shelf (WHIS) thickness of 47.5 m from ice cores collected between 1982 and 1986. Water profiles collected between 1983 and 1999 showed a 22% reduction in depth of the epishelf freshwater layer, which measured 35 m in 1999 (Jeffries and Krouse 1987; Veillette et al. 2008; Vincent et al. 2001). Localized ice thickness estimates based on the freeboard height of floating ice blocks (July-August 2002) situated in a fracture south of Ward Hunt Island showed a further reduction in ice thickness (~25 m thick; Mueller et al. 2003). Overall, thinning of ~15 m likely occurred on WHIS occurred between 1981 and 2002 (Braun et al. 2004a; Braun 2011; Jeffries 1985; Mueller et al. 2003). This thinning was proportionally greater for the WHIS than the Milne Ice Shelf because the mean ice thickness of WHIS is less.

5.3 Milne and northern Ellesmere Island ice shelf mass balance

Direct long-term mass balance measurements are not available for the Milne Ice Shelf. However, area and volume reductions, increases in lake development, and glacier retreat collectively demonstrate that Milne Ice Shelf's mass balance has been negative since at least 1950. Accumulation from factors such as precipitation, basal accretion and glacier input has not balanced out losses due to calving, surface and basal melt, and glacier retreat. Mean annual mass balance computed from the direct line comparison ranged from -0.10 m w.e. yr^{-1} to -0.34 m w.e. yr^{-1} for the period 1981 – 2008/2009 (section 4.4.1.1).

Negative mass balances have been measured for the WHIS, where surface measurements are available for 1966 – 2003. Over the 37 year period, mean annual surface mass balance for the WHIS was -0.07 m w.e. yr^{-1}, with negative summer balances (mean: -0.20 m w.e. yr^{-1}) dominating positive winter balances (mean: +0.15 m w.e. yr^{-1}) (Braun 2004a; Braun 2011). Positive mass balance years were only observed on WHIS for 1963 – 1965 and 1972-1973. Total cumulative surface mass balance of WHIS was -3.1 m w.e. over the period 1966-2003. It should be noted that these measurements only provide data on surface lowering, however, and do not include mass gains or losses from the ice shelf base or from internal accumulation. Given that total thinning on WHIS has been significantly greater than 3.1 m w.e. over the period of study, it appears that net losses have occurred from the ice shelf base.

Comparison of total annual mass balance for the Milne Ice Shelf with annual surface mass balances measured for the Ward Hunt Ice Shelf suggests that losses at the ice shelf base (basal melt) are highly significant. Although it is acknowledged that the two ice shelves are not directly comparable, if a rate of surface mass loss similar to that observed for the Ward Hunt Ice Shelf (-0.07 m w.e. yr^{-1}) were applied to the Milne Ice Shelf, thinning due to basal melt would range from 30% (-0.03 m w.e. yr^{-1}) to 79% (-0.27 m w.e. yr^{-1}) of total thickness change This comparison suggests the importance of basal melt in ice shelf mass loss on northern Ellesmere Island. The importance of basal melt on ice shelf losses has also

been observed in the Antarctic Peninsula, where disintegration of the Larsen A and B Ice Shelves was preceded by a prolonged period of thinning which occurred almost entirely from melt at the ice shelf base (Shepherd et al. 2003).

5.3.1 Milne Ice Shelf mass balance gradient

The spatial distribution of thinning across the Milne Ice Shelf appears to be uneven, with DEM differencing over the period 1981 to 2008/2009 revealing slight loss at the front of the ice shelf, but increasingly large losses towards the centre and rear of the ice shelf. This is consistent with the mass balance conditions observed along the northwest coast of Ellesmere Island, where surface snow accumulation is highest near the coast due to proximity to open water (Braun 2011; Koerner 1979). For example, Pope (2010) noted decreasing snow accumulation with distance from the coast over a 20 km long north-south GPR transect in Yelverton Inlet in early June 2009. The accumulation gradient further impacts mass balance, because the higher albedo of fresh snow near the coast retards melt compared to the rear of the ice shelf where lower albedo and higher rates of ablation are observed (Braun 2011; Vincent et al. 2001).

Ground observations also confirm the presence of higher surface ablation towards the rear of the Milne Ice Shelf. Jeffries (1986b) suggested that the presence of lichens on moraines at the back of the ice shelf and the absence of lichens on rock outcrops near Glacier 1 located near the front of the ice shelf (Figure 2.18) meant that the moraines towards the rear had been exposed for some time. The higher rates of backwasting of tributary glaciers observed towards the rear of the ice shelf (section 4.6.1) suggest a more negative mass balance with distance from the coast. Collectively, these observations reinforce the idea that the mass balance gradient for the Milne Ice Shelf is *reversed* (compared to that observed on most glaciers and Antarctic ice shelves), with less negative mass balances near the ice shelf front and more negative mass balances towards the rear.

5.4 Comparison with Canadian Arctic Archipelago glaciers and ice caps

The temporal trend in mass loss for the Milne Ice Shelf is consistent with that observed for glaciers and ice caps of the Canadian Arctic Archipelago (CAA), which have been in an overall state of negative mass balance since measurements began in 1959, with increasingly negative mass balances since the 1990s. Mass balance studies for glaciers and ice caps on the northwest coast of Ellesmere Island do not exist, although there are mass balance programs on north-central Ellesmere Island (Simmons and Murray Ice Caps: 1963 – 2003), eastern Ellesmere Island (Prince of Wales Ice Cap: 1963 – 2003), Drambuie Glacier (northeast side of Agassiz Ice Cap: 1977 - 2003), Axel Heiberg Island (White Glacier: 1960 – 2003) and Meighen Island (Meighen Ice Cap: 1960 - 2003) which provide a long term regional context in which to interpret the Milne Ice Shelf changes.

Mass balance records for the Murray and Simmons Ice Caps show negative balances observed during the early 1960s (measurements began in ~1963), after which a period of net accumulation and positive mass balance was observed from the late 1960s to early 1970s. Aside from a few positive balance years (e.g. 1982/1983), mass balances have been negative since then, with increasingly negative mass balances since the 1990s (Braun et al. 2004b). Records from stake measurements for the Drambuie Glacier show increasingly negative mean surface mass balances between 1977 (when records began) and 2003 (Braun 2011; Koerner 2002). When iceberg calving is included, overall mass balance for the 19,325 km^2 Prince of Wales Icefield, eastern Ellesmere Island, was also negative for the period 1963 – 2003 (Mair et al. 2009). Similar trends are observed for White Glacier and Meighen Ice Cap, where the decadal mean annual mass balances for the period 1961 – 2000 were -0.14 m w.e. yr^{-1} and -0.08 m w.e. yr^{-1} respectively (Braun 2011; Koerner 2005). For most glaciers and ice caps monitored, summer balances are more variable and appear to dominate the overall trend (Koerner 2002; Koerner 2005).

5.5 Recent observations in context of long-term northern Ellesmere Island ice shelf history

Ice shelf formation requires cold temperatures and sufficient precipitation. These conditions were present ~5500 - 3500 B.P., during a period of climate cooling, when ice shelf formation along northern Ellesmere is thought to have occurred (England et al. 2011). The first recorded human visit to the ice shelves in the late 19th century coincided with the end of the Little Ice Age, a period of colder than normal temperatures (England et al. 2008). Since the explorations of Aldrich (1875/1876) and Peary (1906), the known extent of the once-continuous 'Ellesmere Ice Shelf' has reduced by >90% (Copland et al. 2007; Dowdeswell and Jeffries 2011; Vincent et al. 2001). Because the surface mass balance of ice shelves without significant glacier mass input, like those observed along Ellesmere Island, is largely determined by climate variables, Milne Ice Shelf change must therefore be interpreted in the context of the region's short (years to decades) and long-term (decades to centuries) climate.

It is important to note that the 59 year period of study presented here represents only a brief snapshot of the Milne Ice Shelf's ~5500 year history. The majority of northern Ellesmere's ice shelf mass loss is thought to have occurred during the first half of the 20th century (Koenig et al. 1952), prior to modern scientific observations. By start of the study period in 1950 more than half of the once continuous ~10,000 km^2 'Ellesmere Ice Shelf' had disintegrated, indicating that the ice shelves had been in a state of negative mass balance for some time (Braun et al. 2004a; Copland et al. 2007; Evans and England 1992; Jeffries 2002; Koenig et al. 1952; Mueller et al. 2006; Vincent et al. 2001). This overall negative ice shelf mass balance, observed since at least the early 1900s, became increasingly more negative beginning in the ~1950s (Braun 2011). The measured reductions in Milne Ice Shelf area (1950 – 2009) appear to coincide with acceleration of negative mass balances for both northern Ellesmere Island's ice shelves and for glaciers and ice caps in the northern CAA (section 5.4).

5.6 Ice shelf-climate context

5.6.1 Large-scale synoptic influences

The primary synoptic climate regimes affecting the decadal-scale climate of northern Ellesmere Island include the North Atlantic Oscillation (NAO) and the Arctic Oscillation (AO) (Lesins 2010; Mantua et al. 1997; Serrezze and Barry 2005). Lesins et al. (2010) noted significant variability in winter pressure conditions between 1954/1955 and 1980 at Eureka, which he attributed to the strength of the NAO. However, there is insufficient temporal information about recent ice shelf break-up events and changes to evaluate whether they are related to a specific climate index.

5.6.2 Northwest Ellesmere Island climate

Continuous climate observations at the ice shelves have only been available since 2008 (section 3.2.1; http://tinyurl.com/milnewx), so direct long-term comparisons are only possible with the two Environment Canada stations at Alert (82°32'12"N, 62°16'8"W) and Eureka (79°58'8"N, 85°55'8"W), which are both ~320 km from the Milne Ice Shelf (www.weatheroffice.ec.gc.ca). Analysis of climate data from Eureka (1953-2007) revealed a general cooling period between 1953 and 1972, with a few warm years in the 1960s (Lesins et al. 2010). This was followed by pronounced warming between 1972 and the mid-1980s, a brief cooling in the mid-1980s, and then warming that continues to present-day (with stronger increases since the mid-1990s). The overall warming trend since 1972 has resulted in an increase in mean annual temperature of ~3.5°C at Eureka, with warming concentrated in the colder months (Lesins et al. 2010).

The significant distance between the stations at Eureka/Alert and the Milne Ice Shelf means that the conditions they report do not necessarily represent those affecting the Milne Ice Shelf. To address this issue, studies by Copland et al. (2007) and Mueller et al. (2009)

used NCEP/NCAR reanalysis data to reconstruct information about local climate patterns and trends. It should be noted that the relatively low spatial resolution (grid spacing of 2.5° x 2.5°) and low station density from which to derive the interpolated estimates should to be taken into account when interpreting these data sets.

Reanalysis data for a grid point centered over the Ayles Ice Shelf showed warming of 0.37°C decade^{-1} for 1966 – 2003 (Copland et al. 2007). Analysis of reanalysis data for a grid point centered over M'Clintock Fiord (immediately to the west of the Ward Hunt Ice Shelf) between 1949 and 2007 revealed an increase in mean annual surface air temperatures of 0.48°C decade^{-1} (Mueller et al. 2009). Mueller et al. (2009) used lake phenology and direct observations from Alert/Eureka to assess the validity of reanalysis products (NCEP/NCAR) in depicting the meteorological conditions observed along the northern coast of Ellesmere Island. Results from this study showed that climate shifts identified in lake phenology followed closely with the climate data, but that the true conditions observed on the ground fell somewhere between the reanalysis estimates (higher) and the direct meteorological observations (lower) at Alert and Eureka.

In addition to mean air temperatures, the total number of freezing degree days (FDDs) and positive degree days (PDDs) has been used to assess ice shelf changes. Fewer FDDs likely mean reduced ice growth due to reductions in basal freeze on, as well as less cold internal ice temperatures that make ice shelves more vulnerable to summer melting. Positive degree days, on the other hand, can be used as a proxy for summer melt. Together these measures have been used to identify possible limits of thermal viability. For example, in investigating potential causes for the loss of the Ayles Ice Shelf on 13 August 2005, Copland et al. (2007) identified a threshold of 200 PDDs for ice shelf survival; above this threshold ice shelf calving is usually observed. Similar thresholds have been proposed for Antarctic Peninsula ice shelves where a mean annual -5°C isotherm and a mean summer temperature of ~0°C represent the upper limits of Antarctic Ice Shelf viability (Dowdeswell and Jeffries 2011; Mercer 1978; Robin and Adie 1964).

For the northwest CAA, trends for PDDs and FDDs have been established for the last ~60 years. Based on reanalysis data and direct observations at Eureka, a period of high PDDs was observed between 1948 and 1963 and again from the early 1990s to present (2006) (Copland et al. 2007; Lesins et al. 2010; Mueller et al. 2009). This first period of high PDDs corresponds with a period of warmer summers at Eureka in the 1950s through to the late 1960s and breakup of many ice shelves at this time (Hattersley-Smith 1963). The most recent period of high PDDs coincides with higher mean annual air temperatures at Eureka (Lesins et al. 2010) and is consistent with the loss of ~328 km^2 of ice shelves between 2002 and 2008 (Copland 2009). For the Milne Ice Shelf, this warm period (1990s – present) is consistent with observations of more frequent MLSI calving over the last decade and thinning of the Milne Ice Shelf between 1981 and 2008/2009. Finally, longer melt seasons increase ablation and may expose debris which can increase surface melt (Vincent et al. 2001).

In contrast to the variable pattern of PDD changes over time, a large and continuous reduction in FDDs has been observed along the entire NW coast of Ellesmere Island over the last 50+ years, suggesting that warming is concentrated in the winter months (Copland et al. 2007; Mueller et al. 2009). Over the period 1948 – 2006, FDDs for the Ayles ice shelf reduced from ~7000 yr^{-1} in the 1940s to <6000 yr^{-1} in the last decade. In particular, the lowest number of FDDs on record (5472 yr^{-1}) was observed in the winter preceding the loss of the Ayles Ice Shelf (Copland et al. 2007). Less freezing degree days, which are used as a proxy for winter cooling, have an important impact for ice shelves as it means that they are not able to regenerate over the winter from basal freeze-on. Reductions in winter cooling can also help increase the period of summer melt because less energy is required to bring colder ice to the melting point. It has been proposed that winter warming is equally, if not more important than summer temperatures for ice shelf disintegration (Braun 2011; Copland et al. 2007; Lesins 2010; Vincent et al. 2001).

Finally, a 10% increase in precipitable water was observed at Eureka between 1961 and 2007 (Lesins 2010). A similar observation was made by Mueller et al. (2009), who

observed both an increase in precipitation and an increase in temperatures at Alert and Eureka between 1948 and 2007. This suggests that the measured glacier retreats for the Milne Ice shelf's tributary glaciers are likely driven more by temperature than by a reduction in precipitation.

5.7 Assessment of current Milne Ice Shelf stability

Given the evidence presented above, it is clear that the High Arctic has experienced significant warming over the course of the study period (1950 – 2009). Along the northwest coast of Ellesmere Island, dramatic ice shelf loss, reductions in old multiyear landfast sea ice and ice plugs are clear indications that the region's present climate is no longer able to support the existence of these features. Regional-scale evidence of long-term negative mass balance on glaciers and ice caps in the Canadian Arctic Archipelago further corroborates these trends. In this context the measured reductions in Milne Ice Shelf mass can be expected to have negative implications for the future survival of the ice shelf.

Results from this study show that the Milne Ice Shelf has undergone significant mass loss and structural weakening over the last 59 years. Structural weakening is evidenced by the development of new cracks (between 1981 and 2008/2009), as well as the lengthening of existing cracks (between 1950 and 2009). This is important given the fact that the recent (21st century) break-ups of the Ayles and Ward Hunt Ice Shelves have occurred along pre-existing fractures (Copland et al. 2007; Mueller et al. 2008). The rate of lake development, which is also a sign of negative mass balance, appears to have increased over the 59-year study period. Although the ~28.5 km^2 Milne Epishelf Lake was the largest single contributor to lake area, ice-dammed lakes also developed along the sides of Milne Fiord. These developments are important because lakes that penetrate the entire ice shelf depth indicate that the ice shelf has become detached from the fiord walls, making it more vulnerable to future calving events.

Most of the observed northern Ellesmere ice shelf disintegration has been attributed to strong winter warming and overall climate amelioration (Braun et al. 2004b; Copland et al. 2007; Mueller et al. 2009). Reductions in mass input from tributary glaciers further contribute to a negative ice shelf mass balance. This results in a *pre-weakened* ice shelf; meaning that, under the current climate, the Milne Ice Shelf can no longer regenerate and is structurally unstable. Once an ice shelf has entered this state, the presence of MLSI and pack ice is critical to its stability as sea ice provides a buttressing effect and protects the ice shelf against wind, wave and tidal action (Braun 2011; Copland et al. 2007; Glasser and Scambos 2008). Once the sea ice fringe is removed, as was the case during the 2005 and 2008 northern Ellesmere Island ice shelf break-up events (sections 1.1.5 and 2.2.1), the weak ice shelf ice is less able to withstand the effects of tides, waves and offshore winds (Copland et al. 2007; Dowdeswell and Jeffries 2011; Mueller 2008).

The Milne Ice Shelf is currently an artefact formed under past colder conditions that is not in equilibrium with the current climate. As the ice shelf responds to present-day temperatures, it is likely that the complete loss of the Milne Ice Shelf will occur (Braun et al. 2004a; Copland et al. 2007). When placed in the context of 20th and 21st century warming (~0.26°C per decade north of 60°N since the 1960s; ACIA 2004; Lemke et al. 2007) it is likely that the Milne Ice Shelf will continue to deteriorate under future warming scenarios of 3°C to 11°C by the end of the 21st century (Lemke et al. 2007). It is possible that over the next few decades the Milne Ice Shelf will follow the pattern of break-ups observed for all other northern Ellesmere ice shelves. If true, this would be in agreement with the prediction of Hattersley-Smith et al. (1955) that northern Ellesmere's ice shelves will all be lost by 2035.

Chapter 6: References

Abdalati, W. 2006. Recent changes in high-latitude glaciers, ice caps and ice sheets. *Weather,* **61**(4): 95 – 101.

Abdalati, W., Krabbill, W., Frederick, E., Manizade, S., Martin, C., Sonntag, J., Swift, R., Thomas, R., Yungel, J., Koerner, R. 2004. Elevation changes of ice caps in the Canadian Arctic Archipelago. *Journal of Geophysical Research*, **109**(F04007): 1-11.

Adams, W.P., Cogley, J.G., Ecclestone, M.A., Demuth, M.N. 1998. A small glacier as an index of regional mass balance: Baby Glacier, Axel Heiberg Island, 1952 – 1992. *Geografiska Annaler,* **80**(1): 37-50.

Alt, B., Wilson, K., Carrieres, T. 2006. A case study of old-ice import and export through the Peary and Sverdrup Channels in the Canadian Arctic Archipelago: 1998-2005. *Annals of Glaciology*, **44**(1): 329-338.

Andrews, J.T., and Barry, R.G. 1978. Glacial inception and disintegration during the last glaciation. *Annual Reviews Earth Planetary Science,* **6**: 205-228.

Annan, A.P. 2002. GPR – History, Trends, and Future developments. *Subsurface sensing technologies and applications,* **3**(4): 253-270.

Anonymous 1969. Mass-balance terms. *Journal of Glaciology*, **52** (8): 3-7.

Arctic Climate Impact Assessment (ACIA). 2004. Chapter 4: Cryosphere and Hydrology. *Arctic Climate Impact Assessment*.

Bailey, J.T., Evans, S., Robin, G. de Q. 1964. Radio echo sounding of polar ice sheets, *Nature,* **204**(4957): 420 – 421.

Bamber, J.L. and Payne, A.J. 2004. Mass balance of the cryosphere: Observations and modeling of contemporary and future changes. Cambridge University Press. Cambridge, U.K.

Barrett, B.E., Murray, T., Clark, R. 2007. Errors in radar CMP velocity estimates due to survey geometry, and their implications for ice water content estimation, *Journal of Environmental and Engineering Geophysics*, **12**(1): 101-111.

Benn, D., and Evans, D. 2010. Glaciers and Glaciation 2nd Edition. London: Arnold.

Bingham, R.G. and Siegert, M.J. 2007. Radio-echo sounding over polar ice masses, *Journal of Environmental and Engineering Geophysics*, **12**(1): 47-62.

Bingham, R.G. and Siegert, M.J. 2009. Quantifying bed roughness in Antarctica: implications for ice-sheet dynamics and history, *Quaternary Science Reviews*, **28**: 223 – 236.

Black, W.A. 1962. Sea-Ice survey, Queen Elizabeth Island Region, summer 1962. Geographical Paper No. 39. Department of Mines and Technical Surveys, Ottawa.

Boon, S., Burges, D.O., Koerner, R.M., and Sharp, M.J. 2010. Forty-seven years of research on the Devon Ice Cap, Arctic Canada. *Arctic,* **63**(1): 13-29.

Bradley, R.S. 1990. Holocene Paleoclimatology of the Queen Elizabeth Islands, Canadian High Arctic. *Quaternary Science Reviews*, **9**(4): 365-384.

Braun, C. 2011. The surface mass balance of the Ward Hunt Ice Shelf and Ward Hun Ice Rise, Ellesmere Island, Nunavut, Canada. In: Arctic Ice Shelves and Ice Islands. Copland, L. and Mueller, D.R. (eds). Springer-Praxis, Amsterdam.

Braun, C., Hardy, D.R., Bradley, R.S. 2001. Recent recession of small plateau ice cap, Ellesmere Island, Canada. *Journal of Glaciology*, **47**(156): 154-154.

Braun, C., Hardy, D. R., Bradley, R.S. 2004a Surface mass balance of the Ward Hunt Ice Shelf. Ellesmere Island, Nunavut, Canada. *Journal of Geophysical Research,* **109**(D22110):1-9.

Braun, C., Hardy, D.R., and Bradley, R.S. 2004b Mass balance and area changes of four High Arctic plateau ice caps, 1959 – 2002. *Geografiska Annaler*, **86A**(1): 43-52.

Bushnell, V.C. (1956) Marvin's ice shelf journey, 1906. *Arctic*, **9**(3): 166-177.

Campbell, J.B. 2002. Introduction to remote sensing, Third Edition. Guilford Press, New York, New York, U.S.A.

Comiso, J.C. 2003. Large scale characteristics and variability of the global sea ice cover. In: *Sea Ice - An Introduction to its Physics, Biology, Chemistry, and Geology.* Thomas, D. and G.S. Dieckmann (eds.). Blackwell Science, Oxford, UK, pp. 112—142.

Comiso, J.C., Parkinson, C.L., Gersten, R., Stock, L. 2008. Accelerated decline in the Arctic sea ice cover. *Geophysical Research Letters,* 35(L01703):1-6.

Copland, L. 2009. Review of recent changes in Canadian Arctic ice shelves. Internal report for the Canadian Ice Service.

Copland, L., Sharp, M. 2001. Mapping thermal and hydrological conditions beneath a polythermal glacier with radio-echo sounding. *Journal of Glaciology*. **47***(*157): 232-242.

Copland, L., Sharp, M. and Dowdeswell, J. 2003. The distribution and flow characteristics of surge-type glaciers in the Canadian High Arctic. *Annals of Glaciology*, (**36**): 73-81.

Copland, L., Mueller, D.R., Weir, L. 2007. Rapid loss of the Ayles Ice Shelf, Ellesmere Island, Canada. *Geophysical Research Letters*, **34** (L21501): 1-6.

Crabtree, R.D., Doake, C.S.M. 1986. Radio-echo investigations of Ronne Ice Shelf, *Annals of Glaciology*, **8**: 37-41.

Crary, A.P. 1958. Arctic ice island and ice shelf studies, Part I. *Arctic*, **11** (1): 2-34.

Crary, A.P. 1960, Arctic ice island and ice shelf studies, Part II. *Arctic*, **13** (1): 32-50.

DeBeer, C.M. and Sharp, M.J. 2009. Topographic influences on recent changes of very small glaciers in the Monashee Mountains, British Columbia, Canada. *Journal of Glaciology*, **35**(192): 691-700.

Demuth, M. N., and Pietroniro, A. 2007. Climate change impacts on Canadian glaciers: Why worry? Workshop on adapting to water supply issues in a changing climate: Earth Science Contributions.

Dowdeswell, J.A. 2011. Eurasian Arctic ice shelves and tidewater glacier margins. *In* Copland, L. and Mueller, D.R. (eds.), *Arctic Ice Shelves and Ice Islands*. Springer SBM, Dordrecht.

Dowdeswell, J.A. and Jeffries, M.O. 2011. Arctic ice shelves: an introduction. In: Arctic Ice Shelves and Ice Islands. Copland, L. and Mueller, D.R. (eds). Springer-Praxis, Amsterdam.

Dunse, T., Eisen, O., Helm, V., Rack, W., Steinhage, D., Parry, V., 2008. Characteristics and small-scale variability of GPR signals and their relation to snow accumulation in Greenland's percolation zone. *Journal of Glaciology*, **54**(185), 333-342.

Duguay, C. R. 2006. Recent trends in Canadian lake ice cover. *Hydrological Processes*, ***20***: 781-801.

Dyke, A.S., England, J., Reimnitz, E., Jette, H. 1997. Changes in driftwood delivery to the Canadian Arctic Archipelago: the hypothesis of postglacial oscillations of the Transpolar Drift. *Arctic*, 50(1): 1-16.

England, J.H., Lakeman, T.R., Lemmen, D.S., Bednarski, J.M., Stewart, T.G., Evans, D.J.A. 2008. A millennial-scale record of Arctic Ocean sea ice variability and the demise of the Ellesmere Island ice shelves. *Geophysical Research Letters*, **35** (L19502): 1-5.

England J.H., Evans, D.J.A., Lakeman, T. 2011. Holocene history of Arctic ice shelves. *In* Copland, L. and Mueller, D.R. (eds.), *Arctic Ice Shelves and Ice Islands*. Springer SBM, Dordrecht.

Environment Canada. 2009. Weather Data: Canadian Climate Normals: Alert and Eureka. http://www.climate.weatherofice.ec.gc.ca/climate_normals/index_e.html.

European environmental agency. 2008. Energy and Environment. European Union publications office, Copenhagen, Denmark.

Evans S. and Robin, G. de Q. 1966. Glacier depth sounding from the air. *Nature*. **210** (5039): 883 – 885.

Evans, D.J.A. and England, J. 1992. Geomorphological evidence of Holocene climatic change from northwest Ellesmere Island, Canadian High Arctic. *The Holocene,* **2**:148-158.

Gardner, A.S. and Sharp, M. 2007. Influence of the Arctic circumpolar vortex on the mass balance of Canadian High Arctic glaciers. *Journal of Climate*, **20**: 4586-4598.

Glasser, N.F., Kulessa, B., Luckman, A., Jansen, D., King, E.C., Sammonds, P.R., Scambos, T.A., Jezek, K.C. 2009. Surface structure and stability of the Larsen C ice shelf, Antarctic Peninsula. *Journal of Glaciology*, **55** (191): 400-410.

Glasser, N.F. and Scambos, T.A. 2008. A structural glaciological analysis of the 2002 Larsen B ice shelf collapse. *Journal of Glaciology,* **54**(184): 3 – 16.

Grant, K.L., Stokes, C.R., Evans, I.S. 2009. Identification and characteristics of surge-type glaciers on Novaya Zemlya, Russian Arctic. *Journal of Glaciology*, **55** (194): 960 – 972.

Hamran, S-E., Guneriussen, T., Hagen, J.O., Odegard, R. 1997. Ground penetrating radar and ERS SAR data for glacier monitoring, *Proc. IGARSS –Remote Sensing- A Scientific Visions for Sustainable Development*, 634-636.

Hattersley-Smith, G. 1957. The rolls on the Ellesmere ice shelf. *Arctic*, **10**: 32-44.

Hattersley-Smith, G. 1963. The Ward Hunt ice Shelf: recent changes of the ice front. *Journal of Glaciology*, **4**: 415-424.

Hattersley-Smith, G. 1969. Results of radio echo sounding in Northern Ellesmere Island, 1966. *The Geographical Journal*, **135** (4): 553-557.

Hattersley-Smith, G., A.P. Crary, Christie, R.L., 1955. Northern Ellesmere Island, 1953 and 1954. Arctic, **8**(1): 3-36.

Hattersley-Smith, G., Fuzey, A., Evans, S. 1969. Glacier depths in northern Ellesmere Island: Airborne radio echo sounding in 1966. DREO Technical note no. 69-6. Defense research board, department of national defense Canada, defense research establishment Ottawa: geophysics section.

Hattersley-Smith, G., and Serson, H. 1970. Mass balance of the Ward Hunt Ice Rise and Ice Shelf: a 10-year record. *Journal of Glaciology,* **9**(56): 247-252.

Hock, R. 2003. Temperature index modeling in mountain areas. *Hydrology,* **282**(1-4): 104-115.

Holdsworth, G. 1987. *The surface waveforms on the Ellesmere Island ice shelves and ice islands*. Workshop on Extreme Ice Features, Technical Memorandum 141 (NRCC 28003), National Research Council of Canada, 385 – 403.

Holdsworth, G. and Glynn, J. 1978. Iceberg calving from floating glaciers by a vibrating mechanism. *Nature*, **274**: 464 – 466.

Hubbard, B. and Glasser, N. 2005. Field techniques in glaciology and glacial geomorphology. John Wiley and Sons Ltd., West Sussex, U.K.

Huss, M., Stockli, R, Kappenberger, G., Blatter, H. 2008. Temporal and spatial changes of Laika Glacier, Canadian Arctic, since 1959, inferred from satellite remote sensing and mass-balance modeling. *Journal of Glaciology*, **54**(188):857 – 866.

Irvine-Fynn, T.D.L., Moorman, B.J., Williams, J.L.M., Walter, F.S.A., 2006. Seasonal changes in ground-penetrating radar signature observed at a polythermal glacier, Bylot Island, Canada. *Earth Surface Processes and Landforms,* **31**(7), 892-909.

Jeffries, M.O. 1984. Milne Glacier, northern Ellesmere Island, N.W.T., Canada: a surging glacier?, *Journal of Glaciology*, **30**(105): 251-253.

Jeffries, M.O. 1985. *Physical, chemical and isotopic investigations of Ward Hunt Ice Shelf and Milne Ice Shelf, Ellesmere Island, NWT.* Ph.D. Thesis. The University of Calgary. Calgary, Canada.

Jeffries, M.O. 1985. Ice shelf studies off Northern Ellesmere Island, spring 1983. *Arctic*, **38**(3): 174-177.

Jeffries, M.O. 1986a. Ice island calvings and ice shelf changes, Milne Ice Shelf and Ayles Ice Shelf, Ellesmere Island, N.W.T., *Arctic*, **39**(1): 15-19.

Jeffries, M.O. 1986b. Glaciers and the morphology and structure of Milne Ice Shelf, Ellesmere Island, N.W.T., *Canada. Arctic and Alpine Research*. **18**(4): 397-405.

Jeffries, M.O. 1987. The growth, structure and disintegration of Arctic ice shelves. *Polar Record*, **23**(147): 631-649.

Jeffries, M.O. 1992a. Arctic ice shelves and ice islands: origin, growth and disintegration, physical characteristics, structural-stratigraphic variability, and dynamics. *Reviews of Geophysics*, **30**(92): 245-267.

Jeffries, M.O. 1992b. The source and calving of ice island ARLIS-II, *Polar Record*, **28**(165): 137-144.

Jeffries, M.O. 2002. Glaciers of North America – Glaciers of Canada. Glaciers of the Arctic islands. Ellesmere Island Ice Shelves and Ice Islands. Satellite Image Atlas of Glaciers of the World. U.S. Geological Survey Professional Paper 1386-J-1.

Jeffries, M.O. 2011. The Ellesmere Ice Shelves, Nunavut, Canada. In: Arctic Ice Shelves and Ice Islands. Copland, L. and Mueller, D.R. (eds). Springer-Praxis, Amsterdam.

Jeffries, M.O. and Krouse, H.R. 1987. Snowfall and oxygen-isotope variations off the north coast of Ellesmere Island, N.W.T., Canada, *Journal of Glaciology*, **33**(114): 195 – 199.

Jeffries, M.O. and Sackinger, W.M. 1990. Ice island detection and characterization with airborne synthetic aperture radar. *Journal of Geophysical Research*, **95**(C4): 5371-5377.

Jeffries, M.O., Reynolds, G.J., Miller, J.M. 1992. First Landsat multi-spectral scanner images of the Canadian Arctic north of 80°N. *Polar Record,* **28**(164): 1 – 6.

Jeffries, M.O and Shaw, A.M. 1993. The drift of ice islands from the Arctic Ocean into the Channels of the Canadian Arctic Archipelago: the history of Hobson's Choice Ice Island. *Polar Record*, **29**: 305-312.

Johnston, M.E. and Timco, G.W. 2008. Understanding and Identifying Old Ice in Summer. Canadian Hydraulics Centre, National Research Council, Canada.

Kalnay, E., Kanamitsu, M., Kistler, R., Collins, W., Deaven, D., Gandin, L., Iredell, M., Sasha, S., White, G., Woolen, J., Zhu, Y., Leetmaa, A., Reynolds, B., Chelliah, M., Ebisuzaki, W., Higgins, W., Janowiak, J., Mo, K.C., Ropelewski, C., Wand, J., Jenne, R., Joseph, D. 1996. The NCEP/NCAR 40-Year reanalysis project. *Bulletin of the American Meteorological Society*, **77**: 437-472.

Koenig, L.S., Greenaway, K.R., Dunbar, M., Hattersley-Smith, G. 1952. Arctic ice islands. *Arctic*, **5**: 67-103.

Koerner, R.M., 1979, Accumulation, ablation and oxygen isotope variations on the Queen Elizabeth Islands ice caps, Canada. *Journal of Glaciology*, **22**(86), 25-41.

Koerner, M.R. 2002. Glaciers of North America – Glaciers of Canada, Glaciers of the Arctic Islands, Glaciers of the High Arctic Islands. Satellite Image Atlas of Glaciers of the World. U.S. Geophysical Survey Professional Paper 1386-J-1.

Koerner, M.R. 2005. Mass balance of glaciers in the Queen Elizabeth Islands, Nunavut, Canada. *Journal of Glaciology*, **42**: 417 – 423.

Koerner, R.M. and Paterson, W.S.B. 1974. Analysis of a core through the Meighen Ice Cap, Arctic Canada, and its paleoclimatic implications. *Quaternary Research*, **4**: 253-263.

Kovacs, A. and Morey, R. 1978. Radar anisotropy of sea ice due to preferred azimuthal orientation of the horizontal c-axis of ice crystals. *Journal of Geophysical Research,* **83**(C12): 6037 – 6049.

Kwok, R. and Cunningham, G.F. 2010. Contributions of melt in the Beaufort Sea to the decline in Arctic multiyear sea ice coverage: 1993 – 2009. *Geophysical Research Letters,* **37**(L20501): 1-5.

Lemke, P., Ren, J., Alley, R.B., Allison, I., Carrasco, J., Flato, G., Fujii, Y., Kaser, G., Mote, P., Thomas, R.H., Zhang, T. 2007. Observations: Changes in Snow, Ice and Frozen Ground. In: Climate Change 2007: The Physical Science Basis. Contribution of Working Group I to the Fourth Assessment Report of the Intergovernmental Panel on Climate Change [Solomon, S., D. Qin, M. Manning, Z. Chen, M. Marquis, K.B. Averyt, M. Tignor and H.L. Miller (eds.)]. Cambridge University Press, Cambridge, United Kingdom and New York, NY, USA.

Lemmen, D.S., Evans, D.J.A., England, J. 1988. Canadian Landform Examples – 10: Ice Shelves northern Ellesmere Island, N.W.T. *The Canadian Geographer*, **32**(4): 363-367.

Lesins, G., Duck, T.J., Drummond, J.R. 2010. Climate trends at Eureka in the Canadian High Arctic, *Atmosphere-Ocean*, **48**(2): 59-80.

Lillesand, T.M., Kiefer, R.W., Chipman, J.W. 2008. Remote sensing and image interpretation, sixth edition. John Wiley and Sons Inc., USA.

Lindsay, D.G. 1975. Sea ice Atlas of Arctic Canada, 1961-1968. Energy, Mines and Resources Canada, Ottawa.

Lindsay, D.G. 1977. Sea-ice Atlas of Arctic Canada, 1969-1974. Energy, Mines and Resources Canada, Ottawa.

Lindsay, D.G. 1981. Sea-ice Atlas of Arctic Canada, 1975-1978. Energy, Mines and Resources Canada, Ottawa.

Lindsay, D.G. Seifert, W and Anderson, N. 1968. Ice Islands, 1967. *Arctic*, **21**: 103-106.

Lyons, J.B., Mavin, S.M., A.J. Tamburi, 1971, Basement Ice, Ward Hunt Ice Shelf, Ellesmere Island, Canada. Journal of Glaciology, **10**(58): 93-100.

Macheret, Y.Y., Moskalevsky, M.Y., Vasilenko, E.V. 1993. Velocity of radio waves in glaciers as an indicator of their hydrothermal state, structure and regime, *Journal of Glaciology*, **39**(132): 373–384.

Mair, D., Burgess, D., Sharp, M., Dowdeswell, J.A., Benhan, T., Marshall, S., Cawkwell, F. 2009. Mass balance of the Prince of Wales Icefield, Ellesmere Island, Nunavut, Canada. *Journal of Geophysical Research,* **114**(F02011): 1-15.

Marshall, E.W. 1960. Structure and stratigraphy of T-3 and the Ellesmere Ice Shelf, in *Scientific Studies of Fletcher's Ice Island, T-3, 1952 – 1955*, Res. Pap. 63, pp. 47 – 57, U.S. Air Force, Cambridge Research Center, Bedford, Mass.

Maslanik, J.A., Fowler, C., Stroeve, J., Drobot, S., Zwally, J., Yi, D., Emery, W. 2007. A younger, thinner Arctic ice cover: Increased potential for rapid, extensive sea-ice loss. *Geophysical Research Letters*, **34** (L24501): 1-5.

Mercer J.H. 1978. West Antarctic ice sheet and CO2 greenhouse effect: a threat of disaster. *Nature,* **271**: 321-325.

Miller, G.H., Bradley, R.S., and Andrews, J.T. 1975. The glaciation level and lowest equilibrium line altitude in the High Canadian Arctic: maps and climatic interpretation. *Arctic and Alpine Research,* **7**(2): 155-168.

Mueller, D.R. 2008. Examining arctic ice shelves prior to the 2008 breakup. *EOS, Transactions of the American Geophysical Union*, **89**(49): 502-503.

Mueller, D.R., Vincent, W.F., Jeffries, M.O. 2003. Break-up of the largest Arctic ice shelf and associated loss of an epishelf lake. *Geophysical research letters*, **30**(20): 2031.

Mueller, D.R., Vincent, W.F., Jeffries, M.O. 2006. Environmental gradients, fragmented habits, and microbiota of northern ice shelf cryoecosystem, Ellesmere Island, Canada. *Arctic, Antarctic, and Alpine Research*, **38**(4): 593-607.

Mueller, D.R., Van Hove, P., Antoniades, D., Jeffries, M.O., Vincent, W.F. 2009. High Arctic lakes as sentinel ecosystems: Cascading regime shifts in climate, ice cover, and mixing. *Limnology Oceanogr*, **54**(5): 1-15.

Narod, B.B. and Clarke, G.K.C. 1983. UHF radar system for airborne surveys of ice thickness. *Canadian Journal of Earth Sciences*, **20**: 1073 – 1086.

Narod, B.B., Clarke, G.K.C., Prager, B.T. 1988. Airborne UHF sounding of glaciers and ice shelves, northern Ellesmere Island, Arctic Canada. *Canadian Journal of Earth Sciences*, **25**: 95-105.

National Snow and Ice Data Center. 2009. Arctic sea ice news and analysis. July 2009. http://nsidc.org/arcticseaicenews.

National Oceanic and atmospheric administration national climatic data center, prepared for the Bulletin of the American Meteorological Society (2010). BAMS state of the climate report 2009. http:www.ncdc.noaa.gov/bams-state-of-the-climate.

Newell, J.P. 1993. Exceptionally large icebergs and ice islands in eastern Canadian waters: a review of sightings from 1900 to present. *Arctic*, **46** (3): 205-211.

Nghiem, S.V., Rigor, I.G., Perovich, D.K., Clemente-Colon, P., Weatherly, J.W., Neumann, G. 2007. Rapid reduction of Arctic perennial sea ice. *Geophysical Research Letters,* **34**(L19504): 1-6.

Nutt, D.C. 1966. The Drift of Ice Island WH-5. *Arctic*, **19**: 244-262.

Nyland, D. 2004. Profiles of floating ice in arctic regions using GPR. *The Leading Edge,* **23**: 665- 668.

Pälli, A., Kohler, J.C., Isaksson, E., Moore, J.C., Pinglot, J.F., Pohjola, V.A., Samuelsson, H., 2002. Spatial and temporal variability of snow accumulation using ground-penetrating radar and ice cores on a Svalbard glacier. *Journal of Glaciology*, **48**(162): 417-424.

Perovich, D.K., Richter-Menge, J.A., Jones, K.F., Light, B. 2008. Sunlight, water, and ice: Extreme Arctic sea ice melt during the summer of 2007. *Geophysical Research Letters*, **35**(L11501): 1 – 4.

Plewes, L, A., and Hubbard, B., 2001. A review of the use of radio-echo sounding in glaciology. *Progress in Physical Geography,* **25**(2): 203-236.

Pope, S.G. 2010. *Changes in Multiyear Landfast Sea Ice in the Northern Canadian Arctic Archipelago.* M.Sc. Thesis University of Ottawa. Ottawa, Canada.

Pope, S., Copland, L., Alt, B. 2011. Recent changes in sea ice plugs along the Northern Canadian Arctic Archipelago. *In* Copland, L. and Mueller, D.R., (eds.). *Arctic Ice Shelves and Ice Islands*. Springer SBM, Dordrecht.

Prager, B. T. 1983. *Digital signal processing of UHF radio echo sounding data from Northern Ellesmere Island.* M.Sc. Thesis University of British Columbia, Vancouver, Canada.

Pringle, D., Dubuis, G., Eicken, H. 2009. Impedance measurements of the complex dielectric permittivity of sea ice at 50 MHz: pore microstructure and potential for salinity monitoring. *Journal of Glaciology*, **55**(189): 81 – 94.

PulseEKKO Pro User Guide. 2006. Technical User Guide. *Sensor's and Software: Subsurface Imaging Solutions*.

Reeh, N., Thomsen, H.H., Higgins, A.K., Weidick, A. 2001. Sea ice and the stability of north and northeast Greenland floating glaciers. *Annals of Glaciology*. (**33**): 474-480.

Rignot, E. and Thomas, R.H. 2002. Mass balance of Polar ice sheets. *Science*, **297**: 1502-1506.

Robin, G. de Q. and Adie, R.J. 1964. The Ice Cover. In: Antarctic Research (R. Priestley, R.J. Adie and G. de Q. Robin, eds), Butterworths, London.

Robin, G. de Q., Swithinbank, C.W.M., Smith, B.M.E. 1970. Radio echo exploration of the Antarctic ice sheet, *International Symposium on Antarctic Glaciological Exploration, Hanover, N.H., September 3 – 7, 1968 –Intern. Assoc. Sci. Hydrol., Commission of Snow and Ice,* **86**: 97 – 115.

Rothrock, D.A., Yu, Y., Maykut, G.A. 1999. Thinning of the Arctic sea-ice cover. *Geophysical Research Letters*, **26**(23): 3469 – 3472.

Sackinger, W.M**.**, Jeffries, M.O., Li, F., Lu, M. 1991. Ice Island Creation, drift, recurrences, mechanical properties, and interactions with arctic offshore oil production structures. *U.S. Department of Energy Final Report DOE/MC/25027-3112*.

Sanderson, T.J.O. 1979. Equilibrium profile of ice shelves. Journal of Glaciology, **22**(88): 435-460.

Scambos, T.A., Bohlander, J.A., Shuman, C.A., Skvarca, P. 2004. Glacier acceleration and thinning after ice shelf collapse in the Larsen B embayment, Antarctica. *Geophysical Research Letters*, **31**(L18402): 1-4.

Serreze, M.C., and Barry, R.G. 2005. The Arctic Climate System. Cambridge, England: Cambridge University Press.

Serreze, M.C., Holland, M.M., Stroeve, J. 2007. Perspectives on the Arctic's shrinking sea-ice cover. *Science*, **315**: 1533-1536.

Serson, H.V. 1979. *Mass Balance of the Ward Hunt ice rise and ice shelf: an 18-year record*. Defence Establishment Pacific, Victoria, Victoria, B.C., Canada.

Shepherd, A., Wingham, D., Payne, T., Skvarca, P. 2003. Larsen ice shelf has progressively thinned. Science, **302**: 856-859.

Smith, J.A., Bentley, M.J., Hodgson, D.A., Cook, A. J. 2007. George VI Ice Shelf: past history, present behavior and potential mechanisms for future collapse. *Antarctic Science*, **19**(1): 131 – 142.

Sneed, W.A., Hooke, R. LeB., Hamilton, G.S. 2008. Thinning of the south dome of Barnes Ice Cap, Arctic Canada, over the past two decades. *Geology*, **36**(1): 71 – 74.

Stroeve, J. Holland, M.M., Meier, W., Scambos, T., Serreze, M. 2007. Arctic sea ice decline: faster than forecast. *Geophysical Research Letters*, **34**(L09501): 1-5.

VanWychen, W. and Copland, L. 2011. Ice island drift mechanisms in the Canadian High Arctic. *In* Copland, L. and Mueller, D.R., (eds.). *Arctic Ice Shelves and Ice Islands*. Springer SBM, Dordrecht.

Vaughan, D.G. 1998. A new classification scheme for ice shelves based on mechanisms of mas gain and loss. *Polar Record,* **34**(188): 56 – 58.

Vaughan, D.G., and Doake, C.S.M. 1996. Recent atmospheric warming and retreat of ice shelves on the Antarctic Peninsula. *Nature*, **376**: 328-331.

Vincent, W.F., Gibson, J.A.E., Jeffries, M.O. 2001. Ice-shelf collapse, climate change, and habitat loss in the Canadian high Arctic. *Polar Record*, **37**(201): 133-142.

Wadhams, P. 2000. Ice in the Ocean. Gordon and Breach Science Publishers, London.

Wang, L., Sharp, M.J., Rivard, B., Marshall, S., Burges, D. 2005. Melt season duration on Canadian Arctic ice caps, 2000-2004. *Geophysical Research Letters*, **32** (L19502): 1-4.

Williamson, S., Sharp, M., Dowdeswell, J., Benham, T. 2008. Iceberg calving rates from northern Ellesmere Island ice caps, Canadian Arctic, 1999-2003. *Journal of Glaciology*, **54**(186): 391-400.

Woodward, J. and Burke, M.J. 2007. Applications of ground-penetrating radar to glacial and frozen materials. *Journal of Environmental and Engineering Geophysics*, **12**(1): 69-85.

Yan, M.H. 1986. *The Relationship Between Ice Island Movement and Weather Conditions.* M.Sc. Thesis, University of Alaska, Fairbanks, U.S.A.

Zemp, M., Jansson, P., Homlund, P., Gartner-Roer, I., Koblet, T., Thee, P., Haeberli, W. 2010. Comparison of glaciological and volumetric mass balance measurements at Storglaciaren, Sweden, *The Cryosphere Discussions*, **4**: 381-408.

Appendix 1

Table A1: Image information for 1950 air photos used for 1950 mosaic.

Line (6" lens)	Photo	Date	Flying altitude (ft. ASL)	Map scale	GCPs	RMSE (m)
T407C 85South	6	15-Jul-50	20 000'	1:40 000	25	39.00
T407C 85South	8	15-Jul-50	20 000'	1:40 000	25	55.31
T407C 85South	10	15-Jul-50	20 000'	1:40 000	16	54.20
T407C 85South	11	15-Jul-50	20 000'	1:40 000	27	6.19
T407C 85South	12	15-Jul-50	20 000'	1:40 000	20	50.70
T407C 86North	204	15-Jul-50	20 000'	1:40 000	20	20.51
T407C 86North	205	15-Jul-50	20 000'	1:40 000	20	13.20
T407C 86North	206	15-Jul-50	20 000'	1:40 000	21	12.10
T407C 86North	207	15-Jul-50	20 000'	1:40 000	22	22.44
T407C 86North	209	15-Jul-50	20 000'	1:40 000	23	19.31
T405C	236	15-Jul-50	20 000'	1:40 000	22	22.42
T405C	237	15-Jul-50	20 000'	1:40 000	23	29.53
Mean						28.74

Table A2: Image information for 1959 air photos used for 1959 mosaic.

Line (6" lens)	Photo	Date	Flying altitude (ft. ASL)	Map scale	GCPs	RMSE (m)
A16706	7	29-Jul-59	30 000'	1:60 000	22	37.09
A16706	9	29-Jul-59	30 000'	1:60 000	23	31.27
A16785	65	17-Aug-59	30 000'	1:60 000	23	29.68
A16785	67	17-Aug-59	30 000'	1:60 000	20	16.80
A16785	68	17-Aug-59	30 000'	1:60 000	22	17.31
A16785	70	17-Aug-59	30 000'	1:60 000	14	52.46
A16785	81	17-Aug-59	30 000'	1:60 000	23	33.00
A16785	83	17-Aug-59	30 000'	1:60 000	23	31.88
A16785	211	17-Aug-59	30 000'	1:60 000	14	20.95
A16785	213	17-Aug-59	30 000'	1:60 000	20	22.77
A16785	213	17-Aug-59	30 000'	1:60 000	16	15.36
A16785	215	17-Aug-59	30 000'	1:60 000	23	16.23
Mean						27.07

Table A3: Image information for 1974 air photos used for 1974 mosaic.

Line (6" lens)	Photo	Date	Flying altitude (ft. ASL)	Map scale	GCPs	RMSE (m)
A29343 H-2-N	70	11-Jul-74	10 000'	1:18 000	25	18.15
A29343 H-2-N	72	11-Jul-74	10 000'	1:18 000	20	21.08
A29343 H-2-N	74	11-Jul-74	10 000'	1:18 000	37	14.41
A29343 H-2-N	75	11-Jul-74	10 000'	1:18 000	24	13.14
A29343 H-2-N	77	11-Jul-74	10 000'	1:18 000	34	16.30
A29343 H-2-N	78	11-Jul-74	10 000'	1:18 000	29	23.26
A29343 H-2-N	79	11-Jul-74	10 000'	1:18 000	38	14.43
A29343 H-2-N	80	11-Jul-74	10 000'	1:18 000	33	21.40
Mean						17.77

Table A4: Image information for 1984 air photos used for 1984 mosaic.

Line	Photo	Date	Flying altitude (ft. ASL)	Map scale	GCPs	RMSE (m)
A26534 MIL 2 SE	3	24-Jul-84	10 000’	1:18000	20	15.70
A26534 MIL 2 SE	5	24-Jul-84	10 000’	1:18000	21	13.08
A26534 MIL 2 SE	7	24-Jul-84	10 000’	1:18000	23	14.00
A26534 MIL 2 SE	8	24-Jul-84	10 000’	1:18000	25	9.62
A26534 MIL 2 SE	10	24-Jul-84	10 000’	1:18000	20	13.47
A26534 MIL 2 SE	11	24-Jul-84	10 000’	1:18000	20	12.00
A26534 MIL 2 SE	12	24-Jul-84	10 000’	1:18000	20	14.80
A26534 MIL 2 SE	13	24-Jul-84	10 000’	1:18000	16	31.20
A26534 MIL 2 SE	15	24-Jul-84	10 000’	1:18000	18	9.59
A26534 MIL 2 SE	17	24-Jul-84	10 000’	1:18000	18	7.19
A26534 MIL 2 SE	19	24-Jul-84	10 000’	1:18000	27	11.91
A26534 MIL 2 SE	21	24-Jul-84	10 000’	1:18000	26	10.49
A26534 MIL 2 SE	23	24-Jul-84	10 000’	1:18000	26	17.53
A26534 MIL 2 SE	25	24-Jul-84	10 000’	1:18000	22	12.42
A26534 MIL 2 SE	27	24-Jul-84	10 000’	1:18000	26	22.87
A26534 MIL 2 SE	29	24-Jul-84	10 000’	1:18000	18	18.98
A26534 MIL 3 NW	31	24-Jul-84	10 000’	1:18000	15	28.08
A26534 MIL 3 NW	33	24-Jul-84	10 000’	1:18000	23	11.92
A26534 MIL 3 NW	35	24-Jul-84	10 000’	1:18000	20	17.63
A26534 MIL 3 NW	35	24-Jul-84	10 000’	1:18000	18	21.80
A26534 MIL 3 NW	37	24-Jul-84	10 000’	1:18000	12	14.86
A26534 MIL 3 NW	39	24-Jul-84	10 000’	1:18000	16	18.78
A26534 MIL 3 NW	41	24-Jul-84	10 000’	1:18000	21	21.51
A26534 MIL 3 NW	43	24-Jul-84	10 000’	1:18000	22	19.16
A26534 MIL 3 NW	45	24-Jul-84	10 000’	1:18000	26	15.07
A26534 MIL 3 NW	47	24-Jul-84	10 000’	1:18000	19	25.99
A26534 MIL 3 NW	48	24-Jul-84	10 000’	1:18000	20	10.46
A26534 MIL 3 NW	49	24-Jul-84	10 000’	1:18000	11	27.56
A26534 MIL 3 NW	51	24-Jul-84	10 000’	1:18000	23	13.35
A26534 MIL 3 NW	53	24-Jul-84	10 000’	1:18000	21	11.07
A26534 MIL 3 NW	55	24-Jul-84	10,000’	1:18000	24	11.27
A26534 MIL 3 NW	57	24-Jul-84	10 000’	1:18000	24	4.00
A26534 MIL 4 SE	59	24-Aug-84	9 800’	1:18000	12	24.62
A26534 MIL 4 SE	61	24-Aug-84	9 800’	1:18000	33	12.51
A26534 MIL 4 SE	63	24-Aug-84	9 800’	1:18000	19	13.18
A26534 MIL 4 SE	64	24-Aug-84	9 800’	1:18000	10	13.24

A26534 MIL 4 SE	65	24-Aug-84	9 800’	1:18000	15	10.97
A26534 MIL 4 SE	66	24-Aug-84	9 800’	1:18000	35	8.78
A26534 MIL 4 SE	67	24-Aug-84	9 800’	1:18000	23	14.57
A26534 MIL 4 SE	68	24-Aug-84	9 800’	1:18000	20	12.10
A26534 MIL 5 NW	69	24-Aug-84	9 790’	1:18000	30	5.17
A26534 MIL 5 NW	70	24-Aug-84	9 790’	1:18000	22	13.26
A26534 MIL 5 NW	72	24-Aug-84	9 790’	1:18000	19	6.94
A26534 MIL 5 NW	73	24-Aug-84	9 790’	1:18000	25	34.47
A26534 MIL 5 NW	74	24-Aug-84	9 790’	1:18000	19	25.07
A26534 MIL 5 NW	75	24-Aug-84	9 790’	1:18000	23	21.27
A26534 MIL 5 NW	76	24-Aug-84	9 790’	1:18000	23	24.40
A26534 MIL 5 NW	77	24-Aug-84	9 790’	1:18000	20	25.40
A26534 MIL 1 NE	81	24-Aug-84	8 000’	1:17000	21	12.41
A26534 MIL 1 NE	82	24-Aug-84	8 000’	1:17000	19	6.87
A26534 MIL 1 NE	83	24-Aug-84	8 000’	1:17000	16	11.33
A26534 MIL 1 NE	84	24-Aug-84	8 000’	1:17000	16	19.33
A26534 MIL 1 NE	85	24-Aug-84	8 000’	1:17000	11	30.07
A26534 MIL 1 NE	86	24-Aug-84	8 000’	1:17000	27	12.88
A26534 MIL 1 NE	87	24-Aug-84	8 000’	1:17000	25	13.65
A26534 MIL 1 NE	88	24-Aug-84	8 000’	1:17000	30	13.36
A26534 MIL 1 NE	89	24-Aug-84	8 000’	1:17000	24	8.51
A26534 MIL 1 NE	90	24-Aug-84	8 000’	1:17000	24	9.44
A26534 MIL 1 NE	91	24-Aug-84	8 000’	1:17000	22	7.46
A26534 MIL 1 NE	92	24-Aug-84	8 000’	1:17000	18	6.33
A26534 MIL 1 NE	93	24-Aug-84	8 000’	1:17000	20	7.55
Mean						15.34